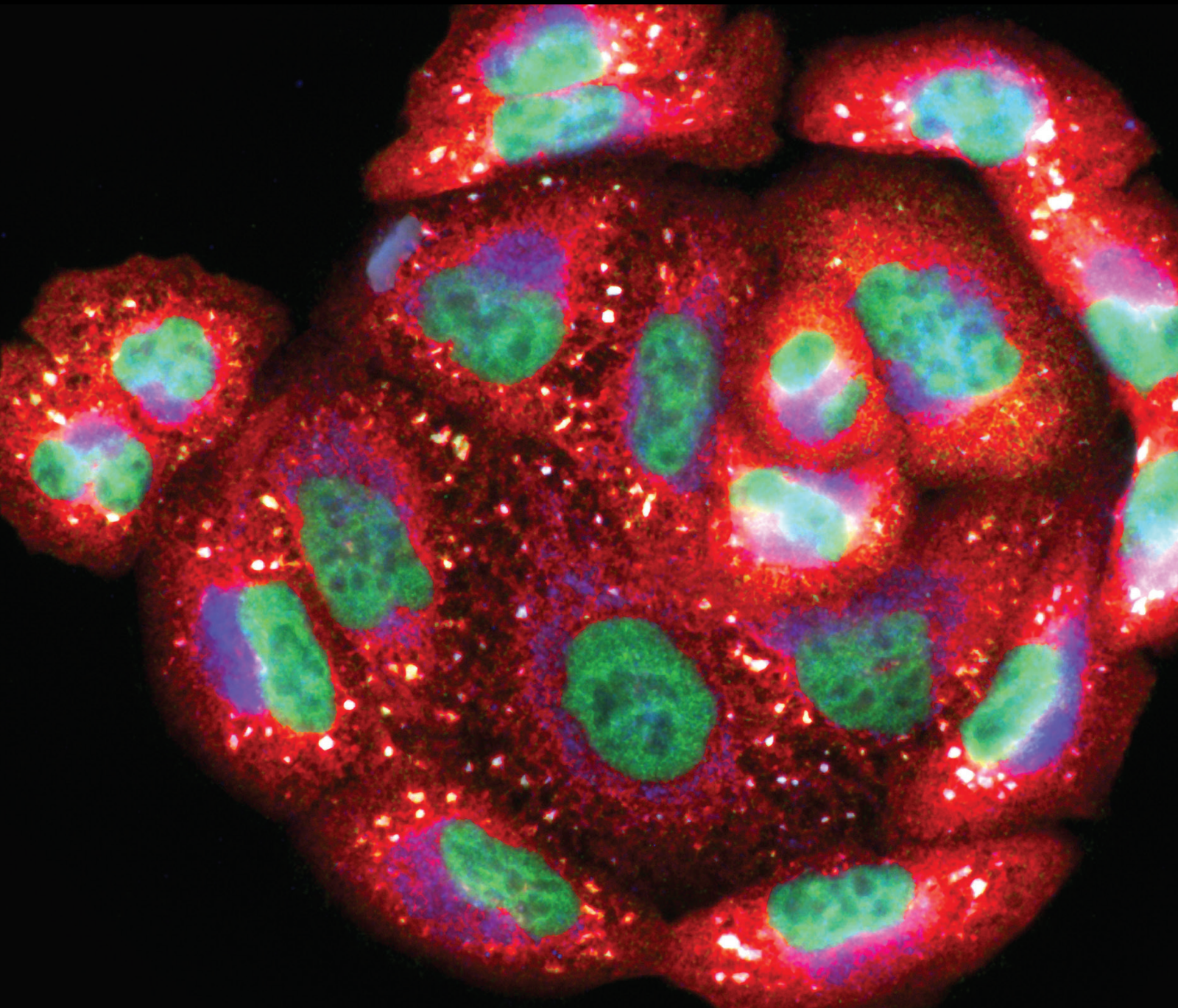


Redox Regulation of Cancer Epigenetics

Lead Guest Editor: Mithun Sinha

Guest Editors: Jayeeta Ghose, Kanhaiya Singh, and Adil Mardinoglu



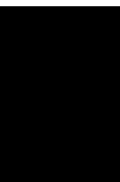
Redox Regulation of Cancer Epigenetics

Oxidative Medicine and Cellular Longevity

Redox Regulation of Cancer Epigenetics

Lead Guest Editor: Mithun Sinha

Guest Editors: Jayeeta Ghose, Kanhaiya Singh, and
Adil Mardinoglu



Copyright © 2022 Hindawi Limited. All rights reserved.

This is a special issue published in "Oxidative Medicine and Cellular Longevity" All articles are open access articles distributed under the Creative Commons Attribution License, which permits unrestricted use, distribution, and reproduction in any medium, provided the original work is properly cited.

Chief Editor

Jeannette Vasquez-Vivar, USA

Associate Editors

Amjad Islam Aqib, Pakistan
Angel Catalá , Argentina
Cinzia Domenicotti , Italy
Janusz Gebicki , Australia
Aldrin V. Gomes , USA
Vladimir Jakovljevic , Serbia
Thomas Kietzmann , Finland
Juan C. Mayo , Spain
Ryuichi Morishita , Japan
Claudia Penna , Italy
Sachchida Nand Rai , India
Paola Rizzo , Italy
Mithun Sinha , USA
Daniele Vergara , Italy
Victor M. Victor , Spain


Academic Editors

Ammar AL-Farga , Saudi Arabia
Mohd Adnan , Saudi Arabia
Ivanov Alexander , Russia
Fabio Altieri , Italy
Daniel Dias Rufino Arcanjo , Brazil
Peter Backx, Canada
Amira Badr , Egypt
Damian Bailey, United Kingdom
Rengasamy Balakrishnan , Republic of Korea
Jiaolin Bao, China
Ji C. Bihl , USA
Hareram Birla, India
Abdelhakim Bouyahya, Morocco
Ralf Braun , Austria
Laura Bravo , Spain
Matt Brody , USA
Amadou Camara , USA
Marcio Carcho , Portugal
Peter Celec , Slovakia
Giselle Cerchiaro , Brazil
Arpita Chatterjee , USA
Shao-Yu Chen , USA
Yujie Chen, China
Deepak Chhangani , USA
Ferdinando Chiaradonna , Italy

Zhao Zhong Chong, USA
Fabio Ciccarone, Italy
Alin Ciobica , Romania
Ana Cipak Gasparovic , Croatia
Giuseppe Cirillo , Italy
Maria R. Ciriolo , Italy
Massimo Collino , Italy
Manuela Corte-Real , Portugal
Manuela Curcio, Italy
Domenico D'Arca , Italy
Francesca Danesi , Italy
Claudio De Lucia , USA
Damião De Sousa , Brazil
Enrico Desideri, Italy
Francesca Diomede , Italy
Raul Dominguez-Perles, Spain
Joël R. Drevet , France
Grégory Durand , France
Alessandra Durazzo , Italy
Javier Egea , Spain
Pablo A. Evelson , Argentina
Mohd Farhan, USA
Ioannis G. Fatouros , Greece
Gianna Ferretti , Italy
Swaran J. S. Flora , India
Maurizio Forte , Italy
Teresa I. Fortoul, Mexico
Anna Fracassi , USA
Rodrigo Franco , USA
Juan Gambini , Spain
Gerardo García-Rivas , Mexico
Husam Ghanim, USA
Jayeeta Ghose , USA
Rajeshwary Ghosh , USA
Lucia Gimeno-Mallench, Spain
Anna M. Giudetti , Italy
Daniela Giustarini , Italy
José Rodrigo Godoy, USA
Saeid Golbidi , Canada
Guohua Gong , China
Tilman Grune, Germany
Solomon Habtemariam , United Kingdom
Eva-Maria Hanschmann , Germany
Md Saquib Hasnain , India
Md Hassan , India




Tim Hofer , Norway
John D. Horowitz, Australia
Silvana Hrelia , Italy
Dragan Hrnčić, Serbia
Zebo Huang , China
Zhao Huang , China
Tariq Hussain , Pakistan
Stephan Immenschuh , Germany
Norsharina Ismail, Malaysia
Franco J. L. , Brazil
Sedat Kacar , USA
Andleeb Khan , Saudi Arabia
Kum Kum Khanna, Australia
Neelam Khaper , Canada
Ramoji Kosuru , USA
Demetrios Kouretas , Greece
Andrey V. Kozlov , Austria
Chan-Yen Kuo, Taiwan
Gaocai Li , China
Guoping Li , USA
Jin-Long Li , China
Qiangqiang Li , China
Xin-Feng Li , China
Jialiang Liang , China
Adam Lightfoot, United Kingdom
Christopher Horst Lillig , Germany
Paloma B. Liton , USA
Ana Lloret , Spain
Lorenzo Loffredo , Italy
Camilo López-Alarcón , Chile
Daniel Lopez-Malo , Spain
Massimo Lucarini , Italy
Hai-Chun Ma, China
Nageswara Madamanchi , USA
Kenneth Maiese , USA
Marco Malaguti , Italy
Steven McAnulty, USA
Antonio Desmond McCarthy , Argentina
Sonia Medina-Escudero , Spain
Pedro Mena , Italy
V́ctor M. Mendoza-Núñez , Mexico
Lidija Milkovic , Croatia
Alexandra Miller, USA
Sara Missaglia , Italy

Premysl Mladenka , Czech Republic
Sandra Moreno , Italy
Trevor A. Mori , Australia
Fabiana Morroni , Italy
Ange Mouithys-Mickalad, Belgium
Iordanis Mourouzis , Greece
Ryoji Nagai , Japan
Amit Kumar Nayak , India
Abderrahim Nemmar , United Arab Emirates
Xing Niu , China
Cristina Nocella, Italy
Susana Novella , Spain
Hassan Obied , Australia
Pál Pacher, USA
Pasquale Pagliaro , Italy
Dilipkumar Pal , India
Valentina Pallottini , Italy
Swapnil Pandey , USA
Mayur Parmar , USA
Vassilis Paschalis , Greece
Keshav Raj Paudel, Australia
Ilaria Peluso , Italy
Tiziana Persichini , Italy
Shazib Pervaiz , Singapore
Abdul Rehman Phull, Republic of Korea
Vincent Pialoux , France
Alessandro Poggi , Italy
Zsolt Radak , Hungary
Dario C. Ramirez , Argentina
Erika Ramos-Tovar , Mexico
Sid D. Ray , USA
Muneeb Rehman , Saudi Arabia
Hamid Reza Rezvani , France
Alessandra Ricelli, Italy
Francisco J. Romero , Spain
Joan Roselló-Catafau, Spain
Subhadeep Roy , India
Josep V. Rubert , The Netherlands
Sumbal Saba , Brazil
Kunihiro Sakuma, Japan
Gabriele Saretzki , United Kingdom
Luciano Saso , Italy
Nadja Schroder , Brazil




Anwen Shao , China
Iman Sherif, Egypt
Salah A Sheweita, Saudi Arabia
Xiaolei Shi, China
Manjari Singh, India
Giulia Sita , Italy
Ramachandran Srinivasan , India
Adrian Sturza , Romania
Kuo-hui Su , United Kingdom
Eisa Tahmasbpour Marzouni , Iran
Hailiang Tang, China
Carla Tatone , Italy
Shane Thomas , Australia
Carlo Gabriele Tocchetti , Italy
Angela Trovato Salinaro, Italy
Rosa Tundis , Italy
Kai Wang , China
Min-qi Wang , China
Natalie Ward , Australia
Grzegorz Wegrzyn, Poland
Philip Wenzel , Germany
Guangzhen Wu , China
Jianbo Xiao , Spain
Qiongming Xu , China
Liang-Jun Yan , USA
Guillermo Zalba , Spain
Jia Zhang , China
Junmin Zhang , China
Junli Zhao , USA
Chen-he Zhou , China
Yong Zhou , China
Mario Zoratti , Italy

Contents







Laser Capture Microdissection in the Spatial Analysis of Epigenetic Modifications in Skin: A Comprehensive Review

Theja Bhamidipati, Mithun Sinha , Chandan K. Sen , and Kanhaiya Singh 
Review Article (12 pages), Article ID 4127238, Volume 2022 (2022)









Effects of MicroRNA-195-5p on Biological Behaviors and Radiosensitivity of Lung Adenocarcinoma Cells via Targeting HOXA10

Cheng Yuan , Rui Bai, Yanping Gao, Xueping Jiang, Shuying Li, Wenjie Sun, Yangyi Li, Zhengrong Huang, Yan Gong , and Conghua Xie 
Research Article (18 pages), Article ID 4522210, Volume 2021 (2021)

Methylation of CALCA and CALCB in Pancreatic Ductal Adenocarcinoma

Feng Gao , Guozhong Liu, Jingwen Wang, Shirong Huang , Fadian Ding , Wei Lian, Xiaoting Lv , Yujia Guo, Xiangqun Fan, Sheng Zhang , and Qicai Liu 
Research Article (13 pages), Article ID 2088345, Volume 2021 (2021)


Exosomal lncRNA PVT1/VEGFA Axis Promotes Colon Cancer Metastasis and Stemness by Downregulation of Tumor Suppressor miR-152-3p

Shiue-Wei Lai , Ming-Yao Chen , Oluwaseun Adebayo Bamodu , Ming-Shou Hsieh , Ting-Yi Huang , Chi-Tai Yeh , Wei-Hwa Lee , and Yih-Giun Cherng 
Research Article (19 pages), Article ID 9959807, Volume 2021 (2021)




Role of RONS and eIFs in Cancer Progression

Yasmeen Ahmed Salaheldin , Salma Sayed Mohamed Mahmoud, Ebenezeri Erasto Ngowi , Vivian Aku Gbordzor, Tao Li, Dong-Dong Wu , and Xin-Ying Ji 
Review Article (14 pages), Article ID 5522054, Volume 2021 (2021)

Integrated Analysis to Identify a Redox-Related Prognostic Signature for Clear Cell Renal Cell Carcinoma

Yue Wu, Xian Wei, Huan Feng, Bintao Hu, Bo Liu, Yang Luan, Yajun Ruan, Xiaming Liu, Zhuo Liu, Jihong Liu, and Tao Wang 
Research Article (35 pages), Article ID 6648093, Volume 2021 (2021)



Exploring the Role and Mechanism of pAMPK α -Mediated Dysregulation of Brf1 and RNA Pol III Genes

Teng Wu, Dongkun Zhang, Mingen Lin, Lihong Yu, Ting Dai, Shuai Li, Fenghai Yu, Lei Lu , Liling Zheng , and Shuping Zhong 
Research Article (15 pages), Article ID 5554932, Volume 2021 (2021)

Advances in Understanding Mitochondrial MicroRNAs (mitomiRs) on the Pathogenesis of Triple-Negative Breast Cancer (TNBC)

Hung-Yu Lin  and Pei-Yi Chu 
Review Article (17 pages), Article ID 5517777, Volume 2021 (2021)

HIF-1 Inhibitor YC-1 Reverses the Acquired Resistance of EGFR-Mutant HCC827 Cell Line with MET Amplification to Gefitinib

Qian Jin , Jisheng Zheng, Ming Chen, Na Jiang, Xianrong Xu, and Feihua Huang 

Research Article (9 pages), Article ID 6633867, Volume 2021 (2021)

Review Article

Laser Capture Microdissection in the Spatial Analysis of Epigenetic Modifications in Skin: A Comprehensive Review

Theja Bhamidipati,¹ Mithun Sinha ,² Chandan K. Sen ,² and Kanhaiya Singh ²

¹Kansas City University, 1750 Independence Avenue, Kansas City, MO, USA

²Indiana Center for Regenerative Medicine and Engineering, Department of Surgery, Indiana University School of Medicine, Indianapolis, IN, USA

Correspondence should be addressed to Kanhaiya Singh; kanh@iu.edu

Received 21 June 2021; Revised 29 October 2021; Accepted 24 December 2021; Published 9 February 2022

Academic Editor: Alin Ciobica

Copyright © 2022 Theja Bhamidipati et al. This is an open access article distributed under the Creative Commons Attribution License, which permits unrestricted use, distribution, and reproduction in any medium, provided the original work is properly cited.

Each cell in the body contains an intricate regulation for the expression of its relevant DNA. While every cell in a multicellular organism contains identical DNA, each tissue-specific cell expresses a different set of active genes. This organizational property exists in a paradigm that is largely controlled by forces external to the DNA sequence *via* epigenetic regulation. DNA methylation and chromatin modifications represent some of the classical epigenetic modifications that control gene expression. Complex tissues like skin consist of heterogeneous cell types that are spatially distributed and mixed. Furthermore, each individual skin cell has a unique response to physiological and pathological cues. As such, it is difficult to classify skin tissue as homogenous across all cell types and across different environmental exposures. Therefore, it would be prudent to isolate targeted tissue elements prior to any molecular analysis to avoid a possibility of confounding the sample with unwanted cell types. Laser capture microdissection (LCM) is a powerful technique used to isolate a targeted cell group with extreme microscopic precision. LCM presents itself as a solution to tackling the problem of tissue heterogeneity in molecular analysis. This review will cover an overview of LCM technology, the principals surrounding its application, and benefits of its application to the newly defined field of epigenomics, in particular of cutaneous pathology. This presents a comprehensive review about LCM and its use in the spatial analysis of skin epigenetics. Within the realm of skin pathology, this ability to isolate tissues under specific environmental stresses, such as oxidative stress, allows a far more focused investigation.

1. Introduction

The premise behind cellular analysis rests largely on the assumption that tissue samples consist of homogenous cells. Historically, this process has disregarded the spatial aspect of the tissue in question. More so, the assumption of tissue homogeneity ignores the fact that identical biologic stressors can cause different reactions in different cell types [1]. Thus, having the ability to specify both spatial and cellular criteria, such as in a biopsy of a suspicious lesion, can allow the identification of molecular pathways that can distinguish between a metastatic process and a more benign etiology [2]. The current dogma behind these molecular pathways is that they rely heavily on heterogeneous cell populations due to their reliance on low abundance molecules, their spa-

tial nature, and their interrelation [3]. Epigenetic modification, in particular, must use downstream cascades in order to properly affect gene transcription simply due to the extracellular nature of the modification. Of note, these downstream cascades are highly variable among different tissue types and even among similar tissues that exist in different environments. When focusing on epigenetic analysis, processes such as CpG methylation are extremely specific to parts of the DNA sequence. Properly isolating target cells and tissue would thus be even more important in the analysis of epigenomics when compared to more standard analytic tools that analyze protein structure or RNA content. The applications of this “microdissection” can be applied to nearly every field for molecular investigation including proteomics and transcriptomics [4] (Figure 1).

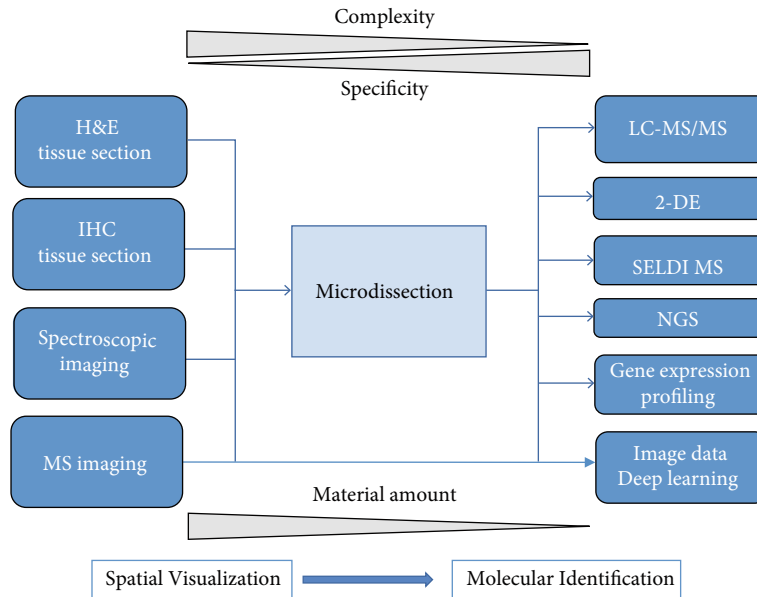


FIGURE 1: Many downstream analysis relies on the fundamental principle behind microdissection. An inappropriate tissue dissection would then be implicated in lower yield results and contamination. Reproduced under the terms of the Creative Commons CC BY license published by John Wiley and sons. The following original report is credited: von Eggeling and Hoffmann [4].

As the DNA sequence has become more understood with the completion of the Human Genome Project in 2003, there has been a shifting focus from solely identifying the genetic component of many diseases to detecting the progression of these same diseases [5–7]. High-risk cancerous tissue, for example, can be analyzed for certain epigenetic modifications which can be used as a proxy for potential malignant transformation [8]. The ability to identify potential malignancy offers avenues for early intervention to prevent morbidity and mortality. The analysis of these types of tissue has historically been done using techniques such as Southern blot analysis and polymerase chain reaction. However, there is a growing need for a new generation of sequencing techniques that can fine-tune the selection of tissue in regard to spatial location and pathological stresses.

When used in unison, isolation of discrete cell types/tissues and new sequencing platforms can create a genome-wide profile that has the power to unveil new information that can challenge previous dogmas. For example, Li et al. demonstrated the necessity for precise tissue sampling by showing that the difference between young and old skin did in fact have different dermal molecular expression in the dermis [9]. This difference was previously ignored because tissue samples rarely were separated from their epidermal components. Clearly, the ability to differentiate between seemingly insignificant parts of the same tissue can have profound implications.

Laser microbeam microdissection (LMM) and its successor laser capture microdissection (LCM) represent the newest technologies meant to overcome the inherent heterogeneity of tissue samples. By using the principles behind ultraviolet and infrared laser, the specificity of cell samples taken in situ is orders of magnitude greater. Thus, further

downstream analysis, such as in epigenetics, becomes far more sensitive and specific.

2. Laser Capture Microdissection

2.1. Overview. The use of applying focused lasers to isolate target tissues first began in the early 20th century but has advanced in recent years [1]. The initial need for a faster process than manual microdissection led to the introduction of microbeams. LMM focused primarily on using an ultraviolet laser on membrane-mounted sections of tissue. The membrane offers good optical quality without interfering with the downstream analysis. Pulses of ultraviolet lasers cause local dissection of the membrane-tissue complex due to photolysis [10]. The dissected tissue would then be taken out and used for further analysis. However, while LMM offered quality dissection with little dispersion of the tissue, it required a great deal of dexterity and is time-consuming. LCM was then introduced by the National Cancer Institute of the National Institutes of Health in Bethesda as the newest generation of laser capture technology. Within the past decade, it has been used to isolate tumor cells, neurons, virus-infected cells, and even specific organelles such as nuclei [11, 12]. Figure 2 pictorially represents the ability of LCM to isolate specific tissue elements [4].

In 1976, Isenberg et al. were the first to use this laser technology but in surgery [13]. It required massive space to dissect out tissue subpopulations. In response, LCM was devised by Emmert-Buck and their team [13]. They recognized a need for a system for efficient dissection of cells of solid tumors to fully utilize analytical technologies. This process quickly moved to a commercial platform by Arcturus Engineering under the name Veritas Systems (Mountain View, CA) [11, 14]. PALM Microbeam system (Carl Zeiss

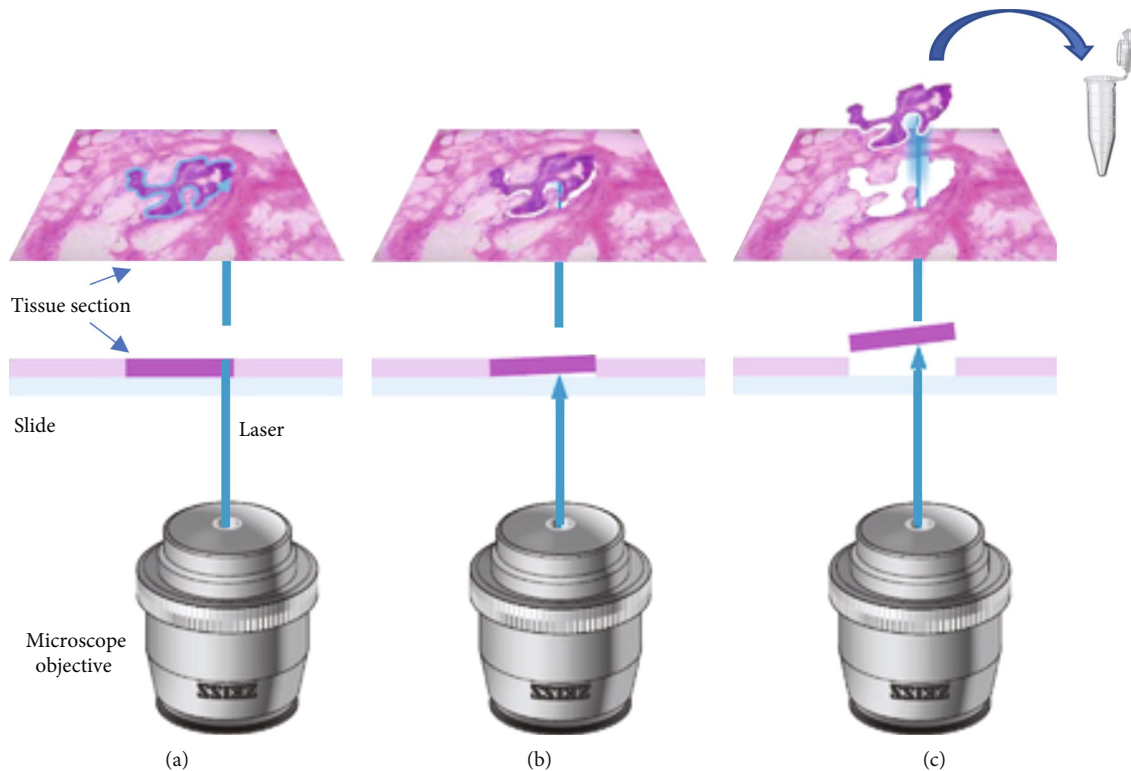


FIGURE 2: Inverted microscope used in laser microbeam (LMM) and laser capture microdissection (LCM) deploying ultraviolet or infrared laser pulses to target specific tissue sections. The laser-based microdissection is performed in three steps. (a) The laser coupled in the objective separated the desired area from the surrounding tissue. (b) The capture of the marked sample is then initiated using a single laser pulse. (c) The marked sample is then transferred to the desired capture device for downstream analyses. Reproduced under the terms of the Creative Commons CC BY license published by John Wiley and sons. The following original report is credited: von Eggeling and Hoffmann [4].

MicroImaging GmbH, Bernried, Germany) and the Leica LMD6000 (Leica Microsystems Inc., Bannockburn, IL, USA) further commercialized the technology making its use ubiquitous in researchers' labs across the world.

2.2. Components of LCM. The components for a LCM are (i) visualization of target cells using traditional microscopy, (ii) having the ability to transfer photoenergy to either a polymer-cell composite or directly to photolyze tissue, and (iii) being able to isolate and remove the target sample. This is done with the use of an inverted microscope, an infrared laser, control unit for the laser, a control mechanism for the microscope stage, a digital camera, and a monitor for target visualization [14]. A prototypical setup for large-scale microdissection is shown in Figure 3. Two large classes of LCM that exist are infrared and ultraviolet. Infrared LCM (IR-LCM) primarily uses large wavelength light at approximately 810 nm while ultraviolet LCM (UV-LCM) uses a shorter wavelength at approximately 355 nm [15]. While IR-LCM utilizes photoenergy to melt polymer caps in order to isolate tissue samples, UV-LCM directly photoablates the tissues around cells of interest. The differences and advantages between the two will be discussed in next sections; however, more modern systems are relying on combination of IR and UV-LCM such as the Arcturus XT (Thermo Fisher Scientific).

2.3. Infrared LCM (IR-LCM). Emmert-Buck and coworkers in 1996 at the National Institutes of Health developed an IR-LCM system [13]. By using very short pulses of infrared lasers with wavelengths of about 810 nm, the IR-LCM system is based on a thin thermoplastic film over the tissue section. The IR beams can melt the polymers overlying the collected tissue sample. This creates a tissue-polymer complex that can isolate target cells. More so, the thermofilm functions as a barrier to the damage from the light preserving the tissue [16]. The focused pulse of IR directed at the thermofilm causes a conformational change and adherence of the tissue to the polymer [17]. At the end of the dissection, cells of interest that are adhered to the film can be detached and transferred for analysis. However, due to this thin polymer, there is a risk of the sample becoming attached to the adhesive film running the risk for contamination. More so, this process is heavily user dependent with operator skill being a limiting factor.

2.4. Ultraviolet LCM (UV-LCM). Using smaller wavelength light of about 355 nm, UV-LCM is able to more specifically ablate tissue adjacent to the cells of interest [17]. First developed by Schutze and Lahr in 1998, this platform uses tissue that has been mounted directly on a membrane. Direct visualization by microscopy then allows direct isolation of cell populations without adjacent unwanted tissue [13, 16].

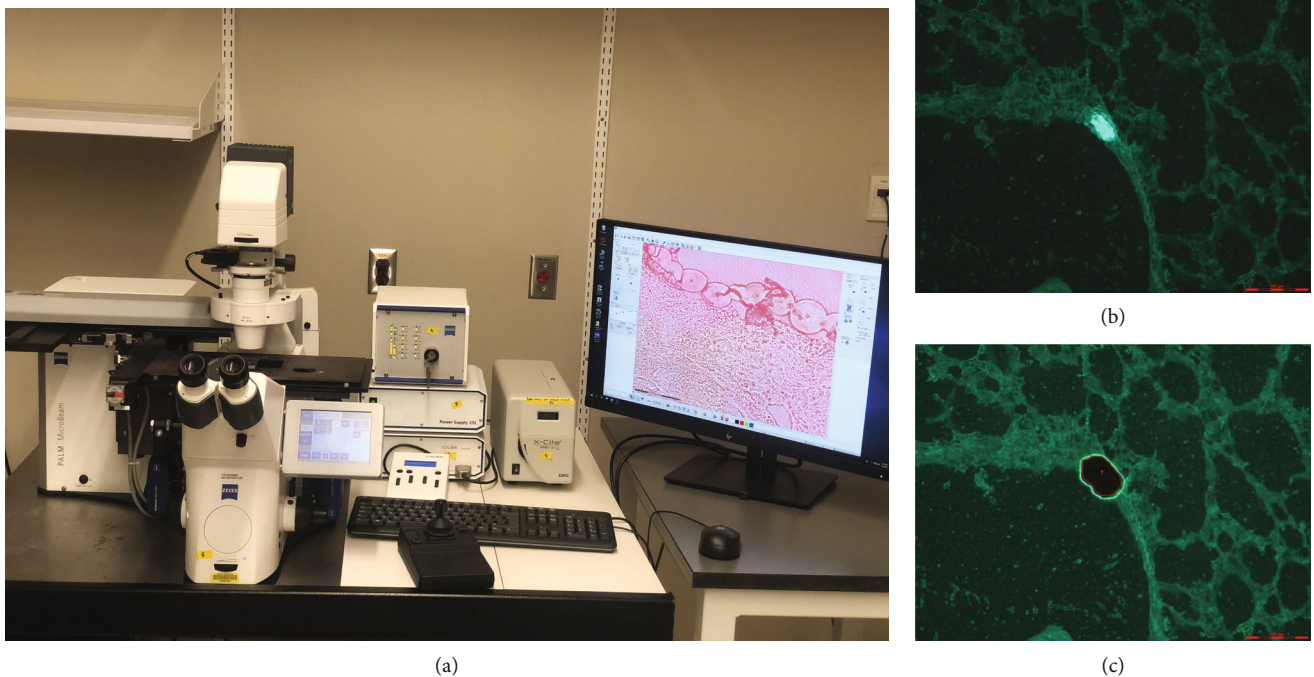


FIGURE 3: (a) Zeiss PALM Microbeam Laser Microdissection System located at the Indiana Center for Regenerative Medicine and Engineering, Indiana University. Prototypical laser setup showcases the components of LCM. (b) Before and (c) after laser capture microdissection of lung tissue sample done under fluoroscopy. Photographs showing of a lung section before and after images during capture of a cluster of fluorescent neuroendocrine cells, known as a neuroepithelial body. (b, c) Reproduced with permission from John Wiley and sons. The following original report was credited: Jensen [18].

When compared to its IR counterpart, UV avoids the issue surrounding adhering of unwanted cells due to the ability to directly photoablate the sample. More so, the smaller wavelength used in this system allows for more precise beam focus around smaller cells or even organelles. The target cells are then retrieved via photonic pressure or gravity which launches them into the collector cap [17].

2.5. Advantages and Limitations of LCM. The advantages of LCM stem from the ability to isolate very small and spatially unique cellular elements. Depending on the laser size and tissue sample, thousands of unique cellular elements can be collected in a fraction of the time that manual microdissection would require. This notion brings up the next advantage of LCM which is the wide-scale application of a fast and easy-to-use technology that does not require substantial manual dexterity or training. Jensen showcased how sensitive tissue from lung biopsies could be easily identified and dissected using LCM [18] (Figure 3). In fact, many LCM microscopes are easily adjusted to correspond with the skill of the operator. When comparing LCM to more conventional techniques, it is important to examine the quality of the tissue samples collected. In 1999, Banks et al. found no gross changes in the protein profiles [19]. The worry about lower quality dissection samples thus does not limit the implementation of LCM in cell and tissue analysis.

However, there are noticeable limitations of LCM which primarily reflect the limitations of microdissection. The narrow band of wavelength offers a physical limit on how small the dissection can be done on subcellular structures [20].

Another issue that is not only seen in LCM is the worry about optical resolution of tissue. Samples in LCM do not require the use of a cover slip. Thus, dehydrated tissue without a coverslip can make precise microdissection difficult. Investigators can however use special staining to highlight the tissue target in question [21]. And while LCM does offer an easier operator learning curve, the physical removal of cells from the slide is operator dependent. This event usually occurs with frozen sections and can be avoided with paraffin wax sections. Luo et al. demonstrate the optimal transfer conditions of frozen tissue sections with specific stains [22]. These immunohistochemistry stains offer their own set of problems. For example, eosin can interfere with certain 2D-Page Gel electrophoresis [23].

However, even when taking into consideration the limitations of laser capture microdissection, the speed, easy handling, and precision make this modality the ideal tool for collection of large amounts of specific tissue and cells.

3. Applications of LCM to Epigenetic Studies

3.1. Overview. Epigenetic modification is the broad-encompassing term that denotes hereditary inheritance that occurs outside of the DNA sequence [24]. These modifications mostly target the storage activation and inactivation of DNA. The three prototypical examples include (i) DNA methylation, (ii) histone modifications, and (iii) chromatin remodeling [25]. As outlined in Figures 4 and 5, these modifications have the ability to change the ability of DNA to be transcribed [26, 27].

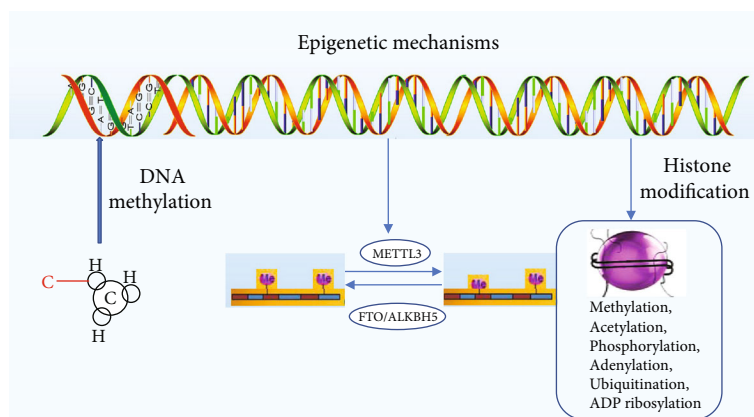


FIGURE 4: Modification to DNA or RNA through methylation or histone modifications changes the storage and packaging of DNA. Downstream, this can limit transcription. DNA methylation is one of the most studied epigenetic mechanisms, which occurs on CpG islands located in different repetitive genome regions or, more commonly, in promoter regions. Other epigenetic mechanisms known as histone modifications mainly include the methylation, ubiquitylation, acetylation, sumoylation, and phosphorylation of the histone tails. N6-Methyladenosine (m6A) is the most common mRNA modification. m6A modification is conducted by its “readers,” “erasers,” and “writers” to remove, add, or preferentially bind to m6A. m6A methylation occurs at once after pre-mRNA transcription by METTL3-containing methyltransferases, while the demethylation of m6A is by fat mass and obesity associated (FTO) and alpha-ketoglutarate-dependent dioxygenase AlkB homolog 5 (ALKBH5). Reproduced with permission from John Wiley and sons. The following original report was credited: Sang and Deng [26].

DNA methylation is a silencing tool associated with cytosine-guanine dinucleotide repeats found primarily on gene promoters. Recruitment of these additional methyl (CH₃) groups to the cytosine base forms a genetically stable carbon-carbon bond resulting in the formation of 5-methylcytosine (5mc) [28]. CpG methylation at these sites on promoters has been associated with gene silencing [28–30]. The CpG methylation events are carried out by DNA methyltransferases (DNMTs) or by the ten-eleven translocation family (TET) [31–33] (Figure 6). In particular, DNMT1, DNMT3A, DNMT3B, TET1, TET2, and TET3 have been shown to be associated with the pathological transcriptional deregulation in many diseases [27]. These diseases range from hematologic malignancies to solid tumor growth. More so, the causes of methylation have been linked environmental and lifestyle factors [34].

On the other hand, histone modifications occur on a larger scale and control gene transcription. As chromatin DNA becomes more condensed and organized, it becomes associated with histone proteins to form a nucleosome [27]. In particular, the four core histone proteins of the nucleosome (H2A, H2B, H3, and H4) are particularly susceptible to modification. Acetylation of these abovementioned histone proteins induces changes in the chromatin configuration that increases gene transcription [27]. Primary histone acetylation is done by acetyltransferases (HAT). On the other hand, deacetylation which is performed by histone deacetylases (HDAC) tightens the conformation of the nucleosome and limits transcription [25].

“Epigenomics” therefore is the study of these epigenetic modifications that occur outside of the genome itself. Of note, there is a strong inheritance pattern exhibited by epigenomics. However, there are also environmental factors that can cause epigenetic changes [35]. This is in stark contrast

to proteomics or genomics where the given DNA sequence is all but permanent. The ability to modify environmental variables makes the understanding of epigenomics extremely important for early therapeutic interventions.

3.2. Epigenetic Investigation. Advances in the past decade have mushroomed the amount of investigation into genes and genome knowledge (genomics). However, the first paper to study epigenetic modification on microdissected cells was by Wu et al. showing the role of hypermethylation in endometriosis [36]. New pursuits into epigenetic modifications have outlined the extracellular modifications in the heritable transfer of genetic material. These epigenetic modifications are independent of primary DNA sequence changes. More so, epigenetic modifications are strongly linked to environmental cues. As such, the precision offered by LCM becomes even more paramount when different cell types and different physiological cues can vastly confound downstream analysis.

LCM has been now being extensively used in epigenetic studies. Examination of methylation patterns, for instance, has been long used as a prognostic factor for predicting cancers [2]. LCM functions as an integral part of the cancer epigenetic repertoire. Examining the frequency of epigenetic modifications in cancerous lesions is all but useless if there is no normal sample to compare. When collection is done in situ, it is difficult to differentiate between normal tissue samples and lesions of interest. The issue is further complicated when one considers the spatial heterogeneity of many tissue samples. This heterogeneity is nearly eliminated when the technology of LCM is applied, and precise dissections are able to isolate the sample of interest.

As mentioned earlier, Li et al. (2016) already demonstrated the importance of LCM. COX2 mRNA expression has been long theorized to play a role in the normal aging

3D Structure

DNA is tightly folded in the nucleus.

The connections between and within chromosomes are dynamic and non-random.

The 3D structure can associate genes with 'transcription factories' and can promote interactions between long-range enhancers and promoters of gene enhancing transcription

Histone Code

Sections of DNA (146bp) is wound around histone proteins to make up a nucleosome.

The tails of these histone proteins can be modified by the addition of chemical groups. These additions are catalyzed by a vast array of enzymes including histone methyltransferases, acetyltransferases, and deacetylases.

Modifications at certain parts of the histone cause DNA to unwind and activate transcription. Other modifications cause repression of transcription.

DNA Methylation

The DNA sequence can be modified by adding a methyl group (usually to a cytosine residue).

DNA Methylation is catalyzed by DNA methyltransferases.

The methylated cytosine can be chemically modified to a hydroxymethyl cytosine as well as formyl- and carboxy-methyl cytosine – these seem to have different functions.

Where DNA methylation occurs relative to the gene influences the function of this modification

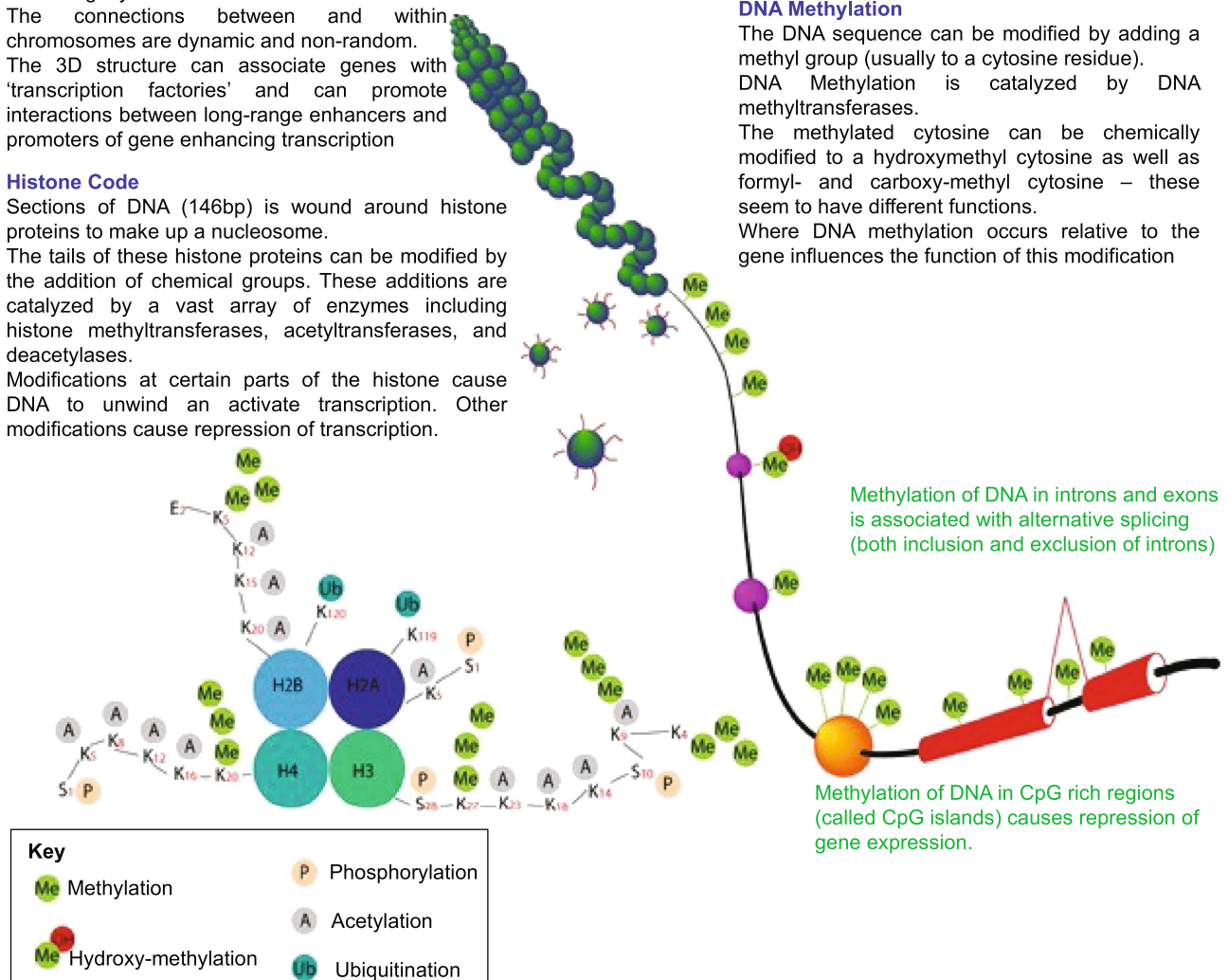


FIGURE 5: Epigenetic modifications can alter the spatial arrangement of DNA. This rearrangement changes the ability for transcription factors and other modifiers to access the DNA sequence. Reproduced with permission from John Wiley and sons. The following original report was credited: Duncan et al. [27].

process of skin. However, the levels expressed in whole skin preparations did not account for that difference. Only after LCM was used to separate dermal from epidermal constituents did a noticeable difference in mRNA expression via quantitative polymerase chain reaction (qPCR) become visible [37]. Skin in particular lends itself to LCM due to the large role that environmental factors can play. There exists so much variance in sun exposure, gland density, heat/cold tolerance, and wound susceptibility that it is impossible to treat in situ skin samples as homogenous and uniform. Naturally, there is a progression toward using LCM and not just applying it to epigenetic studies but applying it specifically to pathology of the skin.

3.3. LCM-Based Epigenetic Studies of the Skin. Cutaneous manifestations of injury are one of the largest areas for epigenetic investigation. The principles surrounding wound injury and healing revolve around the interplay of genetic

and environmental factors. Even minor changes in the environment, such as sun exposure, can create an entirely different milieu for the wound to develop. As such, any investigation into the causality of wound healing will revolve around the role of epigenetics [38]. However, the intrinsic variability surrounding human cutaneous wounds makes the isolation of target cells extremely difficult. In situ biopsy of the tissue such as via punch biopsy or excisional biopsy runs the risk introducing unwanted heterogeneity to the tissue sample [39]. Even more, the epidermal and dermal layers of the skin contain a vast array of cells that grossly differ from each other. Thus, the role of LCM becomes paramount in isolating purely pathologic tissue. Figure 7 demonstrates pictorially how LCM can target specific areas of the skin and avoid unwanted cell types [40].

Biopsies collected from clinical human cutaneous wounds are highly heterogeneous in cellular composition [38]. Furthermore, the composition of the tissue varies based

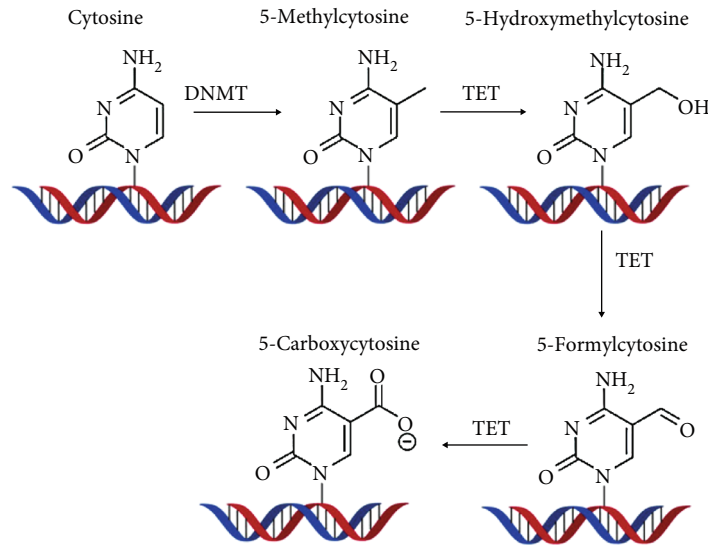


FIGURE 6: Both DNMT and TET enzymes have elaborated roles in the methylation of DNA. Their clinical significance ranges from solid cell tumors to hematologic malignancies. Reproduced with permission from John Wiley and sons. The following original report was credited: Beyer et al. [33].

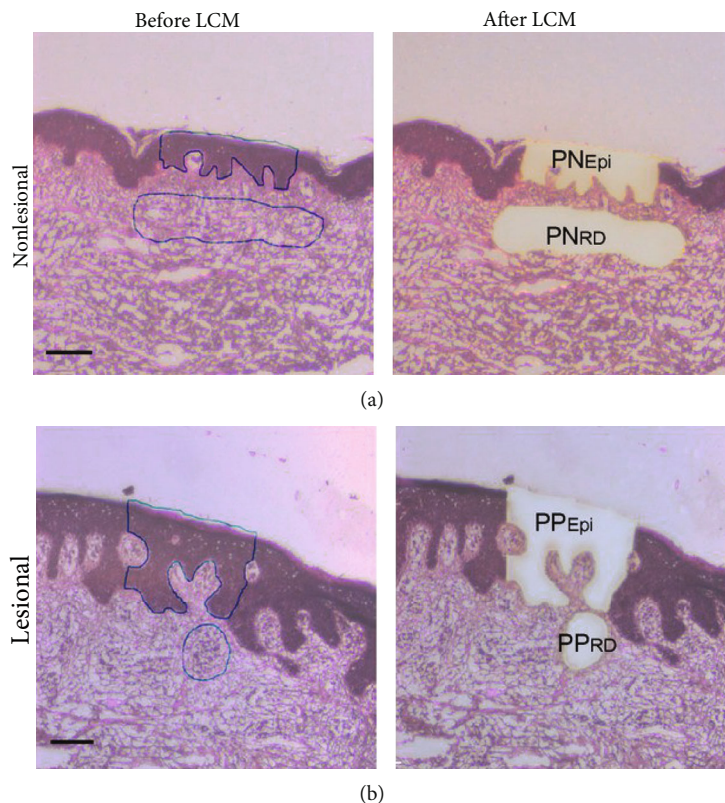


FIGURE 7: Laser capture microdissection (LCM) can be combined with small RNA sequencing to identify specific miRNA signatures in psoriatic plaque epidermis and dermis. LCM was performed by authors on both (a) normal psoriatic skin and (b) psoriatic plaque samples. Special attention is paid to the cellular differences in the epidermal layers requiring microdissection for downstream analysis. PNEpi: normal psoriatic epidermis; PPRD: psoriatic plaque dermal infiltrates. Reproduced with permission from John Wiley and sons. The following original report was credited: Lovendorf et al. [40].

on collection procedure complicating comparison of results derived from tissue homogenates. Thus, the utility of such tissue material is primarily limited to histological studies.

Nothing exemplifies the persistent nature of cutaneous disorders more than that of chronic diabetic ulcers (DCU). DCUs represent the intersection between poor wound repair

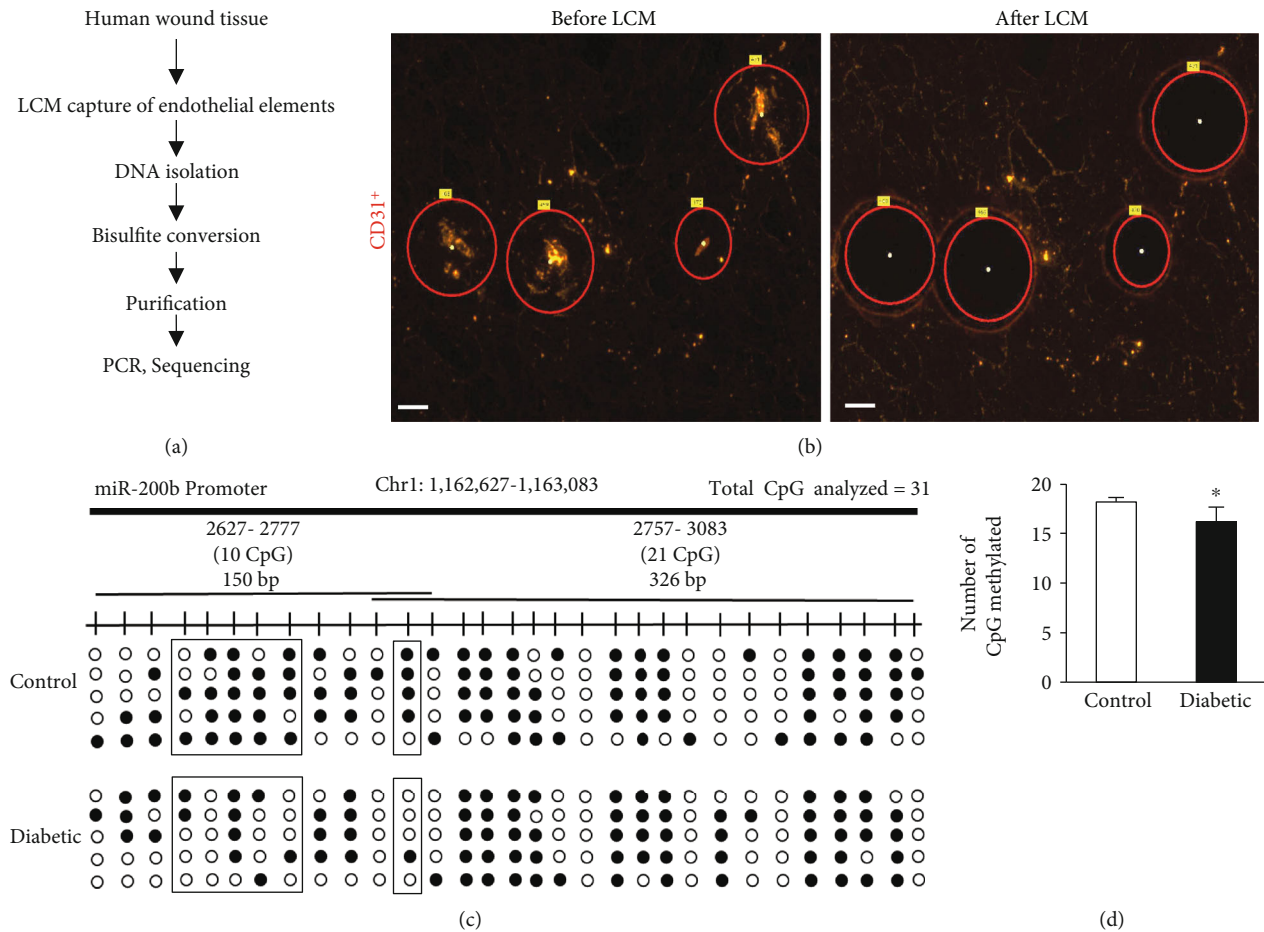


FIGURE 8: Figure showing connection between microdissection and epigenetic analysis as published by our group [42]. (a) Schematic diagram showing experimental design of miR-200b promoter methylation analysis in endothelial elements collected from human chronic wounds. (b) Representative figure shows the selection of CD31⁺ tissue elements (red) and their collection before and after the laser capture microdissection (LCM). Scale bar, 150 μ m. (c, d) Methylation profile and quantitation of methylated CpG islands present in miR-200b promoter in diabetic wounds compared to normoglycemic wounds. Reproduced with permission from the American Society of Gene and Cell Therapy. The following original report was credited: Singh et al. [42].

and specific environmental factors that can affect the progression of proper healing. Nie et al. recently reviewed the role of microRNAs (miRNAs) in nearly all aspects of skin healing including angiogenesis, epithelialization, and tissue remodeling [41]. These factors create a triad of interest when trying to understand the poor healing associated with DCUs. Investigators found multiple distinct pathways regulating miRNAs during chronic wound healing including the Wnt/B-catenin pathway, NF- κ B pathway, and PI3K/AKT/mTOR pathway. In particular, the epigenetic regulation of miRNA promoters has been shown to be a determinant of angiogenesis [42]. The role of angiogenesis thus requires further investigation as it is a hallmark of proper wound healing through the supply of nutrients.

In order to further understand the role of epigenetics and angiogenesis, Singh et al. utilized laser capture technologies to specifically target wound edges in diabetic patients (Figure 8) and in mice [42]. This tissue was precisely selected for its microenvironment. Downstream analysis of this tissue showed stark differences in the expression of miRNA-

200b profiles of diabetic mice as compared to nondiabetic cohorts [42]. This specific capture of tissue would not have been possible with traditional methods where the specific wound edge environment could be isolated.

A further investigation into the poor revascularization factors of diabetic wounds was also performed by the same group in 2019 [43]. This second investigation showed that there is a required process, similar to the epithelial-mesenchymal transition, which must be activated in order for proper wound healing. In particular, transcription factor ZEB1 was implicated to be an activator of this transition process primarily via vascular endothelial growth factor (VEGF) [43]. The mechanism of this pathway was shown to be *via* many miRNAs with special attention focused to miR-200b. Investigators in this report once again used LCM to target regions of human wounds with rich epithelial cell density. The captured cells were then subjected to downstream analysis. The results supported the hypothesis that at the wound edge, low levels of ZEB1 resulted in compromised angiogenesis and delayed wound closure.

The complexity of cell types and samples seen at wound sites makes the specific analysis of epigenetics and other downstream events difficult. LCM offers a new gold standard for the acquisition of tissue samples. The possible implications of having a comprehensive understanding of angiogenesis in cutaneous wounds include the development of therapeutic drugs used for diabetic or other chronic wounds.

3.4. LCM to Study miRNA Regulation. miRNAs act as important posttranscriptional regulators of gene expression. One of the factors to make a rational choice for miRNAs as biomarker or drug targets is posed by exactly this intrinsic heterogeneity in miRNA expression between different cell types and intrinsic cellular complexity of an organ or tissue. LCM helps in disentangling tissue heterogeneity, and when combined with RT-qPCR analysis, it can reveal compartment-specific miRNA expression signatures. This helps in linking miRNA signature to histopathology [44]. This approach for spatial miRNA expression analysis in complex tissues enables discovery of disease mechanisms, biomarkers, and drug candidates. Simoes et al. performed LCM on murine oral mucosal wound tissue to identify miRNA signature in the epithelial tissues [45]. Sinha et al. laser captured the wound-site macrophages during the healing phase to identify their plasticity to fibroblast-like cells [46]. The authors observed increased expression of miR-21 in these LCM-captured macrophages which displayed plasticity. Similar studies using miR-21 were reported by Bejerano et al. Here, the authors used LCM to spatially monitor the response to miR-21 delivery in the macrophage-enriched zones of heart postmyocardial infarction in a rodent model [47]. Multiple reports have shown that miRNAs are important regulators of pluripotency and differentiation. To unravel the function of specific miRNAs, it is important not only to analyze miRNA expression in the entire blastocyst but also to determine the site and level of expression in the inner cell mass (ICM) versus trophectoderm (TE). Using the LCM technology, it was identified that miR-155 was 50-fold highly expressed in ICM than in TE [48]. Though most of the reports have utilized LCM on cryopreserved tissue in optimal cutting temperature (OCT) compound, Majer and Booth have performed LCM on formalin-fixed FPPE brain tissue following virus infection to identify differentially expressed miRNAs [49]. The above studies utilized LCM in conjugation with RT-qPCR. With better capture techniques, LCM-captured spatial tissues are being subjected to next-generation sequencing (NGS). LCM coupled with NGS was utilized to study the specific miRNA expression profiles in the epidermis and dermal inflammatory infiltrates of psoriatic skin of patients [40]. The authors identified 24 deregulated miRNAs in the epidermis and 37 deregulated miRNAs in the dermis of psoriatic plaque compared with normal psoriatic skin. Thus, they were able to demonstrate that LCM combined with NGS provided a robust approach to explore the global miRNA expression in the epidermal and dermal compartments of the skin [40].

4. LCM-Based Epigenetic Studies in Skin-Related Cancer

Melanoma and nonmelanoma skin cancers such as basal cell carcinoma (BCC) and squamous cell carcinoma are the most widespread cancer in the world [50]. These cancers become even more important when it is acknowledged that sun exposure and other behaviors are the risk factors for the future development of skin cancer. With proper diagnostic steps, these cancers can be innocuous and treated. However, delayed treatment is common and is associated with increased mortality and morbidity. Early detection of suspicious skin lesions could therefore offer the opportunity for early intervention and reduced morbidity. Methylation markers for instance have been shown to be an independent prognostic indicator for skin cancer [39]. However, analysis of these markers stems on the ability to specify tissue cells of interest without unnecessary heterogeneity.

When examining melanoma in particular, a particular prognostic factor that is frequently examined is the EMT, often called mesenchymal mimicry [51]. Wouters et al. examined this transition using LCM technology to isolate melanoma cells based on their unique morphology, a task which is notoriously difficult given the large heterogeneity that exists among cutaneous cancers [51]. These cells were isolated using a Leica DM6000B and used for downstream analysis. Immunohistochemical staining was performed looking specifically for the epithelial-mesenchymal transition marker, fibronectin 1 (FN1). FN1-high melanoma cells were found to reside in hypoxic environments suggesting that there exists an interplay between environmental cues and the aggressiveness of melanoma cells [17]. Subsequently, the study raises the question about how these environmental cues affect melanoma cells.

Further elucidation of the role of epigenetic modification in cutaneous cancers is needed to understand the etiology of the disease. Cutaneous melanoma has also been a target for epigenetic investigation. In particular, the methylation status of CDKN2A and RASS1FA has been long implicated in the progression of cancer and the inactivation of p16 and p14 tumor suppressor genes [39]. However, it has also been shown that gene hypomethylation can contribute to tumorigenesis. For example, hypomethylation of long interspersed nucleotide element-1 (LINE-1) is the most studied repetitive genome-wide hypomethylation loci. Tellez et al. further linked cutaneous melanoma to increased levels of LINE-1 hypomethylation [52]. However, the largest limitation was the need for highly purified neoplastic cells. Thurin et al. outline the use of LCM (Arcturus XT) isolated purified tumor cells for downstream analysis such as qPCR or quantitative methylation specific PCR (qMSP) [39]. In their analysis, formalin-fixed paraffin-embedded tissues were cut with LCM at 5 μm . The resulting tissue was prepared with hematoxylin and eosin stain, and downstream analysis confirmed the connection between LINE-1 hypomethylation and tumorigenesis.

A deeper analysis of skin samples with cutaneous T cell lymphoma (CTL) was done in 2014 and outlined the intersection between LCM and measuring DNA methylation

TABLE 1: LCM-based studies for cutaneous manifestations.

Study and author	Disease model	Tissue element captured	Type of epigenetic modification studied
Singh et al. [42]	Diabetes	CD31 ⁺ endothelial element	Methylation of miR-200b promoter
Ren et al. [8]	Ovarian cancer	Tissue from ovarian carcinoma	Inactivation of hMLH1 during malignancy
Li et al. [9]	Aging	Dermal and epidermal elements	Expression of PTGES1 and COX2 mRNA expression
Wu et al. [36]	Endometriosis	Epithelial component of endometriotic implants	Methylation status of progesterone receptors (PRA, PRB)
Greenspan et al. [2]	Colon tumorigenesis	Colonic epithelial elements	Methylation status of RASSF1A
Sigalotti et al. [39]	Melanoma	Cutaneous melanoma cellular elements	Methylation of <i>LINE-1</i>
Nie et al. [41]	Chronic wounds	Diabetic ulcers	miRNA expression of NFkB, TGF-B/SMED
Singh et al. [43]	Wound angiogenesis	Human dermal microvascular endothelial cells	E-Cadherin/ZEB1 expression
Wu et al. [53]	Cutaneous T cell lymphoma	Human CTCL lines HH, Sz4, MyLa, Hut 78	CpG methylation of <i>FAS/CD95</i>
Masterson et al. [54]	Merkel cell carcinoma	Tumor resection epithelial elements	Expression of KRT20, KIF3A, and MUC11

[53]. Target biopsies from patients with CTL were able to be isolated from 5 μ m tissue samples via LCM. Microdissected sections were then lysed and DNA was precipitated. Promoter region *FAS* gene was amplified via PCR in place in Pyromark Q96 MD machine (GE Healthcare, Piscataway, NJ, USA) for sequencing. Pyromark Q-CpG software can then be used to analyze demethylation rates at the *FAS*-ligand promoter [53]. The authors were able to determine the level of DNA methylation of cancerous skin biopsies when compared to treatment groups receiving methotrexate.

Further analysis into cutaneous cancers showed that there exist rare prognostic markers for the poorly understood Merkel cell carcinoma (MCC) [54]. MCC has entered the forefront of investigative efforts due to its new association with the novel Merkel polyomavirus and its exploding incidence [17]. The prognosis of MCC is very poor as evident by its mortality which is over four times that of melanoma. Thus, there is a shifting focus to the possibility of early interventions to prevent this mortality. Having the information to identify MCC in an earlier, less malignant stage can also offer some preventative measures. Of note, Masterson et al. (2014) used IR-LCM and UV-LCM in combination to isolate tumor cells and identify select markers that were upregulated [37]. In particular, *mucin 1*, *KIT*, and *kinesin family member 3A* were all implicated with a poor prognosis. Epigenetic analysis of these genes would create a viable opportunity for further therapeutic interventions for MCC. The need for epigenetic analysis is ongoing, and the outlined utilization of LCM is principal.

5. Future Directions and Conclusion

Epigenetics has been shown to be a burgeoning field of study with huge implications in early therapeutic intervention. Of particular interest is the interplay that exists between epigenetic and environmental cues. These cues in turn are the driving force behind the extragenomic modifications as outlined in this review. Finding prognostic markers or loci of

interest exists in abundance among the current literature. However, there is a noticeable dearth of information that accounts for this same approach when taking into consideration the sheer variety that certain cellular environments can have on gene expression patterns. Isolation of cells taken *in vivo* comes with the caveat that these cells will be subject to a huge array of confounding exposures that can drastically alter protein, gene, and epigenetic expression. As such with traditional capture technologies, any downstream protein or gene analysis will always run the risk of having unwanted cell types. LCM operates at this intersection. By isolating unique cells with a high degree of accuracy, LCM is able to control for the large amount of heterogeneity that is seen among *in vivo* tissue samples (Table 1). The widespread integration of LCM into laboratory settings offers an exciting new approach in the analysis of downstream cellular cascades. Cutaneous disease in particular comes into play when acknowledging the vast diversity that exists. Arguably more so than any other field of study, dermatologic pathology contains hundreds of complex cells that change rapidly based on autocrine and paracrine modifications that are heavily dependent on environmental cues. Epigenetic modifications have been shown to play a role in angiogenesis, tissue remodeling, and wound closure. These all play pivotal roles in the healing of chronic cutaneous wounds, yet another burgeoning field of interest. The application of LCM to cutaneous research has already challenged preexisting paradigms surrounding aging and cancer markers. Further investigation of these variables (such as tissue hypoxia, aging, sunlight, and carcinogen exposure) will inevitably result in different gene expression profiles than when compared to cells that were traditionally captured. In the future, larger incorporation of LCM technology can create cell samples to be used for cancer screening, regenerative medicine, and pharmacological intervention.

Data Availability

No data were used to support this review article.

Conflicts of Interest

The authors declare no conflict of interest.

Authors' Contributions

Theja Bhamidipati, Mithun Sinha, Chandan K Sen, and Kanhaiya Singh wrote the manuscript. All authors reviewed and approved the final manuscript.

Acknowledgments

This work was supported in part by the National Institutes of Health grants GM108014, DK128845, DK125835, and NR015676. This work was also supported in part by the Department of Defense grant W81XWH-21-1-0033 to C.K.S. Research programs led by CKS were supported by the Lilly Endowment INCITE (Indiana Collaborative Initiative for Talent Enrichment) program and John Templeton Foundation grant ID-61742.

References

- [1] S. Datta, "Laser capture microdissection: Big big data from small samples," *Histology Histopathology*, vol. 30, pp. 1255–1269, 2015.
- [2] E. J. Greenspan, "Epigenetic alterations in RASSF1A in human aberrant crypt foci," *Carcinogenesis*, vol. 27, pp. 1316–1322, 2006.
- [3] M. Brioschi, "A mass spectrometry-based workflow for the proteomic analysis of in vitro cultured cell subsets isolated by means of laser capture microdissection," *Analytical and Bioanalytical Chemistry*, vol. 406, pp. 2817–2825, 2014.
- [4] F. von Eggeling and F. Hoffmann, "Microdissection-an essential prerequisite for spatial cancer omics," *Proteomics*, vol. 20, article e2000077, 2020.
- [5] K. Decarlo, A. Emley, O. E. Dadzie, and M. Mahalingam, "Laser capture microdissection: methods and applications," *Methods in Molecular Biology*, vol. 755, pp. 1–15, 2011.
- [6] P. Sluka, L. O'Donnell, R. I. McLachlan, and P. G. Stanton, "Application of laser-capture microdissection to analysis of gene expression in the testis," *Progress in Histochemistry and Cytochemistry*, vol. 42, pp. 173–201, 2008.
- [7] R. M. Greene and M. M. Pisano, "Palate morphogenesis: current understanding and future directions," *Birth Defects Research. Part C, Embryo Today*, vol. 90, pp. 133–154, 2010.
- [8] F. Ren, D. Wang, Y. Jiang, and F. Ren, "Epigenetic inactivation of hMLH1 in the malignant transformation of ovarian endometriosis," *Archives of Gynecology and Obstetrics*, vol. 285, pp. 215–221, 2012.
- [9] Y. Li, "Age-associated increase in skin fibroblast-derived prostaglandin E2 contributes to reduced collagen levels in elderly human skin," *The Journal of Investigative Dermatology*, vol. 135, pp. 2181–2188, 2015.
- [10] M. Bohm, I. Wieland, K. Schutze, and H. Rubben, "Microbeam MOMeNT: non-contact laser microdissection of membrane-mounted native tissue," *The American Journal of Pathology*, vol. 151, pp. 63–67, 1997.
- [11] K. Gousset, A. Gordon, S. Kumar Kannan, and J. Tovar, "A novel microproteomic approach using laser capture microdissection to study cellular protrusions," *International Journal of Molecular Sciences*, vol. 20, 2019.
- [12] E. Kummari, S. X. Guo-Ross, and J. B. Eells, "Laser capture microdissection—a demonstration of the isolation of individual dopamine neurons and the entire ventral tegmental area," *Journal of Visualized Experiments*, vol. 96, 2015.
- [13] M. R. Emmert-Buck et al., "Laser capture microdissection," *Science*, vol. 274, pp. 998–1001, 1996.
- [14] J. L. Hunt and S. D. Finkelstein, "Microdissection techniques for molecular testing in surgical pathology," *Archives of Pathology & Laboratory Medicine*, vol. 128, pp. 1372–1378, 2004.
- [15] R. I. Gallagher, S. R. Blakely, L. A. Liotta, and V. Espina, "Laser capture microdissection: Arcturus(XT) infrared capture and UV cutting methods," *Methods in Molecular Biology*, vol. 823, pp. 157–178, 2012.
- [16] B. Aguilar-Bravo and P. Sancho-Bru, "Laser capture microdissection: techniques and applications in liver diseases," *Hepatology International*, vol. 13, pp. 138–147, 2019.
- [17] S. K. Hussain, J. Sundquist, and K. Hemminki, "Incidence trends of squamous cell and rare skin cancers in the Swedish national cancer registry point to calendar year and age-dependent increases," *The Journal of Investigative Dermatology*, vol. 130, pp. 1323–1328, 2010.
- [18] E. Jensen, "Laser-capture microdissection," *Anat Rec (Hoboken)*, vol. 296, pp. 1683–1687, 2013.
- [19] R. E. Banks, "The potential use of laser capture microdissection to selectively obtain distinct populations of cells for proteomic analysis—preliminary findings," *Electrophoresis*, vol. 20, pp. 689–700, 1999.
- [20] F. Fend and M. Raffeld, "Laser capture microdissection in pathology," *Journal of Clinical Pathology*, vol. 53, pp. 666–672, 2000.
- [21] F. Fend, "Immuno-LCM: laser capture microdissection of immunostained frozen sections for mRNA analysis," *The American Journal of Pathology*, vol. 154, pp. 61–66, 1999.
- [22] L. Luo, "Gene expression profiles of laser-captured adjacent neuronal subtypes," *Nature Medicine*, vol. 5, pp. 117–122, 1999.
- [23] R. A. Craven, N. Totty, P. Harnden, P. J. Selby, and R. E. Banks, "Laser capture microdissection and two-dimensional polyacrylamide gel electrophoresis: evaluation of tissue preparation and sample limitations," *The American Journal of Pathology*, vol. 160, pp. 815–822, 2002.
- [24] A. Boskovic and O. J. Rando, "Transgenerational epigenetic inheritance," *Annual Review of Genetics*, vol. 52, pp. 21–41, 2018.
- [25] S. Booth and G. Collins, "Epigenetic targeting in lymphoma," *British Journal of Haematology*, vol. 192, pp. 50–61, 2021.
- [26] Y. Sang and Y. Deng, "Current insights into the epigenetic mechanisms of skin cancer," *Dermatologic Therapy*, vol. 32, article e12964, 2019.
- [27] E. J. Duncan, P. D. Gluckman, and P. K. Dearden, "Epigenetics, plasticity, and evolution: how do we link epigenetic change to phenotype?," *Journal of Experimental Zoology. Part B, Molecular and Developmental Evolution*, vol. 322, pp. 208–220, 2014.
- [28] K. Singh and K. Singh, "Carcinogenesis and diabetic wound healing: evidences of parallelism," *Current Diabetes Reviews*, vol. 11, pp. 32–45, 2015.

- [29] K. Singh, "Genetic and epigenetic alterations in toll like receptor 2 and wound healing impairment in type 2 diabetes patients," *Journal of Diabetes and its Complications*, vol. 29, pp. 222–229, 2015.
- [30] K. Singh, "Differential expression of matrix metalloproteinase-9 gene in wounds of type 2 diabetes mellitus cases with susceptible -1562C>T genotypes and wound severity," *The International Journal of Lower Extremity Wounds*, vol. 13, pp. 94–102, 2014.
- [31] G. Rajendran, "Epigenetic regulation of DNA methyltransferases: DNMT1 and DNMT3B in gliomas," *Journal of Neuro-Oncology*, vol. 104, pp. 483–494, 2011.
- [32] W. Li and L. Xu, "Epigenetic function of TET family, 5-methylcytosine, and 5-hydroxymethylcytosine in hematologic malignancies," *Oncol Res Treat*, vol. 42, pp. 309–318, 2019.
- [33] J. N. Beyer, N. R. Raniszewski, and G. M. Burslem, "Advances and opportunities in epigenetic chemical biology," *Chembiochem*, vol. 22, pp. 17–42, 2021.
- [34] M. Gardiner-Garden and M. Frommer, "CpG islands in vertebrate genomes," *Journal of Molecular Biology*, vol. 196, pp. 261–282, 1987.
- [35] NIH-NHGRI, *Epigenomics Fact Sheet*, 2020, <https://www.genome.gov/about-genomics/fact-sheets/Epigenomics-Fact-Sheet>.
- [36] Y. Wu, E. Strawn, Z. Basir, G. Halverson, and S. W. Guo, "Promoter hypermethylation of progesterone receptor isoform B (PR-B) in endometriosis," *Epigenetics*, vol. 1, pp. 106–111, 2006.
- [37] E. Chen Gonzalez and J. S. McGee, "Research techniques made simple: laser capture microdissection in cutaneous research," *The Journal of Investigative Dermatology*, vol. 136, pp. e99–e103, 2016.
- [38] S. Roy and C. K. Sen, "Study of the human chronic wound tissue: addressing logistic barriers and productive use of laser capture microdissection," *Methods in Molecular Biology*, vol. 1037, pp. 233–243, 2013.
- [39] L. Sigalotti, E. Fratta, G. Parisi, S. Coral, and M. Maio, "Epigenetic markers of prognosis in melanoma," *Methods in Molecular Biology*, vol. 1102, pp. 481–499, 2014.
- [40] M. B. Lovendorf, "Laser capture microdissection followed by next-generation sequencing identifies disease-related microRNAs in psoriatic skin that reflect systemic microRNA changes in psoriasis," *Experimental Dermatology*, vol. 24, pp. 187–193, 2015.
- [41] X. Nie, "Exploring microRNAs in diabetic chronic cutaneous ulcers: regulatory mechanisms and therapeutic potential," *British Journal of Pharmacology*, vol. 177, pp. 4077–4095, 2020.
- [42] K. Singh, "Epigenetic modification of microRNA-200b contributes to diabetic vasculopathy," *Molecular Therapy*, vol. 25, pp. 2689–2704, 2017.
- [43] K. Singh, "Cutaneous epithelial to mesenchymal transition activator ZEB1 regulates wound angiogenesis and closure in a glycemic status-dependent manner," *Diabetes*, vol. 68, pp. 2175–2190, 2019.
- [44] S. Skalicky, "Combining laser microdissection and microRNA expression profiling to unmask microRNA signatures in complex tissues," *BioTechniques*, vol. 67, pp. 276–285, 2019.
- [45] A. Simoes, "Laser capture microdissection of epithelium from a wound healing model for microRNA analysis," *Methods in Molecular Biology*, vol. 1733, pp. 225–237, 2018.
- [46] M. Sinha, "Direct conversion of injury-site myeloid cells to fibroblast-like cells of granulation tissue," *Nature Communications*, vol. 9, p. 936, 2018.
- [47] T. Bejerano, S. Etzion, S. Elyagon, Y. Etzion, and S. Cohen, "Nanoparticle delivery of miRNA-21 mimic to cardiac macrophages improves myocardial remodeling after myocardial infarction," *Nano Letters*, vol. 18, pp. 5885–5891, 2018.
- [48] K. Goossens, "Differential microRNA expression analysis in blastocysts by whole mount in situ hybridization and reverse transcription quantitative polymerase chain reaction on laser capture microdissection samples," *Analytical Biochemistry*, vol. 423, pp. 93–101, 2012.
- [49] A. Majer and S. A. Booth, "Isolation of viral-infected brain regions for miRNA profiling from formalin-fixed paraffin-embedded tissues by laser capture microdissection," *Methods in Molecular Biology*, vol. 1733, pp. 41–51, 2018.
- [50] American Cancer Society, *I. Basal and Squamous Cell Skin Cancer*, 2021, <https://www.cancer.org/cancer/basal-and-squamous-cell-skin-cancer>.
- [51] J. Wouters, "A novel hypoxia-associated subset of FN1 high MITF low melanoma cells: identification, characterization, and prognostic value," *Modern Pathology*, vol. 27, pp. 1088–1100, 2014.
- [52] C. S. Tellez, "CpG island methylation profiling in human melanoma cell lines," *Melanoma Research*, vol. 19, pp. 146–155, 2009.
- [53] J. Wu, "Quantitative gene analysis of methylation and expression (Q-GAME) in fresh or fixed cells and tissues," *Experimental Dermatology*, vol. 23, pp. 304–309, 2014.
- [54] L. Masterson, "Gene expression differences predict treatment outcome of Merkel cell carcinoma patients," *Journal of Skin Cancer*, vol. 2014, 2014.

Research Article

Effects of MicroRNA-195-5p on Biological Behaviors and Radiosensitivity of Lung Adenocarcinoma Cells via Targeting HOXA10

Cheng Yuan ^{1,2}, Rui Bai,¹ Yanping Gao,¹ Xueping Jiang,¹ Shuying Li,¹ Wenjie Sun,¹ Yangyi Li,¹ Zhengrong Huang,¹ Yan Gong ³, and Conghua Xie ^{1,4,5}

¹Department of Radiation and Medical Oncology, Zhongnan Hospital of Wuhan University, Wuhan, Hubei 430071, China

²Department of Gynecological Oncology, Zhongnan Hospital of Wuhan University, Wuhan 430071, China

³Department of Biological Repositories, Zhongnan Hospital of Wuhan University, Wuhan, Hubei 430071, China

⁴Hubei Key Laboratory of Tumour Biological Behaviors, Zhongnan Hospital of Wuhan University, Wuhan, Hubei 430071, China

⁵Hubei Cancer Clinical Study Center, Zhongnan Hospital of Wuhan University, Wuhan, Hubei 430071, China

Correspondence should be addressed to Yan Gong; yan.gong@whu.edu.cn and Conghua Xie; chxie_65@whu.edu.cn

Cheng Yuan and Rui Bai contributed equally to this work.

Received 20 June 2021; Revised 19 October 2021; Accepted 8 November 2021; Published 7 December 2021

Academic Editor: Kanhaiya Singh

Copyright © 2021 Cheng Yuan et al. This is an open access article distributed under the Creative Commons Attribution License, which permits unrestricted use, distribution, and reproduction in any medium, provided the original work is properly cited.

Objective. To explore the effects of miR-195-5p and its target gene HOXA10 on the biological behaviors and radiosensitivity of lung adenocarcinoma (LUAD) cells. **Methods.** The effects of miR-195-5p on LUAD cell proliferation, migration, invasion, cycle arrest, apoptosis, and radiosensitivity were investigated by *in vitro* experiments. The bioinformatics analysis was used to assess its clinical value and predict target genes. Double-luciferase experiments were used to verify whether the miR-195-5p directly targeted HOXA10. A xenograft tumor-bearing mouse model was used to examine its effects on the radiosensitivity of LUAD *in vivo*. **Results.** Both gain- and loss-of-function assays demonstrated that miR-195-5p inhibited LUAD cell proliferation, invasion, and migration, induced G1 phase arrest and apoptosis, and enhanced radiosensitivity. Double-luciferase experiments confirmed that miR-195-5p directly targeted HOXA10. Downregulation of HOXA10 also inhibited LUAD cell proliferation, migration, and invasion, induced G1 phase arrest and apoptosis, and enhanced radiosensitivity. The protein levels of β -catenin, c-myc, and Wnt1 were decreased by miR-195-5p and increased by its inhibitor. Moreover, the effects of the miR-195-5p inhibitor could be eliminated by HOXA10-siRNA. Furthermore, miR-195-5p improved radiosensitivity of LUAD cells *in vivo*. **Conclusion.** miR-195-5p has excellent antitumor effects via inhibiting cancer cell growth, invasion, and migration, arresting the cell cycle, promoting apoptosis, and sensitizing LUAD cells to X-ray irradiation by targeting HOXA10. Thus, miR-195-5p may serve as a potential candidate for the treatment of LUAD.

1. Introduction

Lung cancer is the leading cause of cancer-related deaths worldwide, with over 2 million new cases diagnosed [1]. As the most common pathological type, lung adenocarcinoma (LUAD) has strong invasive ability and generally poor prognosis [2, 3]. As a primary epithelial tumor of the lung, LUAD pathogenesis involves many factors such as environment, heredity, and living habits [4]. However, its cause has not yet

been fully elucidated. Because LUAD often manifests as peripheral lung cancer clinically, the early clinical symptoms are often atypical, leading to the difficulty of early diagnosis. Some LUAD have metastasized or invaded to the pleura at the time of diagnosis, resulting in a generally poor prognosis for patients [5, 6]. Therefore, it is very important and urgent to identify effective biomarkers for its early diagnosis.

Radiotherapy is a local treatment of a tumor, which is widely used in the clinical treatment of LUAD. Nevertheless,

TABLE 1: PCR primer sequence.

Primer name	Sequence (5' to 3')
miR-195-5p forward	GTCTAGCAGCACAGAAATA
miR-195-5p reverse	GTGCAGGGTCCGAGGT
miR-195-5p RT	GTCGTATCCAGTGCAGGGTCCGAGGTATTTCGACTGGATACGACGCCAA
U6 forward primer	CTCGCTTCGGCAGCACA
U6 reverse primer	AACGCTTCACGAATTTGCGT
HOXA10 forward	GGGTAAGCGGAATAAACT
HOXA10 reverse	GCACAGCAGCAATACAATA
GAPDH forward	GGAGCGAGATCCCTCCAAAAT
GAPDH reverse	GGCTGTTGTCATACTTCTCATGG

many patients have radiotherapy resistance, which often limits the therapeutic effects of radiotherapy. Previous researches reported that radiotherapy caused changes in the expression profile of miRNAs in LUAD patients, and these miRNAs might be related to their radiosensitivity [7–9].

Previous studies [10–12] have confirmed that miR-195-5p had significant antitumor effects. Feng et al. [10] found that miR-195-5p increased chemosensitivity and apoptosis in chemoresistant colorectal cancer cells. A similar phenomenon was also observed [11], which indicated that miR-195-5p could reduce chemoresistance by inhibiting the stem cell-like ability of colorectal cancer cells. Chai et al. found that miR-195-5p, acting as tumor suppressors of melanoma, inhibited A375 cell proliferation, migration, and invasion, arrested the cell cycle, and induced cell apoptosis [12]. In our previous work, we revealed that miR-195-5p had high diagnostic values for LUAD [13]. Higher expression of miR-195-5p indicated better LUAD prognosis. Therefore, in our current research, we explored its roles in response to radiation in LUAD cells and mouse model.

2. Materials and Methods

2.1. Target Prediction and Function of miR-195-5p. Three different databases (TargetScan, miRDB, and DIANA-TarBase) were adopted to predict miRNA target genes. Based on TCGA-LUAD expression profile data, the upregulated genes in LUAD tissues ($\log_2FC > 1$, $\text{adjust } P < 0.05$) were selected. The ROC diagnostic test and Kaplan-Meier plots were then used to evaluate the diagnostic and prognostic values. The cut-off value was $AUC > 0.8$, $HR > 1$, and $\log \text{rank } P < 0.05$. In order to further explore the function of target genes, single gene set enrichment analysis (GSEA) was used to explore the functional signaling pathways related to the target genes.

2.2. Cells Culture and Transfection. PC9 and A549 cells were cultured in RPMI medium (Gibco, USA) containing 10% fetal calf serum. The miR-195-5p mimic, inhibitor, and negative control (NC) were provided by RiboBio, China, and the corresponding transfection reagent was Lipofectamine 2000 (Invitrogen, USA). Three siRNA duplexes (GenePharma, China) were designed to target human HOXA10, transfected with jetPRIME (PolyPlus-transfection).

2.3. Total RNA Extraction and qRT-PCR. TRIzol was used to extract total RNA directly from PC9 and A549 cells. The PrimeScript™ RT Reagent Kit with gDNAEraser was adopted to detect the levels of mature miR-195-5p. The levels of mRNAs were detected by PrimeScript™ RT Reagent Kit and gDNAEraser and SYBR Advantage qPCR Premix (Takara). GAPDH and U6 were used as references. Table 1 provides all PCR-related primer sequences.

2.4. Cell Proliferation, Migration, and Invasion Assays. The cell viability at different time points was measured by the Cell Counting Kit-8 (CCK-8, Beyotime). The migration of LUAD cells was examined by the wound healing assay. LUAD cells were cultured and incubated until the cell confluence was over 90% in 6-well plates. A clean pipette tip (200 μL) was applied to create a scratch in the middle of the cell monolayer. After being cultured with fresh serum-free medium for 48 h, the wound was photographed with an inverted microscope. DiI (5 μM , Google Bio, China) was used 30 min before the observation. For invasion assays, the lower chambers of transwell were filled with 700 μL complete medium. The 1×10^5 LUAD cells were seeded into the upper chambers. The invasive cells were stained with 1% crystal violet solution. Images of invading cells were captured under an inverted microscope.

2.5. Cell Cycle and Apoptosis Assays. After transfection or irradiation (4 Gy) for 48 h, the apoptotic/necrotic cells (1×10^3 cells/ μL) were suspended in 400 mL binding buffer and stained using 5 μL Annexin V/FITC for 15 min and 10 μL PI for 5 min by using Annexin V/PI staining kit (BestBio, China). For cell cycle assays, the cells (2×10^5 cells/well) were stained with 1 mL DNA staining solution (containing RNase A: 0.1 mg/mL) and 10 μL PI (0.5 mg/mL) mixed solution by using a cell cycle staining kit (MultiSciences Biotech, China). Cell cycle and apoptosis assays were measured by using BD FACSVerser™.

2.6. Colony Survival Assay. PC9 and A549 cells, transfected with mimics, inhibitors, siRNA, and corresponding NC, were seeded in 6-well plates (100, 200, 400, 600, 800, 1000, and 2000 cells/well) and exposed to the following radiation (0, 1, 2, 4, 6, 8, and 10 Gy) correspondingly. After 13 days, the colonies were counted and cell survival was evaluated.

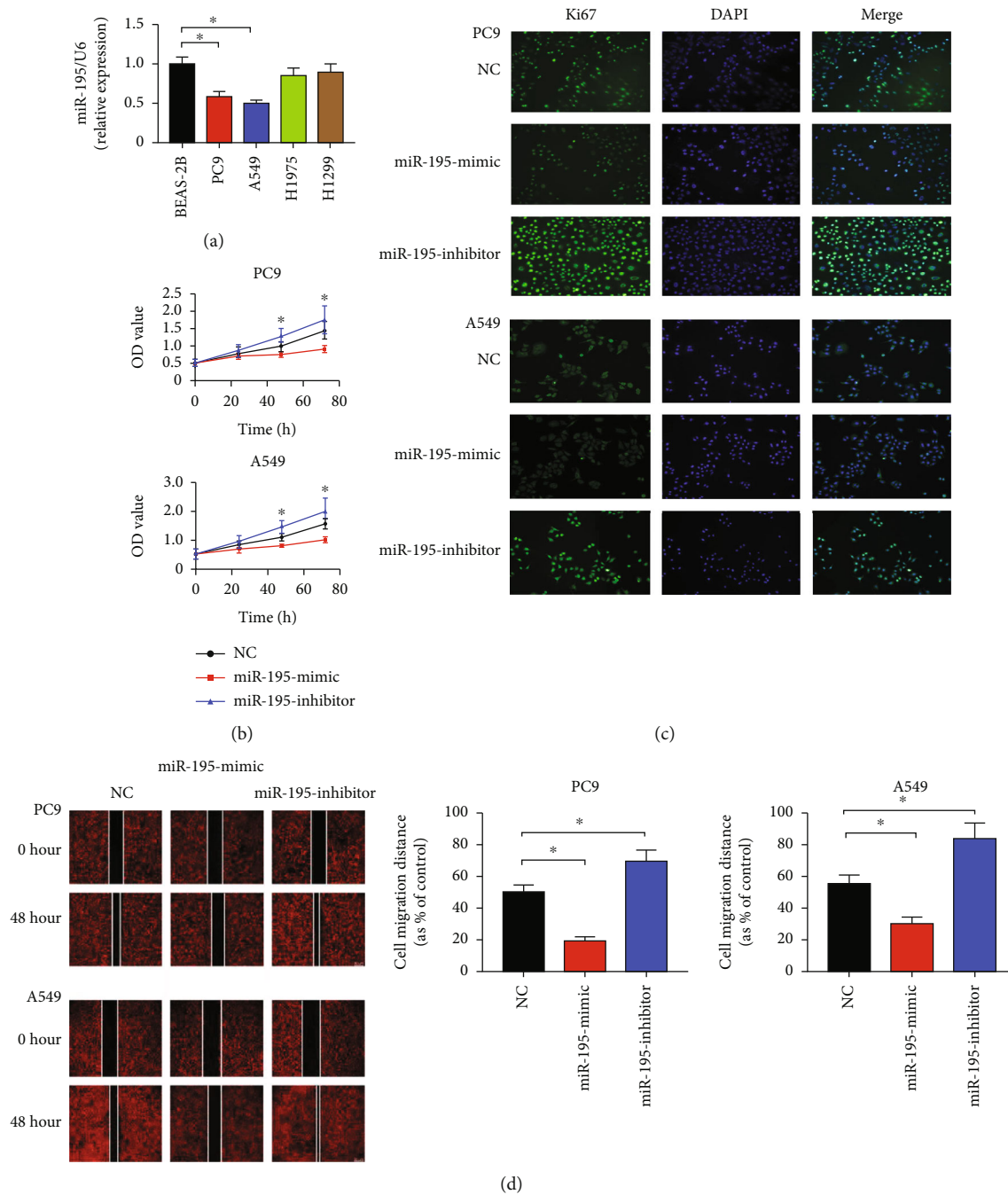


FIGURE 1: Continued.

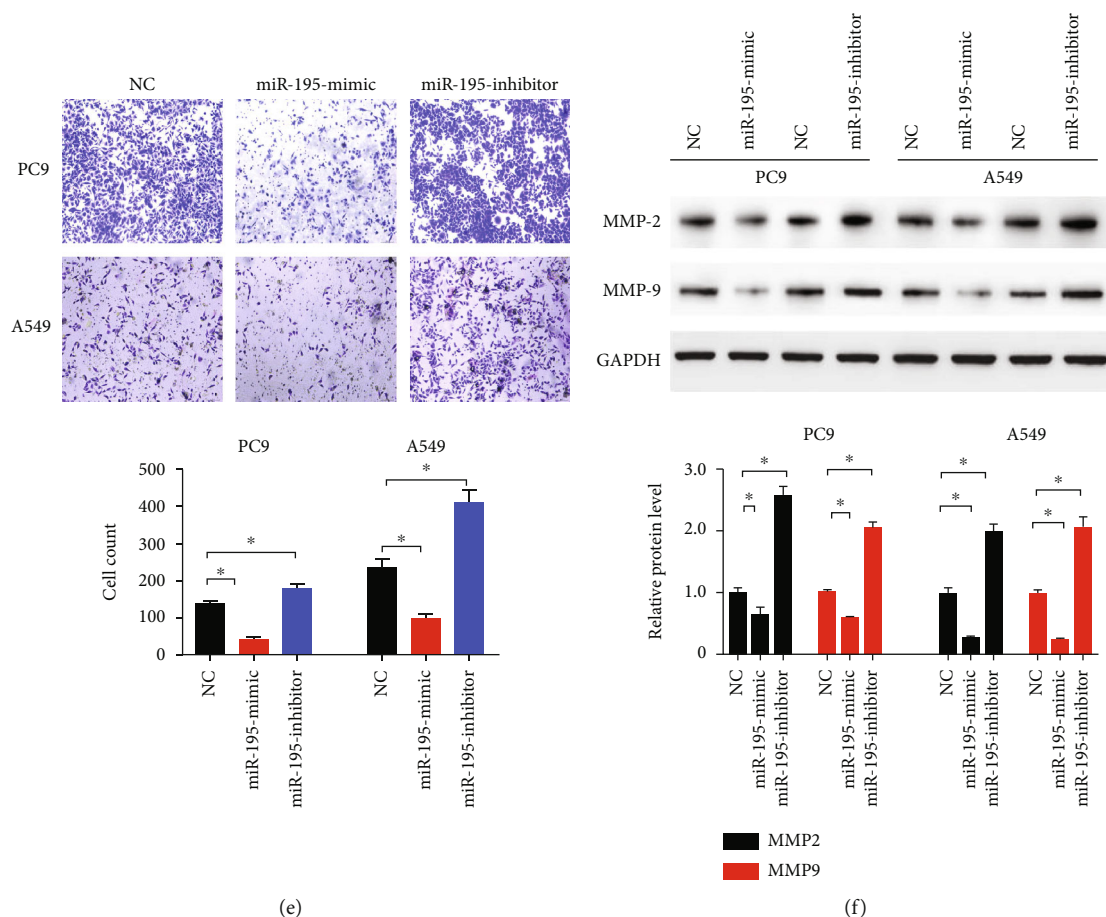


FIGURE 1: miR-195-5p inhibited proliferation, invasion, and metastasis of LUAD cells. (a) The expression levels of miR-195-5p in B4E2, PC9, A549, H1975, and H1299 cell lines. (b) CCK-8 assays of PC9 and A549 cells transfected with the miR-195-5p mimic, inhibitor, and NC. (c) Representative immunofluorescent images of Ki67. (d) Representative images and quantification of wound healing assays in PC9 and A549 cells. (e) Representative images and quantification of transwell migration assays of PC9 and A549 cells. (f) Representative immunoblotting of MMP2 and MMP9 in A549 and PC9 cells. $n = 3$; $*P < 0.05$ vs. B4E2 or NC.

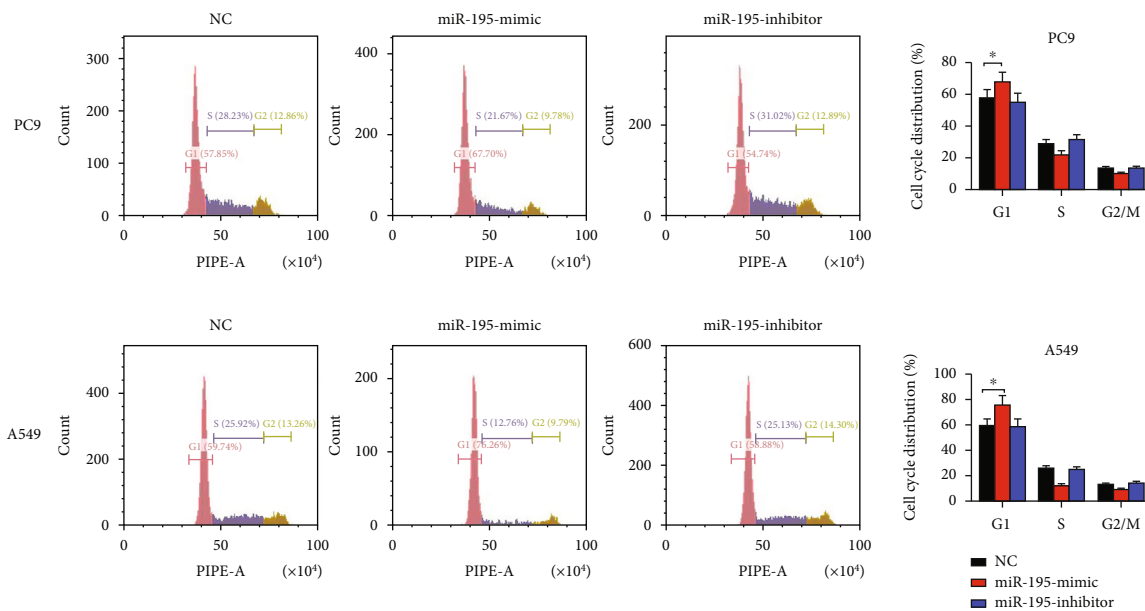
Specifically, colonies with more than 50 cells were counted, and the survival fraction was calculated by the ratio of the colony number and seed cell number.

2.7. Luciferase Assay. To construct a HOXA10 3'-untranslated region- (UTR-) luciferase plasmid, the HOXA10 3'-UTR fragments containing the miR-195-5p-binding (HOXA10-3'UTR-wt) or HOXA10 3'-UTR-mutated (HOXA10-3'UTR-mut) site were inserted into the pSI-Check2 vector, which contains a luciferase reporter gene. After constructing the HOXA10 3'-UTR-luciferase plasmid, 293T cells were transfected. Then, Firefly and Renilla luciferase activities were tested.

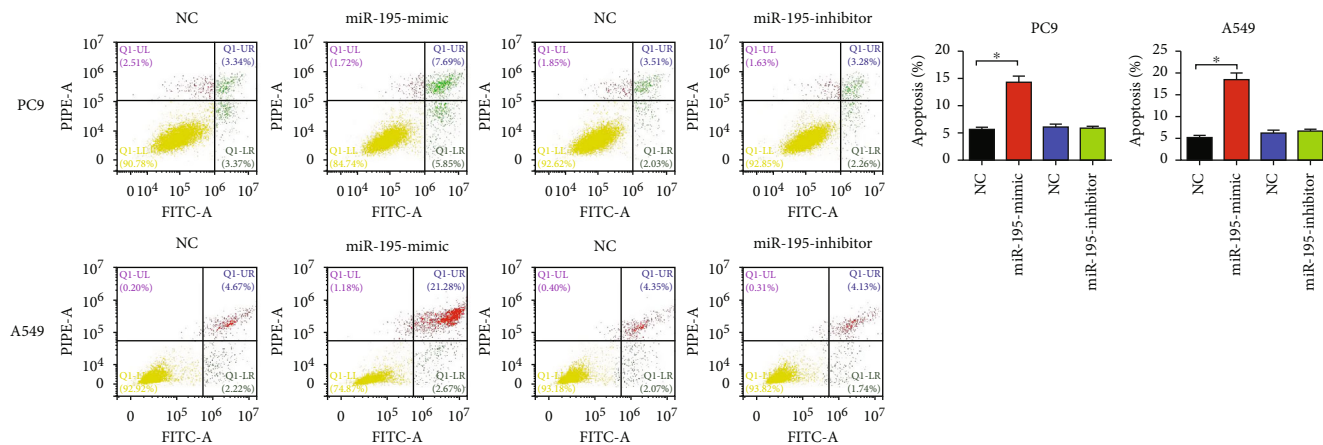
2.8. Immunoblotting. The antibodies of BCL2, Bax, MMP-2, MMP-9, cyclin D1, and c-myc were from Wuhan Sanying, China. The antibodies of β -catenin and Wnt1 were purchased from Cell Signaling Technology, USA, and the antibody of HOXA10 was from Abcam, UK. The proteins were extracted by using RIPA buffer with 1% PMSF and then loaded onto an SDS-PAGE minigel. After being transferred onto PVDF membranes, the primary and correspond-

ing secondary antibodies were used to label the target proteins. GAPDH was used as an endogenous protein for normalization.

2.9. Tumor Formation in Nude Mice. The nude mice (BALB/c, 4-6 weeks old) were provided by Vital River Laboratory Animal Technology, China. All mouse feeding and operation processes followed the Experimental Animal Welfare Ethics Committee of Zhongnan Hospital of Wuhan University. PC9 was used to construct a subcutaneous implant tumor model (6×10^6 cells/mouse). miR-195-5p agomir and miR agomir NC were provided by RiboBio, China. Fifteen days after cell injection, they were administered by intratumoral injection (2 nmol/30 μ L PBS) for 5 consecutive days when the tumor volume was approximately 100 mm³. The mice were divided into 2 groups. One group had no additional treatment, and the other group received X-ray irradiation (10 Gy once). Nude mice were executed via anesthesia at 30 days after irradiation, and the tumors were removed for photographing and the tumor volumes were calculated.



(a)



(b)

FIGURE 2: Continued.

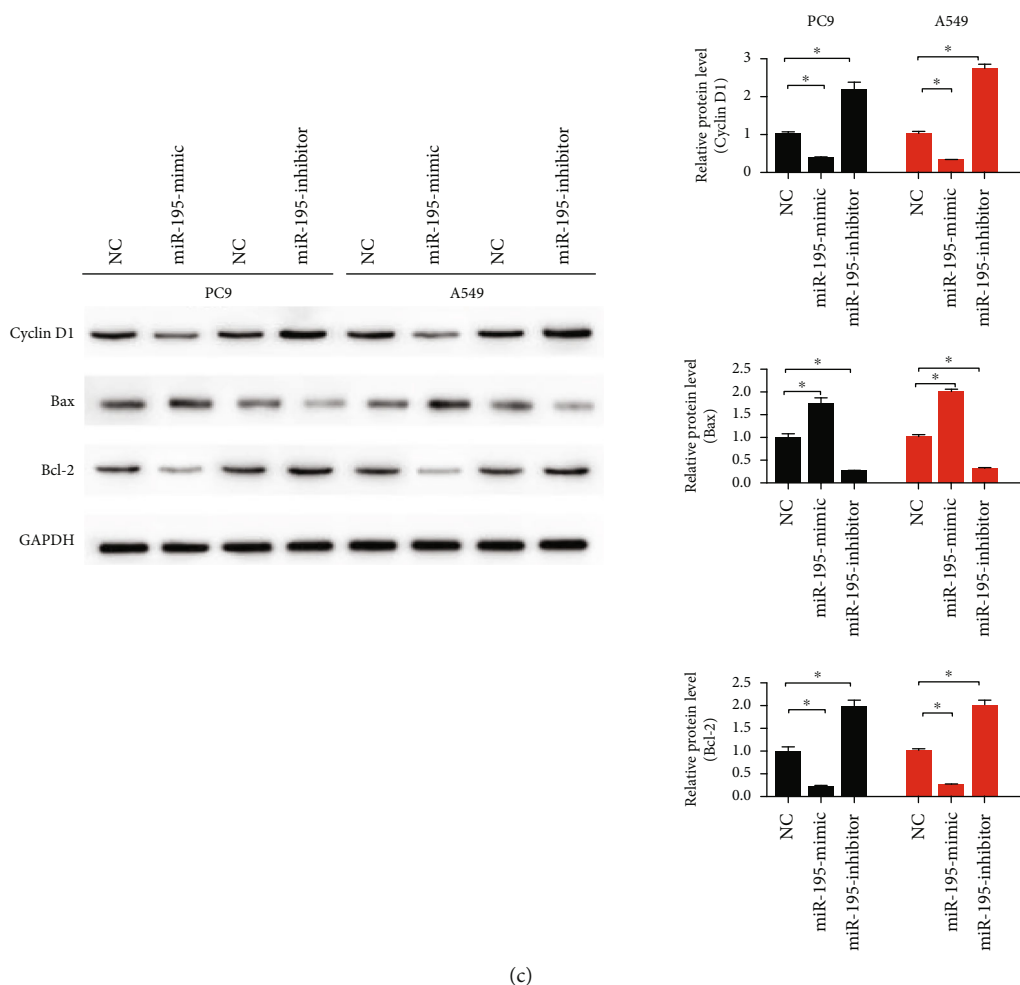


FIGURE 2: miR-195-5p induced apoptosis and blocked the cell cycle. (a) Flow cytometry shows the percentage of cells at different cell cycle phases. (b) Cell apoptosis was detected by flow cytometry at 48 h after being transfected with the miR-195-5p mimic, inhibitor, and NC. (c) The expression levels of cycle- and apoptosis-related proteins (cyclin D1, Bax, and Bcl-2) were measured by immunoblotting. $n = 3$; $*P < 0.05$ vs. NC.

2.10. Statistical Analysis. The results were presented as means \pm standard deviation (SD). One-way analysis of variance (ANOVA) or Student's t -test was performed to estimate the significance between groups. $P < 0.05$ was considered statistically significant.

3. Results

3.1. miR-195-5p Inhibited Proliferation, Invasion, and Migration of LUAD Cells. Compared with the normal lung epithelial cell line (BASE-2B), miR-195-5p levels were significantly lower in A549 and PC9 cells (Figure 1(a)). The results of cell viability assays suggested that the proliferation of A549 and PC9 cells was restrained by the miR-195-5p mimic (Figure 1(b)), which was in accordance with the results of immunofluorescence of Ki67 (Figure 1(c)). The inhibitors of miR-195-5p induced LUAD cell proliferation and increased Ki67 staining. The results of migration and invasion assays indicated that the miR-195-5p mimic reduced PC9 and A549 cell migration, while its inhibitors

had the opposite effects (Figures 1(d) and 1(e)). Immunoblotting confirmed that the miR-195-5p mimic downregulated the protein levels of MMP2 and MMP9, while its inhibitors induced these 2 proteins in A549 and PC9 cells (Figure 1(f)).

3.2. miR-195-5p Enhanced Radiosensitivity. The miR-195-5p mimic increased the numbers of PC9 and A549 cells at the G1 phase, suggesting that the miR-195-5p mimic arrested cells at the G1 phase (Figure 2(a)). In addition, the miR-195-5p mimic also significantly induced LUAD cell apoptosis ($P < 0.05$, Figure 2(b)). The results of immunoblotting demonstrated that miR-195-5p overexpression increased the levels of Bax and reduced cyclin D1 and Bcl-2 expression in PC9 and A549 cells (Figure 2(c)).

To examine whether miR-195-5p affected radiosensitivity of LUAD cells, PC9 and A549 cells were exposed to ionizing radiation (4 Gy). The apoptosis levels of PC9 and A549 cells were measured, and miR-195-5p enhanced LUAD cell apoptosis induced by X-ray (Figure 3(a)). The colony

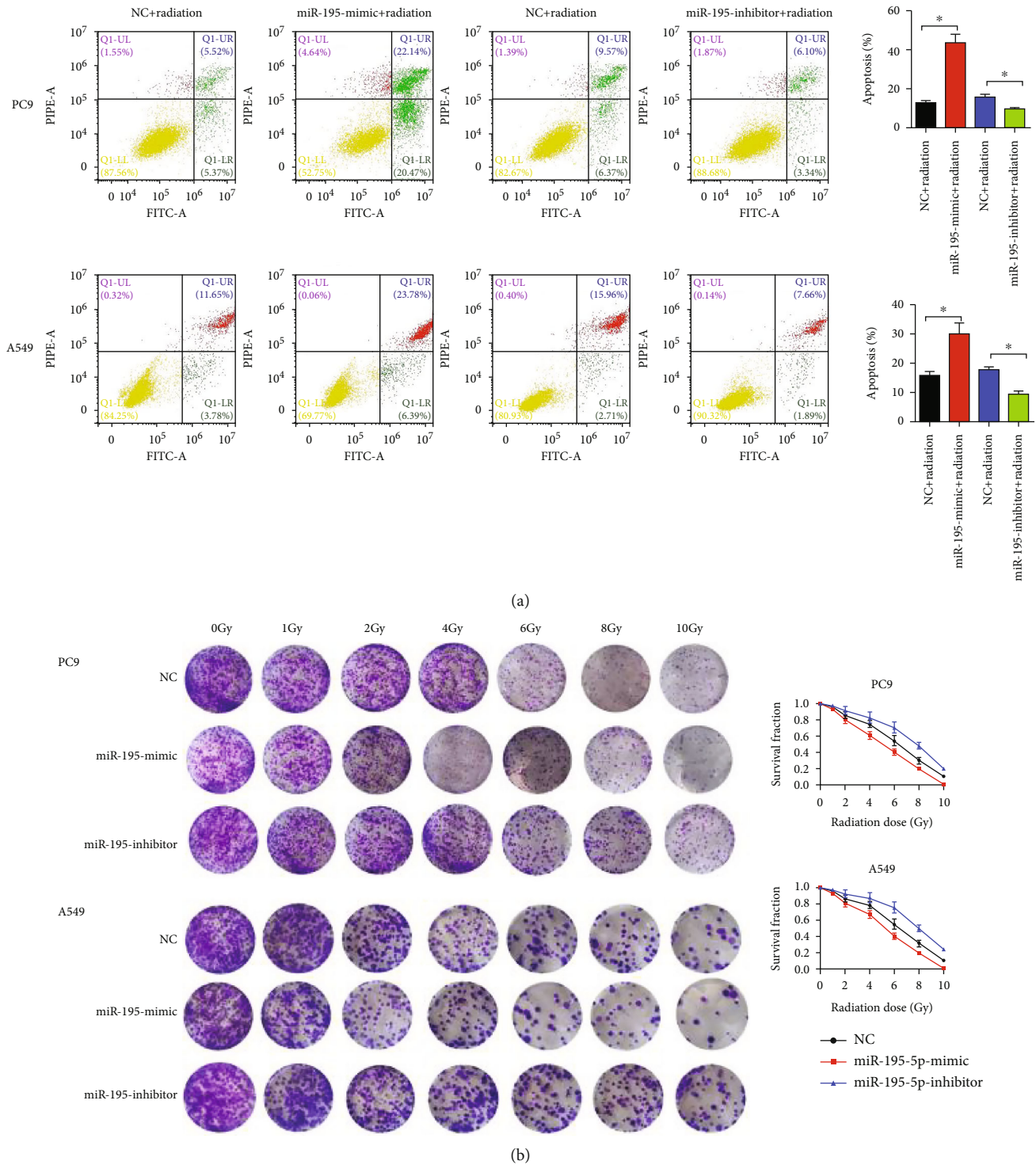


FIGURE 3: miR-195-5p enhanced radiosensitivity of LUAD cells. (a) Cell apoptosis was detected by flow cytometry at 48 h after radiation (4 Gy). (b) Survival fractions were calculated after treatment with 0, 2, 4, 6, 8, and 10 Gy of ionizing radiation. $n = 3$, $*P < 0.05$ vs. NC.

survival assay showed that the miR-195-5p mimic reduced the survival fractions of PC9 and A549 cells at each dose (Figure 3(b)).

3.3. miR-195-5p Targeted HOXA10. Based on TCGA-LUAD profile data, the differentially expressed microRNAs (DEMs) and differentially expressed genes (DEGs) in LUAD tissues

were selected. Three different databases (TargetScan, miRDB, and DIANA-TarBase) were adopted to predict miRNA target genes. When DEMs were matched to GEGs, 34 target genes were screened out (Figure S1). Among them, 16 target genes were the target genes of miR-195-5p. Except TMEM00, RS1, and OSCAR, the remaining genes (CEP55, PSAT1, CHEK1, KIF23, CCNE1, CLSPN, CDC25A, E2F7, CBX2, HOXA10,

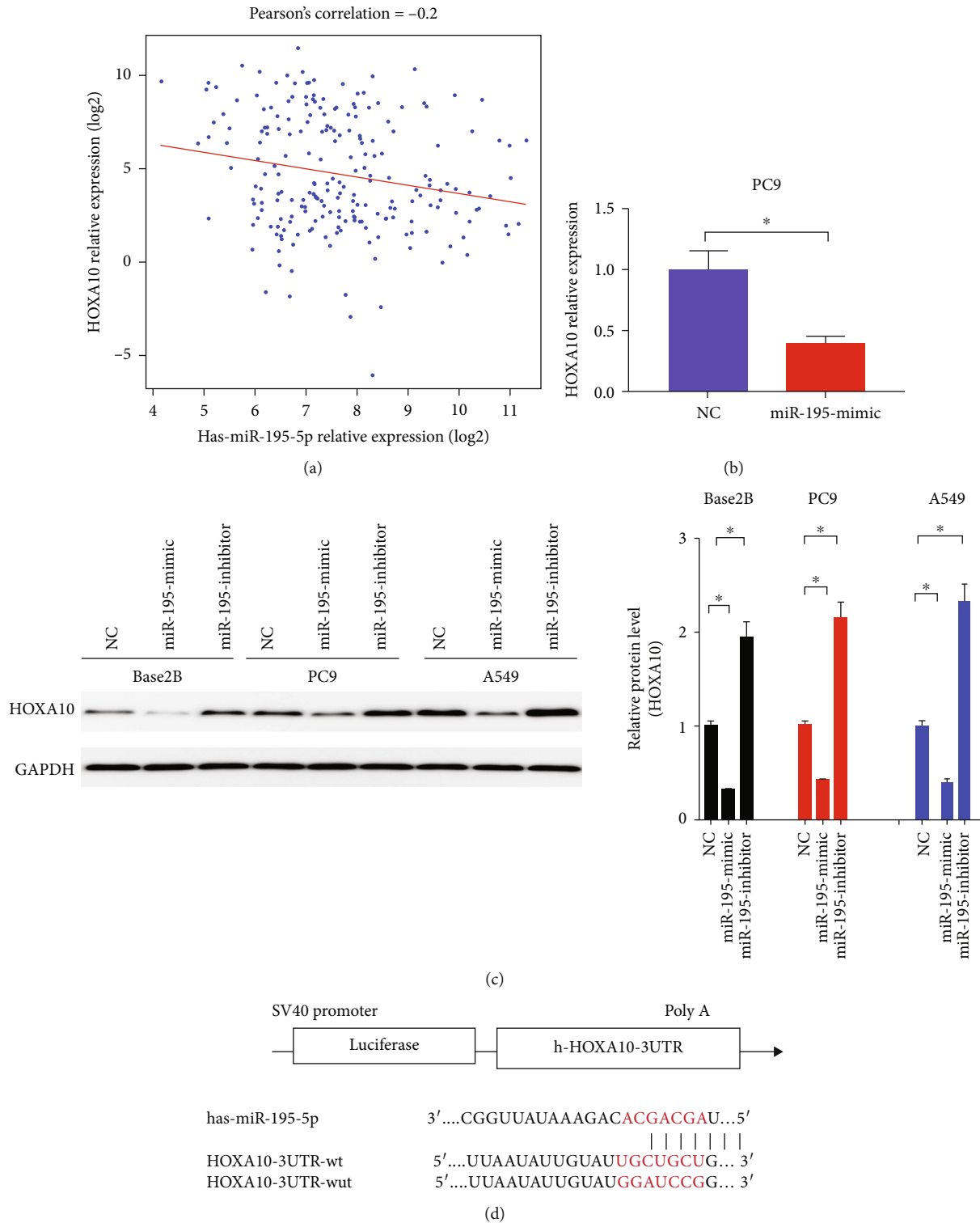


FIGURE 4: Continued.

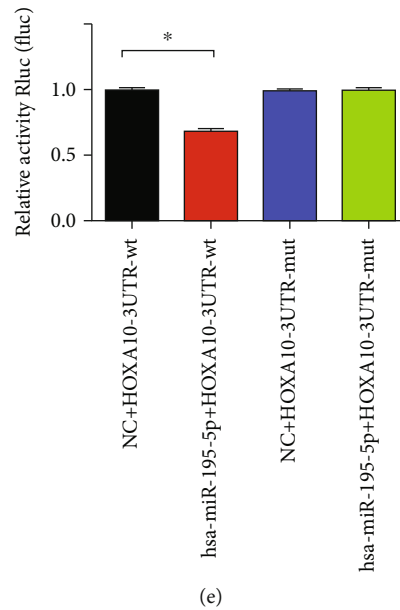


FIGURE 4: miR-195-5p targeted HOXA10. (a) The expression levels of miR-195-5p and HOXA10 showed a negative correlation ($r = -0.2$, $P < 0.05$) in TCGA database. The relative mRNA (b) and protein (c) levels of HOXA10 were detected in PC9 and A549 cells transfected with the miR-195-5p mimic, inhibitor, and NC. (d, e) Dual-luciferase reporter experiments revealed that miR-195-5p directly bound to HOXA10 and reduced its expression. $n = 3$; * $P < 0.05$ vs. NC.

SALL1, TGFBR3, and RET) were upregulated in LUAD tissues (Figure S2). The clinical values of these upregulated target genes were evaluated by diagnostic efficacy and prognostic analysis (Figure S3). The results suggested that HOXA10 might be a hub target gene, which had an important impact on the prognosis of LUAD patients.

Pearson's correlation analysis with TCGA database revealed that the levels of HOXA10 were suppressed by miR-195-5p in LUAD ($r = -0.2$, Figure 4(a)). In LUAD cells, both mRNA and protein levels of HOXA10 were downregulated by the miR-195-5p mimic (Figures 4(b) and 4(c)). Dual-luciferase reporter experiments confirmed that the miR-195-5p mimic downregulated the luciferase expression of HOXA10-3'UTR-wt ($P < 0.001$), indicating a direct targeting. Moreover, the miR-195-5p mimic failed to downregulate the luciferase level of HOXA10-3'UTR-mut (Figures 4(d) and 4(e)), suggesting that miR-195-5p directly targeted HOXA10.

3.4. Effects of HOXA10 on Proliferation, Migration, and Invasion of LUAD Cells. To explore the biological functions of the HOXA10, single gene set enrichment analysis was performed. The logarithm for the fold difference of 18,148 protein coding genes between the high- and low-expression groups was analyzed. The results showed that DNA replication and cell cycle-related signal pathways were activated in the HOXA10 high-expression group (Figure 5(a)). The above results further suggested the importance of HOXA10 in the occurrence and development of LUAD.

After the expression of HOXA10 was downregulated with siRNAs (Figure 5(b)), the proliferation of PC9 and A549 cells was inhibited (Figure 5(c)). This phenomenon

can be confirmed by the detection of Ki67 immunofluorescence (Figure 5(d)). HOXA10-siRNA inhibited LUAD cell migration (Figure 6(a)) and invasion (Figure 6(b)). Immunoblotting results showed that MMP2 and MMP9 protein levels were decreased in the HOXA10-siRNA group compared with NC (Figure 6(c)).

3.5. HOXA10 Decreased Radiosensitivity of LUAD Cells. The results of cell cycle analysis indicated that HOXA10 knockdown blocked the cell cycle at the G1 phase, and the rate of apoptosis was significantly increased (Figures 7(a) and 7(b)). Immunoblotting results showed a decrease in cyclin D1 and Bcl-2 and an increase in Bax protein levels in the HOXA10-siRNA group (Figure 7(c)).

Moreover, HOXA10 knockdown increased the rate of apoptosis induced by radiation (Figure 8(a)). Colony formation assays confirmed that HOXA10 deficiency improved PC9 and A549 cell radiosensitivity (Figure 8(b)). It was worth noting that the enrichment analysis results suggested that HOXA10 might be involved in the regulation of the Wnt pathway (Figure 8(c)). To confirm this prediction, we examined the expression of β -catenin, c-myc, and Wnt1, and their protein levels were inhibited by HOXA10-siRNA (Figure 8(d)).

Therefore, HOXA10 may regulate the tumor biological behaviors and radiosensitivity of the LUAD cells through the Wnt/ β -catenin pathway. To further clarify whether miR-195-5p regulated the Wnt/ β -catenin pathway through HOXA10, we investigated its effects on the expression of Wnt1 and β -catenin in LUAD cells. It was found that the miR-195-5p mimic inhibited the Wnt/ β -catenin pathway, while its inhibitors activated this pathway. Moreover, the

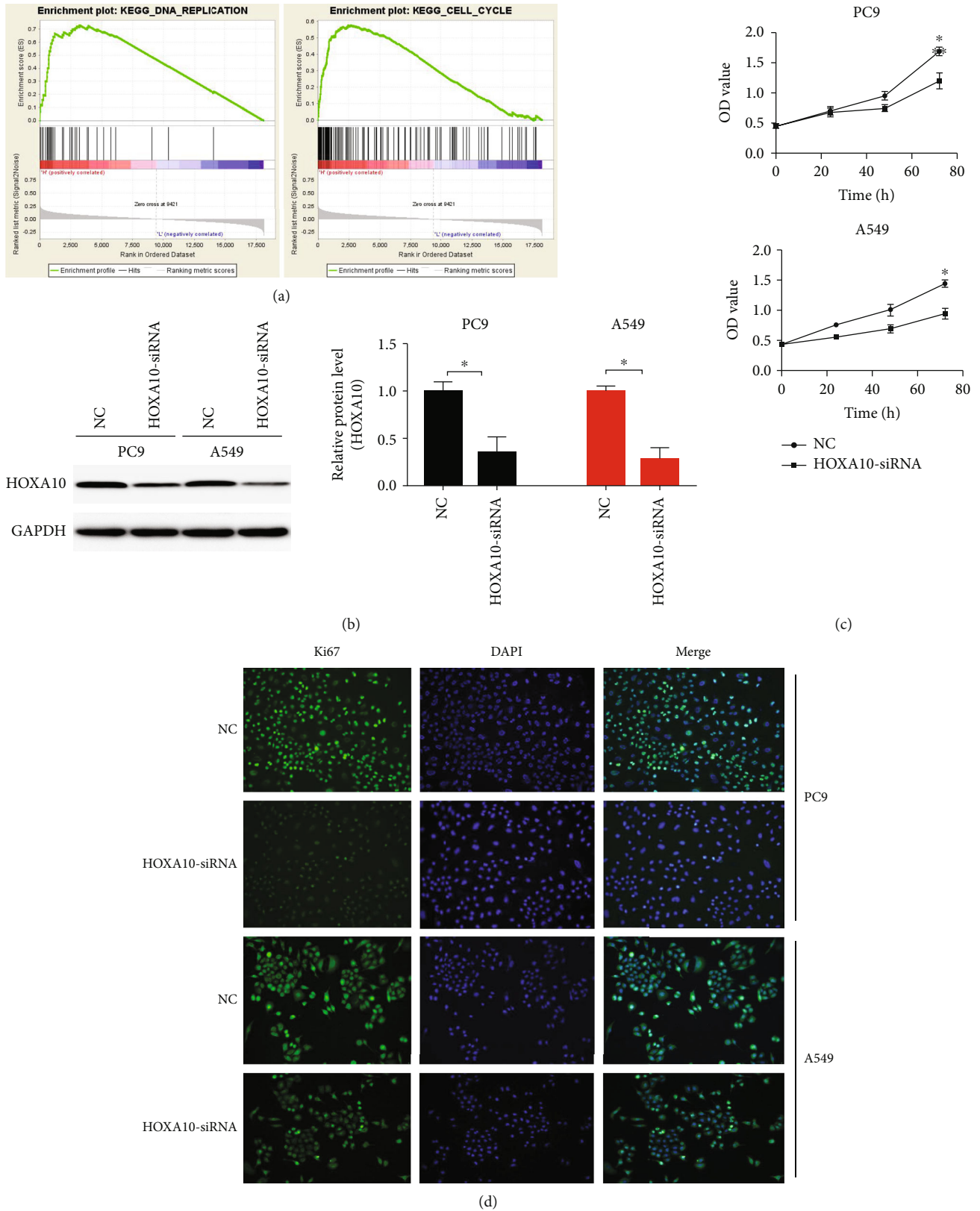


FIGURE 5: HOXA10 downregulation inhibited LUAD cell proliferation. (a) The results of GSEA predicted that DNA replication and cell cycle-related signal pathways were activated in the HOXA10 high-expression group. (b) The protein levels of HOXA10 were detected in PC9 and A549 cells transfected with HOXA10-siRNA and NC. (c) CCK-8 assays of PC9 and A549 cells transfected with HOXA10-siRNA and NC. (d) Representative immunofluorescent images of Ki67 in PC9 and A549 cells transfected with HOXA10-siRNA and NC. $n = 3$; * $P < 0.05$ vs. NC.

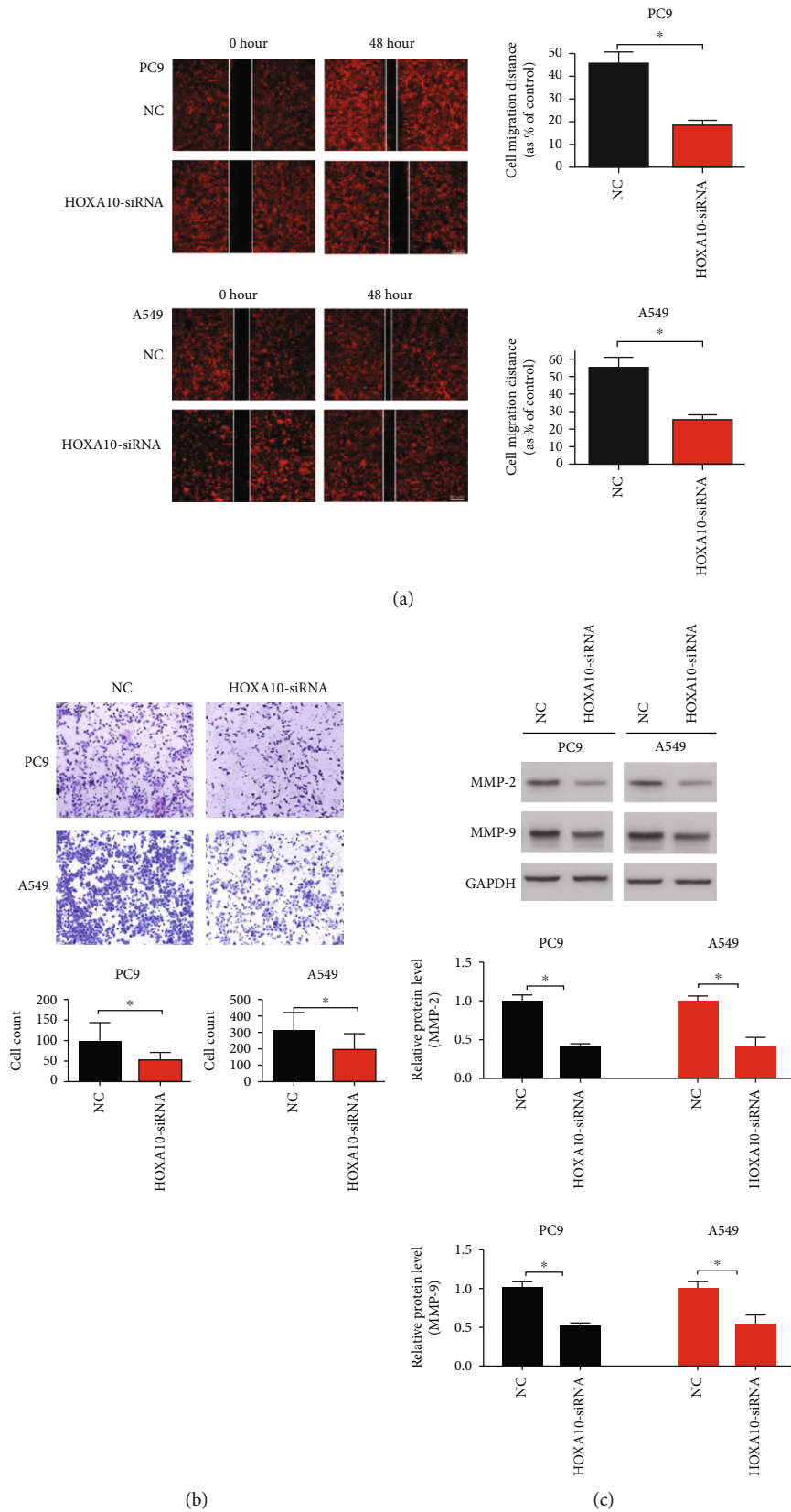


FIGURE 6: HOXA10 downregulation inhibited invasion and metastasis of LUAD cells. (a) Representative images of the wound healing assay in PC9 and A549 cells transfected with HOXA10-siRNA and NC. (b) Representative images of the modified Boyden chamber assay in PC9 and A549 cells transfected with HOXA10-siRNA and NC. (c) Immunoblotting results demonstrated that MMP2 and MMP9 protein levels were decreased in the HOXA10-siRNA group. $n = 3$; $*P < 0.05$ vs. NC.

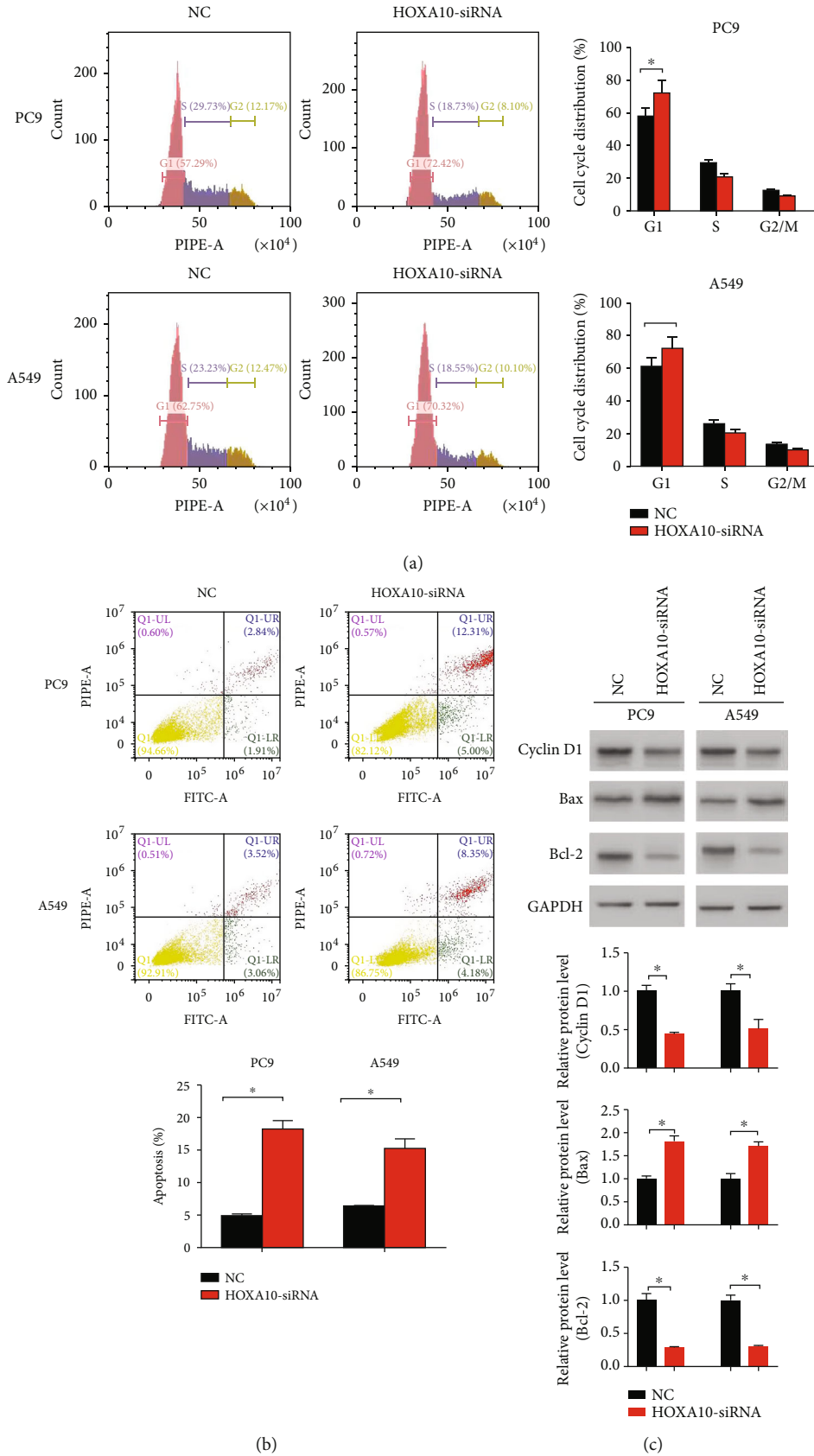


FIGURE 7: HOXA10 downregulation induced LUAD cell apoptosis and blocked the cell cycle. (a) The cell cycle was detected by flow cytometry. (b) Apoptosis was detected by flow cytometry. (c) The levels of cycle- and apoptosis-related proteins (cyclin D1, Bax, and Bcl-2) were measured by immunoblotting. $n = 3$; * $P < 0.05$ vs. NC.

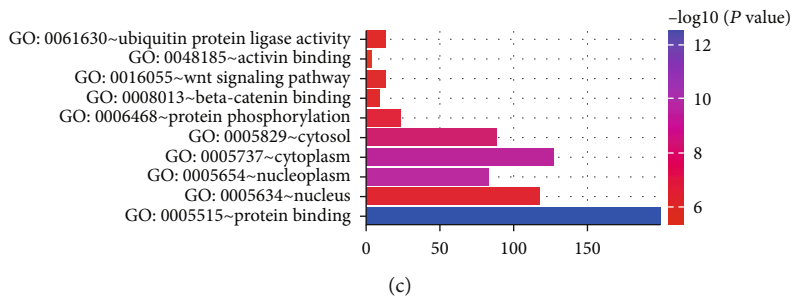
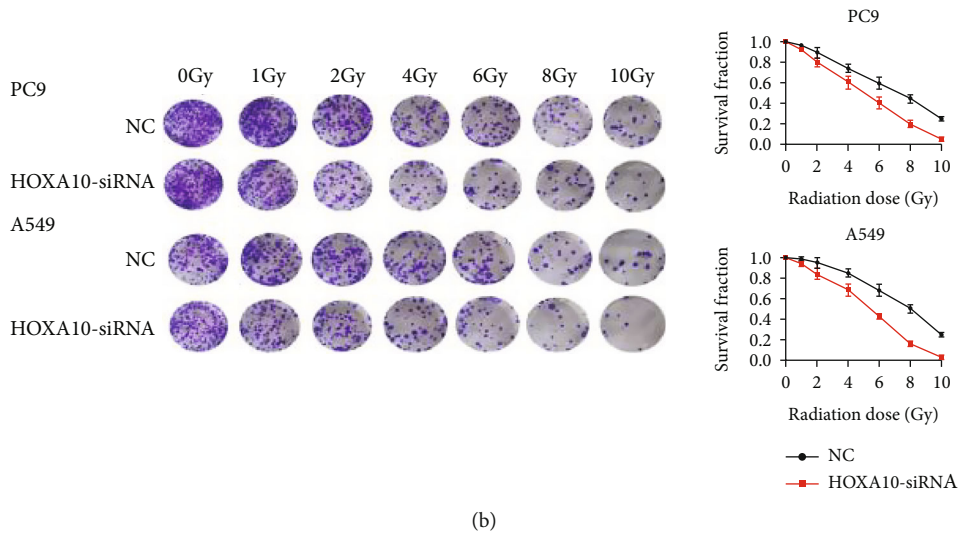
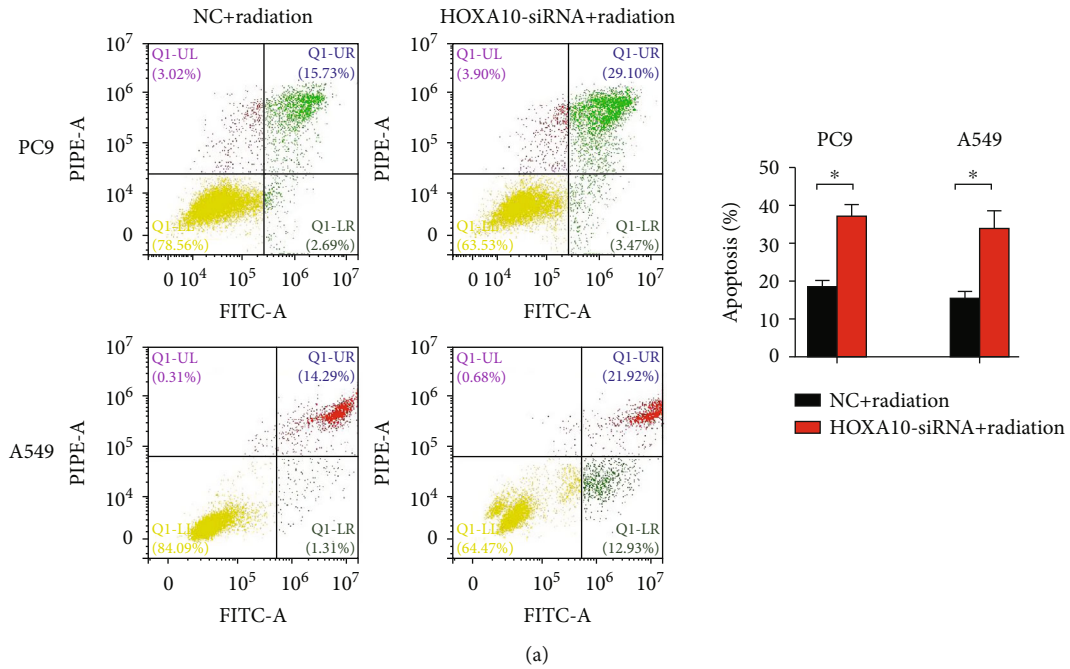


FIGURE 8: Continued.

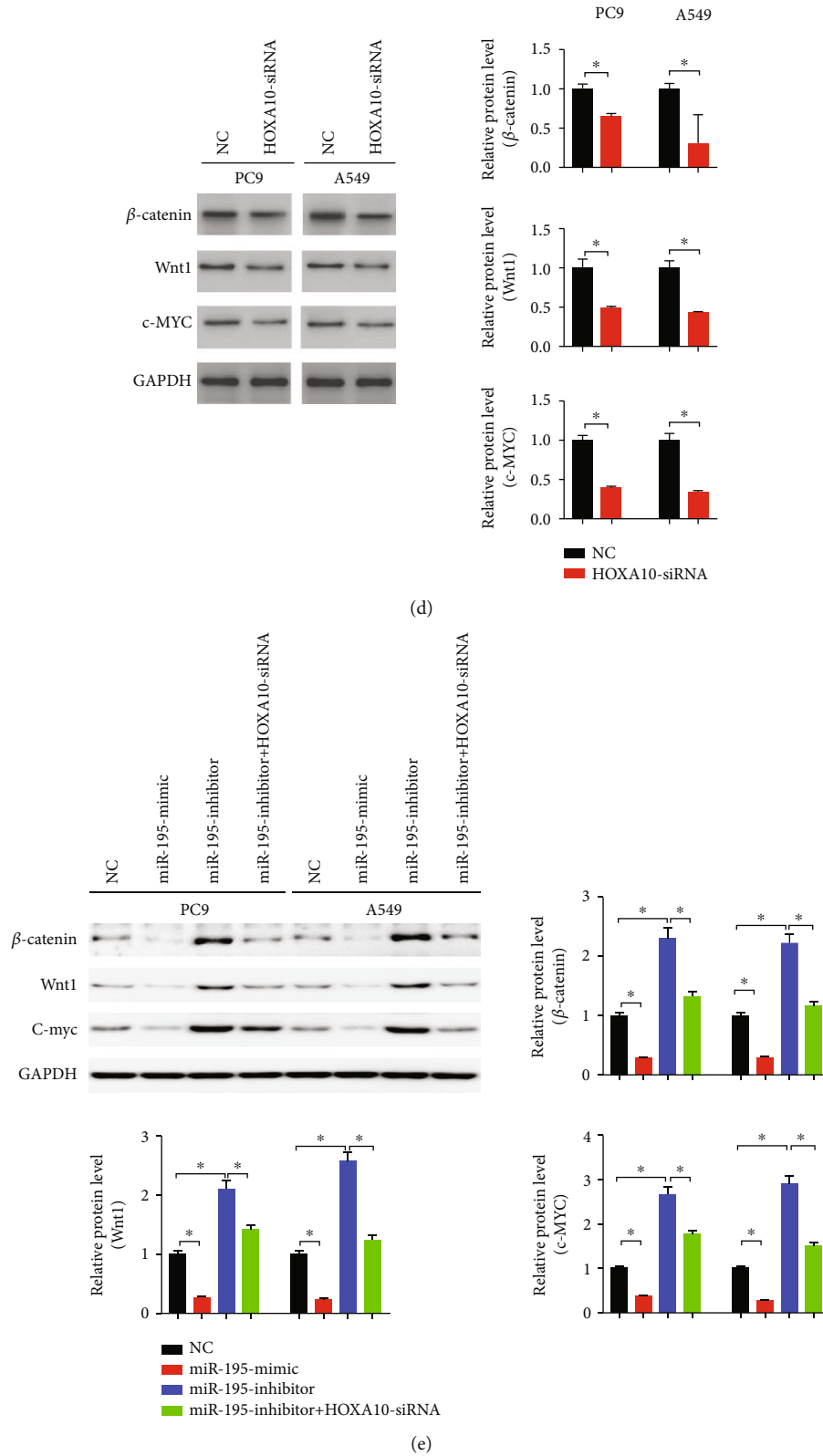


FIGURE 8: HOXA10 downregulation enhanced radiosensitivity of LUAD cells. (a) Cell apoptosis was detected by flow cytometry at 48 h after radiation (4 Gy). (b) Colony formation assays and survival fractions were calculated after treatment with 0, 2, 4, 6, 8, and 10 Gy of ionizing radiation. (c) The enrichment analysis indicated that HOXA10 might be involved in the regulation of the Wnt pathway. (d) Representative immunoblots of β -catenin, c-myc, and Wnt1 in PC9 and A549 cells transfected with HOXA10-siRNA and NC. (e) Representative immunoblots of β -catenin, c-myc, and Wnt1 in PC9 and A549 cells transfected with the miR-195-5p mimic, inhibitor, inhibitor + OXA10-siRNA, and NC. $n = 3$; * $P < 0.05$ vs. NC.

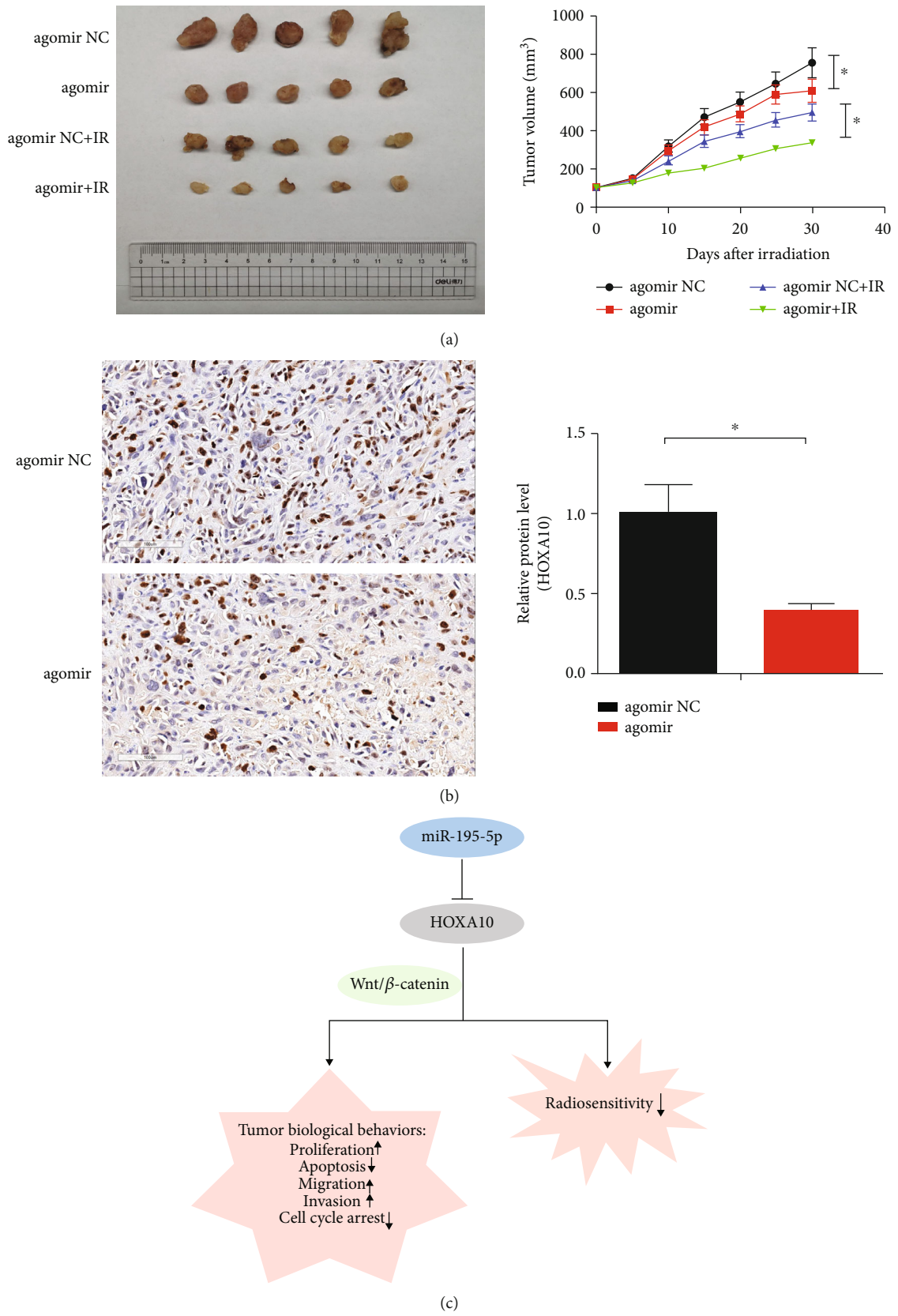


FIGURE 9: Effects of miR-195-5p on the radiosensitivity of the xenograft LUAD tumor. (a) Tumor volume in the nude mice. (b) Representative immunohistochemistry of HOXA10 in the LUAD tissues from nude mice. (c) Hypothesis diagram showing that miR-195-5p targeted HOXA10 to hinder the corresponding cytological behaviors of LUAD cells and enhance radiosensitivity. $n = 5$; * $P < 0.05$ vs. NC.

effects of miR-195-5p inhibitors on the Wnt/ β -catenin pathway could be eliminated by HOXA10-siRNA. Therefore, miR-195-5p regulated the Wnt pathway through HOXA10 (Figure 8(e)).

3.6. miR-195-5p Enhanced the Radiosensitivity of Xenograft-Formed LUAD. The tumor volume in the mice injected with miR-195-5p agomir combined with irradiation was lower than that of agomir NC and radiation alone (Figure 9(a)). In addition, the expression levels of HOXA10 in the tumor tissues of nude mice treated with miR-195-5p agomir were lower than those in the agomir NC tumors (Figure 9(b)).

4. Discussion

Radiotherapy is widely used in the clinical treatment of LUAD. However, some patients have radiotherapy resistance at the beginning or during treatment, which is a challenge. Researchers try to explain the mechanism of radioresistance, including autophagy [14], tumor stem cells [15], and abnormal activation of signal pathways [16]. Previous studies have reported that miRNAs affect radiation damage to cells in different tumors, indicating that miRNAs may play important roles in tumor radiosensitivity [17–19].

Our current study supported that increased miR-195-5p in LUAD cells considerably decreased cell growth, migration, and invasion. Subsequent studies found that miR-195-5p could also increase the cell proportion of the G1 phase in the cell cycle, induce apoptosis, and improve radiosensitivity. Moreover, miR-195-5p could directly regulate HOXA10 expression via targeting its 3'-UTR. It downregulated HOXA10, β -catenin, c-myc, and Wnt1 in PC9 and A549 cells. Finally, miR-195-5p suppressed LUAD growth and enhanced radiosensitivity *in vivo*.

More and more researches supported that miRNAs could be used as biomarkers for malignant tumors. miRNAs were widely present in body fluids and tissues, and their abnormal expression or distribution has important impacts on the biological behaviors [20, 21]. Previous studies suggested that miR-195-5p was proposed to be a biomarker of lung cancer [22]. Our bioinformatics results also showed that miR-195-5p might be a tumor suppressor gene in lung cancer [13], and our *in vitro* experiments were consistent with previous results in non-small-cell lung cancer [23]. Guan et al. reported that HOXA10 mediated EMT in head and neck squamous cell carcinoma and was targeted by miR-195-5p [24]. However, their effects on radiosensitivity were to be investigated.

Previous researches reported that miRNAs affected cell apoptosis and regulated tumor cell radiosensitivity. For example, miR-148b promoted the cell apoptosis and enhances radiosensitivity [25], and miR-185 inhibited the apoptosis of gastric cancer cells [26]. Our studies found that overexpression of miR-195-5p enhanced LUAD radiosensitivity, evidenced by reduced survival fractions and induced apoptosis after miR-195-5p overexpression. In addition, the increase in the cell apoptosis rate was accompanied by induced expression of the proapoptotic molecule Bax, while the levels of Bcl-2 were downregulated. Therefore, it can be

considered that miR-195-5p in LUAD cells might modify the outcome of radiation by the induction of apoptosis.

Dual-luciferase reporter experiments suggested that miR-195-5p directly targeted HOXA10. HOXA10 plays a vital function in embryonic development and cell proliferation and differentiation. Its expression levels are elevated in various tumors. For example, Plowright et al. found that HOXA10 was upregulated in NSCLC [27]. The expression levels of HOXA10 were negatively correlated with the invasion ability of gastric tumor cells. Moreover, Chu et al. reported that HOXA10 induced P53 to exhibit tumor suppressor genes [28]. Therefore, HOXA10 regulated tumor growth in a cancer-specific manner.

The specific functions of HOXA10 in LUAD need to be further explored. The CCK-8 and Ki67 immunofluorescence suggested that HOXA10 downregulation inhibited LUAD cell proliferation, migration, and invasion. The colony formation assay indicated that as radiation dose increased, the colony numbers gradually decreased. At the same dose level, HOXA10 knockdown significantly suppressed colony formation. These results indicated that HOXA10 deficiency induced LUAD cell apoptosis after radiation and reduced cell proliferation and survival. Our findings suggested that miR-195-5p enhanced the radiosensitivity of LUAD cells via inhibiting the HOXA10 expression.

The Wnt/ β -catenin signaling pathway is closely related to the biological behaviors of the tumor. Yang et al. found that miR-183 inhibited osteosarcoma cell growth, migration, and invasion via regulating the Wnt/ β -catenin signaling pathway [29]. Other studies [30–32] also suggested that this pathway was involved in the regulation of radiosensitivity. Interestingly, our results indicated that HOXA10 downregulation significantly inhibited the Wnt/ β -catenin signaling pathway, as well as the biological behaviors of LUAD cells. Moreover, HOXA10 deficiency reversed Wnt/ β -catenin signaling activation induced by the miR-195-5p inhibitor. Therefore, miR-195-5p hindered the activation of the Wnt/ β -catenin signaling pathway via targeting HOXA10, thereby inhibiting the corresponding cytological behaviors of LUAD cells and enhancing radiosensitivity (Figure 9(c)).

Our studies had certain limitations. The results of our researches are to be confirmed with clinical evidence. Furthermore, the direct targeting of HOXA10 and how it affects the Wnt/ β -catenin pathway need further exploration.

In summary, our results demonstrated that miR-195-5p inhibited biological behaviors and sensitized LUAD cells to X-ray irradiation via targeting HOXA10. It provided a novel idea to improve the treatment of LUAD, especially the efficacy of radiotherapy.

Data Availability

The data used to support the findings of this study are available from the corresponding author upon request.

Conflicts of Interest

The authors declare no conflicts of interests.

Authors' Contributions

Cheng Yuan and Rui Bai contributed equally to this work.

Acknowledgments

This study was supported by the National Natural Science Foundation of China (81773236, 81800429, and 81972852), Key Research & Development Project of Hubei Province (2020BCA069), Nature Science Foundation of Hubei Province (2020CFB612), Health Commission of Hubei Province Medical Leading Talent Project, Young and Middle-Aged Medical Backbone Talents of Wuhan (WHQG201902), Application Foundation Frontier Project of Wuhan (2020020601012221), Zhongnan Hospital of Wuhan University Science, Technology and Innovation Seed Fund (znp2019001 and znp2019048), and Translational Medicine and Interdisciplinary Research Joint Fund of Zhongnan Hospital of Wuhan University (ZNYC201922 and ZNYC202007).

Supplementary Materials

Supplementary 1. Supplemental Figure S1: Venn diagrams of differentially expressed microRNA targets. When matched to differentially expressed genes, 34 target genes were screened out.

Supplementary 2. Supplemental Figure S2: expression of the target genes was plotted for LUAD tumor and normal tissues (TCGA dataset). Except TMEM00, RS1, and OSCAR, the remaining genes (CEP55, PSAT1, CHEK1, KIF23, CCNE1, CLSPN, CDC25A, E2F7, CBX2, HOXA10, SALL1, TGFB3, and RET) were upregulated in LUAD tissues.

Supplementary 3. Supplemental Figure S3: the target genes were evaluated by diagnostic efficacy and prognostic analysis. ROC curve analysis was performed based on TCGA dataset. Kaplan-Meier survival curves of the overall survival were shown in the Kaplan-Meier plotter (<https://kmplot.com/analysis/>).

References

- [1] F. Bray, J. Ferlay, I. Soerjomataram, R. L. Siegel, L. A. Torre, and A. Jemal, "Global cancer statistics 2018: GLOBOCAN estimates of incidence and mortality worldwide for 36 cancers in 185 countries," *CA: a Cancer Journal for Clinicians*, vol. 68, no. 6, pp. 394–424, 2018.
- [2] M. Deng, B. Liu, Z. Zhang et al., "Loss of G-protein-signaling modulator 2 accelerates proliferation of lung adenocarcinoma via EGFR signaling pathway," *The International Journal of Biochemistry & Cell Biology*, vol. 122, p. 105716, 2020.
- [3] F. R. Hirsch, G. V. Scagliotti, J. Mulshine et al., "Lung cancer: current therapies and new targeted treatments," *Lancet*, vol. 389, no. 10066, pp. 299–311, 2017.
- [4] V. Relli, M. Trerotola, E. Guerra, and S. Alberti, "Distinct lung cancer subtypes associate to distinct drivers of tumor progression," *Oncotarget*, vol. 9, no. 85, pp. 35528–35540, 2018.
- [5] X. Ai, X. Guo, J. Wang et al., "Targeted therapies for advanced non-small cell lung cancer," *Oncotarget*, vol. 9, no. 101, pp. 37589–37607, 2018.
- [6] A. Zagryazhskaya and B. Zhivotovsky, "miRNAs in lung cancer: a link to aging," *Ageing Research Reviews*, vol. 17, pp. 54–67, 2014.
- [7] B. Tomasik, J. Chałubińska-Fendler, D. Chowdhury, and W. Fendler, "Potential of serum microRNAs as biomarkers of radiation injury and tools for individualization of radiotherapy," *Translational Research*, vol. 201, pp. 71–83, 2018.
- [8] H. Li, M. Jiang, M. Cui et al., "MiR-365 enhances the radiosensitivity of non-small cell lung cancer cells through targeting CDC25A," *Biochemical and Biophysical Research Communications*, vol. 512, no. 2, pp. 392–398, 2019.
- [9] T. Powrozek and T. Malecka-Massalska, "MiRNA and lung cancer radiosensitivity: a mini-review," *European Review for Medical and Pharmacological Sciences*, vol. 23, no. 19, pp. 8422–8428, 2019.
- [10] C. Feng, L. Zhang, Y. Sun et al., "GDPD5, a target of miR-195-5p, is associated with metastasis and chemoresistance in colorectal cancer," *Biomedicine & Pharmacotherapy*, vol. 101, pp. 945–952, 2018.
- [11] Y. Jin, M. Wang, H. Hu, Q. Huang, Y. Chen, and G. Wang, "Overcoming stemness and chemoresistance in colorectal cancer through miR-195-5p-modulated inhibition of notch signaling," *International Journal of Biological Macromolecules*, vol. 117, pp. 445–453, 2018.
- [12] L. Chai, X. J. Kang, Z. Z. Sun et al., "MiR-497-5p, miR-195-5p and miR-455-3p function as tumor suppressors by targeting hTERT in melanoma A375 cells," *Cancer Management and Research*, vol. 10, pp. 989–1003, 2018.
- [13] C. Yuan, L. Xiang, R. Bai et al., "MiR-195 restrains lung adenocarcinoma by regulating CD4+ T cell activation via the CCDC88C/Wnt signaling pathway: a study based on the Cancer Genome Atlas (TCGA), Gene Expression Omnibus (GEO) and bioinformatic analysis," *Annals of Translational Medicine*, vol. 7, no. 12, p. 263, 2019.
- [14] H. Chaachouay, P. Ohneseit, M. Toulany, R. Kehlbach, G. Multhoff, and H. P. Rodemann, "Autophagy contributes to resistance of tumor cells to ionizing radiation," *Radiotherapy and Oncology*, vol. 99, no. 3, pp. 287–292, 2011.
- [15] C. Moncharmont, A. Levy, M. Gilormini et al., "Targeting a cornerstone of radiation resistance: cancer stem cell," *Cancer Letters*, vol. 322, no. 2, pp. 139–147, 2012.
- [16] F. J. Dumont and P. Bischoff, "Disrupting the mTOR signaling network as a potential strategy for the enhancement of cancer radiotherapy," *Current Cancer Drug Targets*, vol. 12, no. 8, pp. 899–924, 2012.
- [17] X. Deng, L. Ma, M. Wu et al., "miR-124 radiosensitizes human glioma cells by targeting CDK4," *Journal of Neuro-Oncology*, vol. 114, no. 3, pp. 263–274, 2013.
- [18] P. Wang, J. Zhang, L. Zhang et al., "MicroRNA 23b regulates autophagy associated with radioresistance of pancreatic cancer cells," *Gastroenterology*, vol. 145, no. 5, pp. 1133–1143.e12, 2013.
- [19] Y. J. Liu, Y. F. Lin, Y. F. Chen et al., "MicroRNA-449a enhances radiosensitivity in CL1-0 lung adenocarcinoma cells," *PLoS One*, vol. 8, no. 4, article e62383, 2013.
- [20] K. B. Marcu, S. A. Bossone, and A. J. Patel, "myc function and regulation," *Annual Review of Biochemistry*, vol. 61, no. 1, pp. 809–858, 1992.
- [21] S. A. Chappell, J. P. LeQuesne, F. E. Paulin et al., "A mutation in the c-myc-IRES leads to enhanced internal ribosome entry

- in multiple myeloma: a novel mechanism of oncogene de-regulation,” *Oncogene*, vol. 19, no. 38, pp. 4437–4440, 2000.
- [22] L. Li, T. Feng, W. Zhang et al., “MicroRNA Biomarkerhsa-miR-195-5pfor detecting the risk of lung cancer,” *International Journal of Genomics*, vol. 2020, Article ID 7415909, 9 pages, 2020.
- [23] J. Zheng, T. Xu, F. Chen, and Y. Zhang, “MiRNA-195-5p functions as a tumor suppressor and a predictive of poor prognosis in non-small cell lung cancer by directly targeting CIAPIN1,” *Pathology Oncology Research*, vol. 25, no. 3, pp. 1181–1190, 2019.
- [24] Y. Guan, A. Guan, L. Chen, and A. Gong, “LINC00461 facilitates HNSCC development and reduces chemosensitivity by impairing miR-195-mediated inhibition of HOXA10,” *Molecular Therapy Oncolytics*, vol. 21, pp. 74–86, 2021.
- [25] Y. Wu, G. L. Liu, S. H. Liu et al., “MicroRNA-148b enhances the radiosensitivity of non-Hodgkin's lymphoma cells by promoting radiation-induced apoptosis,” *Journal of Radiation Research*, vol. 53, no. 4, pp. 516–525, 2012.
- [26] J. Wang, J. He, F. Su et al., “Repression of ATR pathway by miR-185 enhances radiation-induced apoptosis and proliferation inhibition,” *Cell Death & Disease*, vol. 4, no. 6, article e699, 2013.
- [27] L. Plowright, K. J. Harrington, H. S. Pandha, and R. Morgan, “HOX transcription factors are potential therapeutic targets in non-small- cell lung cancer (targeting HOX genes in lung cancer),” *British Journal of Cancer*, vol. 100, no. 3, pp. 470–475, 2009.
- [28] M. C. Chu, F. B. Selam, and H. S. Taylor, “HOXA10 regulates p53 expression and Matrigel invasion in human breast cancer cells,” *Cancer Biology & Therapy*, vol. 3, no. 6, pp. 568–572, 2004.
- [29] X. Yang, L. Wang, Q. Wang, L. Li, Y. Fu, and J. Sun, “MiR-183 inhibits osteosarcoma cell growth and invasion by regulating LRP6-Wnt/ β -catenin signaling pathway,” *Biochemical and Biophysical Research Communications*, vol. 496, no. 4, pp. 1197–1203, 2018.
- [30] M. S. Chen, W. A. Woodward, F. Behbod et al., “Wnt/ β -catenin mediates radiation resistance of Sca1+ progenitors in an immortalized mammary gland cell line,” *Journal of Cell Science*, vol. 120, no. 3, pp. 468–477, 2007.
- [31] N. Gassler, I. Herr, M. Keith et al., “Wnt-signaling and apoptosis after neoadjuvant short-term radiotherapy for rectal cancer,” *International Journal of Oncology*, vol. 25, no. 6, pp. 1543–1549, 2004.
- [32] B. Hai, Z. Yang, S. E. Millar et al., “Wnt/ β -catenin signaling regulates postnatal development and regeneration of the salivary gland,” *Stem Cells and Development*, vol. 19, no. 11, pp. 1793–1801, 2010.

Research Article

Methylation of CALCA and CALCB in Pancreatic Ductal Adenocarcinoma

Feng Gao ¹, Guozhong Liu,² Jingwen Wang,^{1,3} Shirong Huang ⁴, Fadian Ding ², Wei Lian,² Xiaoting Lv ⁵, Yujia Guo,⁶ Xiangqun Fan,⁷ Sheng Zhang ¹ and Qicai Liu ⁶

¹Department of Pathology, 1st Affiliated Hospital, Fujian Medical University, Fuzhou 350005, China

²Department of Hepatobiliary Surgery, 1st Affiliated Hospital, Fujian Medical University, Fuzhou 350005, China

³Department of Neurology, Tiantai People's Hospital of Zhejiang Province, Tiantai 317200, China

⁴Department of Laboratory Medicine, Fujian Medical University, 350004 Fuzhou, China

⁵Department of Respiratory, 1st Affiliated Hospital, Fujian Medical University, Fuzhou 350004, China

⁶Center for Reproductive Medicine, 1st Affiliated Hospital, Fujian Medical University, Fuzhou 350004, China

⁷Center of Prenatal Screening, Fujian Provincial Maternity and Children's Hospital, Fujian Medical University, Fuzhou 350005, China

Correspondence should be addressed to Sheng Zhang; zhgshg@126.com and Qicai Liu; lqc673673673@163.com

Feng Gao, Guozhong Liu, and Jingwen Wang contributed equally to this work.

Received 5 May 2021; Revised 6 June 2021; Accepted 9 July 2021; Published 4 August 2021

Academic Editor: Jayeeta Ghose

Copyright © 2021 Feng Gao et al. This is an open access article distributed under the Creative Commons Attribution License, which permits unrestricted use, distribution, and reproduction in any medium, provided the original work is properly cited.

Calcitonin gene-related peptide (CGRP) plays a diverse and intricate role in chronic low-grade inflammation and is closely related to specific cancers. It includes two subtypes, CALCA (α CGRP) and CALCB (β CGRP), of which α CGRP expression accounts for more than 90%. Here, we show that methylation of CALCA and CALCB in pancreatic ductal adenocarcinoma was significantly higher than that in paracancer. Western blot and immunohistochemistry showed that CGRP, p-AKT, and p-CREB in the tumor tissues were lower than those in the paracarcinoma tissues. *In vivo*, the expressions of p-AKT and p-CREB in the pancreatic tissues of CALCA-KO rats were also lower than those of wild type. Methylation of CALCA and CALCB is increased in pancreatic adenocarcinoma, and under that condition, p-AKT and p-CREB levels were decreased.

1. Introduction

With the mortality approximately equal to the morbidity [1], pancreatic cancer has become one of the most fatal malignant tumors, among which pancreatic ductal carcinoma accounts for more than 90% [2]. However, the mechanism of occurrence and development of pancreatic cancer is still unclear. DNA methylation is an important epigenetic modification, which can regulate cell proliferation, apoptosis, gene expression, and stability, and is closely related to the tumor [3, 4].

Calcitonin gene-related peptide (CGRP) is a member of the calcitonin family of peptides, which can act as a growth or survival factor for several tumors, including endocrine-related tumors [5, 6]. The function of CGRP in stimulating

angiogenesis and lymphangiogenesis may be one of the mechanisms [6]. There are two types that exist in CGRP: (1) α CGRP: the product of alternative splicing of the calcitonin gene (CT/CALCA) in neurons and whose expression accounts for more than 90% and is involved in regulating the function of various organs and (2) calcitonin gene-related peptide beta (CALCB), which has been discovered to form β CGRP, primarily expressed in the enteric sensory system, gut, and inner organs [5–7]. CGRP is one of the strongest vasoactive peptides found *in vivo* so far, which plays a role in relaxing and inhibiting vascular smooth muscle proliferation [6, 7]. At the same time, CGRP can stagnate the cell cycle in G0/G1 phase and thus participate in the regulation of tumor growth [8, 9].

TABLE 1: Primer sequences used to amplify CGRP.

Target gene (promoter region)		CALCA (NC_000011.10 (14966668...14972361, complement))
MSP	Forward	5'-TTTTAGGTTTGGAAAGTATGAGGGTGATG-3'
	Reverse	5'-TTCCCACCACTATAAATCA-3'
	Annealing temperature	53°C
USP	Forward	5'-GTTTTGGAAGTATGAGGGTGACG-3'
	Reverse	5'-TTCCCGCCGCTATAAATCG-3'
	Annealing temperature	53°C
Target gene (promoter region)		CALCB (NC_000011.10 (15073593...15078637))
MSP	Forward	5'-TTTTTAGAAAAGATGGATAGGTCGA-3'
	Reverse	5'-ACCAACACTCACTAAAACAAATACG-3'
	Annealing temperature	45°C
USP	Forward	5'-TTTTTAGAAAAGATGGATAGGTTGA-3'
	Reverse	5'-CCAACACTCACTAAAACAAATACAC-3'
	Annealing temperature	45°C

The literature shows that CGRP plays a key role in the regulation of apoptosis and oxidative stress through the PI3K/Akt pathway [10]. Our previous work showed that abnormal CGRP can drive cell cycle disorder [11]. Therefore, we speculate that CGRP regulated oxidative stress injury, and cell cycle disorder plays an important role in the pathogenesis of pancreatic cancer. However, the epigenetics and expression of CGRP in pancreatic cancer are still unclear.

Therefore, the aims of this study were to investigate the methylation levels of CpG island in the CGRP promoter region of patients with pancreatic cancer by various methods to confirm the relationship between CGRP methylation, CGRP deficiency, and pancreatic cancer. *In vivo*, CGRP knockout rats (CALCA-KO) were also established to explore not only the relationship between CGRP deficiency and pancreatic cancer but also its possible pathogenesis.

2. Materials and Methods

2.1. Study Population. The data of sixty-three patients with pancreatic ductal adenocarcinoma hospitalized at the First Affiliated Hospital were enrolled (45 males and 18 females, male/female ratio≈5:2, range 43-72 years, mean age 57.5 years) between April 2015 and December 2019. In addition, fifteen healthy controls (10 males and 5 females, male/female ratio = 2 : 1, aged 35-60 years, median age 47.5 years) were selected from the physical examination center of our hospital during the same period. Patients were investigated for basic information, including the age of onset and family history. This research project was approved by the Ethics Committee of Fujian Medical University.

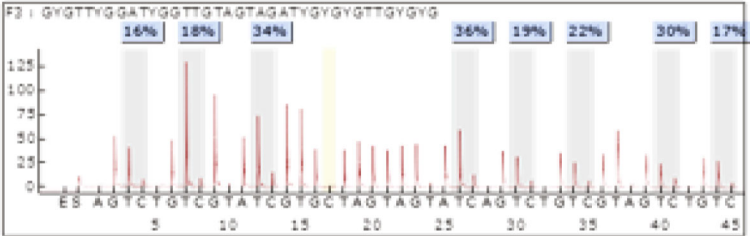
2.2. Pyrosequencing. DNA was extracted from peripheral blood, cancer tissues, and adjacent tissues of patients with pancreatic cancer using the Tiangen DNA Extraction Kit (Tiangen, Beijing, China). DNA was sent directly to Gene Tech (Shanghai) Co., Ltd. (Gene Tech, Shanghai, China)

for pyrosequencing to detect the methylation level of CpG island in the CGRP promoter region.

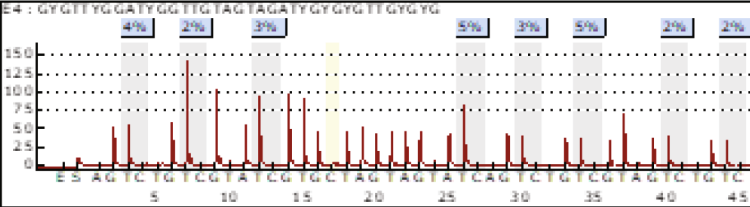
2.3. DNA Bisulfite Conversion and Methylation Detection. The bisulfite conversion of DNA was carried out using Qiagen's EpiTect Fast DNA Bisulfite Kit. The initial sample dose was 1-2 mg, and the procedure was carried out according to the kit instructions. The 0.2 mL PCR tube was added with 20 μ L DNA, 85 μ L freshly prepared bisulfite conversion solution, and 35 μ L DNA protection solution in turn and then was mixed and put into the PCR instrument. The thermal cycle program was performed under the following conditions (step: temperature, time): Step 1: 95°C, 5 min; Step 2: 60°C, 10 min, a total of 2 cycles. Afterwards, conversion products were purified (Table 1).

2.4. Pathological Verification of CGRP-KO Rat Model. In order to investigate whether hypermethylation of CpG island in CGRP may promote the occurrence of pancreatic cancer, we constructed a CGRP knockout rat model to observe the changes in pancreatic tissue after CGRP-KO and to explore the possible mechanism. The model was constructed by GemPharmatech Co., Ltd. The rats were fed at room temperature of 22 \pm 2°C and humidity of 40.00%-60.00%. Adequate rat food was given every day, drinking water was resteaed before being drunk, and the bedding material was changed at least twice a week to ensure that the bedding material was clean. For mating of rats, CGRP-KO (CGRP knockout rats) (> at 8 weeks) were cooped with WT (wild-type rats), with a male to female ratio of 1 : 1 or 2 : 1.

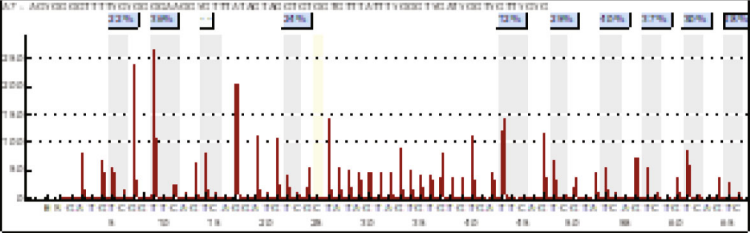
2.5. Immunohistochemistry. Immunohistochemistry (IHC) was performed to detect the expression of CALCA (rabbit antihuman polyclonal antibody, 1 : 100 dilution; A11804, ABclonal, CN), CALCB (rabbit antihuman polyclonal antibody, 1 : 3200 dilution; A5523, ABclonal, CN), AKT (rabbit antihuman polyclonal antibody, 1 : 3200 dilution; AB105,



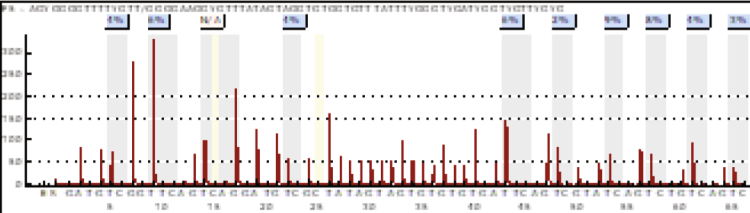
(a)



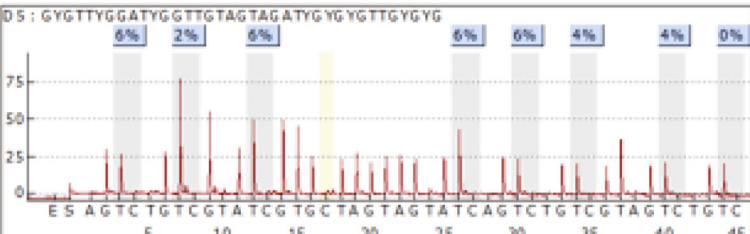
(b)



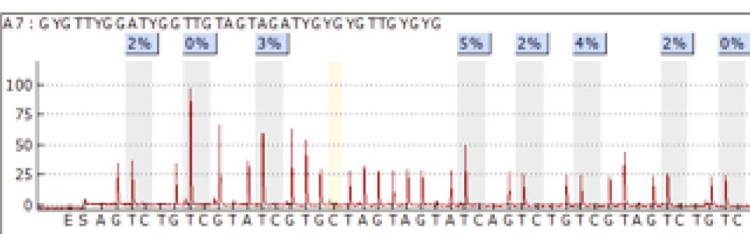
(c)



(d)



(e)



(f)

FIGURE 1: Continued.

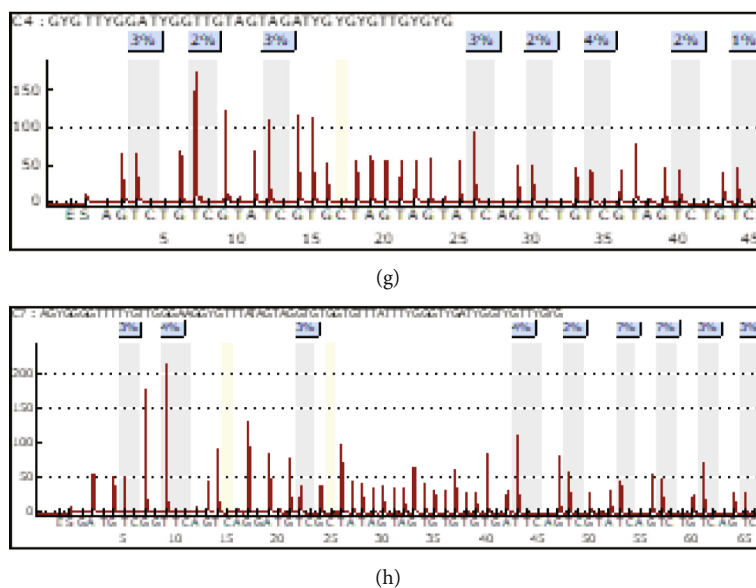


FIGURE 1: Pyrosequencing results of CALCA and CALCB: (a) CALCA pyrosequencing in pancreatic cancer tissue; (b) CALCA pyrosequencing in paracancer tissue; (c) CALCB pyrosequencing in pancreatic cancer tissue; (d) CALCB pyrosequencing in paracancer tissue; (e) CALCA pyrosequencing in peripheral blood of patients with pancreatic cancer; (f) CALCA pyrosequencing in peripheral blood of normal control; (g) CALCB pyrosequencing in peripheral blood of patients with pancreatic cancer; (h) CALCB pyrosequencing in peripheral blood of normal control.

Abclonal, CN), p-AKT1-S473mAb (rabbit antihuman polyclonal antibody, 1:1600 dilution; AP0637, ABclonal, CN), CREB (rabbit antihuman polyclonal antibody, 1:1600 dilution; A10826, ABclonal, CN), and p-CREB-S133pAb (rabbit anti-human polyclonal antibody, 1:1600 dilution; AP0333, ABclonal, CN) proteins, according to the manufacturer's instructions. HRP-conjugated secondary antibody and DAB kit (Dako, Agilent Technologies, USA) were used to visualize antibody binding. Immunostaining reactivity was observed by using light microscopy (Olympus BX-53 with CCD DP73). The optical density value was analyzed with the Motic Med 6.0 analysis system.

2.6. Immunofluorescence. Immunohistochemistry (IHC) was performed to detect the expression of CALCA (rabbit antihuman polyclonal antibody, 1:50 dilution; A11804, ABclonal, CN), CALCB (rabbit antihuman polyclonal antibody, 1:200 dilution; A5523, ABclonal, CN), AKT (rabbit antihuman polyclonal antibody, 1:200 dilution; AB105, ABclonal, CN), p-AKT1-S473mAb (rabbit antihuman polyclonal antibody, 1:100 dilution; AP0637, ABclonal, CN), CREB (rabbit antihuman polyclonal antibody, 1:100 dilution; A10826, ABclonal, CN), and p-CREB-S133pAb (rabbit anti-human polyclonal antibody, 1:100 dilution; AP0333, ABclonal, CN) proteins, according to the manufacturer's instructions. The secondary antibody was rhodamine (TRI-TC)-conjugated goat anti-rabbit IgG or FITC-labeled goat anti-rabbit IgG. Nuclei were stained with DAPI solution.

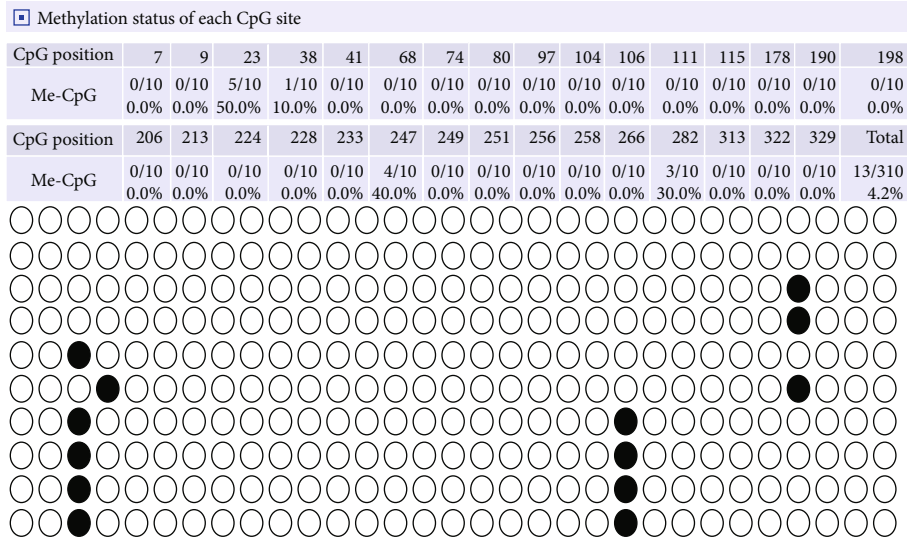
2.7. Western Blot Analyses. Proteins from the pancreas of patients, CGRP-KO rats, and age-matched littermates were separated on 4 to 12% Tris-glycine gels and transferred to nitrocellulose membranes. Membranes were probed with

antibodies directed against CALCA (rabbit anti-human polyclonal antibody, 1:100 dilution; A11804, ABclonal, CN), CALCB (rabbit anti-human polyclonal antibody, 1:3200 dilution; A5523, ABclonal, CN), AKT (rabbit anti-human polyclonal antibody, 1:3200 dilution; AB105, ABclonal, CN), p-AKT1-S473mAb (rabbit anti-human polyclonal antibody, 1:1600 dilution; AP0637, ABclonal, CN), CREB (rabbit anti-human polyclonal antibody, 1:1600 dilution; A10826, ABclonal, CN), and p-CREB-S133pAb (rabbit anti-human polyclonal antibody, 1:1600 dilution; AP0333, ABclonal, CN), and β -actin primary antibody (1:1000) was added and incubated overnight at 4°C. After washing with TBST for 10 min (3 times), the membrane was incubated with the corresponding secondary antibody (1:1000) and kept at room temperature for 2 h. After washing with TBST for 10 min (3 times), ECL developing solution (Beyotime, Shanghai, China, FFN02) was added, and development was carried out with a Bio-Rad gel imager to preserve the image.

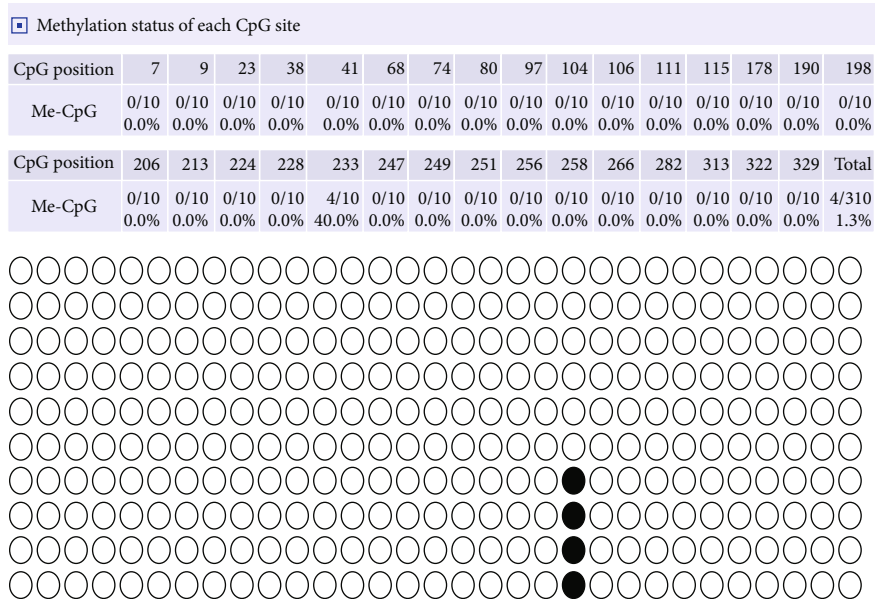
2.8. Statistics. Statistical differences between groups were assessed by the nonparametric Mann-Whitney *U*-test for two groups and the Kruskal-Wallis test for more than two groups. Spearman's rank correlation coefficient estimated the degree of association between two variables. Significance was calculated at $P < 0.05$ by GraphPad Prism 5 (La Jolla, CA).

3. Results

3.1. CGRP Methylation Was Validated by Targeted Pyrosequencing Assays. Pyrosequencing was performed on the pancreatic ductal adenocarcinoma tissues, paracancer tissues, peripheral blood of the patients with pancreatic ductal adenocarcinoma, and healthy controls. It was found that



(a)



(b)

FIGURE 2: Continued.

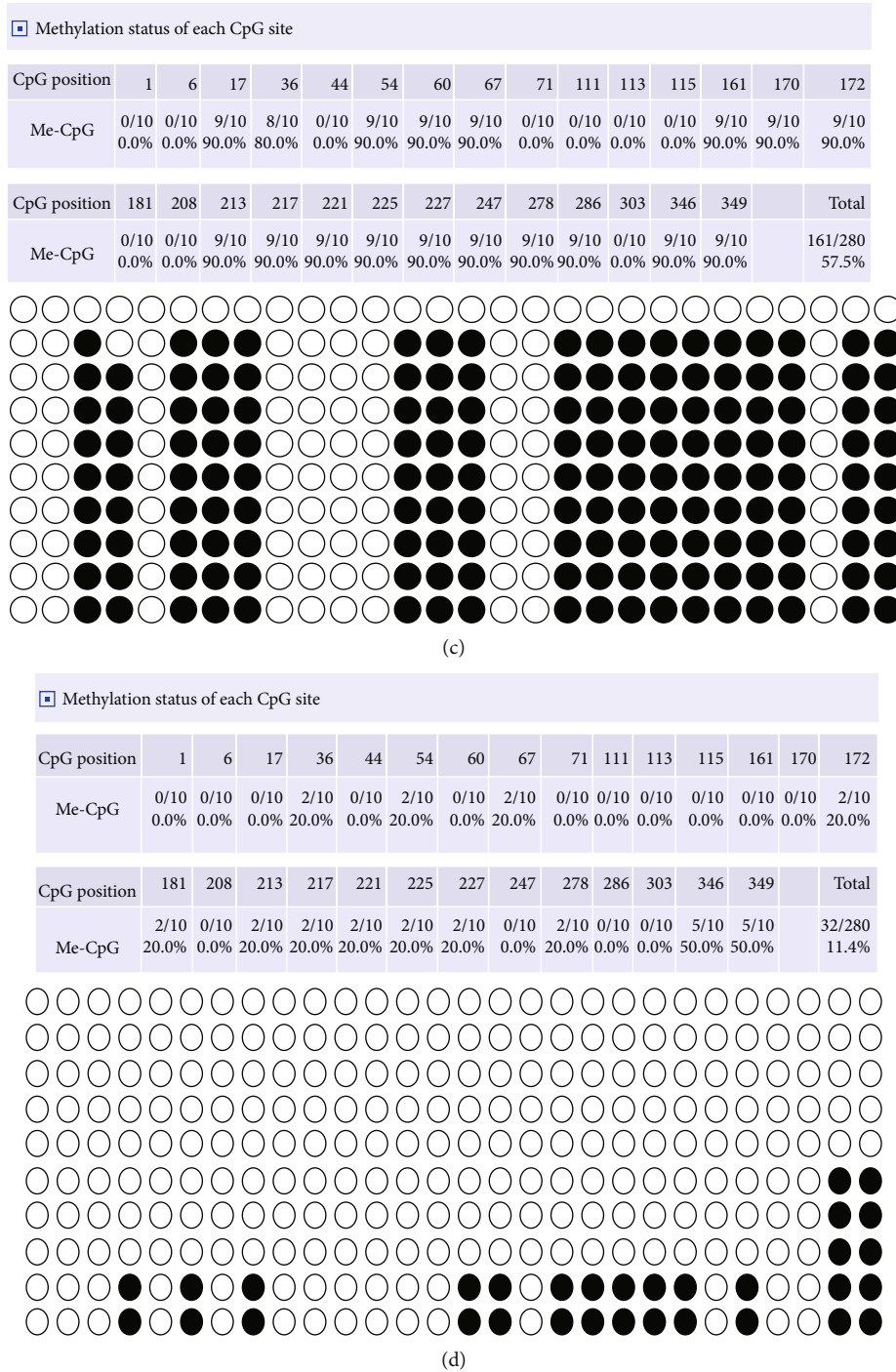
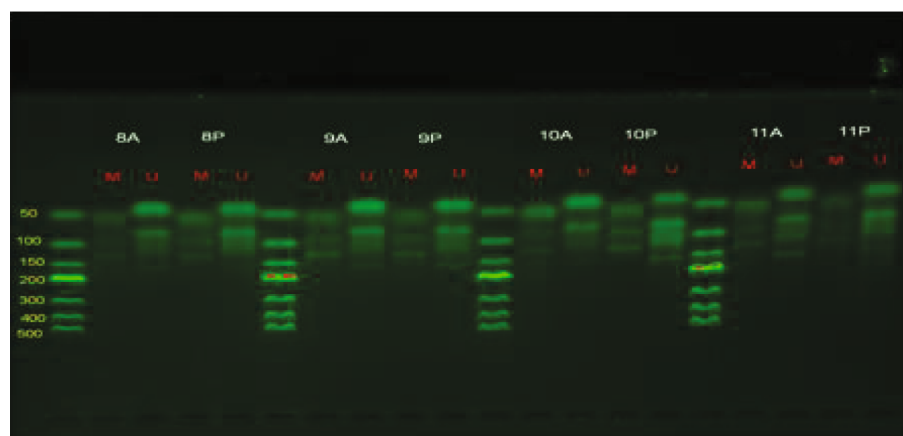


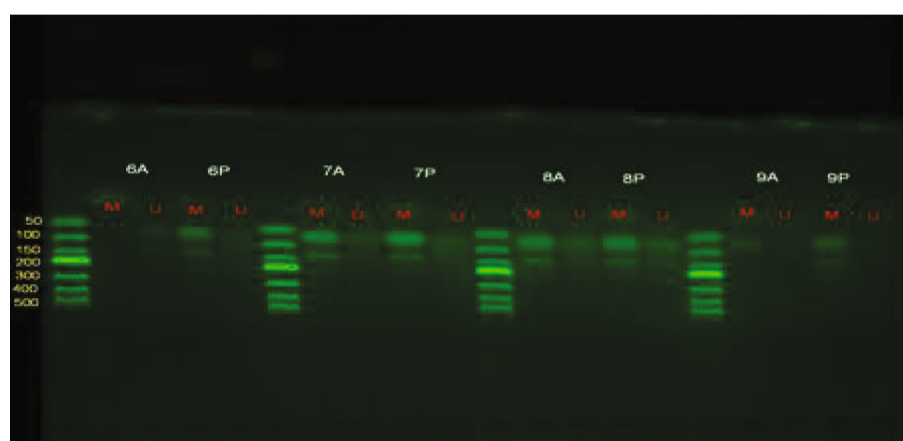
FIGURE 2: Detection of CGRP methylation by bisulfite sequencing PCR (BSP) in pancreatic cancer: (a) CALCA sequencing after pyrobisulfite modification in pancreatic cancer tissues; (b) CALCA sequencing after pyrobisulfite modification of the corresponding pancreatic cancer paratissue; (c) CALCB sequencing after pyrobisulfite modification in pancreatic cancer tissues; (d) CALCB sequencing after pyrobisulfite modification of the corresponding pancreatic cancer paratissue.

the mean percentage of CpG island methylation in the CALCA promoter region in tissues of pancreatic ductal adenocarcinoma (13.14%) was significantly higher than that in paracancer tissues (3.00%, $P = 0.0035$) (Figures 1(a) and 1(b)). However, the mean percentage of CpG island methylation in CALCB was 13.57% in pancreatic cancer which is significantly higher than that in paracancer tissues

(4.29%, $P = 0.005$) (Figures 1(c) and 1(d)). At the whole blood level, there was no statistically significant difference in the percentage of CpG island methylation in the CALCA ($P = 0.1174$) (Figures 1(e) and 1(f)) and the CALCB ($P = 0.4481$) (Figures 1(g) and 1(h)) promoter region between the patients with pancreatic cancer and normal controls.



(a)



(b)

FIGURE 3: Detection of CGRP methylation by methylation-specific PCR (MSP): (a) CpG island methylation of CALCA was found by MSP electrophoresis in pancreatic cancer tissue. A: carcinoma; P: paracancer; M: methylation (target fragment: 132 bp); U: nonmethylation (target fragment: 158 bp). (b) CpG island methylation of CALCB was found by MSP electrophoresis in pancreatic cancer tissue. A: carcinoma; P: paracancer; M: methylation (target fragment: 143 bp); U: nonmethylation (target fragment: 105 bp). There is only one band of M in complete methylation, two bands of M and U in partial methylation, and only one band of U in nonmethylation.

3.2. Detection of CGRP Methylation by Bisulfite Sequencing PCR (BSP). There were thirty CpG island sites in the promoter region of CALCA, with a methylation percentage of 4.2% in pancreatic cancer (Figure 2(a)) and 0.7% in paracancer tissues (Figure 2(b)) determined by BSP. Meanwhile, there were twenty-eight CpG island sites in the CALCB promoter region, with a methylation percentage of 57.5% in pancreatic cancer (Figure 2(c)) and 11.4% in paracancer tissues (Figure 2(d)) determined by BSP. The level of CGRP methylation in pancreatic ductal adenocarcinoma was higher than that in paracancer.

3.3. Detection of CGRP Methylation by Methylation-Specific PCR (MSP). CpG island methylation of CALCA was found in 85.71% (54/63) pancreatic ductal adenocarcinoma tissues. However, there was only 57.14% (36/63) found in paracancer tissues. Among the pancreatic ductal adenocarcinoma tissues, 39 cases presented complete methylation of CALCA (61.90%), and 15 cases presented partial methylation (23.81%). However, in paracancer tissues, the complete

methylation of CALCA was observed in only two cases (3.17%), partial methylation in 34 paracancer (53.97%), and no methylation in 20 paracancer (31.75%) (Figure 3(a)).

For CALCB, there were 88.89% (56/63) patients showing methylation in the CpG island in pancreatic ductal adenocarcinoma, while only 46.03% (29/63) patients showed methylation in the paracancer tissue. In pancreatic ductal adenocarcinoma, 32 patients showed complete methylation of CALCB (50.79%), and 24 patients showed partial methylation (38.10%). In paracancer tissues, partial methylation of CALCB was observed in 29 paracancer (46.03%), and no methylation was observed in 31 paracancer (49.21%) (Figure 3(b)). The results of MSP indicated that the level of CGRP methylation in pancreatic ductal adenocarcinoma was higher than that in paracarcinoma.

3.4. Expression of CGRP in Pancreatic Cancer. Both CALCA (α CGRP) and CALCB (β CGRP) showed lower expression in pancreatic ductal adenocarcinoma tissues than those in normal tissues far away from carcinoma ($P < 0.05$)

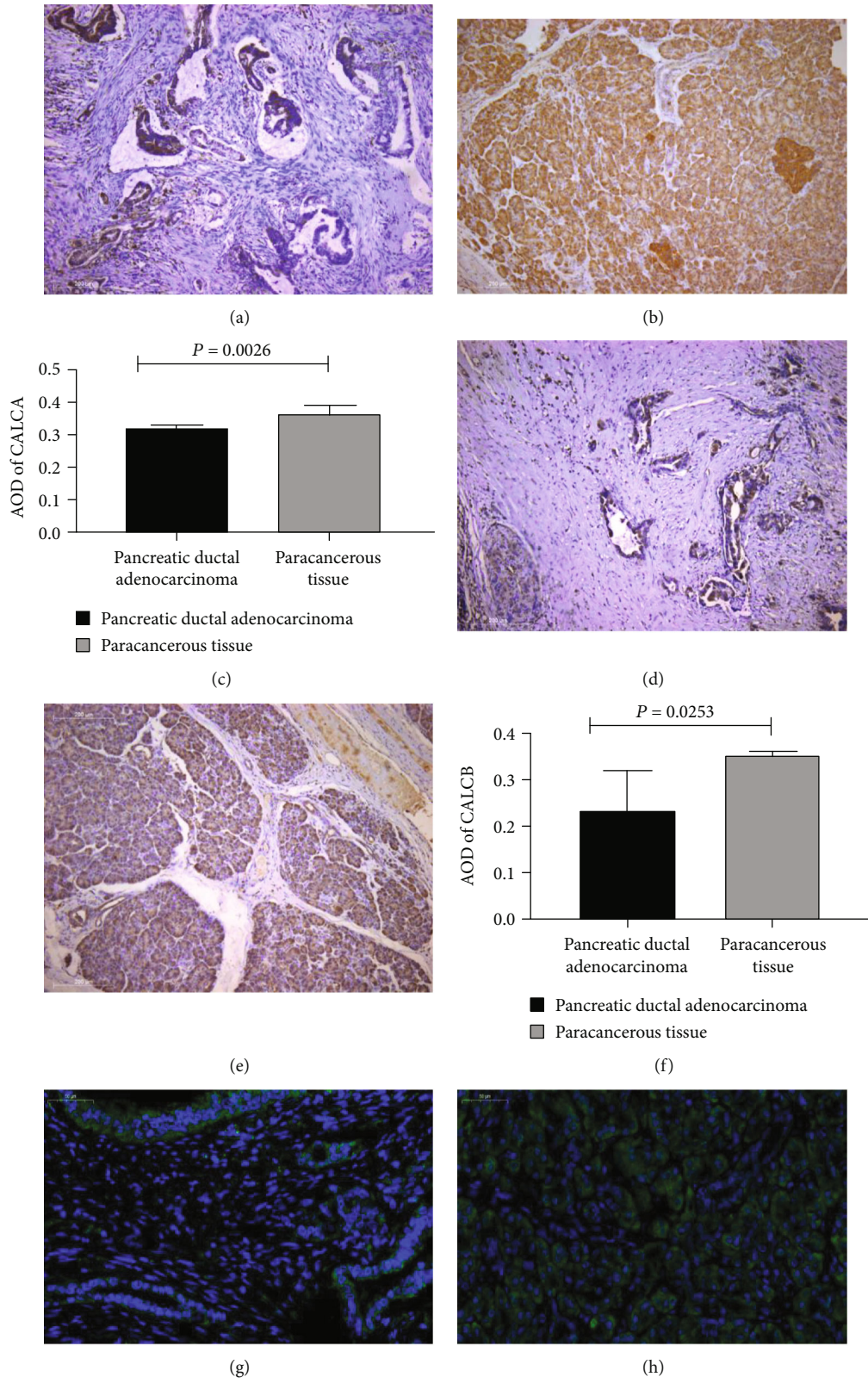


FIGURE 4: Continued.

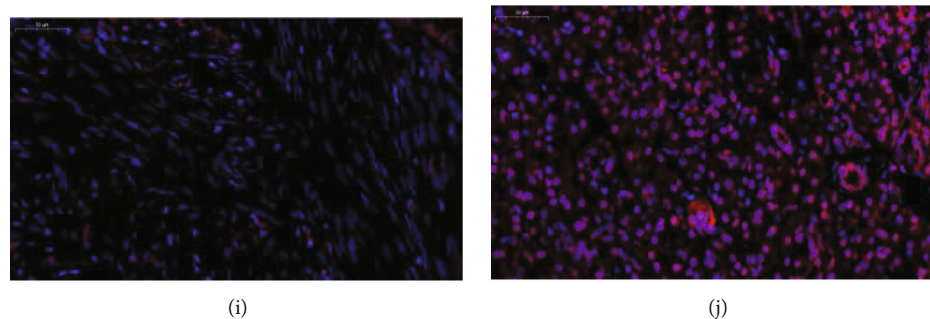


FIGURE 4: Expression of CGRP in pancreatic cancer and adjacent tissues: (a) expression of CALCA in pancreatic cancer tissues (IHC, $\times 100$); (b) expression of CALCA in paracancer tissues (IHC, $\times 100$); (c) differences of CALCA expression between pancreatic cancer tissues and adjacent tissues (IHC, $\times 100$); (d) expression of CALCB in pancreatic cancer tissues (IHC, $\times 100$); (e) expression of CALCB in paracancer tissues (IHC, $\times 100$); (f) differences in CALCB expression between pancreatic cancer tissues and adjacent tissues (IHC, $\times 100$); (g) expression of CALCA in pancreatic cancer tissues (immunofluorescence, $\times 400$); (h) expression of CALCA in paratissue (immunofluorescence, $\times 400$); (i) expression of CALCB in pancreatic cancer tissues (immunofluorescence, $\times 400$); (j) expression of CALCB in paracancer tissues (immunofluorescence, $\times 400$).

(Figures 4(a)–4(f)). Consistently, immunofluorescence also showed that the two subtypes of CGRP were lower expressed in pancreatic ductal adenocarcinoma tissues than those in normal pancreatic tissues (Figures 4(g)–4(j)).

3.5. AKT-CREB Pathway Changes in the Case of CGRP Methylation Validated by Western Blot. CALCA, CALCB, p-CREB/CREB, and p-AKT/AKT in pancreatic ductal adenocarcinoma tissues were downregulated compared with the corresponding paracancer tissues ($P < 0.001$) (Figures 5(a)–5(d)). The expression of p-AKT/AKT and p-CREB/CREB in the pancreatic tissue of CGRP-KO rats was downregulated compared with the wild type ($P < 0.05$) (Figures 5(e)–5(g)).

3.6. Immunohistochemical Staining to Verify AKT-CREB Pathways. The results of immunohistochemistry showed that the expression of AKT ($P = 0.0123$), p-AKT ($P = 0.0357$), CREB ($P = 0.0473$), and p-CREB ($P = 0.0256$) in pancreatic ductal adenocarcinoma was lower than that of paracarcinoma (Figure 6).

In vivo, AKT ($P = 0.0008$), p-AKT ($P = 0.0026$), CREB ($P = 0.0399$), and p-CREB ($P = 0.0256$) in the pancreatic tissue of CGRP-KO rats were lower than those of the wild type (Figure 6).

3.7. The Relationship between CpG Island Methylation in CGRP Promoter Region and Pancreatic Cancer. The hypermethylation of CpG island in the CGRP promoter region leads to low expression of CGRP, which affects the AKT-CREB pathway, thus promoting the development of pancreatic cancer (Figure 7).

4. Discussion

Pyrosequencing showed that methylation of CGRP in pancreatic ductal adenocarcinoma was significantly higher than that in paracancer. BSP and MSP also showed that the methylation level of CpG islands in the promoter region of CGRP in pancreatic cancer tissues was higher than that in paracancerous, indicating that CGRP hypermethylation plays an

important role in the development of pancreatic cancer. However, the results of peripheral blood pyrosequencing demonstrated that there was no significant difference in CGRP methylation between pancreatic cancer patients and normal controls, indicating that CGRP methylation had tissue and organ specificity.

Immunohistochemical staining and immunofluorescence showed that the expression of CGRP in pancreatic cancer tissues was significantly reduced compared with normal pancreatic tissues. Therefore, we speculated that the hypermethylation of CGRP caused the low expression of CGRP and promoted the development of pancreatic cancer. In order to further explore the relationship between hypermethylation or low expression of CGRP and pancreatic cancer, we constructed CGRP-KO models to further explore the function of CGRP.

It was reported that CGRP has a wide range of biological activities, and lower expression of CGRP can promote tumor growth through its ability to promote angiogenesis [12, 13]. The best-known function of CGRP is its effect on the peripheral vasculature. Also, it has been known to modulate the neuromuscular junctions by inhibiting the expression of acetylcholinesterase, which is involved in inflammation within the airways, gastric secretions, and intestinal mobility [12, 13]. It may dampen the immune response primarily by modifying antigen presentation in a variety of antigen-presenting cells and stimulating naive T cells in the primary immune response [14–16]. Tumor development depends on the tumor vascular network to provide adequate oxygen and nutrients, and tumor angiogenesis depends on highly complex growth factor signaling, endothelial cell (EC) proliferation, and other functions [14]. Moreover, CGRP could block the cell cycle from G0/G1 phase to S phase, which may be an important reason for its involvement in tumorigenesis [15, 16]. However, the mechanism by which CGRP deficiency causes pancreatic cancer is not clear.

Protein kinase B (PKB/AKT) plays an important role in carcinogenesis and cell growth control [10, 17], and CGRP activates AKT, which phosphorylates CREB at Ser133 and regulates CREB-mediated gene transcription [18, 19]. The

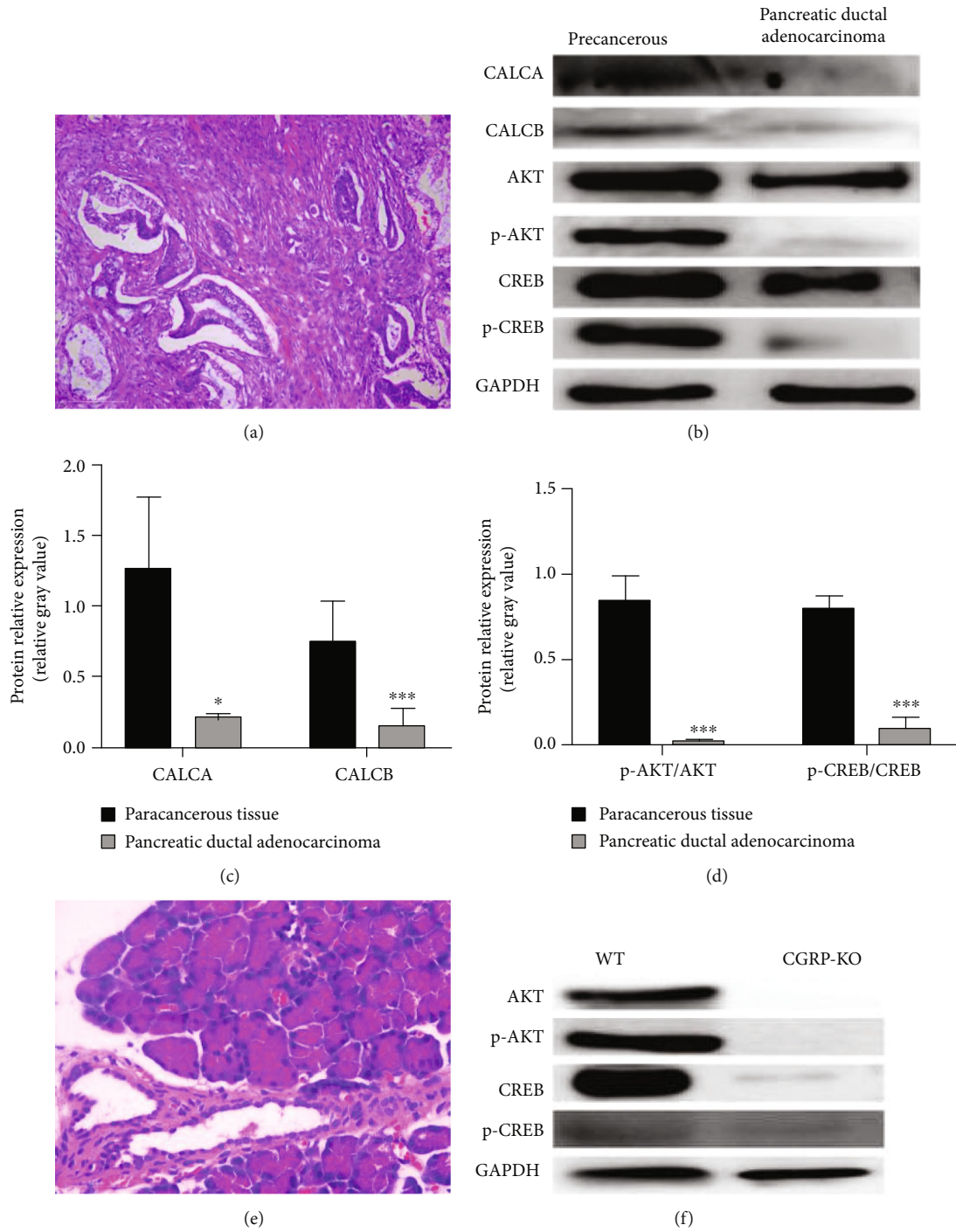
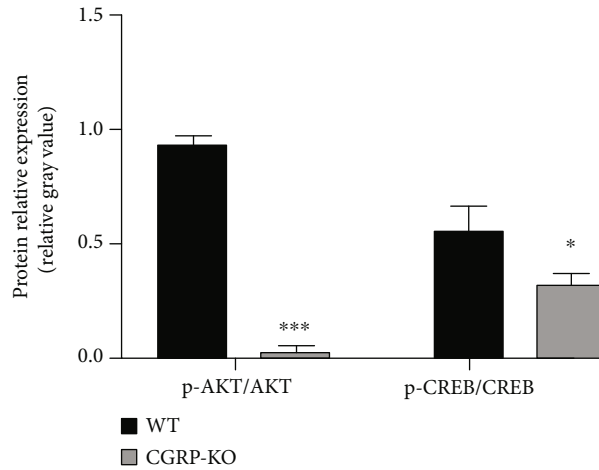


FIGURE 5: Continued.



(g)

FIGURE 5: The possible mechanism of hypermethylation of CGRP promotes the development of pancreatic ductal adenocarcinoma: (a) histopathology of pancreatic ductal adenocarcinoma; (b) Western blot results of pancreatic ductal adenocarcinoma; (c, d) Western blot and grayscale analysis of pancreatic ductal adenocarcinoma; (e) H&E staining of pancreatic tissue from CGRP-KO rat; (f) Western blot results of pancreatic tissue from CGRP-KO rat; (g) Western blot and grayscale analysis of pancreatic tissue from CGRP-KO rat.

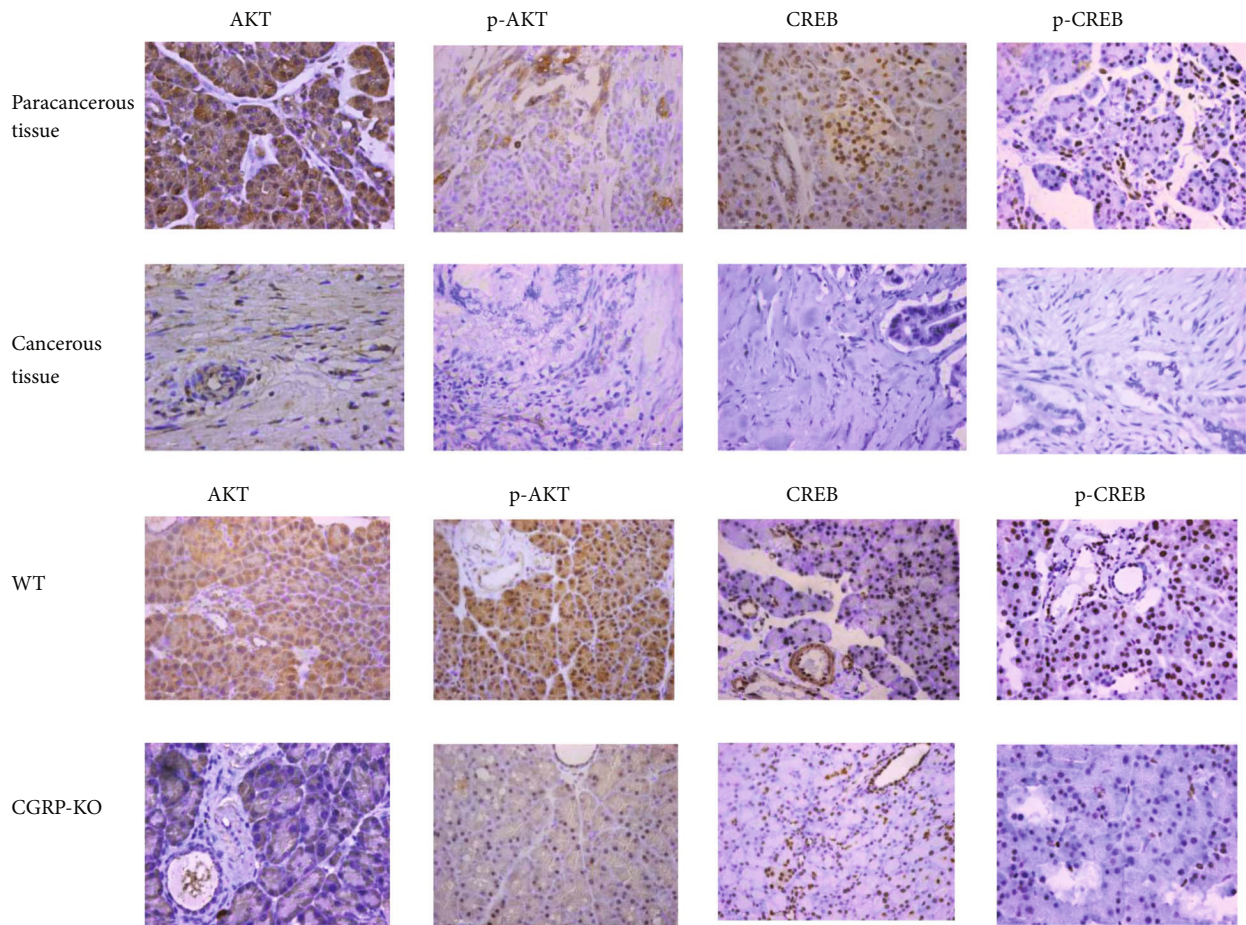


FIGURE 6: Immunohistochemical staining to verify AKT-CREB pathways affected by CGRP deficiency.

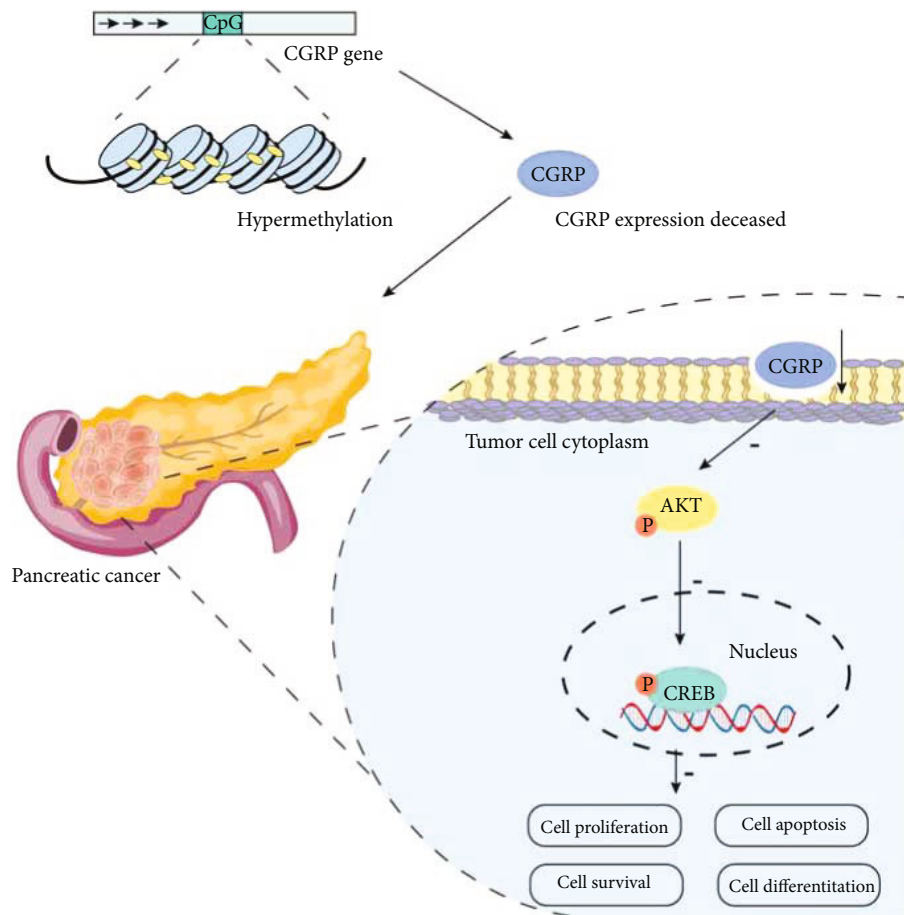


FIGURE 7: Relationship between CpG island methylation in CGRP and the occurrence and development of pancreatic cancer.

AKT-CREB signaling pathway is involved in cell proliferation, apoptosis, differentiation, and survival, and it affects the occurrence and development of tumors [20, 21]. In this study, Western blot results of pancreatic cancer tissues showed that the expression levels of p-AKT/AKT and p-CREB/CREB were both lower than paracancer, and the results were verified by the CGRP knockout model. To further confirm it, we observed downregulation of both AKT and CREB proteins in pancreatic cancer tissue. The deregulated protein expression of the AKT-CREB pathway was also found in CGRP-KO rats.

Data Availability

The data used to support the findings of this study are currently under embargo while the research findings are commercialized. Requests for data, 12 months after publication of this article, will be considered by the corresponding authors.

Ethical Approval

All experimental procedures in animal work were approved by the Ethical Committee of Fujian Medical University. This study was carried out in accordance with the recommendations of the Medical ethics committee of the First Affiliated Hospital of Fujian Medical University. The protocol was

approved by the Medical ethics committee of the First Affiliated Hospital of Fujian Medical University [038].

Disclosure

The funding sources played a key supportive role in sample collection, molecular analysis of patient samples, and bioinformatic analysis.

Conflicts of Interest

The authors have no competing interests to declare.

Authors' Contributions

Q.-C.L., F.G., and S.Z. planned the project. Q.-C.L., J.-W.W., and F.G. conceived and designed the study. G.-Z.L., X.-Q.F., and Q.-C.L. performed the sample collection. S.-R.H., J.-W.W., W.L., X.-T.L., Y.-J.G., and Q.-C.L. performed immunohistochemistry. Q.-C.L., W.L., and X.-T.L. participated in the *in vivo* procedures. Q.-C.L., F.G., and S.Z. performed the expression analysis. Q.-C.L., F.G., and S.Z. analyzed the data and drafted the manuscript. All authors reviewed the manuscript and approved the final version. Feng Gao, Guozhong Liu, and Jingwen Wang are co-first authors. Feng

Gao, Guozhong Liu and Jingwen Wang contributed equally to this work.

Acknowledgments









The authors sincerely thank the participants for their help and willingness to take part in this study. This work was supported by the National Natural Science Foundation of China (nos. 81572442, 81871293, and 81800070), Medical innovation in Fujian Province (2019-CX-27), Youth Fund of Fujian Provincial Department of Health (2019-1-41 and 2019-1-46), and Fujian Provincial Maternity and Children's Health Hospital Foundation (YCXM19-28).

References

- [1] J. Kleeff, M. Korc, M. Apte et al., "Pancreatic cancer," *Nature Reviews Disease Primers*, vol. 2, no. 1, article 16022, 2016.
- [2] W. Chen, R. Zheng, P. D. Baade et al., "Cancer statistics in China, 2015," *CA: a Cancer Journal for Clinicians*, vol. 66, no. 2, pp. 115–132, 2016.
- [3] T. Jenuwein and C. D. Allis, "Translating the histone code," *Science*, vol. 293, no. 5532, pp. 1074–1080, 2001.
- [4] A. Bird, "DNA methylation patterns and epigenetic memory," *Genes & Development*, vol. 16, no. 1, pp. 6–21, 2002.
- [5] L. Schneider, W. Hartwig, T. Flemming et al., "Protective effects and anti-inflammatory pathways of exogenous calcitonin gene-related peptide in severe necrotizing pancreatitis," *Pancreatology*, vol. 9, no. 5, pp. 662–669, 2009.
- [6] D. L. Hay, C. S. Walker, and D. R. Poyner, "Adrenomedullin and calcitonin gene-related peptide receptors in endocrine-related cancers: opportunities and challenges," *Endocrine-Related Cancer*, vol. 18, no. 1, pp. C1–14, 2011.
- [7] M. E. Carter, M. E. Soden, L. S. Zweifel, and R. D. Palmiter, "Genetic identification of a neural circuit that suppresses appetite," *Nature*, vol. 503, no. 7474, pp. 111–114, 2013.
- [8] Z. Du, H. Zhang, Q. Chen, Y. Gao, and B. Sun, "Intranasal calcitonin gene-related peptide protects against focal cerebral ischemic injury in rats through the Wnt/ β -catenin pathway," *Medical Science Monitor*, vol. 24, pp. 8860–8869, 2018.
- [9] M. Naghashpour and G. Dahl, "Sensitivity of myometrium to CGRP varies during mouse estrous cycle and in response to progesterone," *American Journal of Physiology. Cell Physiology*, vol. 278, no. 3, pp. C561–C569, 2000.
- [10] Y. Liu, S. C. Zhang, J. Xue et al., "CGRP reduces apoptosis of DRG cells induced by high-glucose oxidative stress injury through PI3K/AKT induction of heme oxygenase-1 and Nrf-2 expression," *Oxidative Medicine and Cellular Longevity*, vol. 2019, Article ID 2053149, 9 pages, 2019.
- [11] X. T. Lv, F. Gao, S. Y. Zhang et al., "Maladjustment of β -CGRP/ α -CGRP regulation of AQP5 promotes transition of alveolar epithelial cell apoptosis to pulmonary fibrosis," *Journal of Interferon & Cytokine Research*, vol. 40, no. 8, pp. 377–388, 2020.
- [12] C. Yallampalli, Y. L. Dong, and S. J. Wimalawansa, "Calcitonin gene-related peptide reverses the hypertension and significantly decreases the fetal mortality in pre-eclampsia rats induced by N^G-nitro-L-arginine methyl ester," *Human Reproduction*, vol. 11, no. 4, pp. 895–899, 1996.
- [13] K. A. Petersen, S. Birk, H. Doods, L. Edvinsson, and J. Olesen, "Inhibitory effect of BIBN4096BS on cephalic vasodilatation induced by CGRP or transcranial electrical stimulation in the rat," *British Journal of Pharmacology*, vol. 143, no. 6, pp. 697–704, 2004.
- [14] C. Schaeffer, D. Vandroux, L. Thomassin, P. Athias, L. Rochette, and J. L. Connat, "Calcitonin gene-related peptide partly protects cultured smooth muscle cells from apoptosis induced by an oxidative stress via activation of ERK1/2 MAPK," *Biochimica et Biophysica Acta (BBA) - Molecular Cell Research*, vol. 1643, no. 1-3, pp. 65–73, 2003.
- [15] Y. Haibe, M. Kreidieh, H. El Hajj et al., "Resistance mechanisms to anti-angiogenic therapies in cancer," *Frontiers in Oncology*, vol. 10, p. 221, 2020, eCollection 2020.
- [16] Q. C. Liu, F. Chen, C. Y. Wu et al., "CALCB splice region pathogenic variants leading to plasma cell neurotropic enrichment in type 1 autoimmune pancreatitis," *Cell Death Dis.*, vol. 8, no. 2, article e2591, 2017.
- [17] G. Xu, W. Zhang, P. Bertram, X. F. Zheng, and H. McLeod, "Pharmacogenomic profiling of the PI3K/PTEN-AKT-mTOR pathway in common human tumors," *International Journal of Oncology*, vol. 24, no. 4, pp. 893–900, 2004.
- [18] X. Huang, J. Zhang, L. Lu et al., "Cloning and expression of a novel CREB mRNA splice variant in human testis," *Reproduction*, vol. 128, no. 6, pp. 775–782, 2004.
- [19] J. Machado, L. H. Manfredi, W. A. Silveira et al., "Calcitonin gene-related peptide inhibits autophagic-lysosomal proteolysis through cAMP/PKA signaling in rat skeletal muscles," *The International Journal of Biochemistry & Cell Biology*, vol. 72, pp. 40–50, 2016.
- [20] Z. Zhao, P. Zhang, W. Li et al., "Pegylated recombinant human arginase 1 induces autophagy and apoptosis via the ROS-Activated AKT/mTOR pathway in bladder cancer cells," *Oxidative Medicine and Cellular Longevity*, vol. 2021, no. 2, pp. 1–13, 2021.
- [21] Y. Wang, X. Xiao, J. Zhang et al., "A complex network of factors with overlapping affinities represses splicing through intronic elements," *Nature Structural & Molecular Biology*, vol. 20, no. 1, pp. 36–45, 2013.

Research Article

Exosomal lncRNA PVT1/VEGFA Axis Promotes Colon Cancer Metastasis and Stemness by Downregulation of Tumor Suppressor miR-152-3p

Shiue-Wei Lai ^{1,2}, Ming-Yao Chen ^{3,4}, Oluwaseun Adebayo Bamodu ⁵,
Ming-Shou Hsieh ⁵, Ting-Yi Huang ⁵, Chi-Tai Yeh ^{5,6}, Wei-Hwa Lee ⁷,
and Yih-Giun Cherng ^{8,9}

¹Division of Hematology-Oncology, Department of Internal Medicine, Tri-Service General Hospital, National Defense Medical Center, Taipei, Taiwan

²Department of Internal Medicine, Tri-Service General Hospital Penghu Branch, Penghu, Taiwan

³Division of Gastroenterology and Hepatology, Department of Internal Medicine, Taipei Medical University-Shuang Ho Hospital, New Taipei City, Taiwan

⁴Division of Gastroenterology and Hepatology, Department of Internal Medicine, School of Medicine, College of Medicine, Taipei Medical University, Taipei, Taiwan

⁵Department of Medical Research & Education, Taipei Medical University-Shuang Ho Hospital, New Taipei City 235, Taiwan

⁶Department of Medical Laboratory Science and Biotechnology, Yuanpei University of Medical Technology, Hsinchu 300, Taiwan

⁷Department of Pathology, Taipei Medical University-Shuang Ho Hospital, New Taipei City, Taiwan

⁸Department of Anesthesiology, Shuang ho Hospital, Taipei Medical University, New Taipei City, Taiwan

⁹Department of Anesthesiology, School of Medicine, College of Medicine, Taipei Medical University, Taipei, Taiwan

Correspondence should be addressed to Yih-Giun Cherng; stainless@s.tmu.edu.tw

Shiue-Wei Lai and Ming-Yao Chen contributed equally to this work.

Received 19 March 2021; Revised 22 May 2021; Accepted 21 June 2021; Published 20 July 2021

Academic Editor: Jayeeta Ghose

Copyright © 2021 Shiue-Wei Lai et al. This is an open access article distributed under the Creative Commons Attribution License, which permits unrestricted use, distribution, and reproduction in any medium, provided the original work is properly cited.

Background. Treating advanced colon cancer remains challenging in clinical settings because of the development of drug resistance and distant metastasis. Mechanisms underlying the metastasis of colon cancer are complex and unclear. **Methods.** Computational analysis was performed to determine genes associated with the exosomal long noncoding (lncRNA) plasmacytoma variant translocation 1 (PVT1)/vascular endothelial growth factor A (VEGFA) axis in patients with colon cancer. The biological importance of the exosomal lncRNA PVT1/VEGFA axis was examined in vitro by using HCT116 and LoVo cell lines and in vivo by using a patient-derived xenograft (PDX) mouse model through knockdown (by silencing of PVT1) and overexpression (by adding serum exosomes isolated from patients with distant metastasis (M-exo)). **Results.** The *in silico* analysis demonstrated that PVT1 overexpression was associated with poor prognosis and increased expression of metastatic markers such as VEGFA and epidermal growth factor receptor (EGFR). This finding was further validated in a small cohort of patients with colon cancer in whom increased PVT1 expression was correlated with colon cancer incidence, disease recurrence, and distant metastasis. M-exo were enriched with PVT1 and VEGFA, and both migratory and invasive abilities of colon cancer cell lines increased when they were cocultured with M-exo. The metastasis-promoting effect was accompanied by increased expression of Twist1, vimentin, and MMP2. M-exo promoted metastasis in PDX mice. *In vitro* silencing of PVT1 reduced colon tumorigenic properties including migratory, invasive, colony forming, and tumorsphere generation abilities. Further analysis revealed that PVT1, VEGFA, and EGFR interact with and are regulated by miR-152-3p. Increased miR-152-3p expression reduced tumorigenesis, where increased tumorigenesis was observed when miR-152-3p expression was downregulated. **Conclusion.** Exosomal PVT1 promotes colon cancer metastasis through its association with EGFR and VEGFA expression. miR-152-3p targets both PVT1 and VEGFA, and this regulatory pathway can be explored for drug development and as a prognostic biomarker.

1. Introduction

Colon cancer is one of the most prevalent malignancies globally and has consistently ranked in the top three leading causes of cancer-associated death [1]. Treating distant metastasis is one of the most challenging tasks in clinical practice. The liver (approximately 20%–30%) and lungs are the most frequently observed metastatic sites in patients with colon cancer [2]. Despite advancements in the development of chemotherapeutic and targeted therapeutic agents over the past decade, the treatment of metastatic colon cancer remains highly difficult. Therefore, obtaining a better understanding of the molecular and signaling mechanisms involved in the metastatic progression of colon cancer, especially epithelial-to-mesenchymal transition (EMT), can help in designing and developing effective therapeutic agents.

Exosomes or extracellular vesicles are nanosized (30–150 nm) cargos produced by cells for intracellular communication [3]. Because of the presence of proteins, lipids, and nucleic acids in exosomes [3] and the functional attributes of exosomes in tumorigenesis, they have received increasing attention. Accumulating evidence suggests that cancer cells secrete exosomes enriched with various signaling molecules to promote tumor initiation, angiogenesis, distant metastasis, and the development of drug resistance [3]. Various studies have confirmed that noncoding RNAs (ncRNAs) are involved in the development of various cancers through regulation of cell differentiation, proliferation, apoptosis, necrosis, and autophagy [4]. In the past few decades, six ncRNAs have been determined to possess no significant protein-coding potential. Two main members of the ncRNA family, long ncRNA (lncRNA) and microRNA (miRNA), were identified to play key roles in regulating the physiology and pathophysiology of cancer [5]. The structure of lncRNA is similar to that of mRNA except that it contains >200 nucleotides; additionally, some lncRNAs have poly(A) tails. As a miRNA sponge, lncRNAs can negatively regulate miRNA expression through sequence-specific binding. By contrast, miRNAs can also negatively regulate the expression of lncRNAs [6]. A recent study revealed that colon cancer cells secrete exosomes containing an ncRNA, namely, miR-193a, which interacts with major vault protein to promote cancer progression [7]. Moreover, these exosomes can be detected in serum, thus making them ideal prognostic markers. Furthermore, although ncRNA molecules were once considered to be evolutionary remnants, they are now understood to play vital roles in every aspect of cellular activity by performing crucial regulatory functions and providing specificity in gene expression. In this study, we examined plasmacytoma variant translocation 1 (PVT1), an lncRNA locus, which has been identified as a candidate oncogene in several types of tumor, including colon cancer tumors [8]. The abnormal proliferation of tumor cells is a crucial feature that distinguishes tumor tissue from normal tissues. Abnormal proliferation of cells is characterized by cell cycle changes, apoptosis inhibition, and disrupted energy metabolism. PVT1, as a potential oncogene, can promote tumor proliferation [9]. PVT1 is a crucial oncogenic lncRNA that is highly expressed in cancer cells. Multiple miRNA response elements have been

found on PVT1, and PVT1 can bind to specific miRNAs, thereby silencing them and upregulating the expression of certain proteins, ultimately affecting tumor cell proliferation, invasion, and drug resistance [10, 11]. At present, the carcinogenic effect of PVT1 has been confirmed in various cancers such as gallbladder, non-small-cell lung, and colon cancers [12–14]. Therefore, the invasive and metastatic abilities of cancer cells are assessed for cancer staging and prognosis. A study reported that PVT1 is involved in the EMT and distant metastasis of cancer cells as follows [15]. First, the adhesion between tumor cells and surrounding tissues changes and affects the cells and leads to the primary detachment of cells. Then, the degradation of the extracellular matrix occurs. Furthermore, modification of the cytoskeleton enhances the motility of cancer cells, thereby promoting angiogenesis in tumor tissues. In addition, PVT1 acts as a molecular sponge for miRNAs, which can be trimmed and processed into multiple miRNAs (miR-1204, 1205, 1206, 1207-3p, 1207-5p, and 1208) [10]. These miRNAs can regulate tumor development. For example, overexpression of miR-1207-5p reduces the expression of signal transducers and activators of transcription, thereby activating cyclin-dependent kinase inhibitors (CDKN)1A and CDKN1B that regulate the cell cycle and promote tumor cell proliferation [16].

An adequate understanding of the role of EMT and regulatory mechanisms through which EMT promotes distant metastasis in colon cancer remains elusive. EMT has been confirmed to result in distant metastasis and to cause cancer stemness [17, 18]. Therefore, characterizing key molecular players involved in EMT can provide insights into this process and its mechanisms. Notably, numerous EMT markers have been proposed, all of which converge toward angiogenesis, with vascular endothelial growth factor- (VEGF-) associated signaling playing a crucial role in enabling cancer cells to migrate from their primary niche to a secondary site [19]. In addition, EMT has been associated with the emergence of cancer stemness, the initiation of tumors, and the generation of drug-resistant clones [19–21]. Hence, identifying mechanisms or agents that inhibit the members of the VEGF-associated pathway may represent a means to reduce the incidence of distant metastasis. By using the sequencing technology, researchers have classified and sequenced more than 400 tumors based on microarray data obtained from a public data set [22]. These findings can help us analyze the clinical characteristics of colorectal cancer (such as the expression or inhibition of key genes and their effect on overall survival) and identify crucial prognostic markers.

In the present study, we first collected tissues from both healthy individuals and patients with distant metastatic colon cancer and determined that PVT1 expression was significantly increased in patients with metastatic colon cancer. In addition, by analyzing public databases, we determined that exosomes obtained from patients with metastatic colon cancer and patients with disease recurrence contained increased PVT1. Furthermore, we examined the potential of PVT1 to promote cancer development. We observed that PVT1 loss of function resulted in the suppression of colon tumorigenic and metastatic potential, evident in the suppression of colony formation, cell invasion, sphere formation, and related

protein expression *in vitro*. First, we demonstrated that exosomes obtained from patients with metastasis significantly enhanced the migratory and invasive abilities of human colon cancer cell lines HCT116 and LoVo in association with the increased expression of vascular endothelial growth factor A (VEGFA), vimentin, and MMP2. Notably, exosomes isolated from patients with metastatic colon cancer promoted metastasis in patient-derived *in vivo* xenograft mice (with nonmetastatic tumors). *In vitro* results indicated that PVT1-silenced HCT116 and LoVo cells exhibited significantly decreased tumorigenic and oncogenic properties, including decreased colony- and tumorsphere-forming abilities, as well as migratory and invasive potential. Finally, we explored the possible regulatory mechanism of PVT1 and observed that miR-152-3p, a tumor suppressor, contains binding sites at the 3'-UTR of PVT1 and VEGFA. We observed that the regulatory mechanism of the miR-152-3p/PVT1/VEGFA axis causes metastasis in colon cancer through the overexpression and inhibition of miR-152-3p in colon cells. Therefore, targeting this signaling axis can help in developing effective therapeutic agents against metastatic colon cancer.

2. Materials and Methods

2.1. Clinical Sample Collection and Preparation. Written informed consent for the collection of clinical samples was obtained from all participants, and this study was approved by the Medical Ethics Committee of Taipei Medical University-Joint Institutional Review Board (N202104054; Taipei, Taiwan). Serum samples were collected from healthy individuals (control) and patients with treatment-naive primary (P) or metastatic (M) colon cancer based on histological examinations (Table 1). Fresh tissues (tumor, adjacent nontumor, and colon metastasis) obtained from patients with colon cancer were processed within 20 min after resection. The samples were then analyzed and confirmed by two independent pathologists. Venous blood samples from patients were collected, and cell-free serum was isolated using a previously established protocol, which involves initial centrifugation at $1600 \times g$ for 10 min, followed by repeat centrifugation at $16000 \times g$ for 10 min at 4°C . Samples were either used for exosome isolation immediately or were stored at -80°C .

2.2. Cell Culture. The human colon cancer cell lines HCT116 (characteristics: derived from the primary colon ascendens tumor, TGF β 1+/TGF β 2+, suitable transfection host, and tumorigenic in nude/immunodeficient mice) and LoVo (characteristics: derived from metastatic colon cancer, Dukes' type C, grade IV, colorectal adenocarcinoma, MYC+/KRAS+/HRAS+/NRAS+, suitable transfection host, and tumorigenic in immunodeficient mice) were obtained from the American Type Culture Collection (Manassas, VA, USA). The cells were recently authenticated through short tandem repeat profiling. Both the cell lines were maintained and passaged in RPMI-1640 medium (Gibco, Carlsbad, CA, USA) supplemented with 10% fetal bovine serum (Gibco) in a 5% CO₂ humidified incubator at 37°C until 90% conflu-

TABLE 1: Clinical table of metastatic patients that increased PVT1 expression and related information.

Clinicopathological variables	No.	PVT1		X^2	p value
		High	Low		
Age, years					
≤55	17	8	9	0.051	0.822
>55	23	10	13		
Gender					
Male	28	15	13	1.380	0.240
Female	12	4	8		
Tumor differentiation					
Well/moderately	19	9	10	3.536	0.060
Poorly	21	16	5		
Lymph node metastasis					
N0	15	5	10	2.667	0.102
N1–N2	25	15	10		
Distant metastasis					
M0	18	8	10	4.552	0.033
M1	22	17	5		
Primary stage					
I + II	13	6	7	4.000	0.045
III + IV	27	21	6		

ence. Supernatants were collected and centrifuged at $1600 \times g$ for 10 min, followed by repeat centrifugation at $16000 \times g$ for 10 min at 4°C , and then stored at -80°C until exosome extraction.

2.3. Isolation of Exosomes. The serum and culture medium samples were first filtered through a $0.45 \mu\text{m}$ pore polyvinylidene fluoride filter (Millipore, Darmstadt, Germany). ExoQuick solution (System Biosciences, Palo Alto, CA) was added to the serum samples and incubated at room temperature for 30 min, and ExoQuick-TC solution was added to the culture medium samples and incubated at 4°C for 12 h. Exosomes were sedimented and collected through centrifugation ($1500 \times g$, 30 min). The resultant exosome pellets were resuspended in $25 \mu\text{L}$ of phosphate-buffered saline (PBS).

2.4. Transmission Electron Microscopy. Exosomes were diluted to a final concentration of 0.5 mg/mL by using PBS. Exosomes were spotted onto a glow-discharged copper grid and then dried. The samples were stained with a drop of 1% phosphotungstic acid for 5 min and then dried. Morphological analysis of exosomes was performed using a transmission electron microscope (FEI Tecnai, Hillsboro, Oregon) at 200 keV.

2.5. RNA Preparation. Total RNA was isolated from the samples (tumor chunks and cell lines) by using TRIzol reagent (Life Technologies, Carlsbad, CA, USA) and quantified using NanoDrop (Thermo Fisher Scientific, Waltham, MA, USA). RNA from exosomes was extracted using an miRNeasy micro kit (QIAGEN, Hilden, Germany). In brief, the exosome suspension ($20 \mu\text{L}$) was mixed with QIAzol lysis buffer

(700 μ L) and processed according to the manufacturer's protocol. The RNA samples were subsequently eluted with 25 μ L of RNase-free water (repeated twice with the same 25 μ L of RNase-free water to concentrate the samples). The RNA concentration in the samples was again determined using NanoDrop.

2.6. Real-Time Quantitative Reverse-Transcription Polymerase Chain Reaction. Reverse transcription of miRNAs and real-time quantitative reverse-transcription polymerase chain reaction- (qRT-PCR-) based quantification of miRNA levels were performed using the miDETECT A Track miRNA qRT-PCR Starter Kit (RiboBio, Tokyo, Japan). For PVT1 gene expression analysis, the first strand of cDNA was generated using a PrimeScript first-strand cDNA synthesis kit (TaKaRa, Tokyo, Japan). qRT-PCR was performed using the SYBR Premix Ex Taq II kit (Takara, Tokyo, Japan) on a CFX96 real-time PCR detection system (Bio-Rad, Hercules, CA). The qPCR primers used in this study are listed in Supplementary Table 1.

2.7. Migration and Invasion Assays. Colon cancer cells were seeded and cultured in six-well plates for 24 h. The cells were incubated with mitomycin (10 μ g/mL) for 1 h. A linear scratch was created through the cell monolayer by using a 200 μ L pipette tip. Cellular debris was removed, and the cells were allowed to migrate for 24–48 h. Gap healing was determined from micrographs taken before and after the wound creation under a microscope (Nikon, Japan). Migration distance was measured from images (three random fields) obtained at indicated time points. The gap size was subsequently analyzed using ImageJ software. The invasion assay was performed according to a previously established protocol. In brief, 3×10^5 colon cancer cells were seeded onto Matrigel (BD Biosciences, San Jose, CA, USA) in culture plate inserts (pore size: 8 μ m, Corning) in a serum-free medium. Three independent and random fields per well were photographed, and the number of cells in each field was counted. An average of three determinations was obtained for each chamber. Each invasion assay was performed a minimum of three times.

2.8. Tumor Spheroid Formation Assay. Colon cancer cells were transferred into serum-free low-adhesion culture plates containing Dulbecco's modified Eagle's medium/F-12 with N2 supplement (Invitrogen), 20 ng/mL of EGF, and 20 ng/mL of basic-FGF (stem cell medium; PeproTech, Rocky Hill, NJ, USA) for 2 weeks to allow tumorsphere formation. The spheres were counted under a microscope. The tumor ball formation efficiency was calculated as the ratio of the number of balls to the number of implanted cells.

2.9. Cell Transfection. Colon cancer cells (cell lines or clinical samples) were cultured and maintained as described in previous sections. Gene manipulation experiments, namely, PVT1 silencing experiments, were performed using the siRNA technique (Academia Sinica, Taiwan) according to the manufacturer's instructions. Reagents for the miR-152-3p mimic, inhibitor (oligonucleotides), si-PVT1, and their negative controls (si-NC) were purchased from RiboBio (Academia

Sinica, Taiwan), and transfection procedures were performed using Lipofectamine 2000 (Invitrogen, Carlsbad, CA, USA) according to the manufacturer's instructions. The transfected cells were maintained in RPMI-1640 medium (Gibco, Carlsbad, CA, USA) supplemented with 10% fetal bovine serum (Gibco) in a 5% CO₂-humidified incubator at 37°C. The cells were washed three times in PBS (pH 7.4) before transfection to remove the culture medium and serum.

2.10. Western Blot. Total cellular protein lysates from colon cancer cells were extracted using RIPA buffer (Millipore, Darmstadt, Germany), and the lysate concentration was determined using a BCA protein assay kit (Pierce, Rockford, IL, USA). Thirty micrograms of protein were dissolved in SDS-PAGE and transferred onto a PVDF membrane (Millipore, Darmstadt, Germany). After blocking at 37°C for 1 h, the membranes were immunoblotted with different antibodies at 4°C overnight. All antibodies were purchased from Cell Signaling Technology (Danvers, MA) unless otherwise specified. Epidermal growth factor receptor (EGFR) (#2232, 1:400), MMP2 (#13667, 1:300), vimentin (#5741, 1:500), Twist1 (#46702, 1:400), GAPDH (#D16H11, 1:2000), VEGFA (ab52917, 1:500, Abcam, USA), and exosomal markers CD9 (5G6, 1:200) and MCT1 (P14612, 1:500, Invitrogen, USA) were purchased from Novus Biologicals (Centennial, CO, USA).

2.11. In vivo Mouse Studies. Six 8-week-old female nonobese diabetic (NOD)/severe combined immunodeficient (SCID) mice obtained from BioLASCO Taiwan Co. Ltd. (Taipei, Taiwan) were bred under standard experimental pathogen-free conditions. All animal experiments were performed according to protocols approved by the experimental animal welfare committee of our institute (approval number: LAC-2020-0535). For the patient-derived xenograft experiment, pieces of tumor mass (approximately 0.05 cm³ each, obtained from a patient diagnosed as having colon cancer, and nonmetastatic) were subcutaneously implanted into NOD/SCID mice. Tumor growth (until the tumor became palpable) was allowed in tumor-bearing mice, and exosomes isolated from patients with lung metastasis (M-exo) or primary colon cancer (nonmetastatic, P-exo) were systematically injected through the lateral tail vein (20 μ g/mouse, 3 times/week, for 4 weeks); each group contained 10 mice. Tumor growth was monitored and measured using a standard caliper weekly. The tumor volume was determined using the following formula: tumor volume = (width)² \times length/2. Animals were humanely sacrificed following experiments, and their tumor and tissue samples were collected for further analyses.

2.12. Statistical Analysis. SPSS (version 13.0; SPSS Inc., Chicago, IL) was used to perform all statistical analyses. Each experiment was performed three times. All data in figures are expressed as the mean \pm standard deviation (SD). Comparisons between two groups were performed using the *t*-test. All statistical tests were two-sided, and *p* < 0.05 was considered significant. Continuous data were analyzed using the paired samples *t*-test or the Wilcoxon rank test. Categorical data were analyzed using the chi-square test or Fisher's

exact test. Survival analysis was estimated using the Kaplan–Meier method along with the log-rank test to calculate differences between the curves.

3. Results

3.1. PVT1 Is Highly Expressed in Colon Cancer Cells and Affects the Survival Rate. Recent studies have revealed PVT1 to be an oncogenic marker for multiple cancer types. Our analysis of a pan-cancer cohort from the Cancer Genome Atlas (TCGA) public cancer database showed that patients with colorectal cancer exhibited a higher PVT1 expression level (Figure 1(a)). We found that patients with colon cancer (GSE17537) with higher PVT1 expression had significantly shorter overall and disease-free survival durations (Figure 1(b)). Further analysis indicated that the expression of PVT1 in advanced colorectal cancer was more significant (Figure 1(c)). Because advanced colorectal cancer can be defined as colorectal cancer that metastasizes when it appears or recurs, we analyzed the difference in PVT1 expression between primary and metastatic tumors from the GSE49355 dataset. The results revealed that the expression level of PVT1 was higher in metastatic tumors (Figure 1(d)). Finally, we performed a correlation analysis between PVT1 and VEGFA data from the database of TCGA. The results indicated that PVT1 was positively correlated with VEGFA and the exosome biomarker MCT-1 (Figure 1(e)). These results suggest a relationship between the exosomal lncRNA PVT1/VEGFA axis and metastatic colorectal cancer. We investigated the effect of confounding factors such as age, sex, tumor size, and tumor stage on survival by using the GSE17537 dataset. The results revealed that age ($X^2 = 2.229$, $p = 0.135$) and primary tumor stage ($X^2 = 0.900$, $p = 0.343$) were not significantly associated with PVT1 expression; however, female patients demonstrated higher PVT1 expression than male patients ($X^2 = 5.238$, $p = 0.022$; Supplementary Table 2).

3.2. Serum Exosomes Isolated from Patients with Metastatic Colon Cancer Promoted Metastatic Potential in Nonmetastatic Colon Cancer Cells. Table 1 shows the relevant clinicopathological information, including age, sex, and clinical stage, of patients with treatment-I primary or metastatic colon cancer. The results showed that distant metastasis ($X^2 = 4.552$, $p = 0.033$) and primary stage ($X^2 = 4.000$, $p = 0.045$) were significantly associated with PVT1 expression. Because we noted an increased PVT1 level in the tissue or serum samples of patients with colon cancer, we analyzed serum exosomes isolated from these patients. In the representative micrographs, P-exo and M-exo denote exosomes isolated from primary (nonmetastatic) and metastatic samples, respectively. Serum exosomes isolated from normal healthy people were included as the control (normal (N)). The average size of exosomes ranged from 100 to 200 nm. In addition, we detected the expression levels of three tumor-specific biomarkers, namely, CD9, MCT1, and cyclin D1, in exosomes. Western blot results indicated increased expression of CD9 and MCT1 (exosome markers) in the serum samples of patients with metastatic colon cancer com-

pared with those of patients with primary tumor (Figure 2(a)). We cultured human colon cancer cells, namely, HCT116 and LoVo, with P-exo and M-exo under serum-deprived conditions. Subsequently, the findings of qPCR showed that M-exo contained significantly higher levels of PVT1 and VEGFA compared with P-exo (Figure 2(b)). In addition, we found that both cell lines exhibited increased ability to form tumorspheres under the presence of M-exo compared with P-exo (Figure 2(c)). Furthermore, the migratory and invasive abilities of HCT116 and LoVo were significantly increased in the presence of M-exo but not P-exo (Figure 2(d)). The Western blots of both HCT116 and LoVo cells cultured with M-exo demonstrated an increase in EMT markers, namely, Twist1, vimentin, and MMP2, as well as the stemness marker Sox2 compared with HCT116 and LoVo cells cultured with P-exo (Figure 2(e)). In addition, we examined the effects of adding two serum exosomes on the growth of different types of cancer cells, namely, U87 (a human primary glioblastoma cell line), SAS (human squamous cell carcinoma of the tongue), MDA-MB-231 (a triple-negative breast cancer cell line), and HCT116 (a colon cancer cell line), as controls. The results indicated that the cells cultured with M-exo demonstrated increased cell viability (Supplementary Figure S1).

3.3. M-exo Promoted Distant Metastasis in a Patient-Derived Xenograft Mouse Model. Patient-derived xenograft (PDX) mouse models were established using NSG mice bearing patient samples from primary (nonmetastatic) colon cancer tumors. Serum exosomes, M-exo, and P-exo were intravenously injected 1 week following tumor implantation. Injections were administered three times a week for 4 weeks. PDX mice injected with M-exo exhibited significantly higher tumor and tissue growth (Figure 3(a)) and more distant lesions in the lungs compared with other groups (Figure 3(b)); a similar observation was made for lymph node metastasis (Figure 3(c)). In addition, we compared the tumorsphere generation ability among the groups and found that tumor cells harvested from M-exo mice exhibited an enhanced ability to form tumorspheres in terms of both number and size (Figure 3(d)); the number of spheres formed in mice injected with P-exo did not significantly differ from that formed in control mice.

3.4. Inhibition of PVT1 Suppresses the Tumorigenic Properties of Colon Cancer Cells. We examined the functional roles of PVT1 in colon cancer by silencing PVT1 through the siRNA technique. Figure 4(a) shows the siRNA knockdown effect of PVT1 on two colon cancer cell lines. Figure 4(b) presents the basal levels of PVT1 and VEGF (Western blot and gene expression) in cell lysates and exosomes. Supplementary Figure S2 shows the basal levels of the PVT1 and VEGF family in different cancer cell lines, namely, U87, FaDu (hypopharyngeal tumor), MDA-MB-231, and pHCT116 (a colon cancer cell line), that were included as controls. The data were obtained from the Gene Expression Omnibus (GEO) database (GSE36133). We observed that PVT1 promoted angiogenesis by regulating the VEGF signaling pathway in different cancer cells. PVT1-silenced HCT116

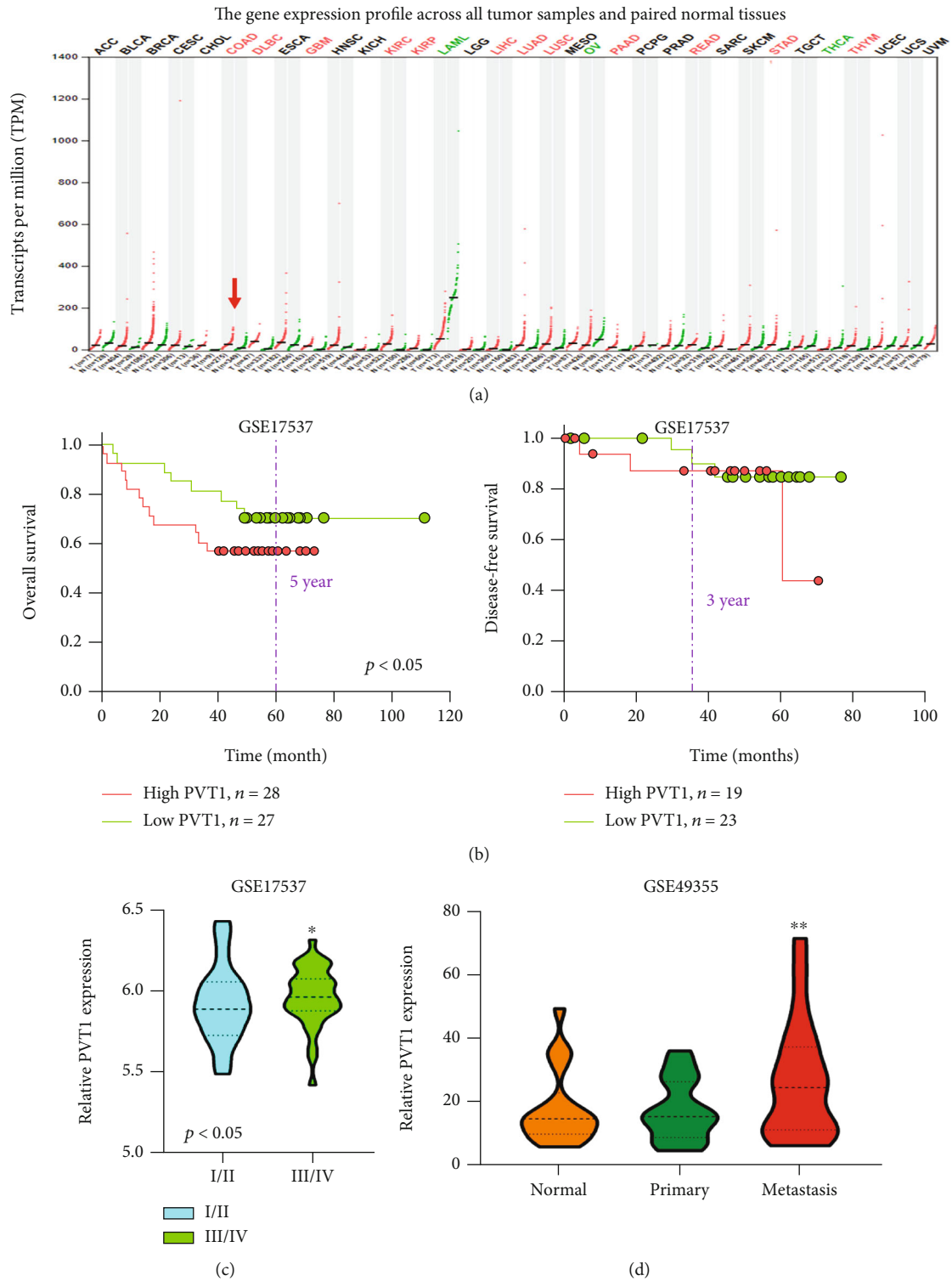


FIGURE 1: Continued.

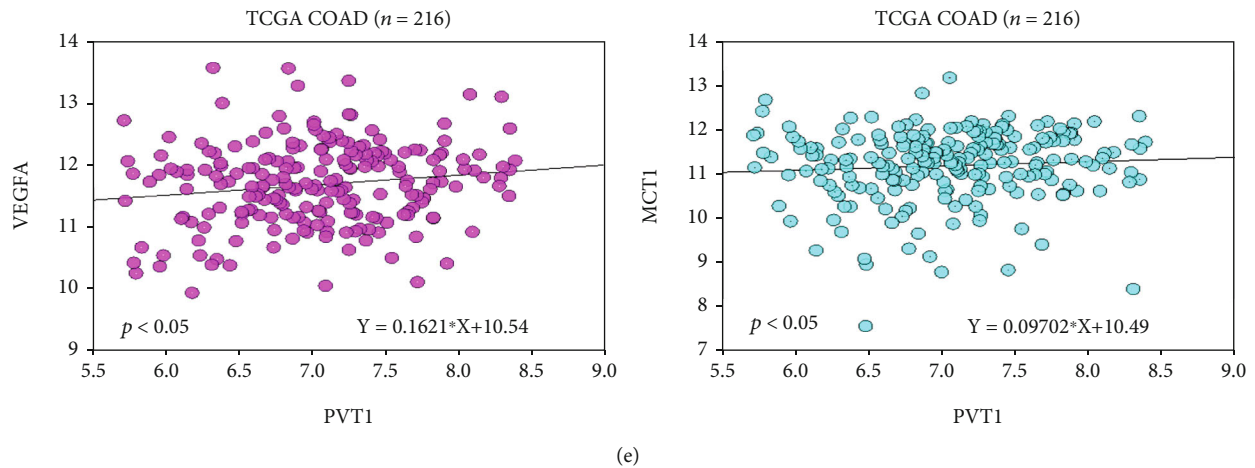


FIGURE 1: Expression analysis of PVT1 in clinical samples of patients with colon cancer. (a) Expression of PVT1 in the pan-cancer analysis from the database of TCGA. The red arrowhead indicates colon adenocarcinoma. (b) The Kaplan–Meier survival curve and disease-free survival durations constructed from the GSE17537 database. Patients with higher PVT1 expression showed a significantly lower disease-specific survival rate. (c) PVT1 expression in different stages of colorectal cancer. The expression of PVT1 in advanced colorectal cancer is significantly upregulated ($p < 0.05$). (d) The difference in PVT1 expression between primary and metastatic tumors from the GSE49355 dataset. (e) The correlation analysis between PVT1 and VEGFA, PVT1, and the exosome biomarker MCT-1 from the database of the TCGA. r : Pearson's correlation index; * $p < 0.05$; ** $p < 0.01$.

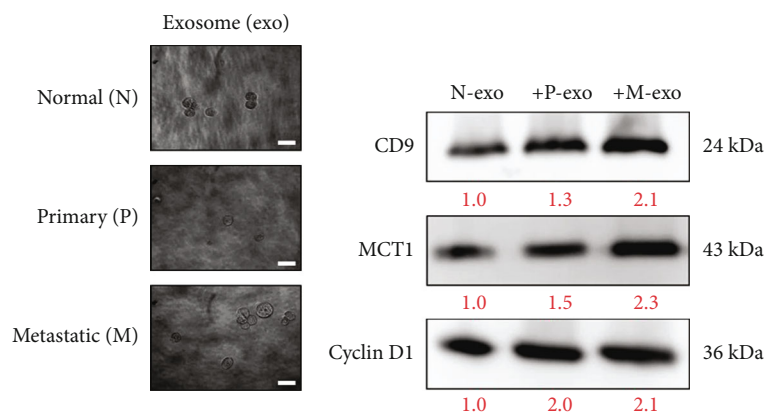
and LoVo cells exhibited significantly decreased colony-forming ability (Figure 4(c)). For example, PVT1-silenced LoVo cells formed approximately 70% fewer colonies than their nonsilenced counterparts (Figure 4(c)). HCT116 and LoVo cells transfected with si-PVT1 were significantly less potent in forming tumorspheres compared with their parental cells (Figure 4(d)). Our bioinformatics research was supported by the fact that PVT1-silenced HCT116 and LoVo cells exhibited significantly lower mRNA (right panels) and protein expression levels of metastatic markers, namely, VEGFA, MMP2, and Twist1, and the oncogenic marker EGFR (left panels; Figure 4(e)). These results indicate markedly suppressed migratory (Figure 4(f)) and invasive abilities (Figure 4(g)). The downregulation of PVT1 suppressed the migration of HCT116 cells by approximately 50% ($p < 0.01$) and that of LoVo cells by approximately 55% ($p < 0.01$); the invasive ability was reduced by at least 50% ($p < 0.01$) in both HCT116 and LoVo cells after PVT1 silencing.

3.5. Tumor Suppressor miR-152-3p Inhibits the Expression of PVT1 and the Metastatic Potential of Colon Cancer. By examining different online platforms, namely, Ensembl (<https://www.ensembl.org/>), LNCipedia (<https://lncipedia.org/>), miRDB (<http://mirdb.org/>), and the ENCORI pan-cancer analysis platform (<http://starbase.sysu.edu.cn/>), we determined that PVT1 and VEGFA are targeted by miR-152-3p, which was identified as a potential inhibitor of PVT1 and VEGFA [23]. The binding sequences are shown in Figure 5(a). The expression of miR-152-3p was higher than that of PVT1 in the early stage, and the expression of PVT1 was higher than that of miR-152-3p in the late stage (Supplementary Figure S3). On the basis of this finding, we examined the effects of the miR-152-3p mimic and inhibitor oligonucleotides on colon tumorigenesis. An increased level

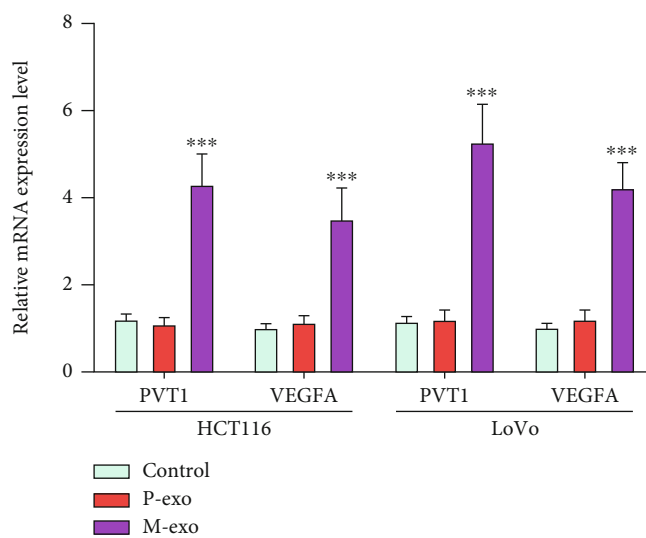
of miR-152-3p in both HCT116 and LoVo cells led to significantly lower expression of PVT1, VEGFA, and EGFR (Figure 5(b)). Moreover, the mimic-induced overexpression of miR-152-3p significantly reduced tumorsphere formation in both cell lines (Figure 5(c)). However, the subsequent addition of the miR-152-3p inhibitor significantly restored tumorsphere formation ability (Figure 5(c)). A similar observation was made for invasive ability. The invasive ability of HCT116 and LoVo cells was significantly reduced when the cells were transfected with the miR-152-3p mimic and oligonucleotides (Figure 5(d)). The invasive ability was restored by the subsequent addition of the miR-152-3p inhibitor (Figure 5(d)). These findings are supported by the results of Western blot analysis that revealed decreased levels of metastasis-associated markers, namely, VEGFA and vimentin, and the oncogenic marker EGFR in mimic-transfected cells (Figure 5(e), lane M); these levels were restored after the addition of the miR-152-3p inhibitor (Figure 5(e), lane I). Furthermore, the analysis of 450 patients with colon cancer from the database of TCGA revealed a negative correlation between the expression of PVT1 and that of miR-152-3p (coefficient r value = -0.149 and $p = 1.58E - 03$; Figure 5(f)).

4. Discussion

Exosomes are small vesicles secreted by cells and are a type of membrane-bound extracellular vesicle; they can be found in various body fluids and participate in communication between cells [24]. Recent studies have indicated that proteins and related RNAs present in exosomes can be used as biological indicators for cancer diagnosis and prognosis assessment. PVT1 is an oncogenic lncRNA and is associated with many cancer types including colorectal and gastric cancers [12–14]. PVT1 contributes to many aspects of cancer

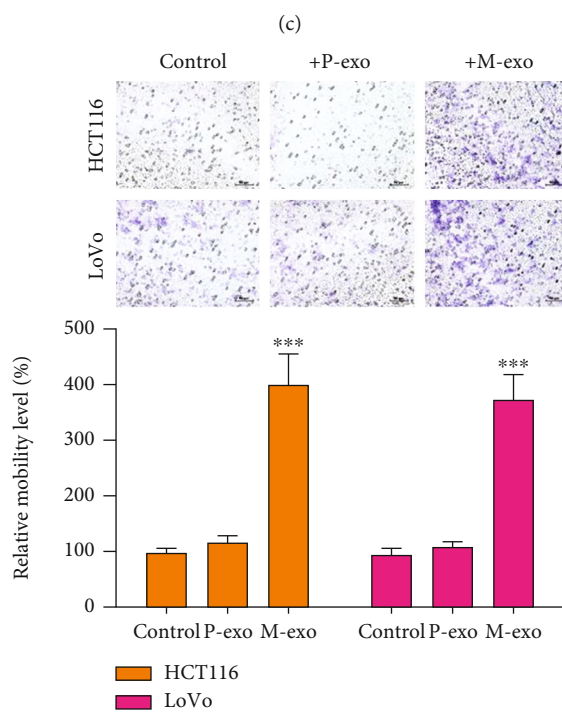
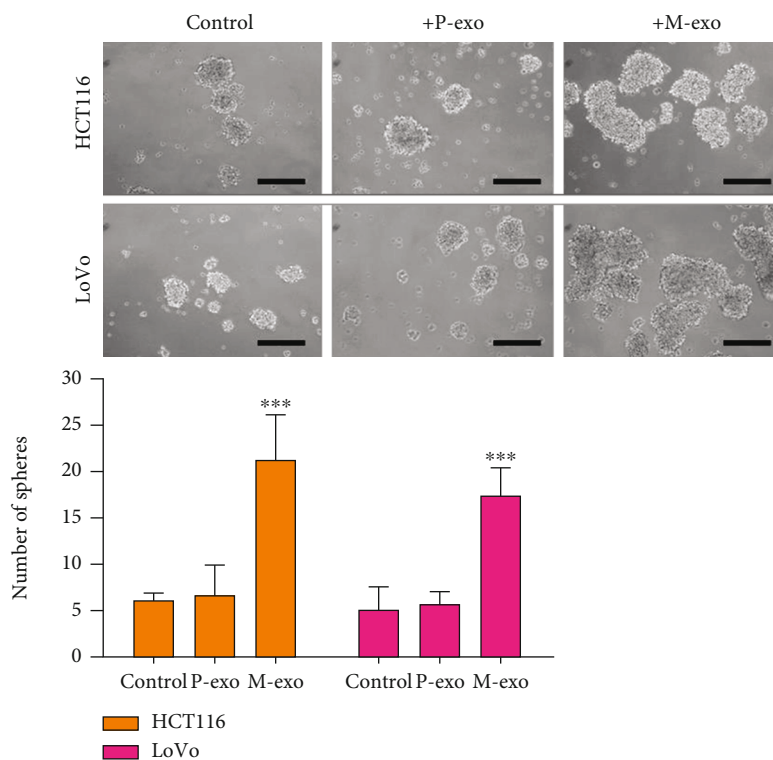


(a)



(b)

FIGURE 2: Continued.



(d)

FIGURE 2: Continued.

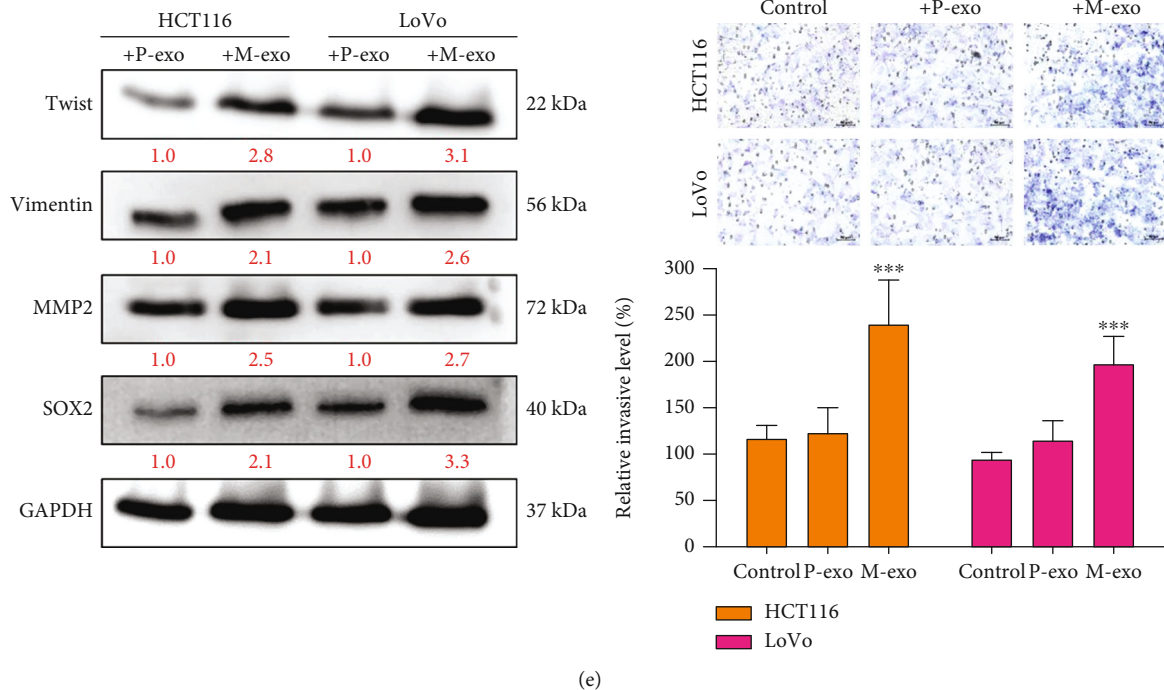


FIGURE 2: Comparative analysis of exosomes from the serum of patients with primary and metastatic colon cancer. (a) Serum exosomes were isolated from patients with primary tumor (P-exo) and distant metastasis (M-exo). Representative electromagnetic images of exosomes are shown. Scale bar: 200 nm. Western blots demonstrated increased CD9 and MCT1 (exosome markers) and cyclin D1 (tumor-specific marker) in the serum of patients with metastatic colon cancer (M, M-exo) compared with that of patients with primary tumor (P, P-exo). Serum exosomes of normal healthy people were included as controls (N, normal). (b) Comparative qPCR analysis showed that the levels of PVT1 and VEGFA were significantly higher in the M-exo than in the P-exo. (c) The sphere-forming assay showed that the addition of M-exo led to formation of an increased number of tumorspheres in both cell lines compared with controls and the group with P-exo. (d) Exosomes and colon cancer cell line coculture experiment. HCT116 and LoVo cells cocultured with M-exo demonstrated enhanced migratory and invasive abilities. (e) Western blot analysis indicated an elevation in metastatic markers, namely, Twist1, vimentin, and MMP2, and the stemness marker Sox2 in HCT116 and LoVo cells cocultured with M-exo compared with their counterparts cultured with P-exo. Coculture with exosomes derived from the serum of healthy individuals served as control. * $p < 0.05$; ** $p < 0.01$; *** $p < 0.001$. Scale bar: 100 μm .

biology through a complex signal network, with a role in tumor growth, metastasis, and response to chemotherapy and radiotherapy [9]. This complex signal network involves interactions with DNA, RNA, and proteins. In the present study, we identified PVT1 as a prognostic biomarker in patients with colon cancer. Notably, patients with a higher PVT1 level exhibited a shorter survival duration than did patients with a lower PVT1 level. In addition, a higher PVT1 level was noted in the serum of patients with recurrent disease. Notably, serum exosomes isolated from patients with metastasis revealed an increased PVT1 level compared with those isolated from patients without metastasis. Moreover, cell line experiments exhibited increased PVT1 levels in HT29 colon spheres compared with their parental counterparts along with increased VEGFA and EGFR levels, the two major metastatic or oncogenic markers in colon cancer. These observations suggest that PVT1 in serum exosomes play a crucial role in promoting metastasis in colon cancer.

Our comparative experiments performed using M-exo and P-exo revealed that M-exo not only contained a significantly higher PVT1 level than did P-exo but also enhanced the migratory and invasive abilities of the human colon cancer cell lines HCT116 and LoVo. This finding indicates that

exosomes enriched with PVT1 are one of the venues for colon cancer cells with metastatic ability to transform neighboring cancer cells. Moreover, this phenomenon was observed in non-small-cell lung cancer wherein the lncRNA MALAT1 was found to be protected by exosomes and involved in the promotion of distant metastasis [25]. Concomitantly, we noted that serum exosomes isolated from patients with metastatic colon cancer contained a higher PVT1 level than did those isolated from patients with primary nonmetastatic colon cancer. Therefore, PVT1-enriched serum exosomes can be used as a potential new prognostic biomarker for metastatic colon cancer.

Another phenomenon observed in our study was the association between increased PVT1 expression and colon tumorsphere generation. In addition, the findings of *in silico* analysis showed that the PVT1 level was significantly higher in HT29 tumorspheres. Furthermore, the results of our *in vitro* experiments revealed that the ability to form tumorspheres was severely compromised when PVT1 expression was inhibited in both HCT116 and LoVo cells. Moreover, M-exo promoted the formation of tumorspheres in our PDX mouse model *in vivo*. This finding provides an indirect link to the EMT-promoted stemness hypothesis first

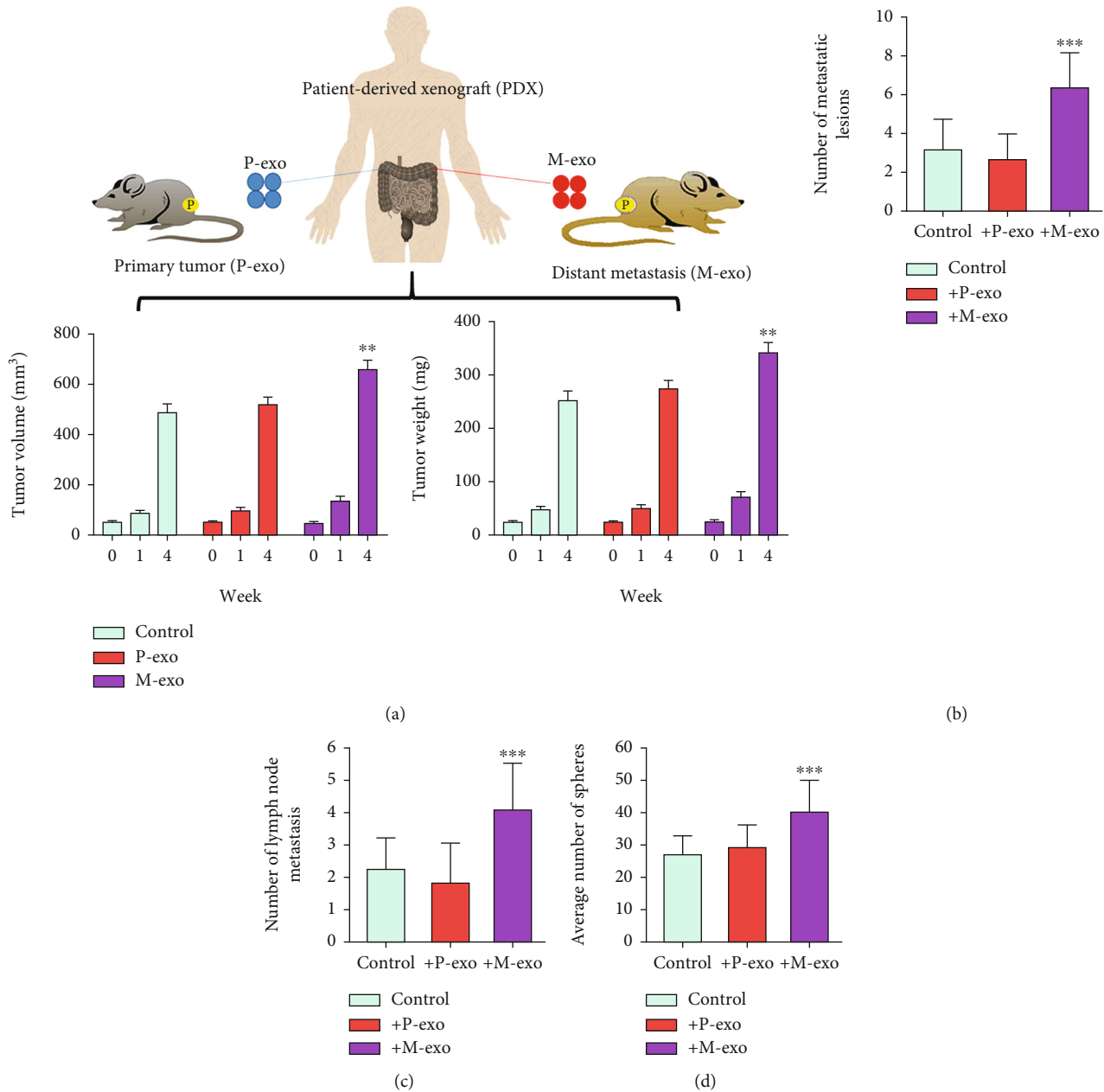
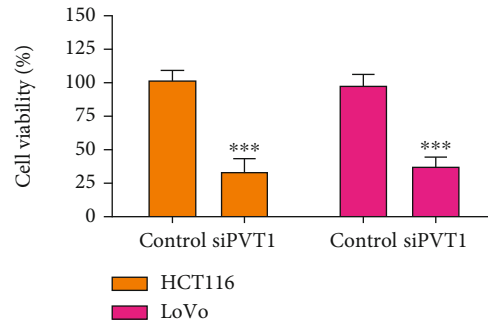


FIGURE 3: M-exo promoted tumor growth and distant metastasis in the PDX mouse model. (a) PDX mice ($n = 10$) were divided into the following groups: control, M-exo, and P-exo. The M-exo group showed a higher tumor volume and weight (week 4) than did control and P-exo groups. Distant (b) lung and (c) lymph node metastasis analysis. Lesions in the lungs from all the three groups were examined and counted. The M-exo group exhibited the highest number of lung lesions, followed by P-exo and control groups. (d) Comparative analysis of tumorsphere-forming ability. Tumor samples harvested from the M-exo group showed a higher number of spheres; no significant difference in the number of spheres was observed between the P-exo and control groups. Mice inoculated with cells cocultured with exosomes derived from the serum of healthy individuals served as control. * $p < 0.05$; ** $p < 0.01$; *** $p < 0.001$.

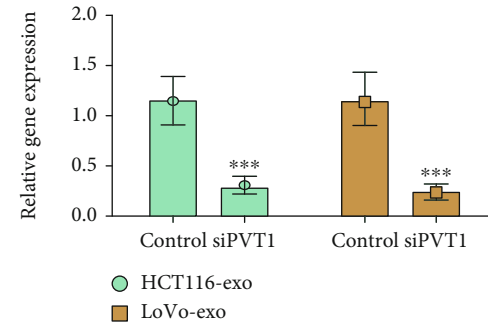
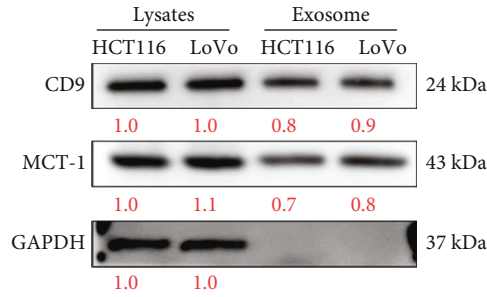
proposed by Shibue and Weinberg [26]. In the case of colon cancer, the presence of CD26(+) cells in primary tumors could predict distant metastasis at follow-up. Moreover, isolated CD26(+) cells, but not CD26(-) cells, caused distant metastasis when injected into mice [27]. This finding is similar to our *in vivo* result that PVT1-enriched M-exo promoted distant metastasis in PDX mice inoculated with primary (nonmetastatic) clinical colon cancer cells. These findings indicate that PVT1-enriched exosomes can function

as an enhancer of the EMT process and cancer stemness in colon cancer. Nevertheless, the exact mechanistic role of PVT1 in the promotion of stemness warrants further investigation and is currently under exploration in our laboratory.

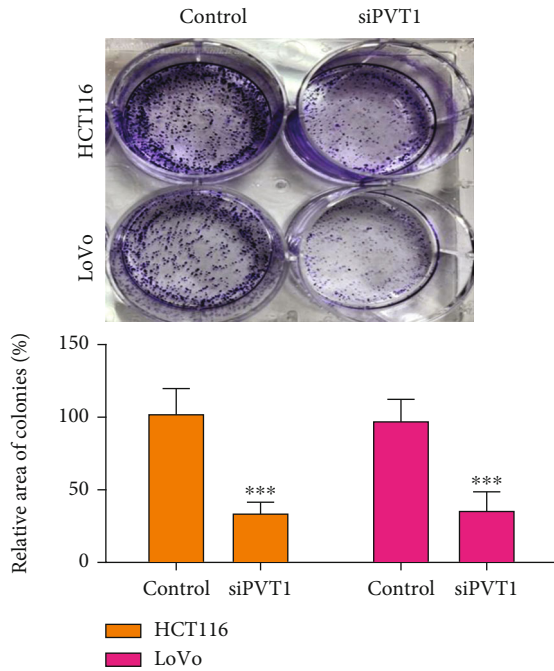
VEGFA plays a major role in promoting colon metastasis by engaging with Sox2-associated signaling [28]. This finding accords with our observation that the addition of exosomes isolated from metastatic colon cancer promoted the generation of tumorspheres in both HCT116 and LoVo cells in



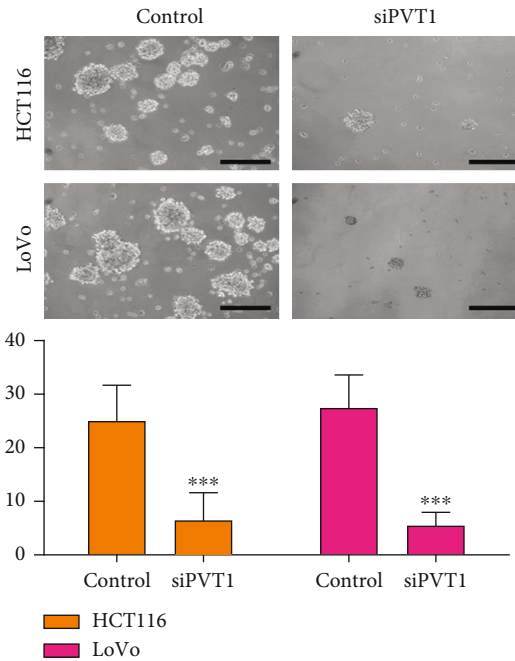
(a)



(b)



(c)



(d)

FIGURE 4: Continued.

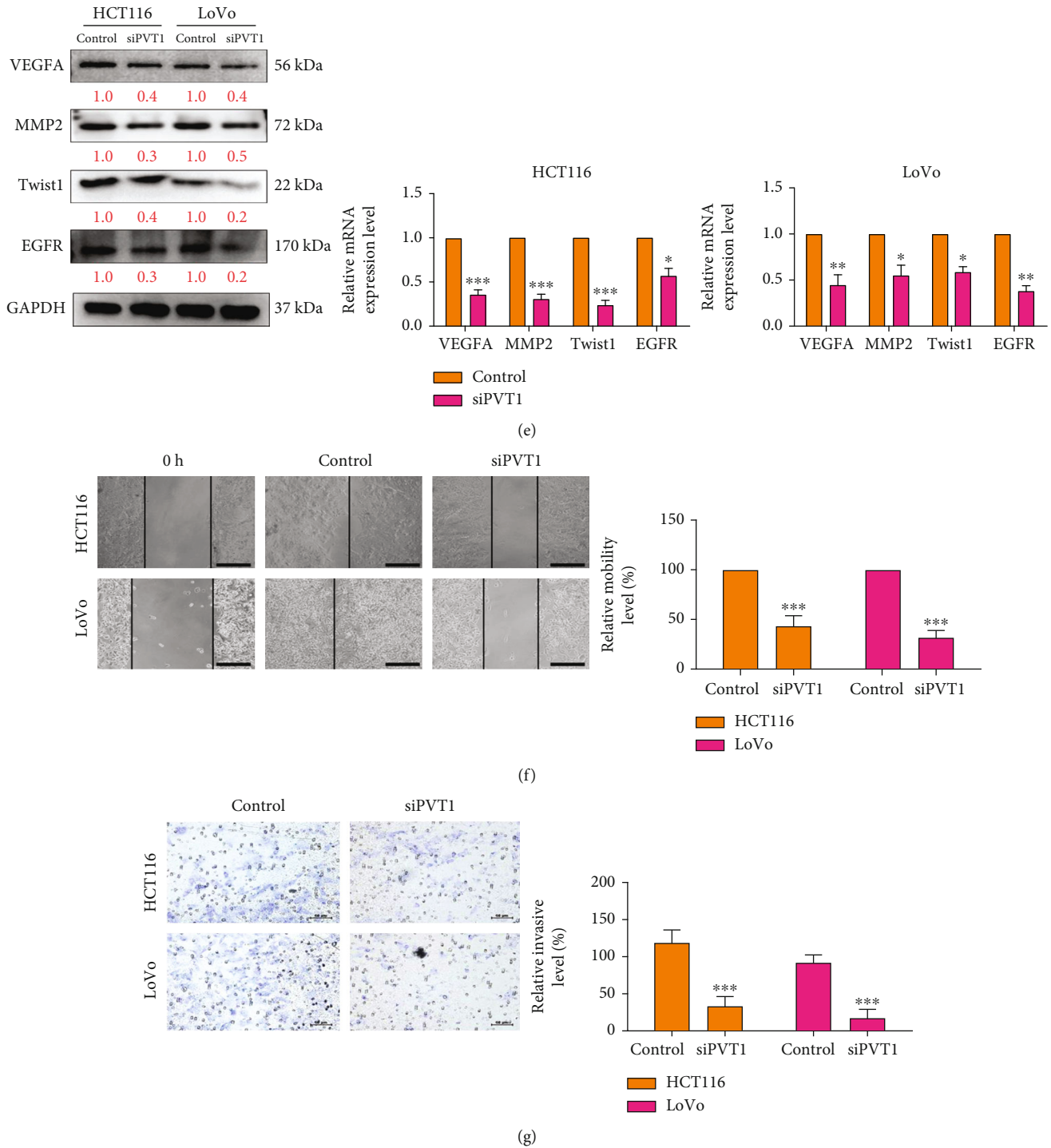


FIGURE 4: PVT1 silencing suppressed colon tumorigenic and metastatic potential. (a) The siRNA knockdown effect of PVT1 on two colon cancer cell lines. (b) The basal levels of PVT1 and VEGF (Western blot and gene expression) in cell lysates and exosomes. (c) Colony formation assay revealed that si-PVT1-transfected HCT116 and LoVo cells formed a significantly lower number of colonies compared with control parental cells. (d) Comparative tumorsphere-forming assay. HCT116 and LoVo cells transfected with si-PVT1 were significantly less potent in forming tumorspheres compared with their parental cells. (e) Comparison of expression between parental colon cancer cells and PVT1-silenced cells. Right panels: qPCR analysis demonstrated markedly decreased expression of metastatic markers, namely, VEGFA, Twist1, and MMP2, and the oncogenic marker EGFR in si-PVT1 colon cells. Left panels: Western blots of parental versus PVT1-silenced HCT116 and LoVo cells. Prominent reduction in the expression of VEGFA, Twist1, MMP2, and EGFR was observed after PVT1 silencing in both cell lines. Effect of PVT1 expression on cell (f) migration and (g) invasion of HCT116 and LoVo cells detected using Transwell assays. NC: negative control (scramble PVT1 oligonucleotides). * $p < 0.05$; ** $p < 0.01$; *** $p < 0.001$. Scale bar: 100 μm .

PVT1: 5'	gcugguggaacCAUGCACUGg 3'
miRNA: 5'	gguucaagacaGUACGUGACu 3'
VEGFA: 5'	ucucgccccaggGCACUGc 3'
miRNA: 5'	gguucaagacaguaCGUGACu 3'

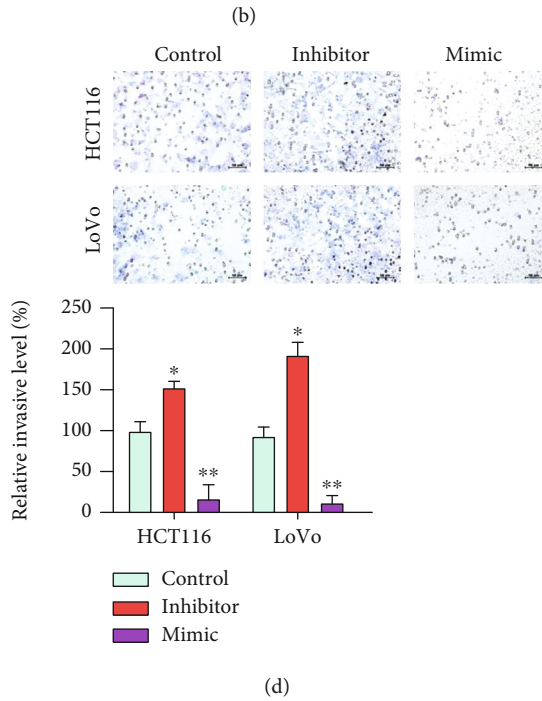
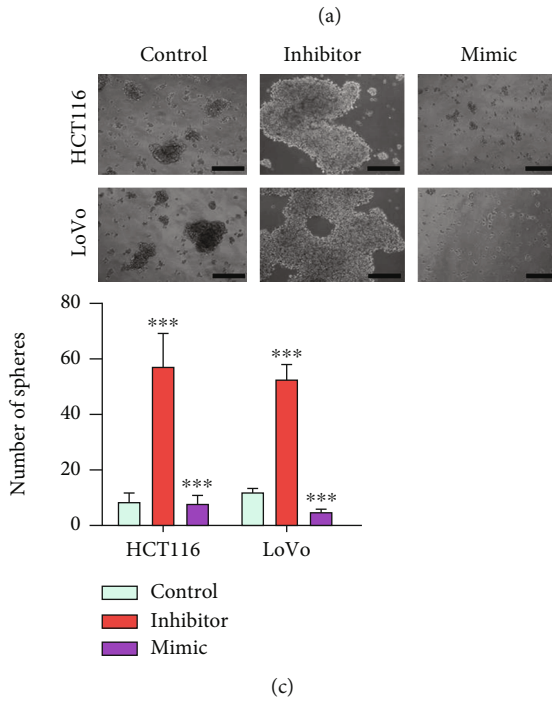
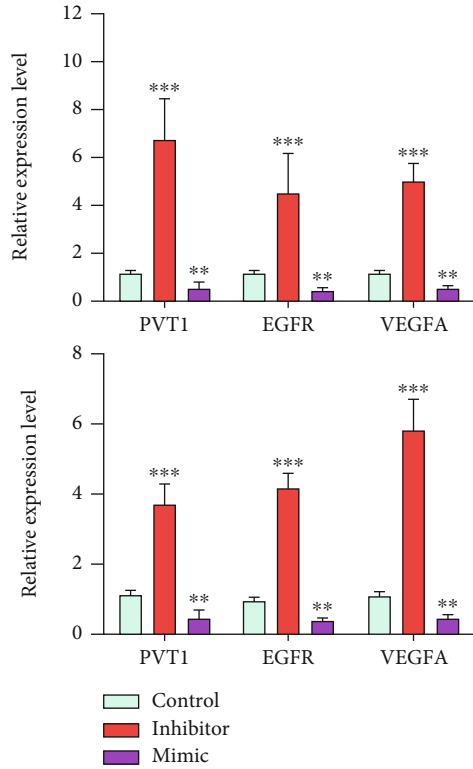


FIGURE 5: Continued.

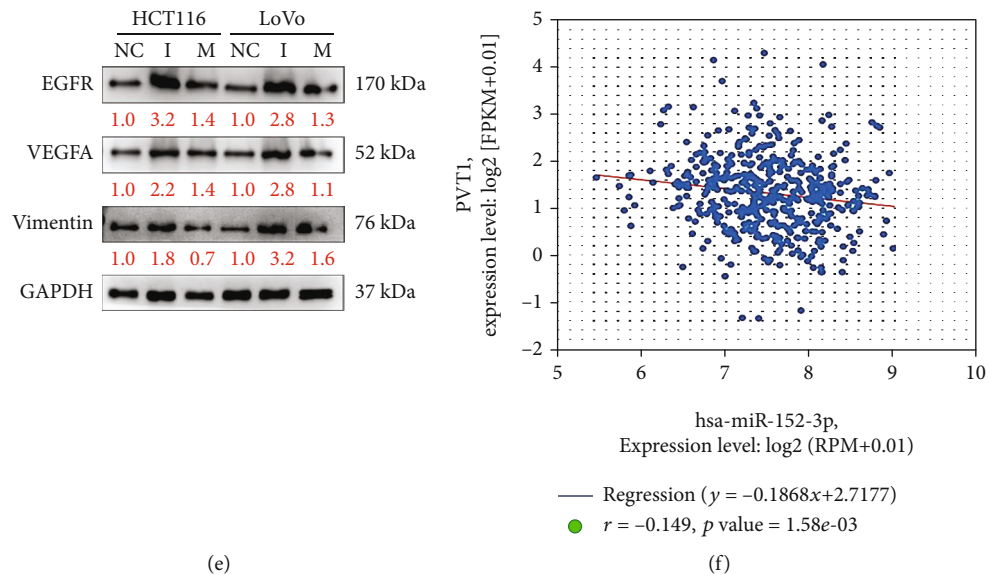


FIGURE 5: Target validation for miR-152-3p and its role in suppressing metastasis. (a) Target binding sequences of miR-152-3p in the 3'-UTR of PVT1 and VEGFA. These binding sites were predicted using both miRmap and MiRanda software. (b) qPCR analysis of PVT1, EGFR, and VEGFA levels in response to the sequential miR-152-3p mimic and inhibitor transfections (the control group did not add any reagents). A significant decrease in the mRNA levels of PVT1, EGFR, and VEGFA was observed after miR16-5p mimic transfection and subsequent restoration with the addition of the miR-152-3p inhibitor. Both HCT116 and LoVo cells showed a similar trend. (c) Tumorsphere formation assay. The tumorsphere-forming ability was considerably inhibited by the transfection of miR-152-3p in both HCT116 and LoVo cells; partial restoration of the tumorsphere-forming ability was noted when the miR-152-3p inhibitor was added. (d) Invasion assay revealed that an increase in miR-152-3p significantly reduced the invasive ability in both HCT116 and LoVo cells; however, the invasive ability was restored by the addition of the miR-152-3p inhibitor. (e) Western blot analysis. The addition of miR-152-3p mimics suppressed the expression of EGFR, vimentin, and VEGFA in both HCT116 and LoVo cells, and the inhibitor restored their expression. (f) A negative correlation was noted between miR-152-3p and PVT1 levels in colon cancer clinical samples from databases of TCGA [12] ($n = 450$). Control/NC: scramble hsa-miR-152-3p oligonucleotides. * $p < 0.05$; ** $p < 0.01$; *** $p < 0.001$. Scale bar: 100 μm .

association with increased Sox2 expression. Notably, EGFR and VEGF mutations are often determined to be associated with increased metastatic incidence and poor prognosis in colon cancer [29]. Our observation of PVT1 downregulation leading to decreased expression of VEGFA, EGFR, Twist1, and MMP2 provides insight into the role of PVT1 in promoting metastasis. Our database analysis indicated that the expression levels of PVT1, VEGFA, and EGFR were significantly elevated in HT29 spheres compared with their parental cells [30]. Although the present study did not establish a causal relationship among the expression of these three molecules, a common regulatory molecule, namely, miR-152-3p, was identified to be an inhibitor of both PVT1 and VEGFA. First, we identified the potential binding sites of miR-152-3p to PVT1 and VEGFA and observed that increased expression of miR-152-3p significantly reduced the expression of PVT1, VEGFA, and EGFR in both HCT116 and LoVo cells. A previous study indicated that PVT1 was linked to the activation of STAT3/VEGFA signaling and promoted angiogenesis in patients with gastric cancer [31]. miR-152-3p has been identified as a tumor suppressor; for example, miR-152-3p was observed to negatively regulate PIK3CA expression, thus inhibiting the activation of AKT and RPS6 in breast cancer cells [32]. In addition, the downregulation of miR-152, which targets DNMT1 (an oncogene or cancer stemness marker), was observed in breast cancer cells [33]. Notably, a negative correlation between the expression levels of PVT1 and

miR-152-3p was identified in TCGA colon cancer database consisting of 450 patient samples [32]. Recent studies have demonstrated that PVT1 regulates the VEGFA/VEGF receptor 1 (VEGFR1)/AKT axis and promotes the tumorigenesis of colorectal cancer; the deletion of PVT1 can reduce tumor volume. Overexpression of VEGFA regulates the AKT signaling cascade by activating VEGFR1 [34]. miR-152-3p has been described as a possible tumor suppressor in numerous studies because its downregulation has been reported in several cancer tissues. Our results indicate that because miR-152-3p may have binding sites for PVT1 and VEGFA, it might regulate the lncRNA PVT1/VEGFA axis. Previous studies have found that PVT1 can promote angiogenesis in tumor tissues. Given the causal relationship between upstream and downstream genes, studies should evaluate whether miR-152-3p can skip PVT1 and directly regulate VEGFA.

Patients with colorectal cancer with high PVT1-214 expression have a shorter survival duration and poor prognosis. The results of in vivo and in vitro studies have indicated that the effects of PVT1-214 exhibit a complex phenotype affecting cell growth, stem-like properties, migration, and invasion [35]. PVT1 can indirectly regulate the expression of four-jointed box 1 (FJX1) by targeting miR-106b-5p. By regulating the miR-106b-5p/FJX1 axis, knockdown of PVT1 can impair cell proliferation, migration, and invasion in colorectal cancer [36]. Many studies have reported that PVT1

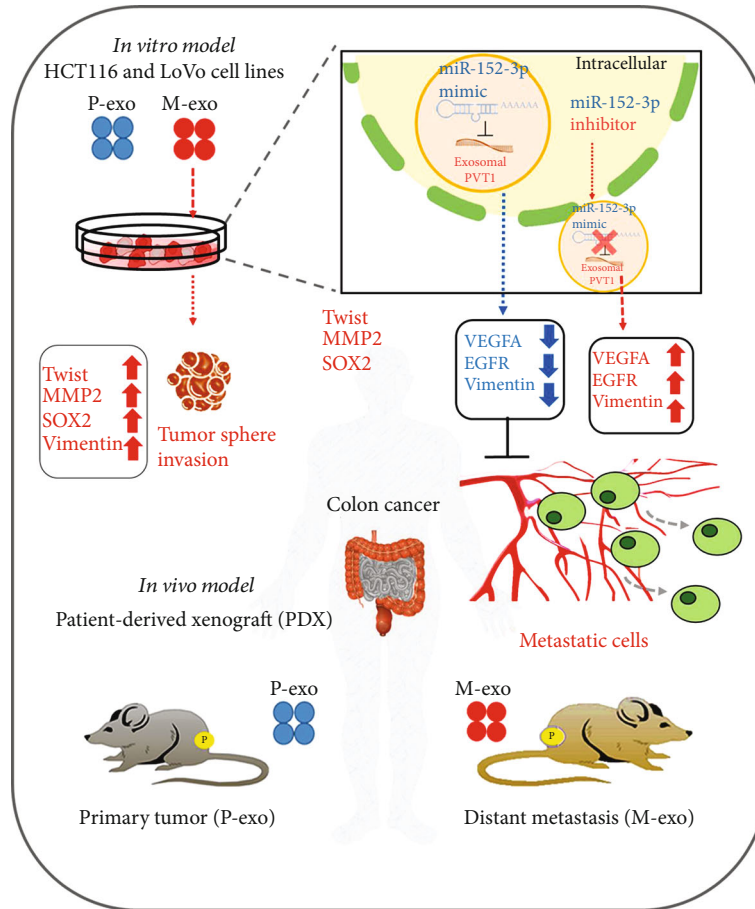


FIGURE 6: Schematic abstract showing that exosomal PVT1 promotes metastasis in colon cancer through its association with EGFR and VEGFA expression.

overexpression was related to cancer growth and proliferation in vivo and in vitro. Moreover, human tissue and mouse xenotransplantation studies have indicated that the overall survival rate and tumor size of many cancer types are related to PVT1 overexpression [37, 38].

lncRNAs are a major type of ncRNA. In addition, the role of PVT1 in cancer development is closely related to miRNAs. PVT1 can be spliced and processed into various miRNAs such as miR-1204 and miR-1207. Furthermore, PVT1 can act as a “sponge” for miRNAs and inhibit their activity, thereby affecting cancer proliferation, invasion, and angiogenesis [39]. Patients with digestive system cancers have a high risk of morbidity and mortality. The expression of PVT1 is elevated in various digestive system cancers and is associated with poor prognosis [40]. Therefore, PVT1 might become a new biomarker for early screening and could potentially be used as a prognostic biomarker and in future targeted therapies to improve the survival rate of patients [40–42]. Liquid biopsy is a novel method used for cancer diagnosis. Circulating ncRNAs such as miRNAs and lncRNAs are biomarkers that can be easily obtained from blood and can be used for early diagnosis and prediction of prognosis and treatment response. lncRNAs can be passively released through tissues or exosomes [43]. Recently, the therapeutic targeting of oncogenic lncRNAs and

lncRNAs related to therapeutic resistance has attracted considerable attention [44]. lncRNAs mediate these functions by interacting with proteins, RNA, and lipids. Unlike other ncRNAs, the functions of lncRNAs cannot be inferred from their sequence or structure [45]. Therefore, experimental evaluations are required to obtain complete and accurate biological annotations. A recent study indicated that lncRNA PVT1 promotes the tumorigenesis of colorectal cancer by stabilizing miR-16-5p and interacting with the VEGFA/VEGFR1/AKT axis [46]. In a mouse xenograft model, the combination of PVT1 loss and miR-16-5p overexpression minimized tumor volume. lncRNA PVT1 acts as a miRNA sponge and negatively regulates miR-16-5p expression. VEGFA is a key regulator of angiogenesis and migration [47]. Angiogenesis is a crucial marker for tumorigenesis, progression, and prognosis [47]. In our study, we discovered the regulatory role of miR-152-3p in the lncRNA PVT1/VEGFA axis, especially exosomes, which are closer to the exploration and application of tumor microenvironment. Our findings regarding the exosomal lncRNA PVT1/VEGFA axis confirms this point. PVT1 in the serum exosomes of patients could affect metastasis and invasion in both in vivo and in vitro models. Exosomes can be used for precise treatment and early diagnosis, thus inspiring novel treatment strategies for colon cancer.

5. Conclusion

Exosomal PVT1 promotes colon cancer metastasis through its association with EGFR and VEGFA expression. miR-152-3p targets both PVT1 and VEGFA, and this regulatory pathway can be explored for drug development and as a prognostic biomarker. A series of experimental designs and their results are shown in the schema abstract in Figure 6. The results of this study indicated the potential role of PVT1/VEGFA-enriched serum exosomes in promoting distant metastasis in colon cancer. Both in vitro and in vivo experiments revealed that increased PVT1 expression was associated with increased metastatic potential and stemness, as reflected by the concomitantly increased expression of VEGFA, EGFR, and Sox2. Moreover, the downregulation of PVT1 significantly suppressed the metastatic ability of colon cancer cells, and PVT1 was observed to be regulated by the tumor suppressor miR-152-3p. Nevertheless, future studies should explore this perspective further and analyze the possibility of designing agents that can increase miR-152-3p expression for treating metastatic colon cancer.

Abbreviations

CSCs: Cancer stem cells
 DTX: Docetaxel
 EMT: Epithelial-to-mesenchymal transition
 ECM: Extracellular matrix
 5-FU: 5-Fluorouracil
 FBS: Fetal bovine serum
 IFC: Immunofluorescence
 SRB: Sulforhodamine B
 TCA: Trichloroacetic acid
 TICs: Tumor-initiating cells.

Data Availability

The authors confirm that the data supporting the findings of this study are available within the article and/or its each supplementary material files. The manuscript is available as a preprint at the following website: <https://www.researchsquare.com/article/rs-116035/v1>.

Additional Points

Highlights. (i) Serum exosomes enriched with lncRNA PVT1/VEGFA in colon cancer. (ii) lncRNA PVT1/VEGFA promotes metastatic potential and stemness. (iii) lncRNA PVT1/VEGF is in association with downregulation of miR-152-3p.

Ethical Approval

This study was approved by the Medical Ethics Committee of Taipei Medical University-Joint Institutional Review Board (N202104054; Taipei, Taiwan). Serum samples were collected from healthy individuals, patients with primary colon cancer, and patients with metastatic colon cancer based on histological examinations.

Consent

Written informed consent for the collection of clinical samples was obtained from all participants.

Conflicts of Interest

The authors declare that they have no potential financial competing interests whereby they may in any way gain or lose financially from the publication of this manuscript at present or in the future. Additionally, no nonfinancial competing interests are involved in the manuscript.

Authors' Contributions

Shiue-Wei Lai conceived and designed the study. Ming-Yao Chen performed the experiments. Oluwaseun Adebayo Bamodu and Ming-Shou Hsieh analyzed the data. Ting-Yi Huang performed the bioinformatics research. Chi-Tai Yeh and Wei-Hwa Lee wrote the manuscript. Yih-Giun Cherng provided reagents, materials, experimental infrastructure, and administrative oversight. All authors read and approved the final version of the manuscript. Shiue-Wei Lai and Ming-Yao Chen contributed equally to this work.

Acknowledgments

The authors thank the laboratory assistant Mr. Alex Fong (Taipei, Taiwan) for his technical assistance. This work was supported by the National Science Council of Taiwan grant to Shiue-Wei Lai (MOST 110-2314-B-016-058). This study was also supported by grants from Tri-Service General Hospital, National Defense Medical Center (TSGH-pH-106-04, TSGH-E-109212, and TSGH-D-110041), to Shiue-Wei Lai.

Supplementary Materials

Supplementary Table 1: primer sequences used in this study. Supplementary Table 2: clinical table (GSE17537) of Figure 1(b). Supplementary Figure S1: cell viability of different cancer cell lines after exosome treatment. Supplementary Figure S2: gene expression of the PVT1 and VEGF family in different cancer cell lines. Supplementary Figure S3: relative gene expression of miR-152-3p and PVT1 in primary stages. Supplementary Figure S4: full-size blots of Figure 2(a). Supplementary Figure S5: full-size blots of Figure 2(e). Supplementary Figure S6: full-size blots of Figure 4(b). Supplementary Figure S7: full-size blots of Figure 4(e). Supplementary Figure S8: full-size blots of Figure 5(e). (*Supplementary Materials*)

References

- [1] K. Jin, H. Lan, F. Cao et al., "Differential response to EGFR- and VEGF-targeted therapies in patient-derived tumor tissue xenograft models of colon carcinoma and related metastases," *International Journal of Oncology*, vol. 41, no. 2, pp. 583–588, 2012.
- [2] A. B. Benson, A. P. Venook, L. Cederquist et al., "Colon cancer, version 1.2017, NCCN clinical practice guidelines in

- oncology,” *Journal of the National Comprehensive Cancer Network: JNCCN*, vol. 15, no. 3, pp. 370–398, 2017.
- [3] M. Colombo, G. Raposo, and C. Thery, “Biogenesis, secretion, and intercellular interactions of exosomes and other extracellular vesicles,” *Annual Review of Cell and Developmental Biology*, vol. 30, no. 1, pp. 255–289, 2014.
 - [4] Y. Chi, D. Wang, J. Wang, W. Yu, and J. Yang, “Long non-coding RNA in the pathogenesis of cancers,” *Cell*, vol. 8, no. 9, article 1015, 2019.
 - [5] M. Zhao, N. Zhu, F. Hao et al., “The regulatory role of non-coding RNAs on programmed cell death four in inflammation and cancer,” *Frontiers in Oncology*, vol. 9, pp. 919–919, 2019.
 - [6] Y. Huang, “The novel regulatory role of lncRNA-miRNA-mRNA axis in cardiovascular diseases,” *Journal of Cellular and Molecular Medicine*, vol. 22, no. 12, pp. 5768–5775, 2018.
 - [7] Y. Teng, Y. Ren, X. Hu et al., “MVP-mediated exosomal sorting of miR-193a promotes colon cancer progression,” *Nature Communications*, vol. 8, no. 1, 2017.
 - [8] Y. Y. Tseng, B. S. Moriarity, W. Gong et al., “_PVT1 dependence in cancer with MYC copy-number increase,” *Nature*, vol. 512, no. 7512, pp. 82–86, 2014.
 - [9] O. T. Onagoruwa, G. Pal, C. Ochu, and O. O. Ogunwobi, “Oncogenic role of PVT1 and therapeutic implications,” *Frontiers in Oncology*, vol. 10, pp. 17–17, 2020.
 - [10] Z. Luo and P. Cao, “Long noncoding RNA PVT1 promotes hepatoblastoma cell proliferation through activating STAT3,” *Cancer Management and Research*, vol. 20, no. 11, pp. 8517–8527, 2019.
 - [11] Y. Xu, X. Luo, W. He et al., “Long non-coding RNA PVT1/miR-150/ HIG2 axis regulates the proliferation, invasion and the balance of iron metabolism of hepatocellular carcinoma,” *Cellular Physiology and Biochemistry*, vol. 49, no. 4, pp. 1403–1419, 2018.
 - [12] J. Chen, Y. Yu, H. Li et al., “Long non-coding RNA PVT1 promotes tumor progression by regulating the miR-143/HK2 axis in gallbladder cancer,” *Molecular Cancer*, vol. 18, no. 1, p. 33, 2019.
 - [13] X. Li, Z. Zhang, H. Jiang et al., “Circular RNA circPVT1 promotes proliferation and invasion through sponging miR-125b and activating E2F2 signaling in non-small cell lung cancer,” *Cellular Physiology and Biochemistry*, vol. 51, no. 5, pp. 2324–2340, 2018.
 - [14] X. Yu, J. Zhao, and Y. He, “Long non-coding RNA PVT1 functions as an oncogene in human colon cancer through miR-30d-5p/RUNX2 axis,” *Journal of BUON*, vol. 23, no. 1, pp. 48–54, 2018.
 - [15] Y. Wu, A. Shao, L. Wang et al., “The role of lncRNAs in the distant metastasis of breast cancer,” *Frontiers in Oncology*, vol. 9, pp. 407–407, 2019.
 - [16] C. Yan, Y. Chen, W. Kong et al., “PVT1-derived miR-1207-5p promotes breast cancer cell growth by targeting STAT6,” *Cancer Science*, vol. 108, no. 5, pp. 868–876, 2017.
 - [17] A. Dongre and R. A. Weinberg, “New insights into the mechanisms of epithelial-mesenchymal transition and implications for cancer,” *Nature Reviews Molecular Cell Biology*, vol. 20, no. 2, pp. 69–84, 2019.
 - [18] Y. Zhang and R. A. Weinberg, “Epithelial-to-mesenchymal transition in cancer: complexity and opportunities,” *Frontiers of Medicine*, vol. 12, no. 4, pp. 361–373, 2018.
 - [19] A. Fantozzi, D. C. Gruber, L. Pisarsky et al., “VEGF-mediated angiogenesis links EMT-induced cancer stemness to tumor initiation,” *Cancer Research*, vol. 74, no. 5, pp. 1566–1575, 2014.
 - [20] H. Lu, K. R. Clauser, W. L. Tam et al., “A breast cancer stem cell niche supported by juxtacrine signalling from monocytes and macrophages,” *Nature Cell Biology*, vol. 16, no. 11, pp. 1105–1117, 2014.
 - [21] X. Ye, W. L. Tam, T. Shibue et al., “Distinct EMT programs control normal mammary stem cells and tumour-initiating cells,” *Nature*, vol. 525, no. 7568, pp. 256–260, 2015.
 - [22] J. K. Teer, “An improved understanding of cancer genomics through massively parallel sequencing,” *Translational Cancer Research*, vol. 3, no. 3, pp. 243–259, 2014.
 - [23] M. Kertesz, N. Iovino, U. Unnerstall, U. Gaul, and E. Segal, “The role of site accessibility in microRNA target recognition,” *Nature Genetics*, vol. 39, no. 10, pp. 1278–1284, 2007.
 - [24] G. Raposo and W. Stoorvogel, “Extracellular vesicles: exosomes, microvesicles, and friends,” *The Journal of Cell Biology*, vol. 200, no. 4, pp. 373–383, 2013.
 - [25] R. Zhang, Y. Xia, Z. Wang et al., “Serum long non coding RNA MALAT-1 protected by exosomes is up-regulated and promotes cell proliferation and migration in non-small cell lung cancer,” *Biochemical and Biophysical Research Communications*, vol. 490, no. 2, pp. 406–414, 2017.
 - [26] T. Shibue and R. A. Weinberg, “EMT, CSCs, and drug resistance: the mechanistic link and clinical implications,” *Nature Reviews Clinical Oncology*, vol. 14, no. 10, pp. 611–629, 2017.
 - [27] R. Pang, W. L. Law, A. C. Y. Chu et al., “A subpopulation of CD26⁺ cancer stem cells with metastatic capacity in human colorectal cancer,” *Cell Stem Cell*, vol. 6, no. 6, pp. 603–615, 2010.
 - [28] M. Kim, K. Jang, P. Miller et al., “VEGFA links self-renewal and metastasis by inducing Sox2 to repress miR-452, driving Slug,” *Oncogene*, vol. 36, no. 36, pp. 5199–5211, 2017.
 - [29] D. N. Rigopoulos, “Deregulation of EGFR/VEGF/HIF-1 α signaling pathway in colon adenocarcinoma based on tissue microarrays analysis,” *Journal of BUON*, vol. 15, no. 1, pp. 107–115, 2010.
 - [30] W.-L. Hwang, M.-H. Yang, M.-L. Tsai et al., “SNAIL regulates interleukin-8 expression, stem cell-like activity, and tumorigenicity of human colorectal carcinoma cells,” *Gastroenterology*, vol. 141, no. 1, pp. 279–291.e5, 2011.
 - [31] J. Zhao, P. du, P. Cui et al., “LncRNA PVT1 promotes angiogenesis via activating the STAT3/VEGFA axis in gastric cancer,” *Oncogene*, vol. 37, no. 30, pp. 4094–4109, 2018.
 - [32] J. H. Li, S. Liu, and H. Zhou, “starBase v2.0: decoding miRNA-ceRNA, miRNA-ncRNA and protein-RNA interaction networks from large-scale CLIP-Seq data,” *Nucleic Acids Research*, vol. 42, no. D1, pp. D92–D97, 2014.
 - [33] Z. Li, Y. Li, Y. Li et al., “Long non-coding RNA H19 promotes the proliferation and invasion of breast cancer through upregulating DNMT1 expression by sponging miR-152,” *Journal of Biochemical and Molecular Toxicology*, vol. 31, no. 9, 2017.
 - [34] H. Liu, Y. Yin, T. Liu et al., “Long non-coding RNA PVT1 regulates the migration of hepatocellular carcinoma HepG2 cells via miR-3619-5p/MKL1 axis,” *Bosnian Journal of Basic Medical Sciences*, vol. 21, no. 2, pp. 187–197, 2021.
 - [35] F. He, Z. Song, H. Chen et al., “Long noncoding RNA PVT1-214 promotes proliferation and invasion of colorectal cancer by stabilizing Lin28 and interacting with miR-128,” *Oncogene*, vol. 38, no. 2, pp. 164–179, 2019.

- [36] F. Liu, R. Wu, L. Guan, and X. Tang, "Knockdown of PVT1 suppresses colorectal cancer progression by regulating miR-106b-5p/FJX1 axis," *Cancer Management and Research*, vol. - Volume 12, pp. 8773–8785, 2020.
- [37] C. Derderian, A. T. Orunmuyi, E. O. Olapade-Olaopa, and O. O. Ogunwobi, "PVT1 signaling is a mediator of cancer progression," *Frontiers in Oncology*, vol. 9, pp. 502–502, 2019.
- [38] Á. Martínez-Barriocanal, D. Arango, and H. Dopeso, "PVT1 long non-coding RNA in gastrointestinal cancer," *Frontiers in Oncology*, vol. 10, pp. 38–38, 2020.
- [39] W. Wang, R. Zhou, Y. Wu et al., "PVT1 promotes cancer progression via microRNAs," *Frontiers in Oncology*, vol. 9, p. 609, 2019.
- [40] D. D. Zhou, X. F. Liu, C. W. Lu, O. P. Pant, and X. D. Liu, "Long non-coding RNA PVT1: emerging biomarker in digestive system cancer," *Cell Proliferation*, vol. 50, no. 6, article e12398, 2017.
- [41] S. N. Shen, K. Li, Y. Liu, C. L. Yang, C. Y. He, and H. R. Wang, "Down-regulation of long noncoding RNA PVT1 inhibits esophageal carcinoma cell migration and invasion and promotes cell apoptosis via microRNA-145-mediated inhibition of FSCN1," *Molecular Oncology*, vol. 13, no. 12, pp. 2554–2573, 2019.
- [42] A. Q. Shang, W. W. Wang, Y. B. Yang et al., "Knockdown of long noncoding RNA PVT1 suppresses cell proliferation and invasion of colorectal cancer via upregulation of microRNA-214-3p," *American Journal of Physiology. Gastrointestinal and Liver Physiology*, vol. 317, no. 2, pp. G222–G232, 2019.
- [43] D. A. Barth, R. Drula, L. Ott et al., "Circulating non-coding RNAs in renal cell carcinoma-pathogenesis and potential implications as clinical biomarkers," *Frontiers in Cell and Developmental Biology*, vol. 8, p. 828, 2020.
- [44] M.-C. Jiang, J.-J. Ni, W.-Y. Cui, B.-Y. Wang, and W. Zhuo, "Emerging roles of lncRNA in cancer and therapeutic opportunities," *American Journal of Cancer Research*, vol. 9, no. 7, pp. 1354–1366, 2019.
- [45] M. Kazimierczyk, M. K. Kasproicz, M. E. Kasprzyk, and J. Wrzesinski, "Human long noncoding RNA interactome: detection, characterization and function," *International Journal of Molecular Sciences*, vol. 21, no. 3, article 1027, 2020.
- [46] H. Wu, M. Wei, X. Jiang et al., "lncRNA PVT1 promotes tumorigenesis of colorectal cancer by stabilizing miR-16-5p and interacting with the VEGFA/VEGFR1/AKT axis," *Molecular Therapy - Nucleic Acids*, vol. 20, pp. 438–450, 2020.
- [47] R. Bhattacharya, F. Fan, R. Wang et al., "Intracrine VEGF signalling mediates colorectal cancer cell migration and invasion," *British Journal of Cancer*, vol. 117, no. 6, pp. 848–855, 2017.

Review Article

Role of RONS and eIFs in Cancer Progression

Yasmeen Ahmed Salaheldin ^{1,2}, **Salma Sayed Mohamed Mahmoud**,^{2,3}
Ebenezeri Erasto Ngowi ^{2,4}, **Vivian Aku Gbordzor**,^{2,5} **Tao Li**,^{2,5} **Dong-Dong Wu** ^{2,6}
and **Xin-Ying Ji** ^{2,7}

¹Department of Pathology, Faculty of Medicine, Ain Shams University, Cairo 11517, Egypt

²International Joint Laboratory for Nucleoprotein Gene Regulation, School of Basic Medical Sciences, Henan University, Kaifeng, Henan 475004, China

³Department of Biochemistry, Faculty of Medicine, Ain Shams University, Cairo 11517, Egypt

⁴Department of Biological Sciences, Faculty of Science, Dar es Salaam University College of Education, Dar es Salaam 2329, Tanzania

⁵Kaifeng Municipal Key Laboratory of Cell Signal Transduction, Engineering Centre for Tumor Molecular Medicine, Henan University, Kaifeng, Henan 475004, China

⁶School of Stomatology, Henan University, Kaifeng, Henan 475004, China

⁷Kaifeng Key Laboratory of Infection and Biological Safety, School of Basic Medical Sciences, Henan University, Kaifeng, Henan 475004, China

Correspondence should be addressed to Dong-Dong Wu; ddwubiomed2010@163.com
and Xin-Ying Ji; 10190096@vip.henu.edu.cn

Received 10 January 2021; Revised 19 April 2021; Accepted 14 May 2021; Published 5 July 2021

Academic Editor: Kanhaiya Singh

Copyright © 2021 Yasmeen Ahmed Salaheldin et al. This is an open access article distributed under the Creative Commons Attribution License, which permits unrestricted use, distribution, and reproduction in any medium, provided the original work is properly cited.

Various research works have piled up conflicting evidence questioning the effect of oxidative stress in cancer. Reactive oxygen and nitrogen species (RONS) are the reactive radicals and nonradical derivatives of oxygen and nitrogen. RONS can act as a double-edged weapon. On the one hand, RONS can promote cancer initiation through activating certain signal transduction pathways that direct proliferation, survival, and stress resistance. On the other hand, they can mitigate cancer progression via their resultant oxidative stress that causes many cancer cells to die, as some recent studies have proposed that high RONS levels can limit the survival of cancer cells during certain phases of cancer development. Similarly, eukaryotic translation initiation factors are key players in the process of cellular transformation and tumorigenesis. Dysregulation of such translation initiation factors in the form of overexpression, downregulation, or phosphorylation is associated with cancer cell's altering capability of survival, metastasis, and angiogenesis. Nonetheless, eIFs can affect tumor age-related features. Data shows that alternating the eukaryotic translation initiation apparatus can impact many downstream cellular signaling pathways that directly affect cancer development. Hence, researchers have been conducting various experiments towards a new trajectory to find novel therapeutic molecular targets to improve the efficacy of anticancer drugs as well as reduce their side effects, with a special focus on oxidative stress and initiation of translation to harness their effect in cancer development. An increasing body of scientific evidence recently links oxidative stress and translation initiation factors to cancer-related signaling pathways. Therefore, in this review, we present and summarize the recent findings in this field linking certain signaling pathways related to tumorigenesis such as MAPK and PI3K, with either RONS or eIFs.

1. Introduction

Cancer is considered the second leading cause of mortality worldwide according to the World Health Organization. Chemotherapy and radiotherapy can help in the management of some types of cancer, but the net outcome of onco-

logical diseases is still far from satisfactory, which directs most of the contemporary medical researchers to focus on this field. Several studies have been conducted to find new molecular therapeutic strategies, to improve the efficacy of cancer treatment and reduce the side effects. Recent research has been focusing on oxidative stress and initiation of

translation as a potential target in cancer treatment. Some types of cancer such as acute lymphocytic leukemia and neuroblastoma are more common in young adults [1, 2], with around 50% of testicular cancer cases occurring in men between the age of 20 and 34 [3]. Cancer diseases are more common among the elderly population due to longer exposure to various risk factors such as exposure to chemicals, radiation, chronic inflammation, unhealthy lifestyle, accumulation of altered macromolecules, and decreased immunity [4]. Patients younger than 20 years old account for only 1.4% of all newly diagnosed cancer cases according to Global Cancer Observatory.

Cancer cells alter mitochondrial dynamics, which include mitochondrial fission and fusion that primarily determine the balance between mitochondrial energy production and cell death programs. Cancer cells cause mitochondrial dynamics to resist apoptosis and adjust their bioenergetic and biosynthetic requirements to support tumor initiation and transformation properties such as autophagy, proliferation, migration, and therapeutic resistance. Microenvironmental stresses impact intratumoral heterogeneity and impose stem-like traits on cancer cells. Major cancer-related pathways such as mitogen-activated protein kinase and phosphatidylinositol-3-kinase, which are both activated by reactive oxygen and nitrogen species, can reprogram mitochondrial function and dynamics. Cancer cells rely on such reprogramming for sustained proliferation, the capacity to metastasize and to resist apoptosis, thus positioning mitochondria as a pivot for major cancer traits [5].

Aerobic eukaryotes are faced with a phenomenon known as the oxygen paradox, where they cannot survive without oxygen, but at the same time, oxygen is considered lethal to their survival. This is due to the presence of unpaired electrons. The mitochondrial electron transport chain produces water from the reduction of oxygen. However, the univalent reduction of oxygen produces reactive intermediates which are frequently encountered within the physiological cellular state [6]. Reactive oxygen species are those reactive intermediates, in other words, partially reduced oxygen molecules that can give rise to functional and morphological cellular disturbances being capable of reacting with almost every component of the cell [7]. On the one hand, RONS can mutate nucleic acid and damage cellular components that raised the assumption many years ago stating that both cellular aging and cancer initiation may reflect accumulated damage of RONS over periods [8]. On the other hand, Gonskikh and Polacek demonstrated that RONS can be beneficial. They explained that reduced protein synthesis caused by oxidative stress is associated with increased production of specific proteins that improve the overall cellular performance [9].

RONS are the reactive radicals and nonradical derivatives of oxygen and nitrogen. They are produced in all aerobic cells and play a key role in cancer. They both originate from endogenous and exogenous sources. Exogenous sources include air and water pollution, drugs (e.g., cyclosporins, tacrolimus, gentamycin, and bleomycin), tobacco, alcohol, heavy metals, industrial solvents, cooking (e.g., smoked meat, waste oil, and fat), and radiation, which are metabolized

inside the body into free radicals, whereas endogenous sources consist of nicotinamide adenine dinucleotide phosphate oxidase, myeloperoxidase, lipoxygenase, and angiotensin II [10, 11]. Oxidative stress is a result of antioxidants and RONS imbalance due to either depletion of antioxidants or accumulation of RONS as shown in (Figure 1). RONS such as superoxide, peroxy radical, hydrogen peroxide, hydroxyl radical, and peroxy nitrite can react with nucleic acids, proteins, and lipids, thus resulting in cell and tissue damage.

Different subcellular compartments including both enzymatic and nonenzymatic reactions produce RONS. The enzymatic reactions include superoxide dismutase, glutathione peroxidase, guaiacol peroxidase, peroxiredoxins, and enzymes of the ascorbate-glutathione cycle, such as ascorbate peroxidase, monodehydroascorbate reductase, dehydroascorbate reductase, and glutathione reductase, whereas non-enzymatic examples include vitamin C, vitamin E, and glutathione molecule [12]. Two main cellular organelles, namely, the endoplasmic reticulum and the mitochondria, are intimately involved in RONS production and their metabolism. They both constitute a fundamental role in redox regulation [13]. Cellular enzymes known as NADPH oxidases produce a considerable amount of RONS in humans [6]. Other cellular sources of RONS include neutrophils, monocytes, cardiomyocytes, endothelial cells, xanthine oxidases, cytochrome P450, lipoxygenases, and nitric oxide synthases [14, 15]. Peroxisomes also produce RONS via both beta-oxidation of fatty acids and flavin oxidase activity [16]. RONS are involved in various physiological processes and essential protective mechanisms that living organisms use for their survival. The protective mechanisms obviously would be the role of the immune defense [17] and vascular tone [18] which aims at maintaining a state of homeostasis. Living organisms strive to keep those highly reactive molecules under tight control with the help of a complex system of antioxidants [19]. Accumulated evidence over time suggested that RONS has a pivotal role in the determination of cell fate, acting as second messengers and modifying various signaling molecules.

Oxidative stress refers to the incapability of the cell to detoxify free radicals produced, resulting in inefficient cellular performance. The mechanism used by the cell in response to oxidant effects is to restore the balance by promoting or inhibiting genes encoding defensive enzymes, transcription factors, and structural proteins [20]. The accumulation of these reactive species affects normal cellular pathways and therefore plays a positive role in cancer by damaging the amino acids, DNA, and lipids that act as building blocks of the body. Intracellular RONS are important components of intracellular signaling cascades [21]. A recent study suggested that RONS act as a double agent by promoting cancer initiation through activating signaling pathways that control proliferation, survival, and stress resistance and on the other side by suppressing cancer initiation and progression via oxidative stress that kills many cancer cells [22].

Initiation of translation is the complex and rate-determining step of protein synthesis. This process is conserved in all eukaryotes, and it involves multiple eukaryotic initiation factors, including but not limited to eIF1, eIF1a,

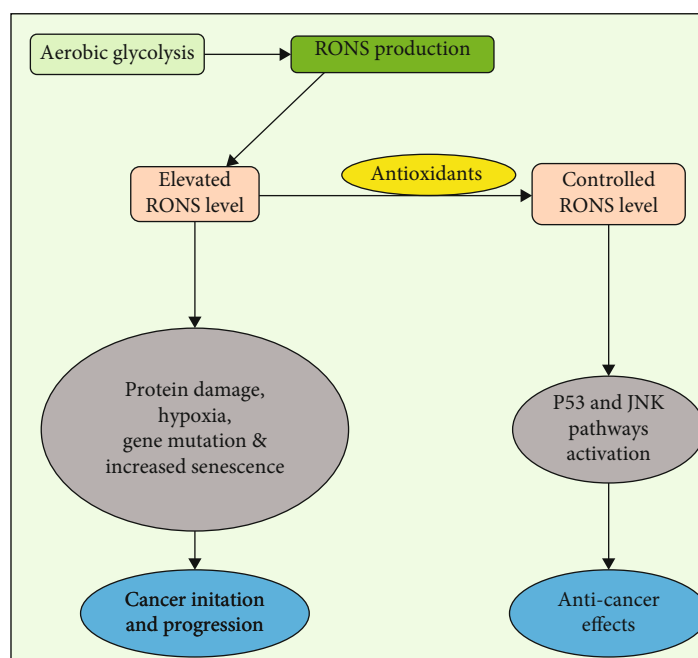


FIGURE 1: A schematic presentation of RONS levels in the cell and their impact, the reasonable amounts of RONS are a key player for activating protective signaling pathways whereas elevated RONS is considered lethal to most cellular functions and may lead to cancer development. RONS: reactive oxygen and nitrogen species; P53: tumor suppressor; JNK: Jun N-terminal kinase.

eIF2, eIF2b, eIF3, eIF4a, eIF4e, eIF4g, eIF4b, eIF4h, eIF5, eIF5b, and eIF6 [23]. eIFs are proteins, most of which are composed of several subunits, and have a major role in the regulation of the translation initiation machinery [24]. Major events in initiation comprise (1) formation of a 43S preinitiation complex which consists of a 40S ribosomal subunit and binds to eIFs 1, 1A, 3, and 5 and also a ternary complex consisting of the initiating methionyl-tRNA which binds to eIF2-Guanosine triphosphate (eIF2-GTP-MettRNAi); (2) assembling of eIF4F complex (eIF4E, eIF4G, eIF4A) on mRNA 5' m7GpppN cap; (3) eIF4F complex facilitating the recruitment of the 43S PIC to the mRNA via eIF4G-eIF3 interaction to form the 43S mRNA initiation complex; (4) in the 43S mRNA initiation complex, scanning of the mRNA 5' of the untranslated region in the 5' to 3' direction to the initiation codon; (5) initiation codon recognition and 48S complex formation; (6) eIF5B promoting the hydrolysis of eIF2-bound guanosine triphosphate, the displacement of eIFs, and the joining of a 60S subunit; (7) GTP hydrolysis by eIF5B and release of eIF1A and guanosine diphosphate-bound eIF5B from assembled elongation-competent 80S ribosomes; (8) formation of an active 80S ribosome to initiate protein synthesis; and (9) eIF5A promoting peptide bond formation and translation elongation. The inactive eIF2-GDP is recycled to active eIF2-GTP by GTP recycling factor eIF2B [23–27]. Dysregulation of translation initiation factors in the form of overexpression, downregulation, or phosphorylation affects cancer cell survival, metastasis, and tumor angiogenesis and aging-related features [23, 27].

Signaling pathways and translation initiation factors have represented a promising aspect for further studies in cancer treatment, as their dysregulation promotes cancer progres-

sion. In addition, *in vivo* trials have provided up-and-coming results, including some that have already moved to the final phase of clinical trial. RONS play a double agent role, depending on their cumulative amount within the cell. The impact of elevated amounts of RONS is of greater importance when it comes to developing new cancer therapeutics; however, targeting RONS requires determining the threshold level of lethal RONS in different cells, opening an opportunity for more research to be done concerning the mechanisms and relevant applications of the proposed approaches.

Blocking dysregulated signaling pathways such as (PI3K/Ak strain transforming/mechanistic target of rapamycin) pathway and translation regulators by kinase inhibitors have yielded promising outcomes as cancer treatment targets. Also, researchers aiming at targeting dysregulated eIFs as a cancer therapy focus on eIF4 complex. This may be achieved in many ways such as suppressing eIF4E activity or targeting its subunits [23]. It may help in controlling the disease and discovering a new vision for cancer treatment in combination with conventional chemotherapeutics. Future studies should focus on determining the clear mechanism and the role of initiation factors in aging. Another study demonstrated that overexpression of forkhead box O6 inhibits the migration and progression of breast cancer cells [28]. Understanding crosstalk between the signaling pathways is the major challenge in targeting signaling pathways, and also, the adverse events associated with drugs make treatment more complicated.

2. RONS in Cancer

At low levels, RONS can be beneficial to cells activating signaling pathways that promote survival. In contrast, at higher

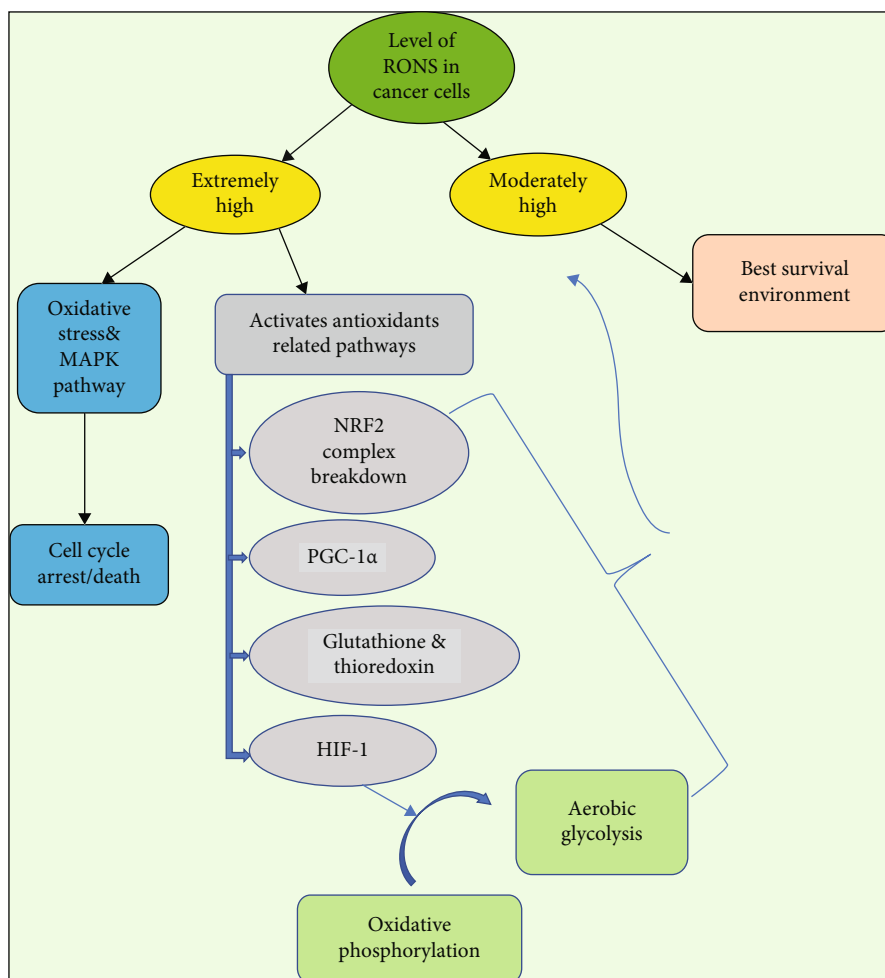


FIGURE 2: A schematic illustration of RONS regulation within cancer cells depicting some of the mechanisms used to reduce the extreme accumulation of RONS to reach the optimum level for cellular performance and survival. Excessive accumulation of RONS enhances cell death notably via ASK1/JNK/P38 MAPK pathway activation. RONS: reactive oxygen and nitrogen species; NRF2: nuclear factor erythroid-derived 2-like 2; PGC-1 α : peroxisome proliferator-activated receptor gamma coactivator one alpha; HIF-1: hypoxic inducible factor one.

levels, RONS can damage or even kill cells by oxidizing cellular components including proteins, lipids, and most importantly nucleic acids. However, recent studies have proposed that high RONS levels can also limit the survival of cancer cells during certain phases of cancer initiation and progression [22]. In some cancer cells, high RONS levels can be attributed to hypoxia, sustained mitochondrial respiration, unfolded protein response, and oncogenesis [29]. Classically, RONS have been demonstrated to promote various types of cancers. This was attributed to their ability to induce DNA damage and thus enhancing the rate of tumor-causing mutations and genetic instability besides their proinflammatory effect. Recent evidence suggests that cancer cells are more sensitive than normal cells to elevated RONS levels [30] and that they rely on glutathione and thioredoxin for protection [31]. In some cancers, including melanomas, oxidative stress acted as a barrier to distant metastasis [32].

Besides, the survival of tumor cells outside of a normal tissue context requires adaptation to the metabolism of different microenvironments. Cancer cells depend on a variety

of mechanisms to suppress RONS and to cope with oxidative stress [22]. Cancer cell uses several mechanisms to avoid the extreme accumulation of radicals as shown in Figure 2. For example, hypoxia-inducible factor, which is a transcription factor that responds to the decrease in available cellular oxygen in response to elevated RONS levels, has been shown to mediate the shift of oxidative phosphorylation of anaerobic glycolysis aiming to decrease RONS levels and eventually increase the survival of cancer cells during their metastasis to the lungs [33]. In a new study, peroxisome proliferator-activated receptor gamma coactivator 1-alpha protein, a key molecule activated by RONS production, involved in mitochondrial biogenesis and antioxidant enzymes activation was identified to promote chemoresistance in response to RONS generated by exposure of cells to ovarian sphere-forming culture conditions [34]. Moreover, nuclear factor-like, an inducible antioxidant program, is a redox stress-sensitive transcription factor that induces several antioxidant and detoxification genes. The activation of the NRF2 antioxidant program in response to cellular stressors results in a decrease

in RONS levels. DeNicola and colleagues have demonstrated that several endogenous oncogenes such as KRAS, BRAF, and Myc in mice can actively induce the NRF2 expression, promoting a RONS detoxification program and hence creating a more “reduced” intracellular environment. This program is what the authors have suggested is required for tumor initiation [35]. NRF2-deficient cancer cells showed impaired cancer progression by globally suppressing protein translation due to unopposed oxidative stress [36]. Multiple transcription factors such as activation transcription factor 4 also cooperate to induce an antioxidant response that promotes survival. NRF2 and ATF4 promote the expression of serine/glycine biosynthesis enzymes to increase glutathione synthesis, which reduces oxidative stress and promotes survival during metastasis [37]. Tumors from approximately 15% of patients with lung cancer harbor somatic mutations in Kelch-like ECH-associated protein 1 that prevent effective NRF2 repression [38].

Some other tumor suppressors also act partly by suppressing RONS production. BCR-ABL-transformed cells (cells with gene translocation between chromosomes 9 and 22, also known as Philadelphia chromosome) show increased intracellular RONS, as well as oxidative DNA damage and chromosomal fragmentation [39]. The oxidative inhibition of phosphatase and TENsin homolog, PTEN, a tumor suppressor gene, by abnormally elevated levels of RONS in many tumors could functionally impair the tumor-suppressing activity of the enzyme, enhancing tumor development [40]. Another study demonstrated a cysteine residue involving the mechanism by which Maspin, another tumor suppressor, reduces RONS production, and RONS scavenging was associated with the inhibition of extracellular signal-regulated kinase 1/2 [41].

2.1. Nuclear Factor Kappa-Light-Chain Enhancer of Activated B Pathway. NF- κ B is a transcription factor that is considered crucial in many processes including inflammatory response, cellular adhesion, differentiation, proliferation, autophagy, senescence, and apoptosis. The disorder of NF- κ B has already been confirmed to be associated with cancer [42]. The bidirectional interrelation was found between both RONS and NF- κ B. The NF- κ B pathway may be activated by at least two distinct pathways named canonical and non-canonical pathways. RONS affect NF- κ B in multiple manners, e.g., RONS can activate the noncanonical pathway, leading to NF- κ B activation [43]. At the same time, the canonical pathway can be inactivated, leading to NF- κ B inhibition. NF- κ B can influence the RONS levels by increasing the expression of various antioxidant proteins [44]. A recent study found that the NF- κ B pathway can also be activated by a tumor necrosis factor receptor that is regulated by eIF3b in human osteosarcoma cells [45].

2.2. Mitogen-Activated Protein Kinase (MAPK) Pathway. Another signaling pathway altered by RONS is the MAPK pathway. MAPK cascades are major intracellular signal transduction pathways that play an important role in various cellular processes such as cell growth, differentiation, development, cell cycle, survival, and cell death. The MAPK/ERK

pathway is activated mainly by growth factors, and this depends primarily on RAS phosphorylation [46]. RONS have been shown to activate the receptors of epidermal growth factor and platelet-derived growth factor in the absence of their corresponding ligands, which can stimulate RAS and the subsequent activation of the MAPK pathway [47]. Also, it has been demonstrated that RONS generated by commensal bacteria in the activated DUSP3 gene by oxidation on Cys-124 results in MAPK pathway activation. DUSP3 gene maps to a region that contains the BRCA-1 locus, which confers susceptibility to breast and ovarian cancer [48]. RONS was also found to activate c-JUN N-terminal kinase pathway that is one of the MAPK cascades [49, 50].

2.3. PI3K/AKT Pathway. The PI3K/AKT pathway is involved in many critical cellular functions, including protein synthesis, cell cycle progression, proliferation, apoptosis, autophagy, and drug resistance [51]. RONS do not only activate PI3K directly but also concurrently inactivates PTEN, which inhibits the activation of AKT. PTEN is a tumor suppressor gene on chromosome 10, and its mutation is linked to many cancers; RONS can also enhance PTEN to enter the proteolytic degradation pathway [52].

2.4. Calcium Signaling Pathway. In eukaryotic cells, calcium acts as one of the most versatile signals involved in the control of cellular processes and functions, such as contraction, secretion, metabolism, gene expression, cell survival, and cell death. A bidirectional interrelation was found between both calcium and RONS [53]. The primary role of calcium is to promote adenosine triphosphate synthesis and RONS generation in mitochondria via stimulating the Krebs cycle enzymes and oxidative phosphorylation [54]. Calcium ion regulates several extramitochondrial RONS generating enzymes, such as NADPH oxidase and nitric oxide synthase [55]. Besides, calcium modulates RONS clearance processes by regulating the antioxidant defense system. Calcium ions can directly activate antioxidant enzymes such as catalase and glutathione reductase, increase the level of superoxide dismutase, and induce mitochondrial glutathione release. Meanwhile, calmodulin, a ubiquitous calcium-binding protein, activates catalase in the presence of calcium and downregulates hydrogen peroxide levels [56]. Moreover, RONS can also influence calcium signaling by oxidizing cysteine thiol groups of the calcium channel [57].

Mitochondria Permeability Transition Pore, a large, non-specific channel spanning the inner and outer mitochondrial membranes, is known to control the lethal permeability changes that initiate mitochondrial-driven death [58]. RONS modulate mPTP opening in two ways: firstly, by directly oxidizing different sites in its structure [55] and secondly by either indirectly increasing the mitochondrial calcium concentration [59] or by activating the Jun N-terminal kinase pathway [50]. In a recent study, opening mPTP was shown to cause RONS to increase and promote apoptosis in cancer cells [60].

2.5. Protein Kinases. RONS function in various cellular processes via oxidizing the sulfhydryl groups of cysteine residues

in various protein kinases such as protein kinase C/D, calmodulin-dependent protein kinase II, and receptor tyrosine kinases such as insulin receptor, epidermal growth factor receptor, and platelet growth factor receptor, resulting in their activation [61, 62]. RONS play a dual role in both stimulation and inactivation of PKC following its concentration: higher doses of oxidants react with catalytically important cysteine residues inactivating PKC whereas low doses induce stimulation of PKC activity [63].

2.6. Ubiquitination/Proteasome System. Ubiquitination/proteasome system plays an indispensable role in a variety of biological processes such as regulation of the cell cycle, inflammatory responses, immune response, protein misfolding, and endoplasmic reticulum-associated degradation of proteins [64]. Oxidative stress affects the process of ubiquitination in different ways. First, the rapid depletion of reduced glutathione and improvement of the levels of oxidized glutathione upon exposure to oxidative stress result in the oxidation of cysteine residues at the active sites of the ubiquitin-activating enzymes E1 and E2 and the generation of mixed disulfide bonds, which block their binding to ubiquitin thus altering its function [65]. Second, it has also been reported that bacteria elicit RONS generation in epithelial cells that inactivate the Ubc12 enzyme by preventing the neddylation of cullin-1, rendering it unable to carry out ubiquitination and thus making it inactive [66]. Third, the proteasome itself is considered a target of oxidative stress, and it was proposed that the 26S proteasome is more susceptible than the 20S proteasome to oxidative inactivation [67].

Meanwhile, ubiquitination impacted by RONS has been studied in some cancers. 3-Hydroxy butyrate dehydrogenase 2 is considered to be an important tumor suppressor in gastric cancer. BDH2 was found to regulate the level of intracellular RONS to mediate the PI3K/Akt pathway through Keap1/Nrf2 signaling, thereby inhibiting the growth of gastric cancer. Mechanistically, BDH2 promoted Keap1 interaction with Nrf2 to increase the ubiquitination of Nrf2 consequently increasing the level of RONS, thereby inhibiting the phosphorylation of AKT and mTOR [68]. Another study handled ubiquitination in thyroid cancer, and they found that vitamin C kills thyroid cancer cells by inhibiting MAPK/ERK and PI3K/AKT pathways via a RONS-dependent mechanism. They suggested that vitamin C eradicated BRAF wild-type thyroid cancer cells through a ROS-mediated decrease in the activity of epidermal growth factor/epidermal growth factor receptor-MAPK/ERK signaling and an increase in AKT ubiquitination [69]. Sajadimajd and Khazaei studied the ubiquitination of NRF2 and its correlation with RONS. They found that under normal conditions, NRF2 is commonly degraded in the cytoplasm by interaction with Keap1 inhibitor as an adaptor for ubiquitination factors. However, a high amount of RONS activates tyrosine kinases to dissociate NRF2: Keap1 complex, nuclear import of NRF2, and coordinated activation of cytoprotective gene expression [70].

2.7. FOXO Apoptotic Pathway. Cancer cells are known by their ability to escape cancer drugs by hijacking autophagy;

in the light of recent studies, it is idealized that blocking autophagy can help in increasing apoptosis through transcriptional factor FOXO3a which links the two processes, by maintaining autophagy equilibrium and controlling a gene responsible for making an apoptosis-facilitating protein called p53 upregulated modulator of apoptosis [71].

FOXO transcription factors are involved in inducing apoptotic injury and RONS regulation in cancer cells. Overexpression of Survivin, an antiapoptotic protein acting on the FOXO3 apoptotic pathway, has been reported in neuroblastoma cells. FOXO3a is shown to prevent reactive oxygen species accumulation and shift energy production from oxidative phosphorylation to glycolysis [72]. The pathway is activated by cellular oxidative stress via PI3K signaling. An elevated level of superoxide dismutase 2 is associated with increased FOXO activity [73], while NAD-dependent deacetylase sirtuin-3 was demonstrated to promote the FOXO3a expression by inhibiting the wingless-related integration site/ β -catenin pathway. They suggested that upregulation of FOXO6 was shown to inhibit epithelial-mesenchymal transition and migration of breast cancer cells and vice versa [28].

2.8. Pentose Phosphate Pathway. The PPP, which branches from glycolysis at the first committed step of glucose metabolism, is required for the synthesis of ribonucleotides and is a major source of NADPH. PPP is crucial for cancer cell survival and lipid biosynthesis. Given that NADPH is central to oxidative stress resistance, cancer cells modulate the PPP to maintain their anabolic demands and keep a state of redox homeostasis. Recently, several neoplastic lesions were shown to have evolved to facilitate the flux of glucose into the pentose phosphate pathway [74]. Circulating microRNA-21, a homotetrameric protein that was found to be highly expressed in many solid tumors, catalyzes the oxidative decarboxylation of malate to yield carbon dioxide and pyruvate, with concomitant reduction of NAD⁺ or NADP⁺. In non-small-cell lung cancer cell lines, MIR-21 depletion caused an inhibition of cell proliferation with induction of cell death accompanied by increased RONS. Furthermore, MIR-21 knockdown impacts phosphoinositide-dependent kinase-1 and PTEN expression, leading to PI3k pathway inhibition [75].

The big picture reflecting the contribution of various mediators plus local environmental factors seems to be the actual determinant for RONS-induced consequences in both physiology and pathology; therefore, it is essential to unravel the not-yet-well-understood parts of this intricate picture for a better understanding of the RONS induced alterations [19]. The net effect of RONS on cancer reflects a complex combination of adaptive and maladaptive consequences within the cells and their environment [22].

3. eIFs in Cancer

Messenger RNA translation or protein synthesis plays a major role in the regulation of the eukaryotic gene expression [76]. Many studies confirmed that dysregulation of the translational machinery, especially in the initiation, can lead to abnormal gene expression and uncontrolled cell growth

TABLE 1: Functions of different eIFs.

Protein	Function	Refs.
eIF1	mRNA screening and delivery of tRNA.	[23, 101]
eIF2	Initiation codon recognition.	[27]
eIF2b	Allows for the next initiation to occur (returns the released GDP to GTP).	
eIF3	Recruiting translation factors and 40S ribosome subunits to the mRNA.	[23, 24, 102]
eIF4F	Multisubunit complex:	[24, 103]
(i) eIF4E	CAP binding activity, a rate-limiting factor.	
(ii) eIF4G	Scaffolding protein and interaction partner for other factors.	
(iii) eIF4A	RNA helicase.	
(iv) eIF4B and eIF4H	mRNA secondary structure unwinding.	
eLF5	Translation elongation and bond formation.	[23]
eIF6	Prevents 60S subunit association with 40S subunit in the absence of mRNA (antiasociation factor).	[25]

eIF: eukaryotic initiation factor; mRNA: messenger RNA; tRNA: transfer RNA; GDP: glutamine dipeptide; GTP: glutamine tripeptide; CAP: catabolite activator protein.

resulting in cancer [25, 77–79]. Regulation of the translational process is mainly achieved by the rate-limiting initiation step, which is organized by multiple eukaryotic initiation factors [20]. Out of many eIFs, only six are involved in translation initiation. Table 1 describes the six factors involved and the role of each one.

Alteration in initiation rate can occur by a change in initiation factors' availability or activation of oncogenic signaling pathways, such as PI3K/AKT/mTOR and MAPK pathways [80]. Many relations have been found between the translation machinery and some oncogenes such as Myc and RAS families and tumor suppressors such as PTEN and p53 [77–79].

Translation initiation factors also have a major role in cellular transformation and tumorigenesis. Dysregulation of translation initiation factors in the form of overexpression, downregulation, or phosphorylation is involved in cancer cell survival, metastasis, and tumor angiogenesis [23, 27]. The regulation of initiation factors including overexpression of eIF4A, eIF4E, and eIF4G; downregulation of eIF4E-binding protein levels; and phosphorylation of eIF2 is involved in various types of cancer as shown in Table 2 [23, 27, 78, 81]. And still, the specific role played by increased initiation factors, levels, or activity in cancer behavior remains poorly understood.

3.1. MAPK/MAPK-Interacting Kinases 1-2 Pathway. MNK1 and MNK2 phosphorylate eIF4E on a single residue Ser209. MAPK and ERK pathways activate MNKs in response to stress and mitogens, respectively [82]. Hyperphosphorylation of eIF4E can lead to an increase in specific mRNA translation that encodes prosurvival proteins such as myeloid cell leukemia-1, invasion, and epithelial to mesenchymal transition promoting proteins and cytokines [83]. Experimental results revealed that complete loss of eIF4E phosphorylation in the absence of MNK1 and MNK2 in the mouse model may delay the development of tumorigenesis [84]. Hence, the

eIF4F complex has an important role in tumorigenesis, which is affected by many oncogenic pathways [85].

3.2. PI3K/AKT Pathway. E74-like factor 4 complex is a multi-subunit which consists of eIF4E, eIF4A, and eIF4G. It is considered as a rate-limiting component in the initiation of translation as its role is to recruit small ribosomal subunits and related factors (43S, PICs) to the 5' end of mRNA [23]. The mTOR has a major role in the regulation of eIF4E [86]. As hyperphosphorylation of eIF4E binding proteins by mTOR enables its dissociation from eIF4E, so eIF4F can interact with eIF4G and form eIF4 complex and continue the translation process [85].

In cancer, activation of oncogenes (e.g., AKT) or loss of tumor suppressors (e.g., PTEN) leads to activation of mTORC1, a hallmark of a cancer cell, which enhances cell proliferation, survival, and invasion [86]. Hyperactivated mTOR can lead to overexpression of eIF4E, which promotes the translation of specific mRNAs which are involved in angiogenesis, cell proliferation, and cell survival, namely, vascular endothelial growth factor-A, cMyc, and B-cell lymphoma 2, respectively [87]. Cellular stresses, such as amino acid deprivation and hypoxia, which are common in tumors, downregulate mTORC1 activity, preventing the formation of the eIF4F complex, and thus downregulating protein synthesis [85].

Previous studies have confirmed that the overexpression of eIF4F or loss of eIF4E-binding protein 1 is the key feature of most poor prognostic and drug-resistant cancer cells [88, 89]. Some studies suggested that increased mTOR activity can also lead to overexpression of eIF4A1 [23, 25]. On the other hand, eIF6 is necessary for ribosome biogenesis in the nucleus. Several studies have described eIF6 as an important factor in age-related diseases such as colorectal cancer, malignant pleural mesothelioma, and breast cancer. In CRC and MPM, eIF6 was overexpressed compared to nonneoplastic tissues, suggesting a key contribution to

TABLE 2: Dysregulated eIFs in different types of cancer.

Protein	Form of dysregulation	Resultant cancer	Refs.
eIF1	Overexpression	HCC	[104]
	Mutation	Thyroid cancer	[105]
eIF2 alpha	Increased Phosphorylation	Oropharyngeal	[95]
	Overexpression	Gastrointestinal	[106]
		NSCL	[107]
		Lymphoma	[23]
		Brain tumor	[108]
		Thyroid carcinoma	[109]
eIF3A	Overexpression	Colorectal	[110]
eIF3B		Esophageal	[111]
eIF3C		Glioma	[112]
eIF3D		Breast	[92]
		Prostate	[93]
		Gastric	[113]
eIF3H		HCC	[114]
eIF3I		Head and neck	[115]
eIF3M		Colorectal	[116]
eIF3E	Downregulation	Breast	[23]
eIF3F		Pancreatic	[117]
		Brain	[108]
		Endometrial	[118]
		Head and neck	[119]
		Bladder	[120]
		Cervical	[121]
		Prostate	[122]
		Colon	[123]
		Liver	[124]
		Lymphoma	[125]
eIF4E	Overexpression	Esophagus	[126]
		Gastric	[127]
		Nasopharyngeal	[128]
		Breast	[80, 129]
		Squamous cell lung cancer	[130]
		Cervical cancer	[81]
		Melanoma	[131]
eIF4A	Downregulation	Breast	[132]
		Lung	[133]
eIF4B	Overexpression	B-cell lymphoma	[134]
eIF4H		Lung	[135]

TABLE 2: Continued.

Protein	Form of dysregulation	Resultant cancer	Refs.
eIF5	Overexpression	HCC	[136]
		Glioblastoma	[137]
		Lung	[138]
		Urinary bladder	[139]
eIF6	Overexpression	Ovarian	[140]
		Colorectal	[141]
		Leukemia	[142]
		Ovarian serous	[143]

HCC: hepatocellular carcinoma; NSCL: non-small-cell lung cancer.

carcinogenesis. In a recent study, the knockdown of eIF6 in adenocarcinoma and squamous cell carcinoma led to pre-rRNA processing and ribosomal 60S maturation defects, and in non-small-cell lung cancer, there was upregulation of eIF6 [90].

3.3. Miscellaneous Pathways Involving eIFs in Cancer. Other studies confirmed that silencing eIF3a reverses the malignant phenotype of human lung and breast cancer cell lines and downregulates the cyclin dependent kinase inhibitor p27 [91]. Silencing eIF3d also showed a role in limiting the proliferation and invasion of cancer cells by suppressing Wnt/B-catenin signaling and cyclin dependent kinase-1 [92, 93]. The overexpression of eIF3f may lead to suppression of AKT and ERK signaling, an increase of p53 protein levels, and inhibition of clusters in protein expression, which also promotes cancer cell proliferation and reduces chemosensitivity [94]. Recent studies also suggest that prolonged eIF2 α phosphorylation, which prevents the conversion of GDP to GTP by increasing the affinity of eIF2B for eIF2-GDP, results in blocking of protein synthesis [27]. eIF2 α can promote cell survival, transformation, and drug resistance, whereas other studies suggest that eIF2 α phosphorylation can trigger apoptosis [95, 96]. Moreover, eIF6 is upregulated and active in many human cancers and may be regulated by protein kinase C by phosphorylation on S235 [97].

4. RONS Impacting eIFs

RONS can affect eIFs in different ways. A study confirmed that specific translational control driven by eIF6 is essential for adjusting a set of RONS-controlling genes in megakaryocytes. Specifically, genes coding for the mitochondrial electron transport chain complex I and complex IV and those involved in RONS production. They identified the pathways of the mitochondrial electron transport chain and oxidative phosphorylation as the most significantly impaired [98]. Another group of researchers investigated the mechanism linking eIF5A2 and RONS. They found that the inhibition of eIF5A2 affects epithelial mesenchymal transition progression so that it decreases the invasion and metastasis of hepatocellular carcinoma cells via RONS-related pathways [99]. Moreover, it is suggested that radiation-induced autophagy

is a prosurvival response initiated by oxidative stress and mediated by eIF2A kinase 3 [100].

5. Conclusion

Oxidative stress and initiation of translation fundamentally influence oncogenesis and age-related diseases by altering the relevant downstream pathways and that can be used to our privilege in treating oncologic diseases. Oxidative stress has been described as one of the main causes of cellular damage and mutations resulting in decreased cellular performance; however, these radicals existing in reasonable amounts within the cell can play a crucial role in the activation of various signaling pathways. Initiation of translation is an important step in synthesizing a protein, altering of which can affect the quantity and quality of the proteins produced. To maintain normal cellular functioning, these proteins need to be degraded; failure of that degradation will lead to accumulated proteins, consequently increasing the possibility of cancer. Moreover, dysregulation of translation initiation factors has been associated with cancer progression; however, more studies are needed to determine the involved mechanism. Hence, future studies should focus more on harnessing the initiation of translation and reactive radicals to target cancer cells. Targeting the pathways associated with the initiation of translation and RONS should be given the utmost priority.

Data Availability

Data are deposited in a repository.

Conflicts of Interest

The authors declare that they have no competing interests.

Acknowledgments

This work was supported by grants from the National Natural Science Foundation of China (Nos. 81802718 and 81670088), the Foundation of Science & Technology Department of Henan Province, China (Nos. 202102310480 and 192102310151), and the Training Program for Young Backbone Teachers of Institutions of Higher Learning in Henan Province, China (No. 2020GGJS038).

References

- [1] J. L. McNeer and A. Bleyer, "Acute lymphoblastic leukemia and lymphoblastic lymphoma in adolescents and young adults," *Pediatric Blood & Cancer*, vol. 65, no. 6, article e26989, 2018.
- [2] E. Olecki and C. N. Grant, "MIBG in neuroblastoma diagnosis and treatment," *Seminars in Pediatric Surgery*, vol. 28, no. 6, article 150859, 2019.
- [3] P. Chieffi, "An up-date on novel molecular targets in testicular germ cell tumors subtypes," *Intractable & rare diseases research*, vol. 8, no. 2, pp. 161–164, 2019.
- [4] I. Liguori, G. Russo, F. Curcio et al., "Oxidative stress, aging, and diseases," *Clinical Interventions in Aging*, vol. Volume 13, pp. 757–772, 2018.
- [5] D. Senft and A. R. Ze'ev, "Regulators of mitochondrial dynamics in cancer," *Current Opinion in Cell Biology*, vol. 39, pp. 43–52, 2016.
- [6] B. Lassègue, A. San Martín, and K. K. Griendling, "Biochemistry, physiology, and pathophysiology of NADPH oxidases in the cardiovascular system," *Circulation Research*, vol. 110, no. 10, pp. 1364–1390, 2012.
- [7] M. Martinez-Cayuela, "Oxygen free radicals and human disease," *Biochimie*, vol. 77, no. 3, pp. 147–161, 1995.
- [8] D. Harman, "Aging: a theory based on free radical and radiation chemistry," *Journal of Gerontology*, vol. 11, no. 3, pp. 298–300, 1956.
- [9] Y. Gonskikh and N. Polacek, "Alterations of the translation apparatus during aging and stress response," *Mechanisms of Ageing and Development*, vol. 168, pp. 30–36, 2017.
- [10] M. Genestra, "Oxyl radicals, redox-sensitive signalling cascades and antioxidants," *Cellular Signalling*, vol. 19, no. 9, pp. 1807–1819, 2007.
- [11] A. Phaniendra, D. B. Jestadi, and L. Periyasamy, "Free radicals: properties, sources, targets, and their implication in various diseases," *Indian Journal of Clinical Biochemistry*, vol. 30, no. 1, pp. 11–26, 2015.
- [12] J. M. McCord and I. Fridovich, "Superoxide Dismutase," *The Journal of Biological Chemistry*, vol. 244, no. 22, pp. 6049–6055, 1969.
- [13] D. Hernández-García, C. D. Wood, S. Castro-Obregón, and L. Covarrubias, "Reactive oxygen species: a radical role in development?," *Free Radical Biology & Medicine*, vol. 49, no. 2, pp. 130–143, 2010.
- [14] F. J. Cubero and N. Nieto, "Arachidonic acid stimulates TNF α production in Kupffer cells via a reactive oxygen species-pERK1/2-Egr1-dependent mechanism," *American Journal of Physiology-Gastrointestinal and Liver Physiology*, vol. 303, no. 2, pp. G228–G239, 2012.
- [15] E. I. Azzam, J. P. Jay-Gerin, and D. Pain, "Ionizing radiation-induced metabolic oxidative stress and prolonged cell injury," *Cancer Letters*, vol. 327, no. 1-2, pp. 48–60, 2012.
- [16] M. Schrader and H. D. Fahimi, "Peroxisomes and oxidative stress," *Biochimica et Biophysica Acta*, vol. 1763, no. 12, pp. 1755–1766, 2006.
- [17] W. Dröge, "Free radicals in the physiological control of cell function," *Physiological Reviews*, vol. 82, no. 1, pp. 47–95, 2002.
- [18] Y. Liu, H. Zhao, H. Li, B. Kalyanaraman, A. C. Nicolosi, and D. D. Gutterman, "Mitochondrial sources of H₂O₂ generation play a key role in flow-mediated dilation in human coronary resistance arteries," *Circulation Research*, vol. 93, no. 6, pp. 573–580, 2003.
- [19] A. A. Alfadda and R. M. Sallam, "Reactive oxygen species in health and disease," *Journal of Biomedicine and Biotechnology*, vol. 2012, 14 pages, 2012.
- [20] E. Birben, U. M. Sahiner, C. Sackesen, S. Erzurum, and O. Kalayci, "Oxidative stress and antioxidant defense," *World Allergy Organization Journal*, vol. 5, no. 1, pp. 9–19, 2012.
- [21] A. Bratic and N. G. Larsson, "The role of mitochondria in aging," *The Journal of Clinical Investigation*, vol. 123, no. 3, pp. 951–957, 2013.

- [22] J. G. Gill, E. Piskounova, and S. J. Morrison, "Cancer, oxidative stress, and metastasis," *Cold Spring Harbor Symposia on Quantitative Biology*, vol. 81, pp. 163–175, 2016.
- [23] M. U. Ali, M. S. Ur Rahman, Z. Jia, and C. Jiang, "Eukaryotic translation initiation factors and cancer," *Tumor Biology*, vol. 39, no. 6, p. 1010428317709805, 2017.
- [24] R. Spilka, C. Ernst, A. K. Mehta, and J. Haybaeck, "Eukaryotic translation initiation factors in cancer development and progression," *Cancer Letters*, vol. 340, no. 1, pp. 9–21, 2013.
- [25] J. Chu, M. Cargnello, I. Topisirovic, and J. Pelletier, "Translation initiation factors: reprogramming protein synthesis in cancer," *Trends in Cell Biology*, vol. 26, no. 12, pp. 918–933, 2016.
- [26] R. J. Jackson, C. U. Hellen, and T. V. Pestova, "The mechanism of eukaryotic translation initiation and principles of its regulation," *Nature Reviews Molecular Cell Biology*, vol. 11, no. 2, pp. 113–127, 2010.
- [27] C. de la Parra, B. A. Walters, P. Geter, and R. J. Schneider, "Translation initiation factors and their relevance in cancer," *Current Opinion in Genetics & Development*, vol. 48, pp. 82–88, 2018.
- [28] R. Li, Y. Quan, and W. Xia, "SIRT3 inhibits prostate cancer metastasis through regulation of FOXO3A by suppressing Wnt/ β -catenin pathway," *Experimental Cell Research*, vol. 364, no. 2, pp. 143–151, 2018.
- [29] C. Gorrini, I. S. Harris, and T. W. Mak, "Modulation of oxidative stress as an anticancer strategy," *Nature Reviews Drug Discovery*, vol. 12, no. 12, pp. 931–947, 2013.
- [30] L. Raj, T. Ide, A. U. Gurkar et al., "Selective killing of cancer cells by a small molecule targeting the stress response to ROS," *Nature*, vol. 475, no. 7355, pp. 231–234, 2011.
- [31] I. S. Harris and J. S. Brugge, "The enemy of my enemy is my friend," *Nature*, vol. 527, no. 7577, pp. 170–171, 2015.
- [32] E. Piskounova, M. Agathocleous, M. M. Murphy et al., "Oxidative stress inhibits distant metastasis by human melanoma cells," *Nature*, vol. 527, no. 7577, pp. 186–191, 2015.
- [33] T. Zhao, Y. Zhu, A. Morinibu et al., "HIF-1-mediated metabolic reprogramming reduces ROS levels and facilitates the metastatic colonization of cancers in lungs," *Scientific Reports*, vol. 4, no. 1, pp. 1–7, 2014.
- [34] B. Kim, J. W. Jung, J. Jung et al., "PGC1 α induced by reactive oxygen species contributes to chemoresistance of ovarian cancer cells," *Oncotarget*, vol. 8, no. 36, pp. 60299–60311, 2017.
- [35] G. M. DeNicola, F. A. Karreth, T. J. Humpton et al., "Oncogene-induced Nrf2 transcription promotes ROS detoxification and tumorigenesis," *Nature*, vol. 475, no. 7354, pp. 106–109, 2011.
- [36] I. I. C. Chio, S. M. Jafarnejad, M. Ponz-Sarvise et al., "NRF2 promotes tumor maintenance by modulating mRNA translation in pancreatic cancer," *Cell*, vol. 166, no. 4, pp. 963–976, 2016.
- [37] G. M. DeNicola, P.-H. Chen, E. Mullarky et al., "NRF2 regulates serine biosynthesis in non-small cell lung cancer," *Nature Genetics*, vol. 47, no. 12, pp. 1475–1481, 2015.
- [38] J. D. Hayes and M. McMahon, "NRF2 and KEAP1 mutations: permanent activation of an adaptive response in cancer," *Trends in Biochemical Sciences*, vol. 34, no. 4, pp. 176–188, 2009.
- [39] M. O. Nowicki, R. Falinski, M. Koptyra et al., "BCR/ABL oncogenic kinase promotes unfaithful repair of the reactive oxygen species-dependent DNA double-strand breaks," *Blood*, vol. 104, no. 12, pp. 3746–3753, 2004.
- [40] M. Benhar, D. Engelberg, and A. Levitzki, "ROS, stress-activated kinases and stress signaling in cancer," *EMBO Reports*, vol. 3, no. 5, pp. 420–425, 2002.
- [41] N. Mahajan, H. Y. Shi, T. J. Lukas, and M. Zhang, "Tumor-suppressive maspin functions as a reactive oxygen species scavenger: importance of cysteine residues," *Journal of Biological Chemistry*, vol. 288, no. 16, pp. 11611–11620, 2013.
- [42] A. S. Baldwin, "Regulation of cell death and autophagy by IKK and NF- κ B: critical mechanisms in immune function and cancer," *Immunological Reviews*, vol. 246, no. 1, pp. 327–345, 2012.
- [43] J.-H. Kim, H.-J. Na, C.-K. Kim et al., "The non-provitamin A carotenoid, lutein, inhibits NF- κ B-dependent gene expression through redox-based regulation of the phosphatidylinositol 3-kinase/PTEN/Akt and NF- κ B-inducing kinase pathways: role of H₂O₂ in NF- κ B activation," *Free Radical Biology and Medicine*, vol. 45, no. 6, pp. 885–896, 2008.
- [44] N. L. Reynaert, A. van der Vliet, A. S. Guala et al., "Dynamic redox control of NF- κ B through glutaredoxin-regulated S-glutathionylation of inhibitory κ B kinase beta," *Proceedings of the National Academy of Sciences*, vol. 103, no. 35, pp. 13086–13091, 2006.
- [45] Y. J. Choi, Y. S. Lee, H. W. Lee, D. M. Shim, and S. W. Seo, "Silencing of translation initiation factor eIF3b promotes apoptosis in osteosarcoma cells," *Bone & joint research*, vol. 6, no. 3, pp. 186–193, 2017.
- [46] A. Plotnikov, E. Zehorai, S. Procaccia, and R. Seger, "The MAPK cascades: signaling components, nuclear roles and mechanisms of nuclear translocation," *Biochimica et Biophysica Acta (BBA) - Molecular Cell Research*, vol. 1813, no. 9, pp. 1619–1633, 2011.
- [47] H. Lei and A. Kazlauskas, "Growth factors outside of the platelet-derived growth factor (PDGF) family employ reactive oxygen species/Src family kinases to activate PDGF receptor α and thereby promote proliferation and survival of cells," *Journal of Biological Chemistry*, vol. 284, no. 10, pp. 6329–6336, 2009.
- [48] C. C. Wentworth, A. Alam, R. M. Jones, A. Nusrat, and A. S. Neish, "Enteric commensal bacteria induce extracellular signal-regulated kinase pathway signaling via formyl peptide receptor-dependent redox modulation of dual specific phosphatase 3," *Journal of Biological Chemistry*, vol. 286, no. 44, pp. 38448–38455, 2011.
- [49] C. Davies and C. Tournier, "Exploring the function of the JNK (c-Jun N-terminal kinase) signalling pathway in physiological and pathological processes to design novel therapeutic strategies," *Biochemical Society Transactions*, vol. 40, no. 1, pp. 85–89, 2012.
- [50] M. Castro-Caldas, A. N. Carvalho, E. Rodrigues, C. Henderson, C. R. Wolf, and M. J. Gama, "Glutathione S-transferase pi mediates MPTP-induced c-Jun N-terminal kinase activation in the nigrostriatal pathway," *Molecular Neurobiology*, vol. 45, no. 3, pp. 466–477, 2012.
- [51] X. Qiu, J. C. Cheng, H. M. Chang, and P. C. Leung, "COX2 and PGE2 mediate EGF-induced E-cadherin-independent human ovarian cancer cell invasion," *Endocrine-Related Cancer*, vol. 21, no. 4, pp. 533–543, 2014.
- [52] N. R. Leslie and C. P. Downes, "PTEN: the down side of PI 3-kinase signalling," *Cellular Signalling*, vol. 14, no. 4, pp. 285–295, 2002.

- [53] J. R. Naranjo and B. Mellström, "Ca²⁺-dependent transcriptional control of Ca²⁺ homeostasis," *Journal of Biological Chemistry*, vol. 287, no. 38, pp. 31674–31680, 2012.
- [54] A. Lewis, T. Hayashi, T. P. Su, and M. J. Betenbaugh, "Bcl-2 family in inter-organelle modulation of calcium signaling; roles in bioenergetics and cell survival," *Journal of Bioenergetics and Biomembranes*, vol. 46, no. 1, pp. 1–15, 2014.
- [55] J. Zhang, X. Wang, V. Vikash et al., "ROS and ROS-Mediated Cellular Signaling," *Oxidative Medicine and Cellular Longevity*, vol. 2016, Article ID 4350965, 18 pages, 2016.
- [56] A. V. Gordeeva, R. A. Zvyagil'skaya, and Y. A. Labas, "Cross-talk between reactive oxygen species and calcium in living cells," *Biochemistry (Moscow)*, vol. 68, no. 10, pp. 1077–1080, 2003.
- [57] R. Chaube, D. T. Hess, Y. J. Wang et al., "Regulation of the skeletal muscle ryanodine receptor/Ca²⁺-release channel RyR1 by S-palmitoylation," *Journal of Biological Chemistry*, vol. 289, no. 12, pp. 8612–8619, 2014.
- [58] G. Morciano, C. Giorgi, M. Bonora et al., "Molecular identity of the mitochondrial permeability transition pore and its role in ischemia-reperfusion injury," *Journal of Molecular and Cellular Cardiology*, vol. 78, pp. 142–153, 2015.
- [59] S. Voronina, E. Okeke, T. Parker, and A. Tepikin, "How to win ATP and influence Ca²⁺ signaling," *Cell Calcium*, vol. 55, no. 3, pp. 131–138, 2014.
- [60] S. NavaneethaKrishnan, J. L. Rosales, and K. Y. Lee, "Loss of Cdk5 in breast cancer cells promotes ROS-mediated cell death through dysregulation of the mitochondrial permeability transition pore," *Oncogene*, vol. 37, no. 13, pp. 1788–1804, 2018.
- [61] A. Eisenberg-Lerner and A. Kimchi, "PKD is a kinase of Vps34 that mediates ROS-induced autophagy downstream of DAPK," *Cell Death & Differentiation*, vol. 19, no. 5, pp. 788–797, 2012.
- [62] C. M. Sag, H. A. Wolff, K. Neumann et al., "Ionizing radiation regulates cardiac Ca handling via increased ROS and activated CaMKII," *Basic Research in Cardiology*, vol. 108, no. 6, pp. 1–15, 2013.
- [63] G. A. Ramirez-Correa, S. Cortassa, B. Stanley, W. D. Gao, and A. M. Murphy, "Calcium sensitivity, force frequency relationship and cardiac troponin I: critical role of PKA and PKC phosphorylation sites," *Journal of Molecular and Cellular Cardiology*, vol. 48, no. 5, pp. 943–953, 2010.
- [64] M. Kim, R. Otsubo, H. Morikawa et al., "Bacterial effectors and their functions in the ubiquitin-proteasome system: insight from the modes of substrate recognition," *Cell*, vol. 3, no. 3, pp. 848–864, 2014.
- [65] M. Obin, F. Shang, X. Gong, G. Handelman, J. Blumberg, and A. Taylor, "Redox regulation of ubiquitin-conjugating enzymes: mechanistic insights using the thiol-specific oxidant diamide," *The FASEB Journal*, vol. 12, no. 7, pp. 561–569, 1998.
- [66] A. Kumar, H. Wu, L. S. Collier-Hyams et al., "Commensal bacteria modulate cullin-dependent signaling via generation of reactive oxygen species," *The EMBO Journal*, vol. 26, no. 21, pp. 4457–4466, 2007.
- [67] T. Reinheckel, O. Ullrich, N. Sitte, and T. Grune, "Differential impairment of 20S and 26S proteasome activities in human hematopoietic K562 cells during oxidative stress," *Archives of Biochemistry and Biophysics*, vol. 377, no. 1, pp. 65–68, 2000.
- [68] J.-Z. Liu, Y.-L. Hu, Y. Feng et al., "BDH2 triggers ROS-induced cell death and autophagy by promoting Nrf2 ubiquitination in gastric cancer," *Journal of Experimental & Clinical Cancer Research*, vol. 39, no. 1, pp. 1–18, 2020.
- [69] X. Su, Z. Shen, Q. Yang et al., "Vitamin C kills thyroid cancer cells through ROS-dependent inhibition of MAPK/ERK and PI3K/AKT pathways via distinct mechanisms," *Theranostics*, vol. 9, no. 15, pp. 4461–4473, 2019.
- [70] S. Sajadimajd and M. Khazaei, "Oxidative stress and cancer: the role of Nrf2," *Current Cancer Drug Targets*, vol. 18, no. 6, pp. 538–557, 2018.
- [71] K. Jiang, C. Zhang, B. Yu et al., "Autophagic degradation of FOXO3a represses the expression of PUMA to block cell apoptosis in cisplatin-resistant osteosarcoma cells," *American Journal of Cancer Research*, vol. 7, no. 7, pp. 1407–1422, 2017.
- [72] J. Hagenbuchner and M. J. Ausserlechner, "Mitochondria and FOXO3: breath or die," *Frontiers in Physiology*, vol. 4, p. 147, 2013.
- [73] H. van Ooijen, M. Hornsveld, C. D.-d. Veen et al., "Assessment of functional phosphatidylinositol 3-kinase pathway activity in cancer tissue using forkhead box-O target gene expression in a knowledge-based computational model," *The American Journal of Pathology*, vol. 188, no. 9, pp. 1956–1972, 2018.
- [74] K. C. Patra and N. Hay, "The pentose phosphate pathway and cancer," *Trends in Biochemical Sciences*, vol. 39, no. 8, pp. 347–354, 2014.
- [75] W. Ren, C. Qiang, L. Gao et al., "Circulating microRNA-21 (MIR-21) and phosphatase and tensin homolog (PTEN) are promising novel biomarkers for detection of oral squamous cell carcinoma," *Biomarkers*, vol. 19, no. 7, pp. 590–596, 2014.
- [76] N. Sonenberg and A. G. Hinnebusch, "Regulation of translation initiation in eukaryotes: mechanisms and biological targets," *Cell*, vol. 136, no. 4, pp. 731–745, 2009.
- [77] D. Ruggero, "Translational control in cancer etiology," *Cold Spring Harbor Perspectives in Biology*, vol. 5, no. 2, pp. a012336–a012336, 2013.
- [78] D. Silvera, S. C. Formenti, and R. J. Schneider, "Translational control in cancer," *Nature Reviews Cancer*, vol. 10, no. 4, pp. 254–266, 2010.
- [79] M. Bhat, N. Robichaud, L. Hulea, N. Sonenberg, J. Pelletier, and I. Topisirovic, "Targeting the translation machinery in cancer," *Nature Reviews Drug Discovery*, vol. 14, pp. 261–278, 2015.
- [80] D. Silvera, R. Arju, F. Darvishian et al., "Essential role for eIF4GI overexpression in the pathogenesis of inflammatory breast cancer," *Nature Cell Biology*, vol. 11, no. 7, pp. 903–908, 2009.
- [81] S. Liang, Y. Zhou, Y. Chen, G. Ke, H. Wen, and X. Wu, "Decreased expression of EIF4A1 after preoperative brachytherapy predicts better tumor-specific survival in cervical cancer," *International Journal of Gynecologic Cancer*, vol. 24, no. 5, pp. 908–915, 2014.
- [82] T. Ueda, R. Watanabe-Fukunaga, H. Fukuyama, S. Nagata, and R. Fukunaga, "Mnk2 and Mnk1 are essential for constitutive and inducible phosphorylation of eukaryotic initiation factor 4E but not for cell growth or development," *Molecular and Cellular Biology*, vol. 24, no. 15, pp. 6539–6549, 2004.
- [83] N. Robichaud and N. Sonenberg, "eIF4E and its binding proteins," in *Translation and Its Regulation in Cancer Biology and Medicine*, pp. 73–113, Springer, Dordrecht, 2014.

- [84] T. Ueda, M. Sasaki, A. J. Elia et al., "Combined deficiency for MAP kinase-interacting kinase 1 and 2 (Mnk1 and Mnk2) delays tumor development," *Proceedings of the National Academy of Sciences*, vol. 107, no. 32, pp. 13984–13990, 2010.
- [85] C. Demosthenous, J. J. Han, M. J. Stenson et al., "Translation initiation complex eIF4F is a therapeutic target for dual mTOR kinase inhibitors in non-Hodgkin lymphoma," *Oncotarget*, vol. 6, no. 11, pp. 9488–9501, 2015.
- [86] A. C. Hsieh, Y. Liu, M. P. Edlind et al., "The translational landscape of mTOR signalling steers cancer initiation and metastasis," *Nature*, vol. 485, no. 7396, pp. 55–61, 2012.
- [87] Y. Mamane, E. Petroulakis, L. Rong, K. Yoshida, L. W. Ler, and N. Sonenberg, "eIF4E - from translation to transformation," *Oncogene*, vol. 23, no. 18, pp. 3172–3179, 2004.
- [88] S. Avdulov, S. Li, D. B. Van Michalek et al., "Activation of translation complex eIF4F is essential for the genesis and maintenance of the malignant phenotype in human mammary epithelial cells," *Cancer Cell*, vol. 5, no. 6, pp. 553–563, 2004.
- [89] D. Ruggero, L. Montanaro, L. Ma et al., "The translation factor eIF-4E promotes tumor formation and cooperates with c-Myc in lymphomagenesis," *Nature Medicine*, vol. 10, no. 5, pp. 484–486, 2004.
- [90] V. Gandin, A. Miluzio, A. M. Barbieri et al., "Eukaryotic initiation factor 6 is rate-limiting in translation, growth and transformation," *Nature*, vol. 455, no. 7213, pp. 684–688, 2008.
- [91] Y. Zhang, J. J. Yu, Y. Tian et al., "eIF3a improve cisplatin sensitivity in ovarian cancer by regulating XPC and p27Kip1 translation," *Oncotarget*, vol. 6, no. 28, pp. 25441–25451, 2015.
- [92] Y. Fan and Y. Guo, "Knockdown of eIF3D inhibits breast cancer cell proliferation and invasion through suppressing the Wnt/ β -catenin signaling pathway," *International Journal of Clinical and Experimental Pathology*, vol. 8, no. 9, pp. 10420–10427, 2015.
- [93] Y. Gao, J. Teng, Y. Hong et al., "The oncogenic role of EIF3D is associated with increased cell cycle progression and motility in prostate cancer," *Medical Oncology*, vol. 32, no. 7, pp. 1–8, 2015.
- [94] J. Y. Lee, H. J. Kim, S. B. Rho, and S. H. Lee, "eIF3f reduces tumor growth by directly interrupting clusterin with anti-apoptotic property in cancer cells," *Oncotarget*, vol. 7, no. 14, pp. 18541–18557, 2016.
- [95] Q. Qiao, C. Sun, C. Han, N. Han, M. Zhang, and G. Li, "Endoplasmic reticulum stress pathway PERK-eIF2 α confers radioresistance in oropharyngeal carcinoma by activating NF- κ B," *Cancer Science*, vol. 108, no. 7, pp. 1421–1431, 2017.
- [96] A. E. Koromilas and Z. Mounir, "Control of oncogenesis by eIF2 α phosphorylation: implications in PTEN and PI3K-Akt signaling and tumor treatment," *Future Oncology*, vol. 9, no. 7, pp. 1005–1015, 2013.
- [97] N. Gantenbein, E. Bernhart, I. Anders et al., "Influence of eukaryotic translation initiation factor 6 on non-small cell lung cancer development and progression," *European Journal of Cancer*, vol. 101, pp. 165–180, 2018.
- [98] S. Ricciardi, A. Miluzio, D. Brina et al., "Eukaryotic translation initiation factor 6 is a novel regulator of reactive oxygen species-dependent megakaryocyte maturation," *Journal of Thrombosis and Haemostasis*, vol. 13, no. 11, pp. 2108–2118, 2015.
- [99] R. R. Liu, Y. S. Lv, Y. X. Tang et al., "Eukaryotic translation initiation factor 5A2 regulates the migration and invasion of hepatocellular carcinoma cells via pathways involving reactive oxygen species," *Oncotarget*, vol. 7, no. 17, pp. 24348–24360, 2016.
- [100] M. Chaurasia, S. Gupta, A. Das, B. S. Dwarakanath, A. Simonsen, and K. Sharma, "Radiation induces EIF2AK3/PERK and ERN1/IRE1 mediated pro-survival autophagy," *Autophagy*, vol. 15, no. 8, pp. 1391–1406, 2019.
- [101] H. Miyasaka, S. Endo, and H. Shimizu, "Eukaryotic translation initiation factor 1 (eIF1), the inspector of good AUG context for translation initiation, has an extremely bad AUG context," *Journal of Bioscience and Bioengineering*, vol. 109, no. 6, pp. 635–637, 2010.
- [102] Z. Sha, L. M. Brill, R. Cabrera et al., "The eIF3 interactome reveals the translatome, a supercomplex linking protein synthesis and degradation machineries," *Molecular Cell*, vol. 36, no. 1, pp. 141–152, 2009.
- [103] D. Walsh, C. Perez, J. Notary, and I. Mohr, "Regulation of the translation initiation factor eIF4F by multiple mechanisms in human cytomegalovirus-infected cells," *Journal of Virology*, vol. 79, no. 13, pp. 8057–8064, 2005.
- [104] S. L. Zhou, Z. J. Zhou, Z. Q. Hu et al., "Tumor-associated neutrophils recruit macrophages and T-regulatory cells to promote progression of hepatocellular carcinoma and resistance to sorafenib," *Gastroenterology*, vol. 150, no. 7, pp. 1646–1658.e17, 2016.
- [105] J. W. Kunstman, C. C. Juhlin, G. Goh et al., "Characterization of the mutational landscape of anaplastic thyroid cancer via whole-exome sequencing," *Human Molecular Genetics*, vol. 24, no. 8, pp. 2318–2329, 2015.
- [106] M. V. Lobo, M. E. Martín, M. I. Pérez et al., "Levels, phosphorylation status and cellular localization of translational factor eIF2 in gastrointestinal carcinomas," *The Histochemical Journal*, vol. 32, no. 3, pp. 139–150, 2000.
- [107] Y. He, H. Yu, L. Rozeboom et al., "LAG-3 protein expression in non-small cell lung cancer and its relationship with PD-1/PD-L1 and tumor-infiltrating lymphocytes," *Journal of thoracic oncology : official publication of the International Association for the Study of Lung Cancer*, vol. 12, no. 5, pp. 814–823, 2017.
- [108] S. Tejada, M. V. Lobo, M. García-Villanueva et al., "Eukaryotic initiation factors (eIF) 2 α and 4E expression, localization, and phosphorylation in brain tumors," *Journal of Histochemistry & Cytochemistry*, vol. 57, no. 5, pp. 503–512, 2009.
- [109] W. Wang, W. Zhao, H. Wang et al., "Poorer prognosis and higher prevalence of BRAF V600E mutation in synchronous bilateral papillary thyroid carcinoma," *Annals of Surgical Oncology*, vol. 19, no. 1, pp. 31–36, 2012.
- [110] J. Haybaeck, O'Connor T, R. Spilka et al., "Overexpression of p150, a part of the large subunit of the eukaryotic translation initiation factor 3, in colon cancer," *Anticancer Research*, vol. 30, no. 4, pp. 1047–1055, 2010.
- [111] B. Xu, L. Chen, J. Li et al., "Prognostic value of tumor infiltrating NK cells and macrophages in stage II+ III esophageal cancer patients," *Oncotarget*, vol. 7, no. 46, pp. 74904–74916, 2016.
- [112] J. Hao, C. Liang, and B. Jiao, "Eukaryotic translation initiation factor 3, subunit C is overexpressed and promotes cell proliferation in human glioma U-87 MG cells," *Oncology Letters*, vol. 9, no. 6, pp. 2525–2533, 2015.

- [113] J. He, X. Wang, J. Cai, W. Wang, and X. Qin, "High expression of eIF3d is associated with poor prognosis in patients with gastric cancer," *Cancer Management and Research*, vol. 9, pp. 539–544, 2017.
- [114] Q. Zhu, G. L. Qiao, X. C. Zeng et al., "Elevated expression of eukaryotic translation initiation factor 3H is associated with proliferation, invasion and tumorigenicity in human hepatocellular carcinoma," *Oncotarget*, vol. 7, no. 31, pp. 49888–49901, 2016.
- [115] M. Ahlemann, R. Zeidler, S. Lang, B. Mack, M. Münz, and O. Gires, "Carcinoma-associated eIF3i overexpression facilitates mTOR-dependent growth transformation," *Molecular Carcinogenesis*, vol. 45, no. 12, pp. 957–967, 2006.
- [116] S.-H. Goh, S.-H. Hong, S.-H. Hong et al., "eIF3m expression influences the regulation of tumorigenesis-related genes in human colon cancer," *Oncogene*, vol. 30, no. 4, pp. 398–409, 2011.
- [117] A. Doldan, A. Chandramouli, R. Shanas et al., "Loss of the eukaryotic initiation factor 3f in pancreatic cancer," *Molecular Carcinogenesis*, vol. 47, no. 3, pp. 235–244, 2008.
- [118] S. B. Korets, S. Czok, S. V. Blank, J. P. Curtin, and R. J. Schneider, "Targeting the mTOR/4E-BP pathway in endometrial cancer," *Clinical Cancer Research*, vol. 17, no. 24, pp. 7518–7528, 2011.
- [119] M. S. Haydon, J. D. Googe, D. S. Sorrells, G. E. Ghali, and B. D. Li, "Progression of eIF4e gene amplification and overexpression in benign and malignant tumors of the head and neck," *Cancer*, vol. 88, no. 12, pp. 2803–2810, 2000.
- [120] J. P. Crew, S. Fuggle, R. Bicknell, D. W. Cranston, A. De Benedetti, and A. L. Harris, "Eukaryotic initiation factor-4E in superficial and muscle invasive bladder cancer and its correlation with vascular endothelial growth factor expression and tumour progression," *British Journal of Cancer*, vol. 82, no. 1, pp. 161–166, 2000.
- [121] J. W. Lee, J. J. Choi, K. M. Lee et al., "eIF-4E expression is associated with histopathologic grades in cervical neoplasia," *Human Pathology*, vol. 36, no. 11, pp. 1197–1203, 2005.
- [122] J. R. Graff, B. W. Konicek, R. L. Lynch et al., "eIF4E activation is commonly elevated in advanced human prostate cancers and significantly related to reduced patient survival," *Cancer Research*, vol. 69, no. 9, pp. 3866–3873, 2009.
- [123] H. J. Berkel, E. A. Turbat-Herrera, R. Shi, and A. de Benedetti, "Expression of the translation initiation factor eIF4E in the polyp-cancer sequence in the colon," *Cancer Epidemiology and Prevention Biomarkers*, vol. 10, no. 6, pp. 663–666, 2001.
- [124] X. L. Wang, H. P. Cai, J. H. Ge, and X. F. Su, "Detection of eukaryotic translation initiation factor 4E and its clinical significance in hepatocellular carcinoma," *World journal of gastroenterology: WJG*, vol. 18, no. 20, pp. 2540–2544, 2012.
- [125] S. X. Yang, S. M. Hewitt, S. M. Steinberg, D. J. Liewehr, and S. M. Swain, "Expression levels of eIF4E, VEGF, and cyclin D1, and correlation of eIF4E with VEGF and cyclin D1 in multi-tumor tissue microarray," *Oncology Reports*, vol. 17, no. 2, pp. 281–287, 2007.
- [126] H. S. Hsu, H. W. Chen, C. L. Kao, M. L. Wu, A. F. Y. Li, and T. H. Cheng, "MDM2 is overexpressed and regulated by the eukaryotic translation initiation factor 4E (eIF4E) in human squamous cell carcinoma of esophagus," *Annals of Surgical Oncology*, vol. 18, no. 5, pp. 1469–1477, 2011.
- [127] C. N. Chen, F. J. Hsieh, Y. M. Cheng, P. H. Lee, and K. J. Chang, "Expression of eukaryotic initiation factor 4E in gastric adenocarcinoma and its association with clinical outcome," *Journal of Surgical Oncology*, vol. 86, no. 1, pp. 22–27, 2004.
- [128] L. Tu, Z. Liu, X. He et al., "Over-expression of eukaryotic translation initiation factor 4 gamma 1 correlates with tumor progression and poor prognosis in nasopharyngeal carcinoma," *Molecular Cancer*, vol. 9, no. 1, p. 78, 2010.
- [129] S. Braunstein, K. Karpisheva, C. Pola et al., "A hypoxia-controlled cap-dependent to cap-independent translation switch in breast cancer," *Molecular Cell*, vol. 28, no. 3, pp. 501–512, 2007.
- [130] S. D. Wagner, A. E. Willis, and D. Beck, "eIF4G," in *In Translation and Its Regulation in Cancer Biology and Medicine*, pp. 163–171, Springer, Dordrecht, 2014.
- [131] A. Parsyan, R. J. Sullivan, A. N. Meguerditchian, and S. Meterissian, "Melanoma and Non-Melanoma Skin Cancers," in *In Translation and Its Regulation in Cancer Biology and Medicine*, pp. 435–452, Springer, Dordrecht, 2014.
- [132] Z. Nasr, F. Robert, J. A. Porco Jr., W. J. Muller, and J. Pelletier, "eIF4F suppression in breast cancer affects maintenance and progression," *Oncogene*, vol. 32, no. 7, pp. 861–871, 2013.
- [133] X. Shaoyan, Y. Juanjuan, T. Yalan, H. Ping, L. Jianzhong, and W. Qinian, "Downregulation of EIF4A2 in non-small-cell lung cancer associates with poor prognosis," *Clinical Lung Cancer*, vol. 14, no. 6, pp. 658–665, 2013.
- [134] E. Horvilleur, T. Sbarrato, K. Hill et al., "A role for eukaryotic initiation factor 4B overexpression in the pathogenesis of diffuse large B-cell lymphoma," *Leukemia*, vol. 28, no. 5, pp. 1092–1102, 2014.
- [135] Y. Bai, C. Lu, G. Zhang et al., "Overexpression of miR-519d in lung adenocarcinoma inhibits cell proliferation and invasion via the association of eIF4H," *Tumour biology: the journal of the International Society for Oncodevelopmental Biology and Medicine*, vol. 39, no. 3, p. 1010428317694566, 2017.
- [136] F. H. Shek, S. Fatima, and N. P. Lee, "Implications of the Use of Eukaryotic Translation Initiation Factor 5A (eIF5A) for Prognosis and Treatment of Hepatocellular Carcinoma," *International journal of hepatology*, vol. 2012, Article ID 760928, 6 pages, 2012.
- [137] M. Preukschas, C. Hagel, A. Schulte et al., "Expression of eukaryotic initiation factor 5A and hypusine forming enzymes in glioblastoma patient samples: implications for new targeted therapies," *PLoS One*, vol. 7, no. 8, article e43468, 2012.
- [138] M. Caraglia, M. H. Park, E. C. Wolff, M. Marra, and A. Abbuzzese, "eIF5A isoforms and cancer: two brothers for two functions?," *Amino Acids*, vol. 44, no. 1, pp. 103–109, 2013.
- [139] W. Chen, J.-H. Luo, W.-F. Hua et al., "Overexpression of EIF-5A2 is an independent predictor of outcome in patients of urothelial carcinoma of the bladder treated with radical cystectomy," *Cancer Epidemiology and Prevention Biomarkers*, vol. 18, no. 2, pp. 400–408, 2009.
- [140] G. F. Yang, D. Xie, J. H. Liu et al., "Expression and amplification of eIF-5A2 in human epithelial ovarian tumors and overexpression of EIF-5A2 is a new independent predictor of outcome in patients with ovarian carcinoma," *Gynecologic Oncology*, vol. 112, no. 2, pp. 314–318, 2009.
- [141] Y. Bao, Y. Lu, X. Wang et al., "Eukaryotic translation initiation factor 5A2 (eIF5A2) regulates chemoresistance in

- colorectal cancer through epithelial mesenchymal transition,” *Cancer Cell International*, vol. 15, no. 1, p. 109, 2015.
- [142] F. Weis, E. Giudice, M. Churcher et al., “Mechanism of eIF6 release from the nascent 60S ribosomal subunit,” *Nature Structural & Molecular Biology*, vol. 22, no. 11, pp. 914–919, 2015.
- [143] R. J. Flavin, P. C. Smyth, S. P. Finn et al., “Altered eIF6 and Dicer expression is associated with clinicopathological features in ovarian serous carcinoma patients,” *Modern Pathology*, vol. 21, no. 6, pp. 676–684, 2008.

Research Article

Integrated Analysis to Identify a Redox-Related Prognostic Signature for Clear Cell Renal Cell Carcinoma

Yue Wu,^{1,2} Xian Wei,^{1,2} Huan Feng,^{1,2} Bintao Hu,^{1,2} Bo Liu,³ Yang Luan,^{1,2} Yajun Ruan,^{1,2} Xiaming Liu,^{1,2} Zhuo Liu,^{1,2} Jihong Liu,^{1,2} and Tao Wang^{1,2} 

¹Department of Urology, Tongji Hospital, Tongji Medical College, Huazhong University of Science and Technology, Wuhan, 430030 Hubei, China

²Institute of Urology, Tongji Hospital, Tongji Medical College, Huazhong University of Science and Technology, Wuhan, 430030 Hubei, China

³Department of Oncology, Tongji Hospital, Tongji Medical College, Huazhong University of Science and Technology, Wuhan, 430030 Hubei, China

Correspondence should be addressed to Tao Wang; tjhwt@126.com

Received 25 November 2020; Revised 3 March 2021; Accepted 12 April 2021; Published 22 April 2021

Academic Editor: Adil Mardinoglu

Copyright © 2021 Yue Wu et al. This is an open access article distributed under the Creative Commons Attribution License, which permits unrestricted use, distribution, and reproduction in any medium, provided the original work is properly cited.

The imbalance of the redox system has been shown to be closely related to the occurrence and progression of many cancers. However, the biological function and clinical significance of redox-related genes (RRGs) in clear cell renal cell carcinoma (ccRCC) are unclear. In our current study, we downloaded transcriptome data from The Cancer Genome Atlas (TCGA) database of ccRCC patients and identified the differential expression of RRGs in tumor and normal kidney tissues. Then, we identified a total of 344 differentially expressed RRGs, including 234 upregulated and 110 downregulated RRGs. Fourteen prognosis-related RRGs (*ADAM8*, *CGN*, *EIF4EBP1*, *FOXM1*, *G6PC*, *HAMP*, *HTR2C*, *ITIH4*, *LTB4R*, *MMP3*, *PLG*, *PRKCG*, *SAA1*, and *VWF*) were selected out, and a prognosis-related signature was constructed based on these RRGs. Survival analysis showed that overall survival was lower in the high-risk group than in the low-risk group. The area under the receiver operating characteristic curve of the risk score signature was 0.728 at three years and 0.759 at five years in the TCGA cohort and 0.804 at three years and 0.829 at five years in the E-MTAB-1980 cohort, showing good predictive performance. In addition, we explored the regulatory relationships of these RRGs with upstream miRNA, their biological functions and molecular mechanisms, and their relationship with immune cell infiltration. We also established a nomogram based on these prognostic RRGs and performed internal and external validation in the TCGA and E-MTAB-1980 cohorts, respectively, showing an accurate prediction of ccRCC prognosis. Moreover, a stratified analysis showed a significant correlation between the prognostic signature and ccRCC progression.

1. Introduction

Renal cell carcinoma (RCC) is one of the most common urogenital tumors, among which clear cell RCC (ccRCC) is the most common subtype, accounting for about 75% of all renal tumors [1]. The standard treatment for ccRCC is surgery, with a high cure rate for localized disease, early and a 5-year survival rate of more than 90%, while the 5-year survival rate for patients with distant metastases

drops to 12% [2]. However, nearly 25-30% of ccRCC patients are diagnosed with advanced cancer, and 30% have distant metastases after surgery for early cancer [3, 4]. In addition, the TNM staging system (tumor, lymph node, and metastasis) currently used clinically cannot effectively predict the invasiveness of ccRCC [5]. Although some renal carcinoma-related biomarkers have been released recently, such as Li et al. [6] have developed a classification system of ccRCC based on PKM alternative splicing; Caliskan et al.

[7] conducted comparative analysis of RNA-seq transcriptome data of different RCC subtypes and found reporter molecules that were specific to each other or subtype; there are still few markers or models that can be used to predict the prognosis of ccRCC patients clinically. Therefore, in-depth exploration of the molecular mechanism of ccRCC, identification of biomarkers that can effectively predict the prognosis and progression of ccRCC, and development of effective early screening and diagnosis methods are of vital importance for improving the treatment effect and quality of life of patients.

The homeostasis system of cellular redox forms a delicate balance between the production of reactive oxygen species (ROS) and the removal of reactive oxygen species by antioxidant enzymes and small-molecule antioxidants, and participates in the regulation of physiological events such as cell signal transduction, proliferation, and differentiation at normal low concentrations [8, 9]. However, excessive intracellular ROS accumulation can cause oxidative stress, which can damage cell membranes, promote mitochondrial damage, and induce cell death, thus negatively affecting cell function and survival [10–12]. It is worth noting that this is largely due to the uncontrolled increase of ROS, which leads to the accumulation of large amounts of free radicals, thus destroying proteins, DNA, and lipid macromolecules, leading to genomic instability and changes in cell growth [13]. It is therefore not surprising that disorders of redox homeostasis are associated with the development of a variety of pathologies, including obesity, diabetes, cardiovascular disease, and neurodegenerative diseases [14–16]. In the past few decades, many studies have also shown that the imbalance of the oxidation-reduction system and the accumulation of ROS and oxidative stress can mediate the occurrence and development of cancer by causing molecular damage [17, 18]. Redox imbalance was also found in the development and progression of renal cell carcinoma [19, 20]. However, there has been no systematic study on the composition of redox-related genes (RRGs) in ccRCC and their relationship with prognosis. Thus, understanding the molecular composition of RRGs and their roles and functions in ccRCC is necessary for improving prognosis and identifying new biomarkers.

In the current study, we download the transcriptome data and corresponding clinical data of ccRCC from The Cancer Genome Atlas (TCGA) database. We identified differentially expressed RRGs and found that these genes were closely related to clinical parameters. Subsequently, we identified the fourteen RRGs most associated with prognosis and constructed a predictive model based on them. Kaplan-Meier survival analysis and time-dependent receiver operating characteristic (ROC) analysis showed that the model had satisfactory predictive potential. Next, we explored the upstream regulatory network of these RRGs and its relationship with immune cell infiltration. We then built a nomogram based on the signature and other clinical parameters and validated it in the TCGA database and ArrayExpress database. Finally, we verified the expression of these RRGs in the Human Protein Atlas (HPA) database.

2. Materials and Methods

2.1. Data Access, Collation, and Differential Expression Analysis. The miRNA sequencing dataset, RNA sequencing dataset, and corresponding clinical data of ccRCC were downloaded from the TCGA (<https://portal.gdc.cancer.gov/>) database. Then, genes related to redox were screened from the OMIM database (<https://www.oncomine.org/resource/>), NCBI gene function module (<https://www.ncbi.nlm.nih.gov/gene/>), GeneCards database (<https://www.genecards.org/>), and GSEA-MSigDB (<https://www.gsea-msigdb.org/gsea/msigdb>) with the keyword “redox” [21]; a total of 4087 RRGs were obtained. In addition, we downloaded the E-MTAB-1980 dataset from the ArrayExpress database (<https://www.ebi.ac.uk/arrayexpress/>) as an external validation cohort. Next, we used edgeR package (<http://www.bioconductor.org/packages/release/bioc/html/edgeR.html>) to preprocess the raw data of the TCGA cohort, including averaging the genes with the same name, removing the genes with an average expression of less than 1, and normalizing the expression data based on trimmed mean of M -values (TMM) algorithm. And for microarray data from ArrayExpress, the data were background adjusted and normalized using the robust multiarray analysis (RMA) method in affy package (<http://www.bioconductor.org/packages/release/bioc/html/affy.html>). Additionally, the data were transformed using a \log_2 transformation, and the probes were converted into gene symbols. When a gene was recorded by multiple probes, its expression level was averaged. $|\log_2$ fold change (FC)| > 2.0 and false discovery rate (FDR) < 0.05 were considered to be differently expressed genes.

2.2. Evaluation of Gene Modules and Their Correlation with Clinical Parameters. We performed weighted correlation network analysis (WGCNA) of differentially expressed RRGs to establish gene interaction modules and to evaluate the relationships between these RRGs and clinical parameters as a whole, according to the WGCNA package. Briefly, after soft threshold (power) was set and cluster modules and genes were obtained, correlation analysis was conducted between clinical parameters (including age, gender, tumor grade, tumor stage, T stage, N stage, and M stage) and module characteristic genes. A $p < 0.05$ was considered statistically significant.

2.3. Establishing Protein-Protein Interaction (PPI) Network and Screening Key Modules. We first identified the protein-protein interaction information of these differentially expressed RRGs through the STRING database (<http://www.string-db.org/>). Then, the PPI network was constructed and visualized using Cytoscape 3.8.0 software. In addition, we used the Molecular Complex Detection (MCODE) plugin to filter the key modules with nodes greater than 10.

2.4. Identification of Prognosis-Related RRGs. First, univariate Cox regression analysis was performed on these key RRGs of the TCGA cohort to identify the RRGs associated with prognosis. Subsequently, we performed the least absolute shrinkage and selection operator (LASSO) regression analysis, Kaplan-Meier test, and multivariate Cox regression analysis

to screen for the RRGs most associated with prognosis. A $p < 0.05$ was considered significant.

2.5. Construction and Evaluation of RRG-Based Prognosis-Related Signature. After screening these prognosis-related RRGs, a multivariate Cox proportional hazards regression model was constructed to predict the prognosis of ccRCC patients. The risk score for each patient in the signature was calculated according to the following formula:

$$\text{Risk score} = \sum_{i=1}^n \text{Exp}i\beta_i. \quad (1)$$

Here, Exp represents the expression of each gene, and β represents the regression coefficient. Subsequently, based on the median risk score, we divided the TCGA cohort into high-risk and low-risk subgroups. Then, we performed the Kaplan-Meier survival analysis to compare the difference in overall survival (OS) between the two subgroups. And the time-dependent ROC curve was used to evaluate the prognostic ability of the signature. In addition, the E-MTAB-1980 cohort was used as an external validation set to verify the stability and accuracy of the signature. Moreover, we also randomly and equally divided the TCGA cohort into two datasets, and further verified the stability and reliability of the signature based on these two datasets.

2.6. The Expression Differences of Signature-Based Risk Score and Prognosis-Related RRGs Stratified by Different Clinicopathological Parameters. We analyzed the expression differences of signature-based risk score stratified by different clinicopathological parameters to explore whether it might affect the progression of ccRCC. In addition, we analyzed the expression differences of prognosis-related RRGs stratified by different clinicopathological parameters to understand the role of redox in ccRCC. A $p < 0.05$ was considered significant.

2.7. Upstream Regulatory Network and Functional Enrichment Analysis of Prognosis-Related RRGs. We first obtained ccRCC miRNA sequencing dataset from the TCGA database. Next, we conducted coexpression analysis of differentially expressed miRNAs and prognosis-related RRGs to explore their regulatory relationships, based on $|\text{Cor}| > 0.1$ and $p < 0.001$ standard. Subsequently, the functional enrichment analysis of these differentially expressed RRGs was detected by the Gene Ontology (GO) and Kyoto Encyclopedia of Genes and Genomes (KEGG) database pathway enrichment analysis. All enrichment analyses were performed by using the clusterProfiler package (<http://www.bioconductor.org/packages/release/bioc/html/clusterProfiler.html>).

2.8. The Infiltration Difference of Tumor-Infiltrating Immune Cells between High-Risk and Low-Risk Groups in the TCGA Cohort Assessed by RRG-Based Prognostic Signature. The degree of infiltration of immune cells in the immune microenvironment is important for tumor progression, treatment, and prognosis. We used the cell-type identification by esti-

imating relative subsets of RNA transcripts (CIBERSORT) and its supplied LM22 gene set to assess the degree of immune cell infiltration in different subgroups. CIBERSORT is a deconvolution algorithm that assesses the relative abundance of immune cell infiltration in each patient based on the expression data of 22 tumor-infiltrating lymphocyte subsets. Here, the number of permutations was set to 1000. $p < 0.05$ was the filtering criterion.

2.9. Construction of a Nomogram. We performed the Cox regression analysis and multiple regression analysis to assess the prognostic significance of different clinical parameters and the prognosis-related signature. Then, to establish a quantitative approach to predict the prognosis of ccRCC patients, we constructed a nomogram combining clinical parameters and RRG-based prognosis-related signature by using rms package. Subsequently, calibration curves at different time intersections were plotted to assess the predictive accuracy of the nomograms. And the TCGA and E-MTAB-1980 datasets were used for Kaplan-Meier survival analysis and ROC analysis to further evaluate the accuracy and stability of the nomogram.

2.10. Validation of Prognosis-Related RRG Expression. We used the immunohistochemical results from the Human Protein Atlas (HPA, <http://www.proteinatlas.org/>) online database to detect the protein expression of these prognosis-related RRGs [22].

3. Results

3.1. Identifying Differentially Expressed RRGs. In this study, we systematically and comprehensively analyzed the role and clinical significance of RRGs in ccRCC. Figure 1 shows a flow chart of the study. A total of 72 normal renal tissue samples and 539 ccRCC samples were analyzed. We identified a total of 4087 RRGs from the GeneCards, OMIM, NCBI, and GSEA-MSigDB databases, and finally, 3845 RRG expression data was obtained according to the TCGA cohort. Next, based on our inclusion criteria ($|\log_2 \text{FC}| > 2.0$ and $\text{FDR} < 0.05$), 344 differentially expressed RRGs were identified, including 234 upregulated and 110 downregulated RRGs. The expression distribution of these RRGs is shown in Figures 2(a) and 2(b).

3.2. Correlation between Gene Modules and Clinical Characteristics. We performed WGCNA analysis to determine the correlation between gene modules and clinical features. Briefly, after extracting gene expression data and corresponding clinical data from the TCGA database, including prognosis status, age, gender, tumor grade, tumor stage, T stage, N stage, and M stage, we then set a soft threshold (power) and obtained the optimal scale-free topology fitting model index (scale-free R^2) and average connectivity. The degree of difference among genes was determined based on topological overlap measure, and the clustering tree diagram of genes was obtained. Finally, the clinical factors and module characteristic genes in TCGA were analyzed by cluster analysis. Figure 2(c) shows the relationships between different gene modules and clinical features such as age, gender,

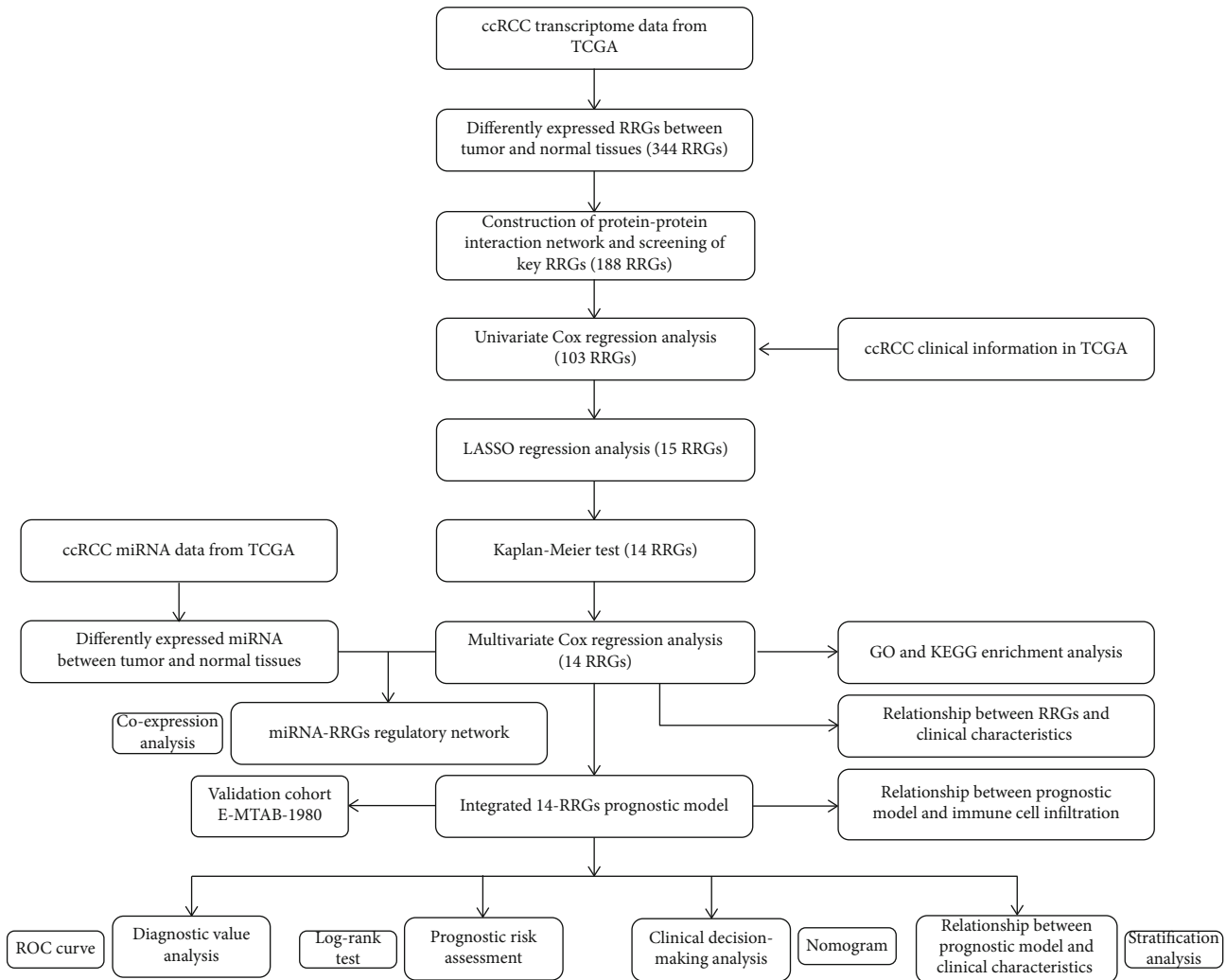


FIGURE 1: The flow chart for analyzing RRG-based model and miRNA-RRG regulatory network in ccRCC.

tumor grade, tumor stage, T stage, N stage, and M stage after WGCNA analysis. Two modules were significantly correlated with tumor grade ($p = 0.025$, $p = 0.025$). One module was significantly correlated with tumor stage ($p = 0.030$). Three modules were negatively correlated with M stage ($p = 0.013$, $p = 0.013$, and $p = 0.017$). Three modules were significantly correlated with N stage ($p = 0.033$, $p = 0.025$, and $p < 0.001$). However, there was no significant correlation between the gene models and age, gender, and T stage. Although our results showed a small effect size, the association was statistically significant, suggesting that RRGs may affect clinical outcomes in ccRCC patients. Therefore, prognostic analysis deserved to be performed subsequently.

3.3. Construction of PPI Network and Screening Key Modules. In order to further explore the role of key RRGs in ccRCC, we used the STRING database and Cytoscape software to analyze these differentially expressed RRGs and construct a PPI network containing 189 nodes and 489 edges (Figure 3(a)). We also used the MCODE plug-in

to filter two key modules. Module 1 contained 23 nodes and 143 edges (Figure 3(b)). And module 2 contained 12 nodes and 32 edges (Figure 3(c)).

3.4. Construction and Evaluation of RRG-Based Prognosis-Related Signature. We first performed univariate Cox regression analysis on these 189 key RRGs and identified 103 prognosis-related RRGs (Supplemental Table S2). Next, LASSO regression analysis was performed for further analysis, and 15 RRGs were identified (Supplemental Figure S1). To further identify the RRGs with the best prognostic significance, we identified 14 RRGs, including *ADAM8*, *CGN*, *EIF4EBP1*, *FOXO1*, *G6PC*, *HAMP*, *HTR2C*, *ITIH4*, *LTB4R*, *MMP3*, *PLG*, *PRKCG*, *SAA1*, and *VWF*, by using the Kaplan-Meier test (Supplemental Figure S2). Next, the GEPIA online tool (<http://gepia.cancer-pku.cn/>) was used to explore the expression levels of these 14 RRGs in different cancer types in the TCGA cohort, and the results are shown in Supplemental Figure S3. Subsequently, a RRG-based prognosis-related signature was established by

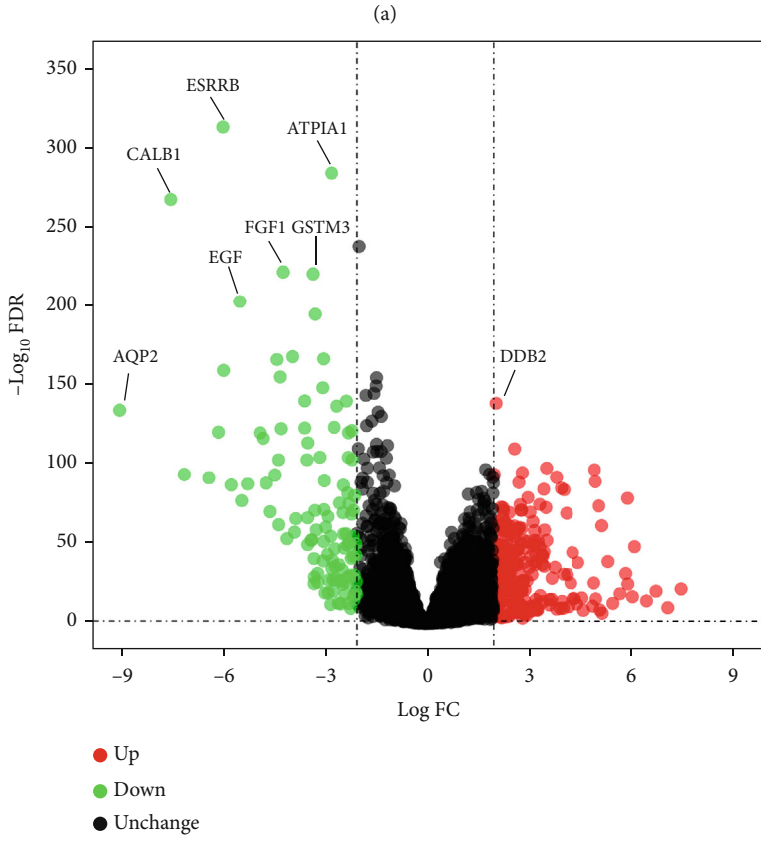
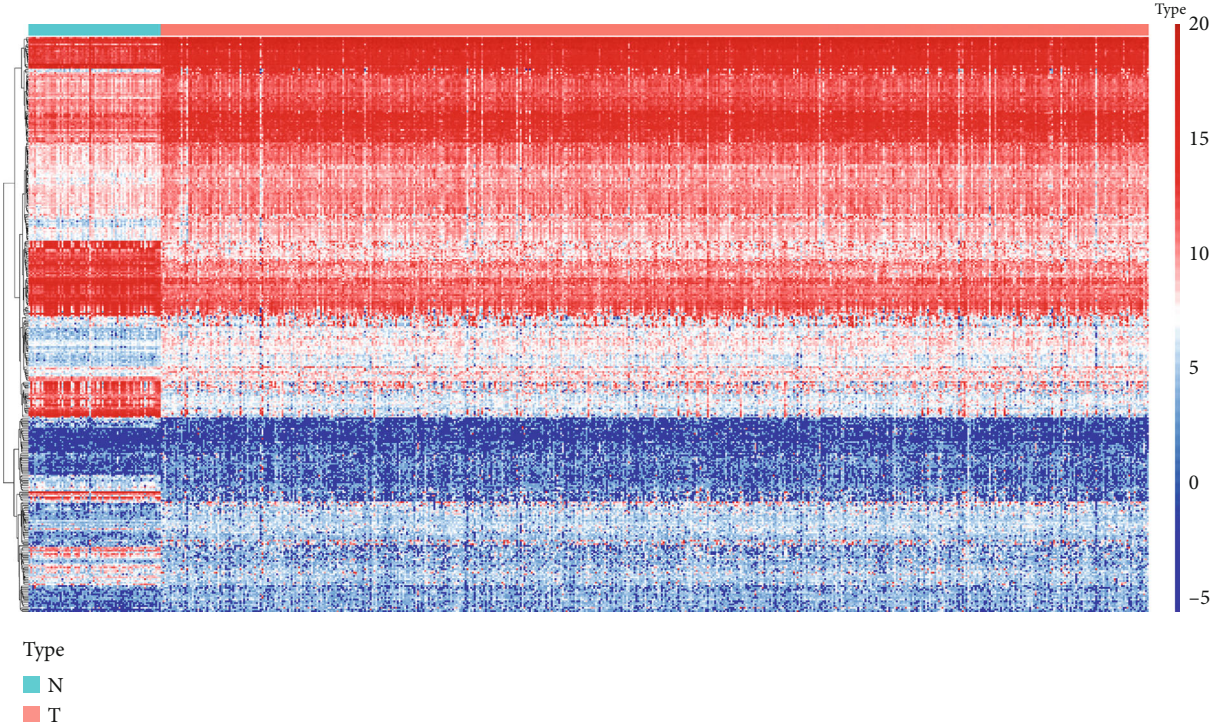


FIGURE 2: Continued.

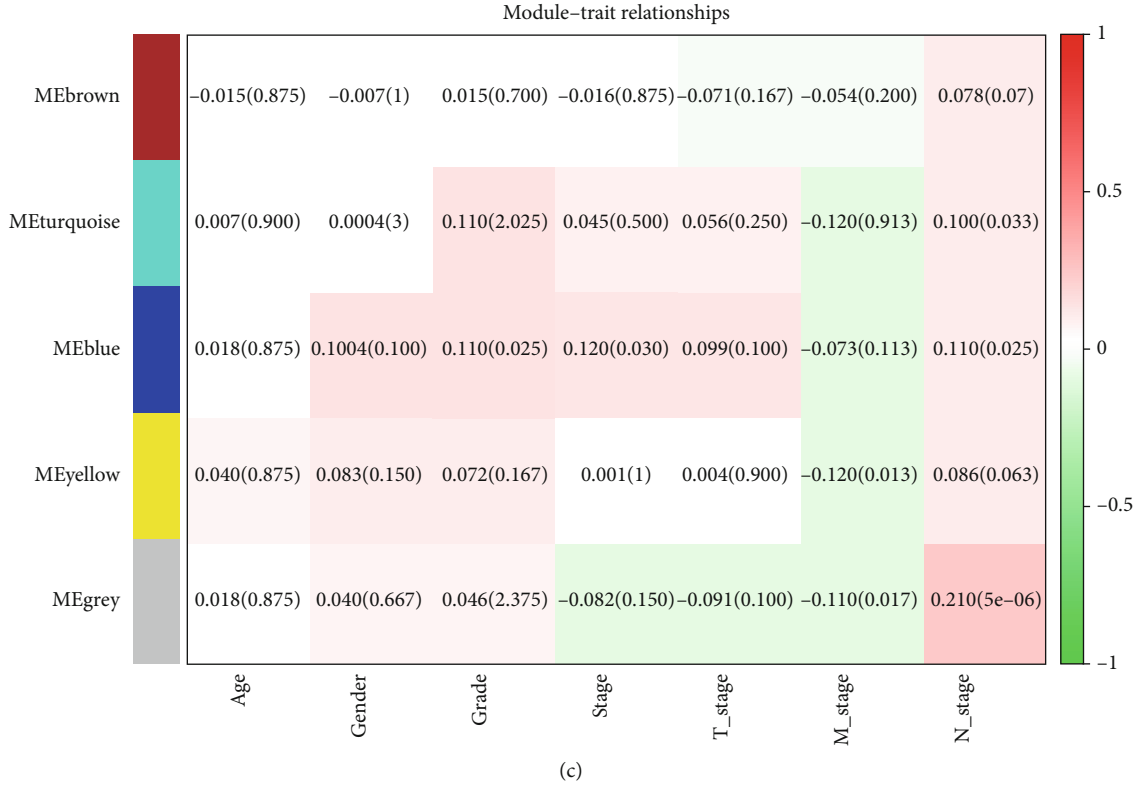


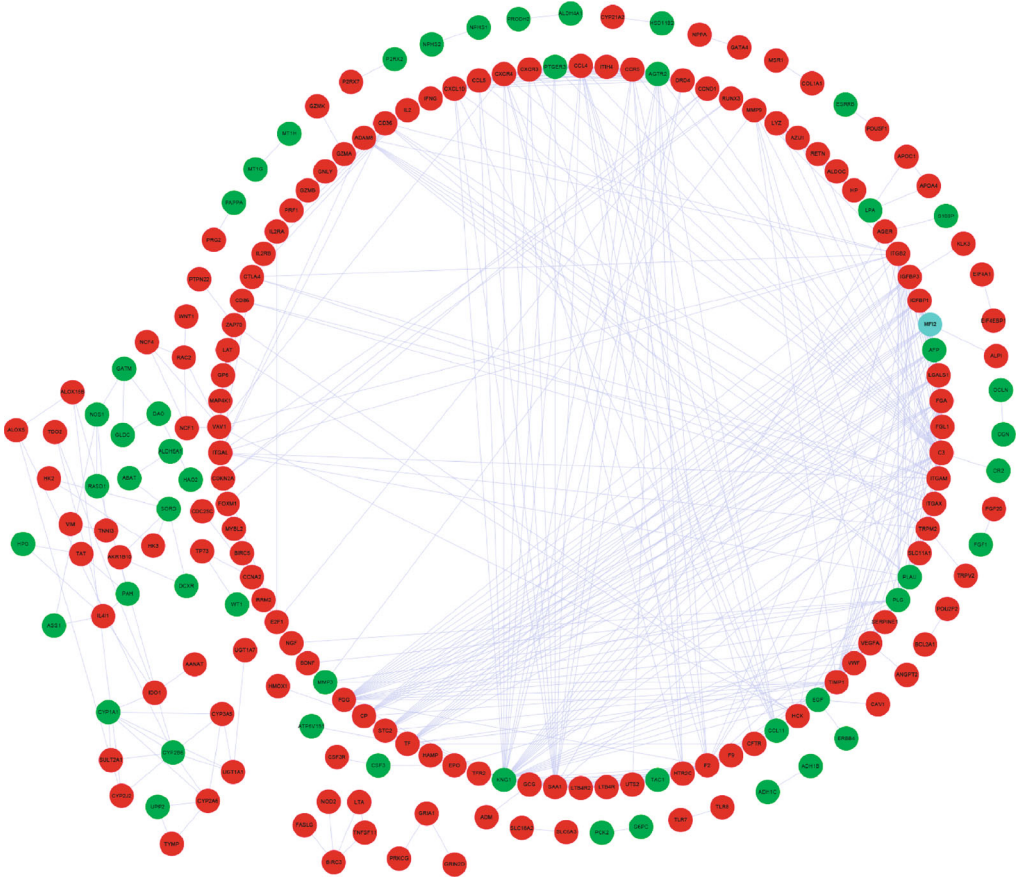
FIGURE 2: Landscape of the expression and distribution of differentially expressed RRGs in ccRCC and the correlation between gene module and clinical parameters based on WGCNA analysis. (a) Heat map of 344 differentially expressed RRGs in the normal renal tissues and ccRCC tissues. (b) Volcano plot shows the \log_2 fold change and q value of each differentially expressed RRG. (c) Module-trait relationships based on WGCNA analysis. Each column represents a clinical trait and each row represents a gene module.

multiple stepwise Cox regression (Table 1). The risk score of each ccRCC patient was calculated as follows:

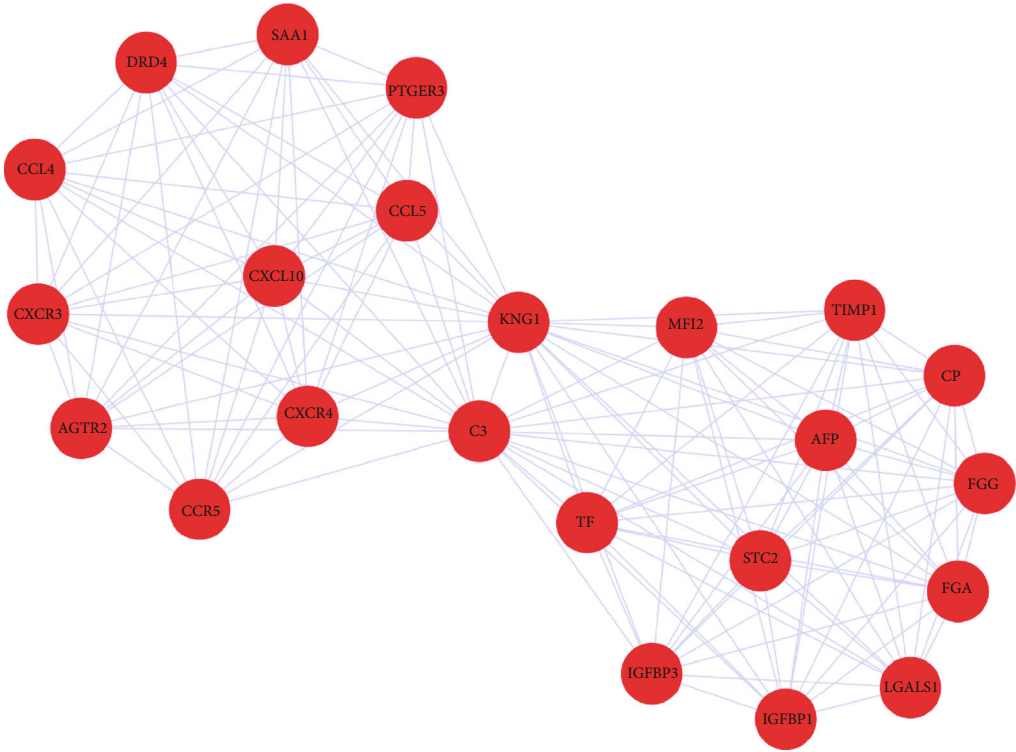
$$\begin{aligned}
 \text{Risk score} = & (0.0632 \times \text{Exp ADAM8 reads}) \\
 & + (-0.0989 \times \text{Exp CGN reads}) \\
 & + (0.1336 \times \text{Exp EIF4EBP1 reads}) \\
 & + (0.1039 \times \text{Exp FOXM1 reads}) \\
 & + (-0.0263 \times \text{Exp G6PC reads}) \\
 & + (0.0258 \times \text{Exp HAMP reads}) \\
 & + (0.1703 \times \text{Exp HTR2C reads}) \\
 & + (0.0460 \times \text{Exp ITIH4 reads}) \\
 & + (0.1244 \times \text{Exp LTB4R reads}) \\
 & + (0.0618 \times \text{Exp MMP3 reads}) \\
 & + (-0.0531 \times \text{Exp PLG reads}) \\
 & + (0.0259 \times \text{Exp PRKCG reads}) \\
 & + (0.0332 \times \text{Exp SAA1 reads}) \\
 & + (-0.0657 \times \text{Exp VWF reads}).
 \end{aligned} \tag{2}$$

Then, according to the median risk score, the TCGA cohort was divided into high-risk and low-risk subgroups. Kaplan-Meier survival analysis showed that patients in the

high-risk group had a worse prognosis than those in the low-risk group ($p = 1.033e - 14$, Figure 4(a)). A time-dependent ROC curve was performed to further evaluate the predictive performance of the signature, and the area under the ROC curve (AUC) for OS was 0.796 at one year, 0.728 at three years, and 0.759 at five years (Figure 4(b)). Next, the external cohort E-MTAB-1980 dataset was used to verify the stability of the RRG-based signature. The Kaplan-Meier survival analysis also showed a poorer prognosis for patients in the high-risk group ($p = 1.164e - 05$, Figure 4(c)). The AUCs of the 1-, 3-, and 5-year survival rates were 0.759, 0.804, and 0.829, respectively (Figure 4(d)). Figures 4(e), 4(g) and 4(f), 4(h) show the survival status and expression heat maps of each patient in the TCGA and E-MTAB-1980 cohort, respectively. Moreover, to further verify the accuracy and stability of the signature, the whole TCGA cohort was randomly divided into training ($n = 270$) and test groups ($n = 269$) for subsequent analysis. The Kaplan-Meier survival analysis also showed a worse prognosis in the high-risk group in both datasets ($p = 1.484e - 08$ and $p = 3.747e - 08$, Figures 5(a) and 5(c)). In the training dataset, the predicted AUCs for 1-, 3-, and 5-year survival rates were 0.771, 0.693, and 0.763, respectively (Figure 5(b)), and in the test dataset, the predicted AUCs for 1-, 3-, and 5-year survival rates were 0.826, 0.767, and 0.756, respectively (Figure 5(d)).



(a)



(b)

FIGURE 3: Continued.

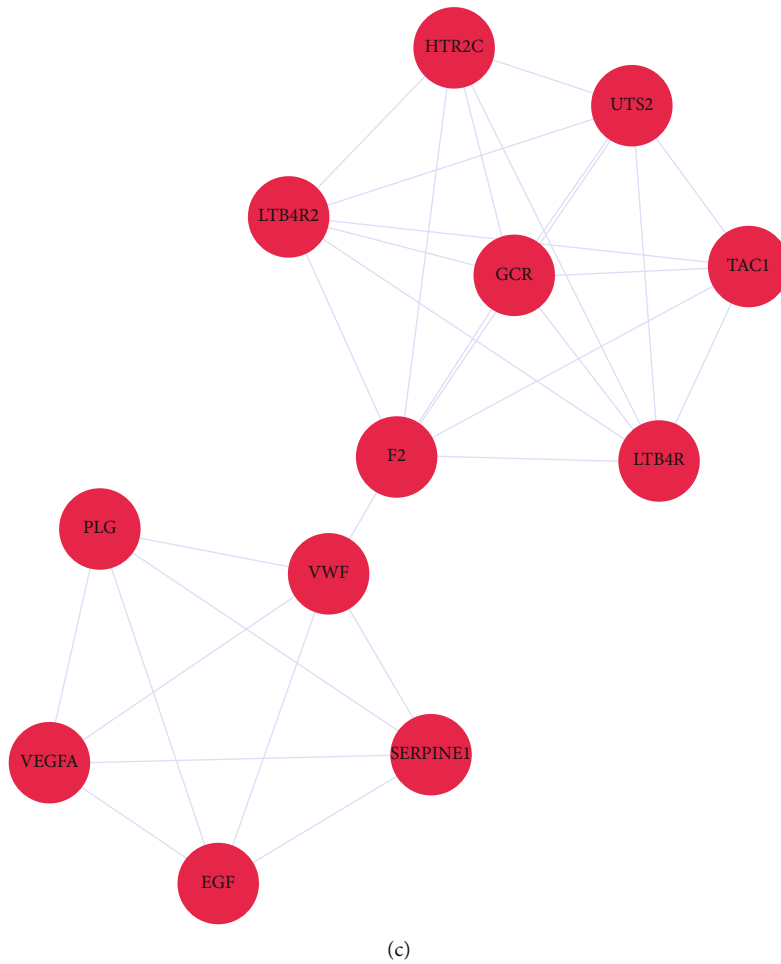


FIGURE 3: Construction of protein-protein interaction network and screening key modules. (a) Protein-protein interaction network of differentially expressed RRGs. (b) Critical module 1 from PPI network based on MCODE plug-in. (c) Critical module 2 from PPI network based on MCODE plug-in. Green circles: downregulation; red circles: upregulation.

Figures 5(e) and 5(h) show the survival status of each patient in the training and test groups, respectively. These results showed that the RRG-based prognosis-related signature has good predictive performance and stability.

3.5. Prognostic Value of the Signature Stratified by Clinical Parameters. To investigate the clinical prognostic value of the 14 RRGs-based prognosis-related signature in the ccRCC patients stratified by different clinical parameters, ccRCC patients were stratified by age, gender, tumor grade, tumor stage, T stage, N stage, and M stage. Kaplan-Meier survival analysis showed poor prognosis in all high-risk groups (Figure 6). These results suggested that the RRG-based prognosis-related signature could predict the prognosis of ccRCC patients without considering clinical parameters.

3.6. The Expression Differences of Signature-Based Risk Score Stratified by Different Clinicopathological Parameters. Next, to explore whether the signature would affect the ccRCC progression, we investigated the correlation between the signature and different clinical parameters. The results showed

that there was no significant correlation between age, gender, N stage, and the signature ($p = 0.174$, $p = 0.321$, and $p = 0.281$, Figures 7(a), 7(b), and 7(f)). However, the risk score of stage I-II was significantly lower than that of stage III-IV ($p < 0.001$, Figure 7(c)), the risk score of grades 1-2 was significantly lower than that of grades 3-4 ($p < 0.001$, Figure 7(d)), the risk score of T1-2 was significantly lower than that of T3-4 ($p < 0.001$, Figure 7(e)), and the risk score of M0 was significantly lower than that of M1-X ($p < 0.001$, Figure 7(g)). These results indicated that the prognostic signature was significantly associated with tumor progression in ccRCC, and the higher the risk score, the more advanced the tumor was.

3.7. The Expression Differences of Prognosis-Related RRGs Stratified by Different Clinicopathological Parameters. Based on the above results, we analyzed the relationship between prognosis-related RRGs and different clinical parameters to further investigate the role of these RRGs in ccRCC. The results showed that the expressions of G6PC and SAA1 were significantly correlated with gender; the expressions of ADAM8, CGN, EIF4EBP1, FOXM1, G6PC, HAMP, HTR2C,

TABLE 1: Multivariate Cox regression analysis to identify prognosis-related redox genes.

Gene	Coef	Exp (coef)	se (coef)	z	Pr (> z)
ADAM8	0.0632	1.0652	0.0834	0.7575	0.4488
CGN	-0.0989	0.9058	0.0569	-1.7376	0.0823
EIF4EBP1	0.1336	1.1430	0.0898	1.4880	0.1367
FOXM1	0.1039	1.1095	0.0773	1.3442	0.1789
G6PC	-0.0263	0.9741	0.0383	-0.6851	0.4933
HAMP	0.0258	1.0261	0.0595	0.4328	0.6651
HTR2C	0.1703	1.1857	0.0707	2.4100	0.0160
ITIH4	0.0460	1.0470	0.0584	0.7873	0.4311
LTB4R	0.1244	1.1324	0.0957	1.3003	0.1935
MMP3	0.0618	1.0637	0.0392	1.5764	0.1149
PLG	-0.0531	0.9483	0.0291	-1.8230	0.0683
PRKCG	0.0259	1.0263	0.0571	0.4536	0.6501
SAA1	0.0332	1.0337	0.0273	1.2146	0.2245
VWF	-0.0657	0.9364	0.0628	-1.0463	0.2954

Coef: coefficient.

ITIH4, LTB4R, MMP3, PLG, PRKCG, SAA1, and VWF were significantly correlated with grade; the expressions of ADAM8, CGN, EIF4EBP1, FOXM1, G6PC, HAMP, ITIH4, LTB4R, MMP3, PLG, PRKCG, SAA1, and VWF were significantly correlated with stage and T stage; the expressions of ADAM8, EIF4EBP1, G6PC, HAMP, LTB4R, PLG, SAA1, and VWF were significantly correlated with M stage. However, no genes were associated with age and N stage (Table 2).

3.8. Multidimensional Regulatory Network and Functional Enrichment Analysis of Prognosis-Related RRGs. The redox-dependent regulation of cell homeostasis is considered to be a multilayered process involving not only protein and enzyme complexes but also noncoding RNAs [23, 24]. These noncoding RNAs, including miRNAs, play important roles in regulating cellular redox homeostasis systems [25]. Some miRNAs have been found to be involved in cellular reactions by altering the expression of genes encoding antioxidant enzymes (SOD, catalase, peroxidase, and glutathione transferase) [26]. Zhang et al. [27] found that miR-206 induces ROS accumulation in vivo and in vitro by binding to SOD1 mRNA, which may be a cause of cardiovascular disease. Gómez de Cedrón et al. [28] reported that miR-661 regulates redox and metabolic homeostasis in colon cancer. Therefore, it is noteworthy to reveal the multidimensional regulatory network in tumor genesis and progression of prognosis-related RRGs and miRNAs in this study. We first investigated the upstream mechanism of RRGs based on the prognosis-related signature. We obtained 2089 miRNA sequencing data from the TCGA database, and 211 miRNAs were obtained after differential analysis, including 115 upregulated and 96 downregulated miRNAs (Figure 8(a)). Next, we conducted coexpression analysis between differentially expressed miRNAs and prognosis-related RRGs, identified a total of 9 miRNAs involved in upstream regulation, and drew a Sankey plot (Figure 8(b)). And all miRNAs positively regulated the corresponding RRGs (Supplemental Table S3).

Subsequently, we conducted GO and KEGG enrichment analysis of these RRGs by using clusterProfiler package to explore the biological functions and molecular mechanisms of these differentially expressed RRGs. GO and KEGG enrichment analysis showed that these RRGs were mainly involved in reactive oxygen species metabolic process, calcium ion homeostasis, antigen processing, treatment, peptide antigen presentation, HIF-1 signaling pathway, transcriptional misregulation in cancer, and PI3K-Akt signaling pathway (Figures 8(c) and 8(d)).

3.9. The Infiltration Difference of Tumor-Infiltrating Immune Cells between High-Risk and Low-Risk Groups in the TCGA Cohort Assessed by Fourteen RRG-Based Prognostic Signature. The degree of immune cell infiltration is critical to tumor progression, treatment, and prognosis. The CIBERSORT algorithm was used to evaluate the differences in immune cell infiltration among different risk subgroups. The results showed that in each sample of the TCGA cohort, there were significant differences in the composition of 22 immune cells (Figure 9(a)). In addition, we found that there were some differences among the cells in different groups. Specifically, the infiltration degree of plasma cells, T cells CD8, T cells CD4 memory activated, T cells follicular helper, T cells regulatory (Tregs), monocytes, macrophages M0, dendritic cells activated, mast cell resting, and eosinophils were significantly different between the two groups (Figure 9(b)). Moreover, the results of correlation matrix showed that T cells CD8 had the strongest positive correlation with T cells regulatory (Tregs), and was also positively correlated with T cells follicular helper. There was also strong positive correlation between T cells follicular helper and T cells regulatory (Tregs) (Figure 9(c)).

3.10. Construction and Validation of a Nomogram. Cox regression analysis was first performed to assess the prognostic value of different clinical parameters and risk score in ccRCC patients. The results indicated that the age

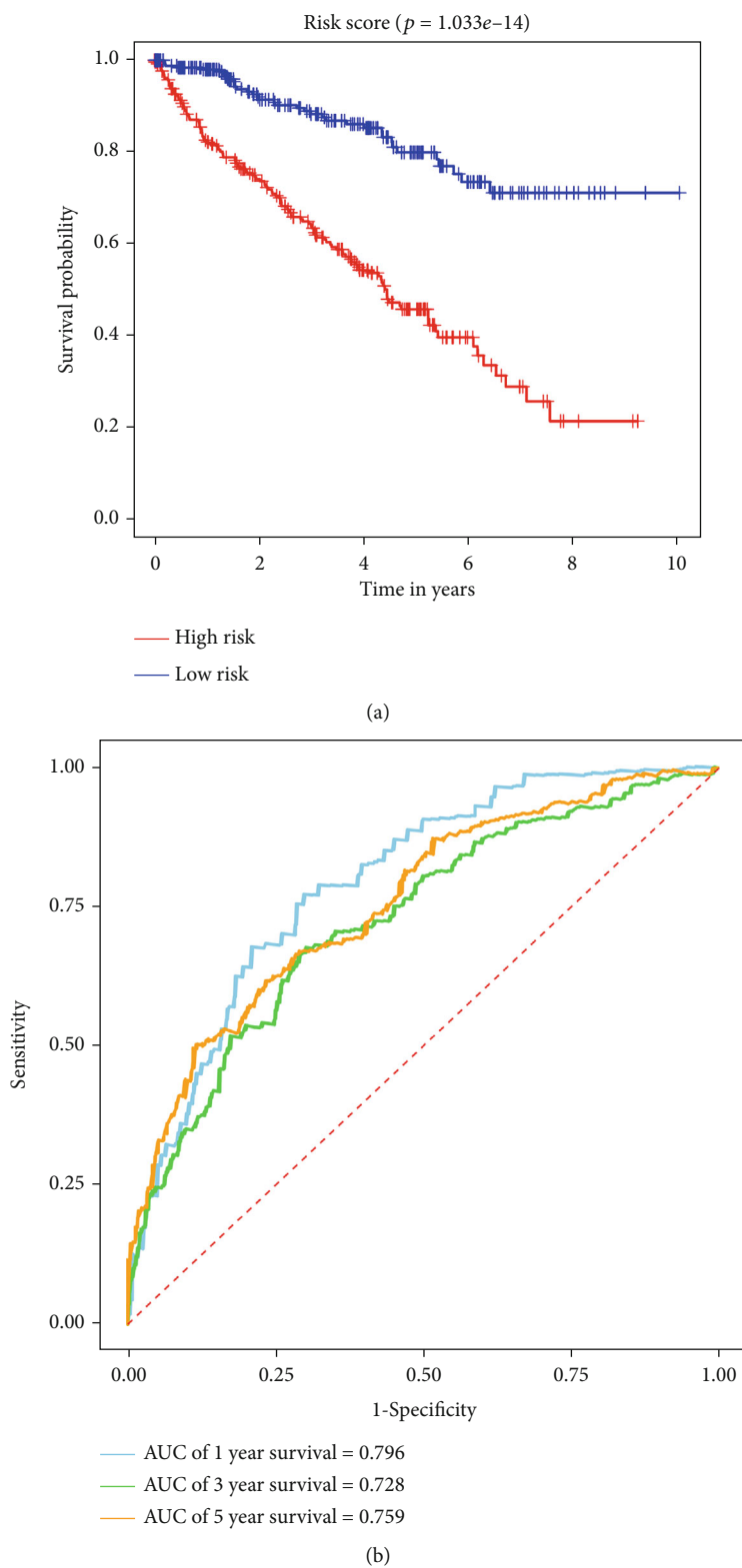
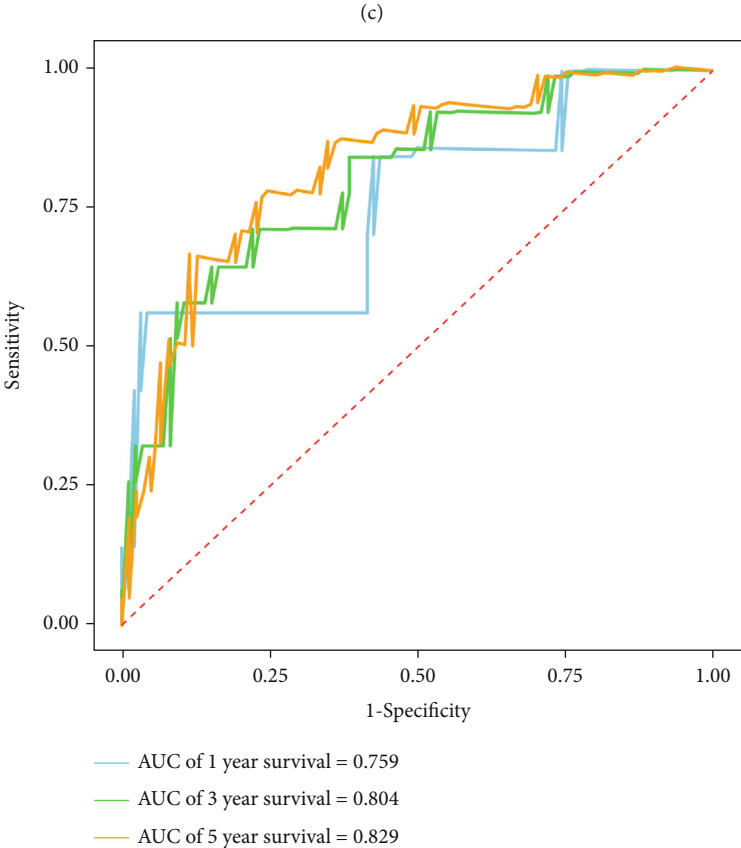
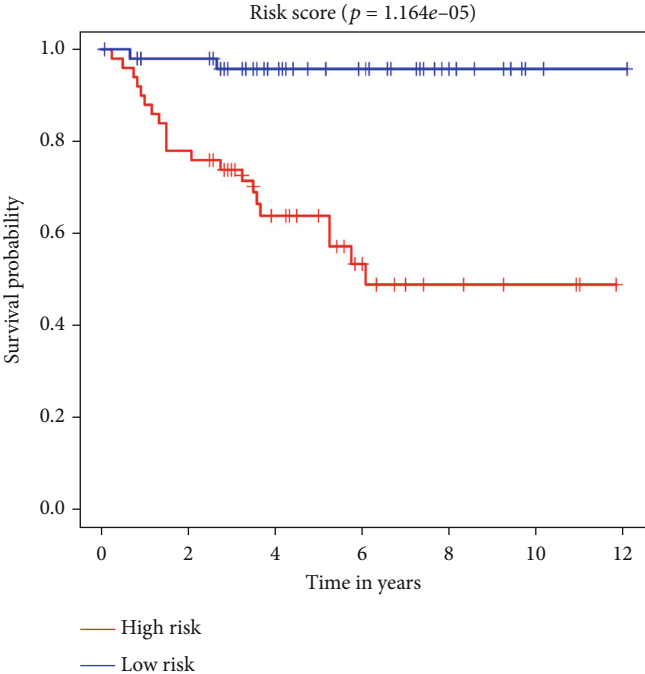
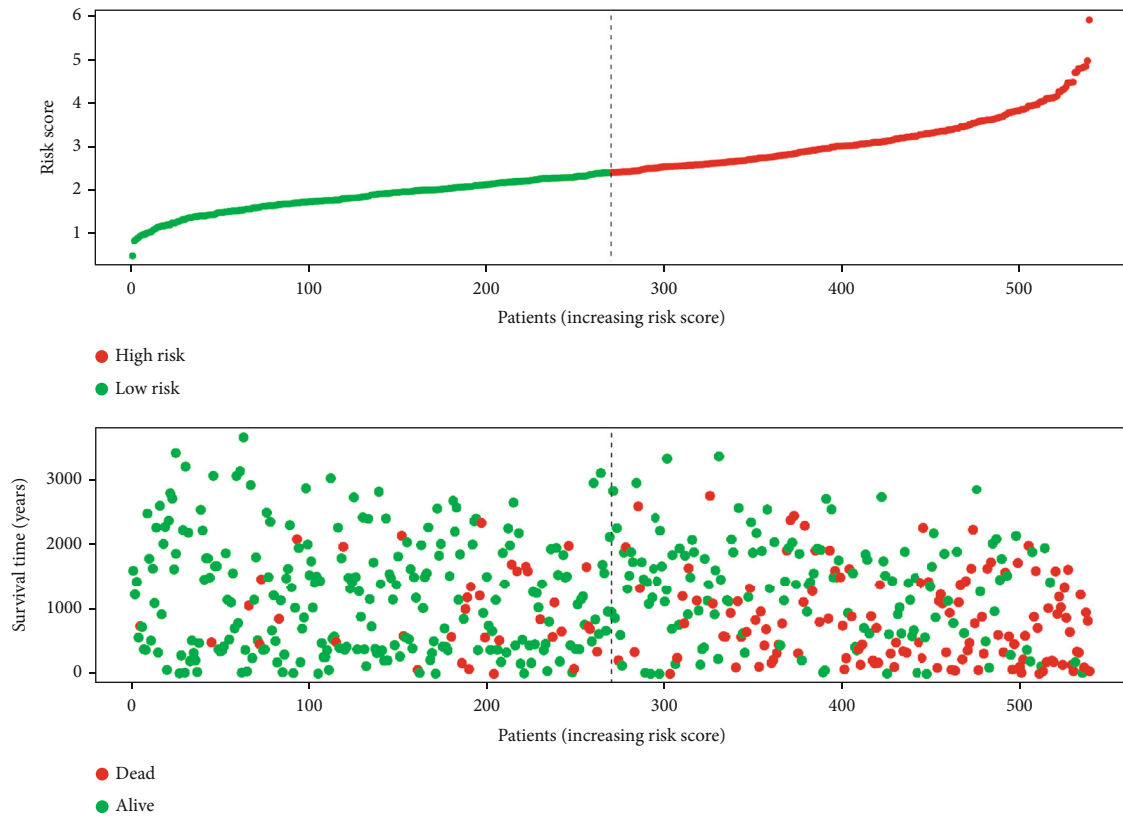


FIGURE 4: Continued.

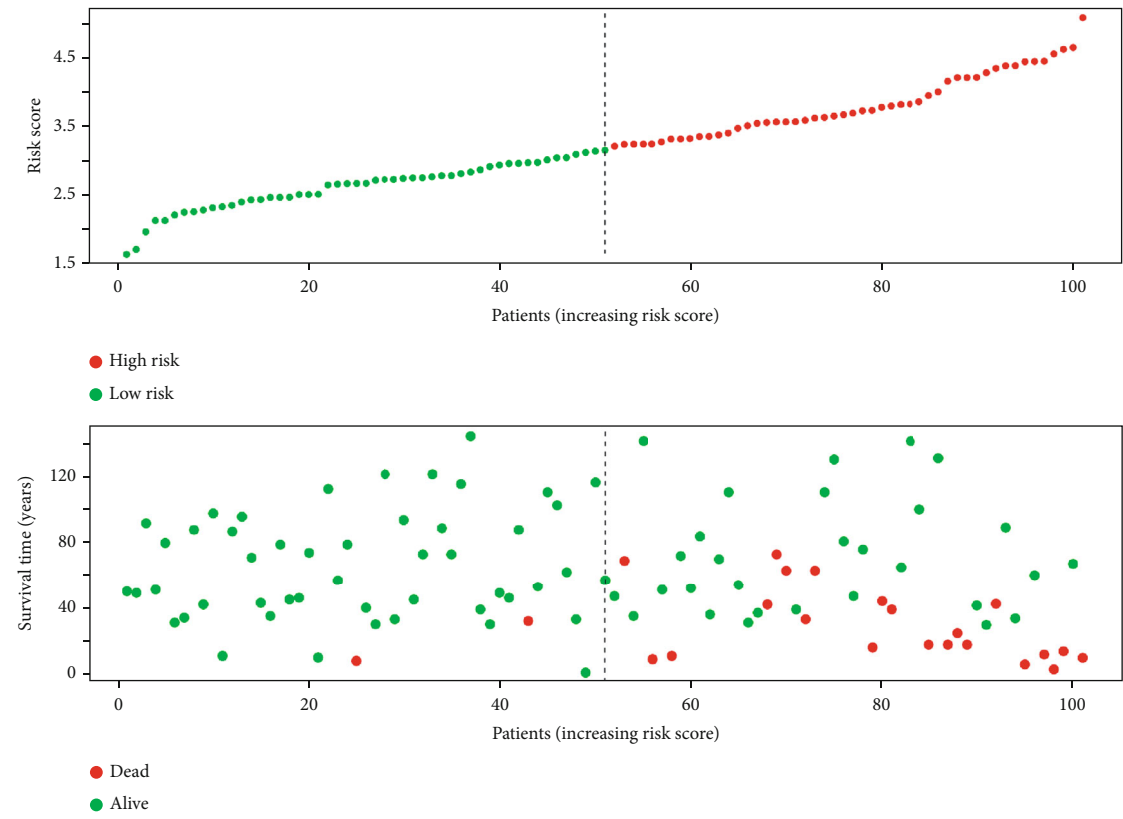


(d)

FIGURE 4: Continued.



(e)



(f)

FIGURE 4: Continued.

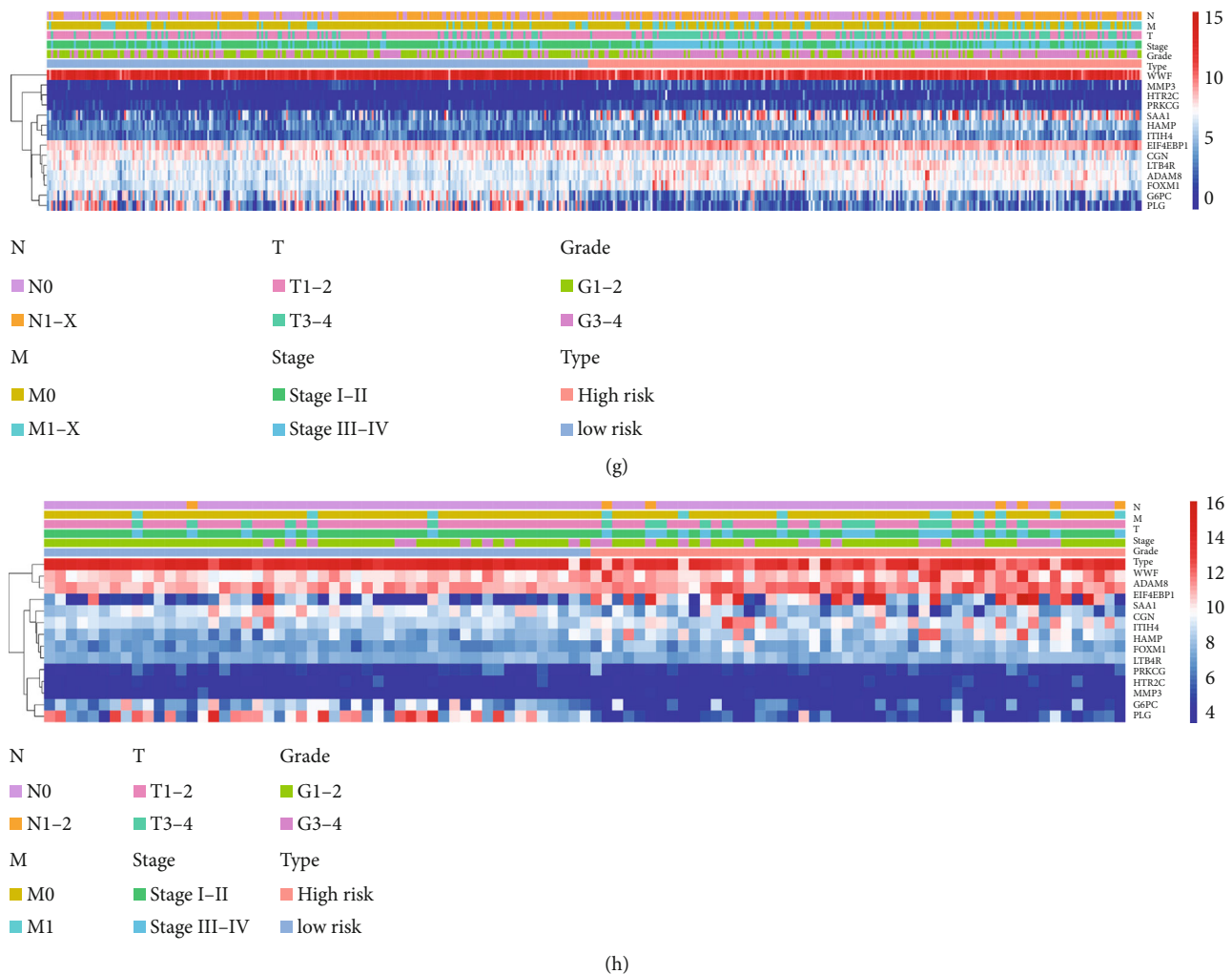
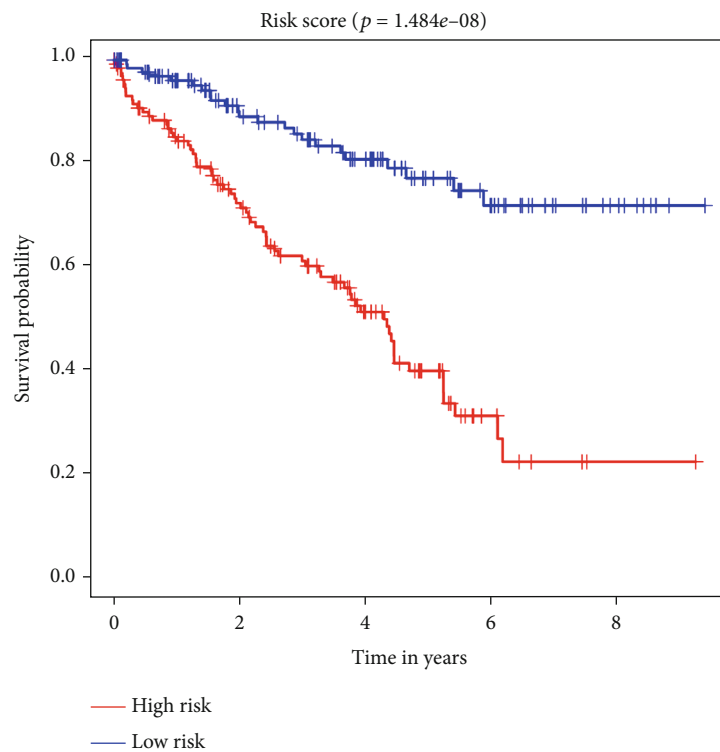


FIGURE 4: Risk score, survival time, and survival status analysis of ccRCC patients based on the fourteen RRGs' prognostic signature in the TCGA and E-MTAB-1980 cohorts. (a) Kaplan-Meier survival curve analysis of OS in the high- and low-risk subgroups of the TCGA cohort. ccRCC patients were grouped according to the median risk score. (b) Time-dependent ROC curves of the RRG-based risk signature for the TCGA cohort. The ROC curves and AUC were shown to predict ccRCC patients at 1, 3, and 5 years. (c) Kaplan-Meier survival curve analysis of OS in the high- and low-risk subgroups of the E-MTAB-1980 cohort. ccRCC patients were grouped according to the median risk score. (d) Time-dependent ROC curves of the RRG-based risk signature for the E-MTAB-1980 cohort. The ROC curves and AUC were shown to predict ccRCC patients at 1, 3, and 5 years. (e) The survival status of each patient in the TCGA cohort assessed by risk score. (f) The survival status of each patient in the E-MTAB-1980 cohort assessed by risk score. (g) Heat map of the fourteen RRGs in the TCGA cohort was evaluated based on risk score combined with other clinical parameters. (h) Heat map of the fourteen RRGs in the E-MTAB-1980 cohort was evaluated based on risk score combined with other clinical parameters.

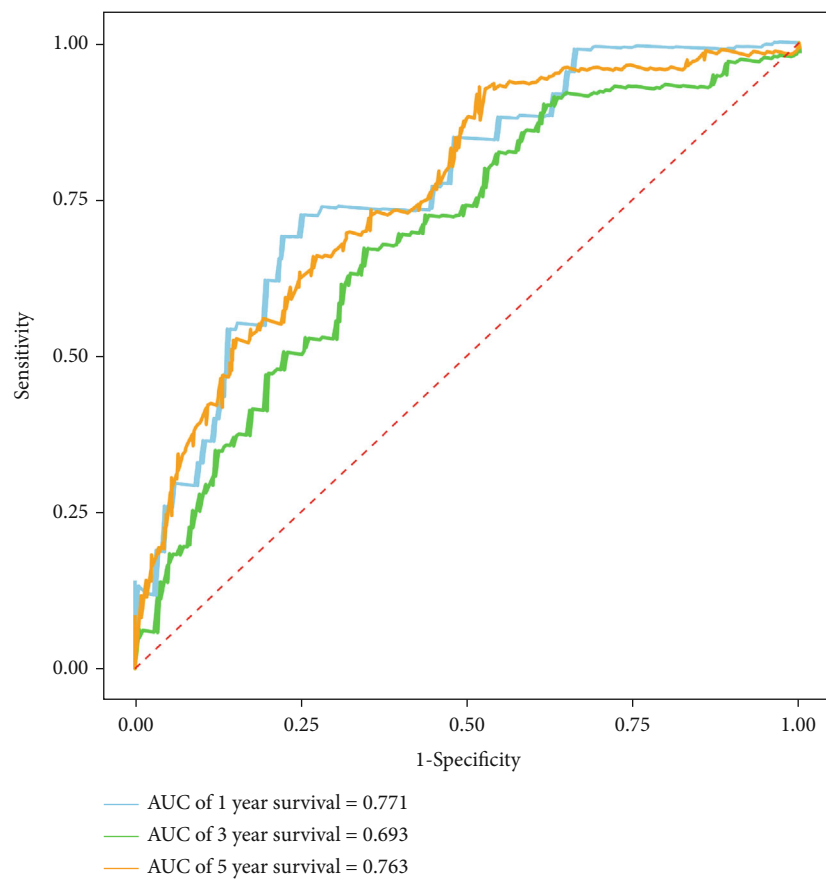
($p < 0.001$), tumor grade ($p < 0.001$), tumor stage ($p < 0.001$), primary tumor location ($p < 0.001$), lymph node infiltration ($p = 0.049$), distant metastasis ($p < 0.001$), and risk score ($p < 0.001$) of ccRCC patients were significantly correlated with OS (Figure 10(a)). However, multiple regression analysis revealed that age ($p = 0.013$), tumor stage ($p < 0.001$), and risk score ($p < 0.001$) were independent prognostic factors associated with OS (Figure 10(b)).

Subsequently, to establish a quantitative approach to predict the prognosis of ccRCC patients, we constructed a nomogram combining clinical parameters and the RRG-based prognosis-related signature by using rms package (Figure 10(c)). We mapped the points of each variable to the corresponding horizontal line and then calculated the

total points of each patient and normalized it to a distribution of 0 to 100. By drawing a line perpendicular to both axes (prognosis axis and total point axis), we can estimate the 1-year, 3-year, and 5-year survival probabilities of ccRCC patients, which may be used as a reference for making clinical decisions. The calibration curve showed that the predicted value of the nomogram has a good correlation with the actual value (Figures 10(d), 10(e), and 10(f)). Moreover, to expand the clinical application and availability of the nomogram based on risk score and clinical parameters, we used TCGA and E-MTAB-1980 datasets for validation, respectively. Kaplan-Meier survival analysis showed that nomogram could better distinguish ccRCC patients with low survival rates in TCGA and E-MTAB-1980 datasets ($p < 0.001$ and

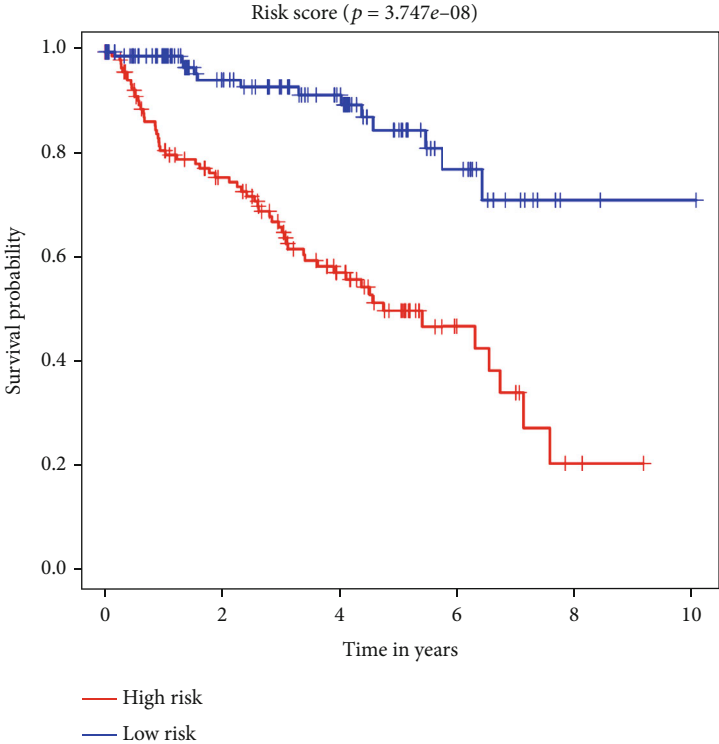


(a)

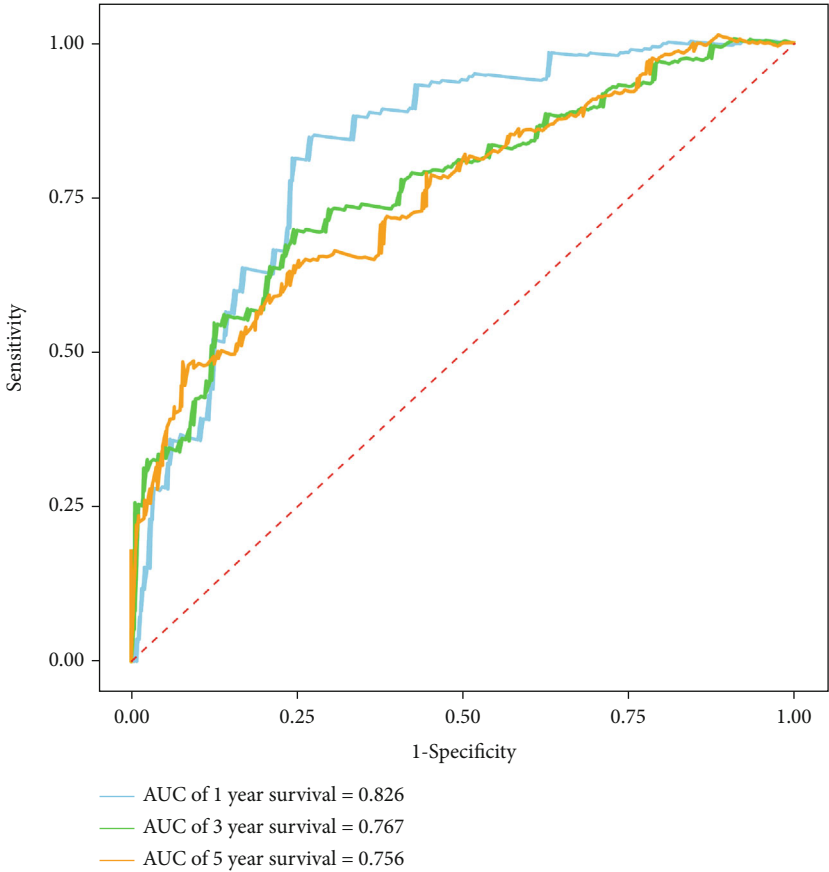


(b)

FIGURE 5: Continued.

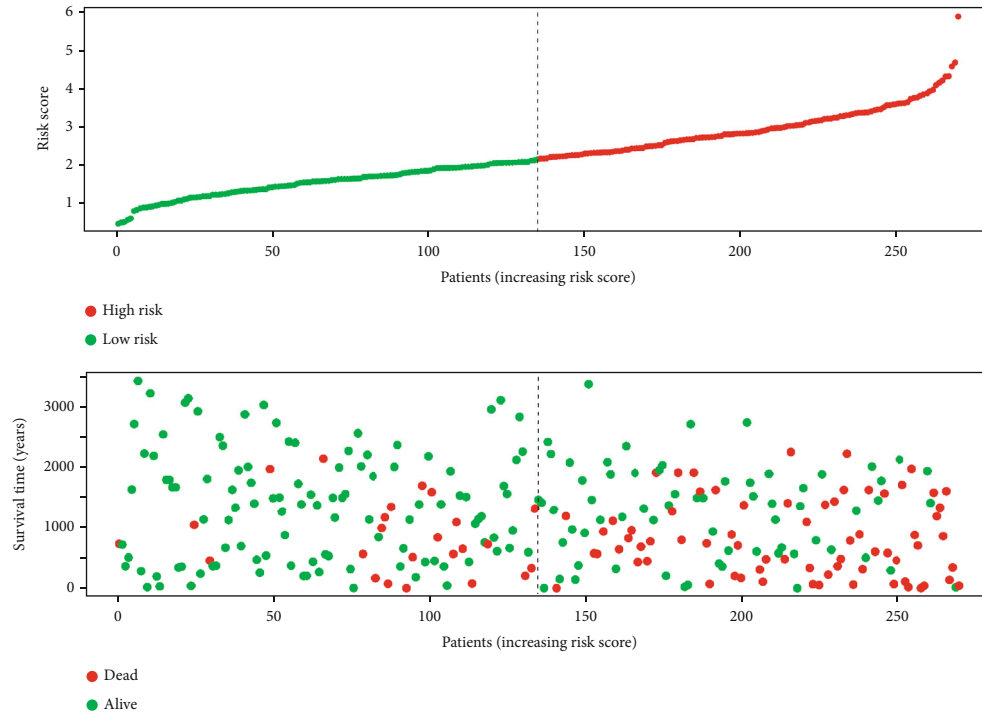


(c)

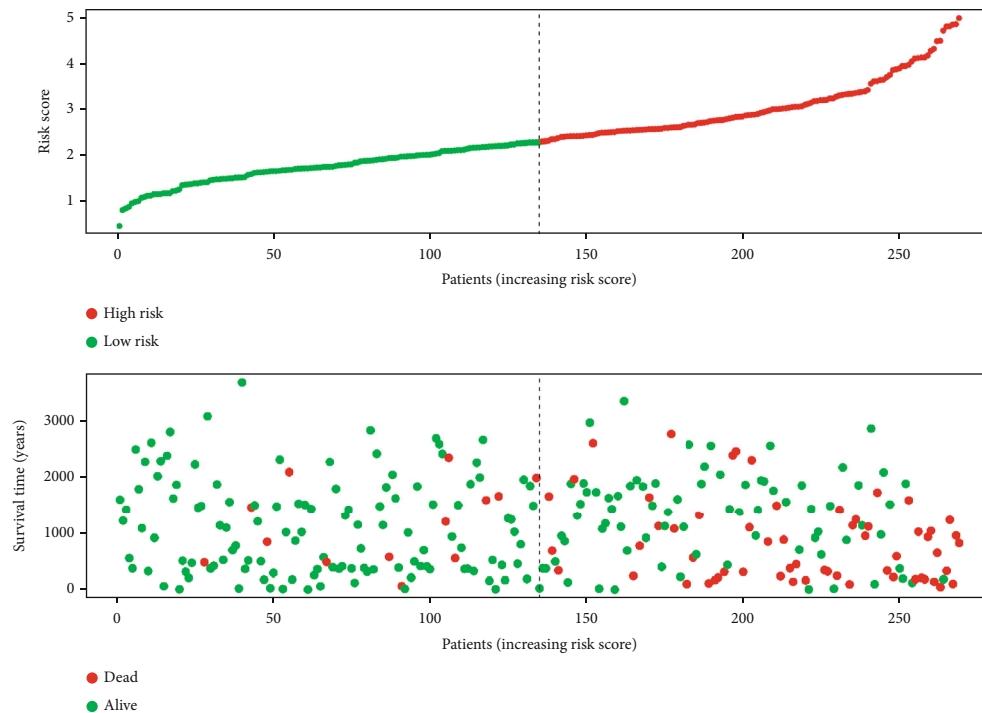


(d)

FIGURE 5: Continued.



(e)



(f)

FIGURE 5: Risk score, survival time, and survival status analysis of ccRCC patients based on the fourteen RRGs' prognostic signature in the training and test groups. (a) Kaplan-Meier survival curve analysis of OS in the high- and low-risk subgroups of the training group. ccRCC patients were grouped according to the median risk score. (b) Time-dependent ROC curves of the RRG-based risk signature for the training group. The ROC curves and AUC were shown to predict ccRCC patients at 1, 3, and 5 years. (c) The survival status of each patient in the training group assessed by risk score. (d) Kaplan-Meier survival curve analysis of OS in the high- and low-risk subgroups of the test group. ccRCC patients were grouped according to the median risk score. (e) Time-dependent ROC curves of the RRG-based risk signature for the test group. The ROC curves and AUC were shown to predict ccRCC patients at 1, 3, and 5 years. (f) The survival status of each patient in the test group assessed by risk score.

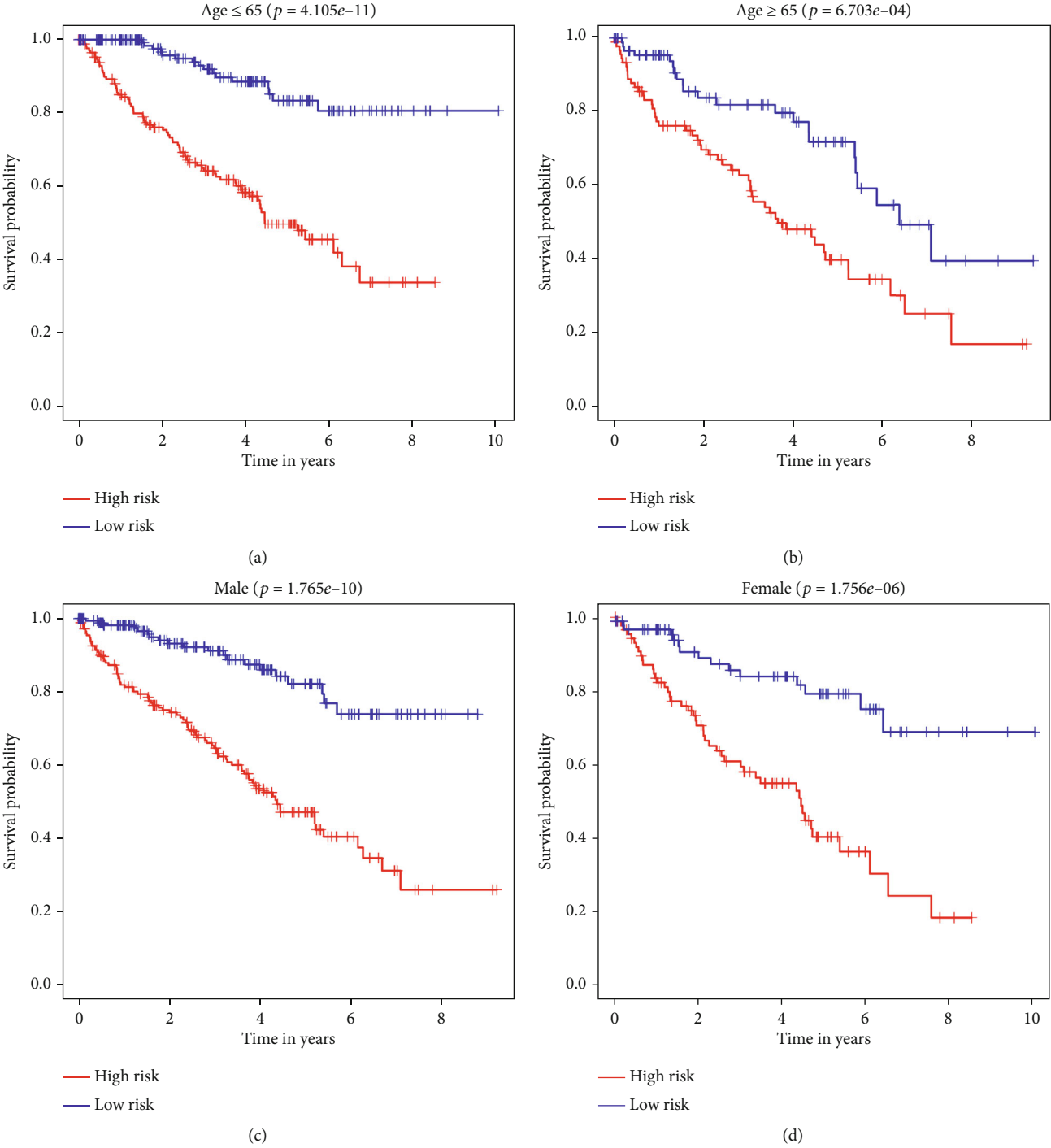
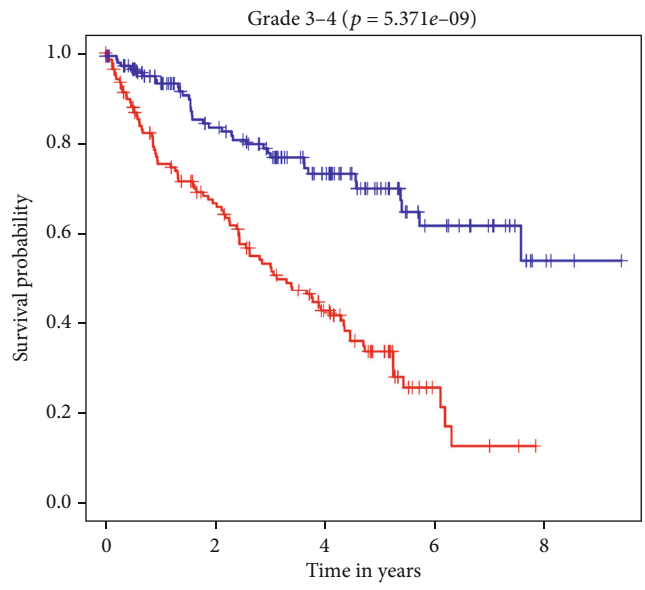
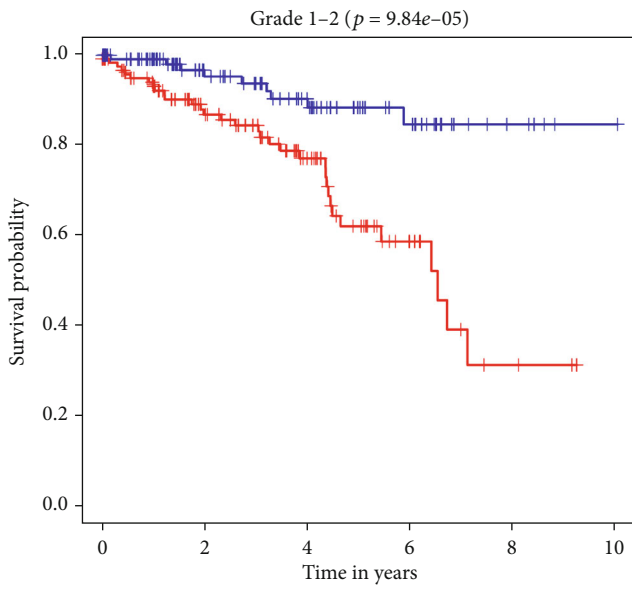
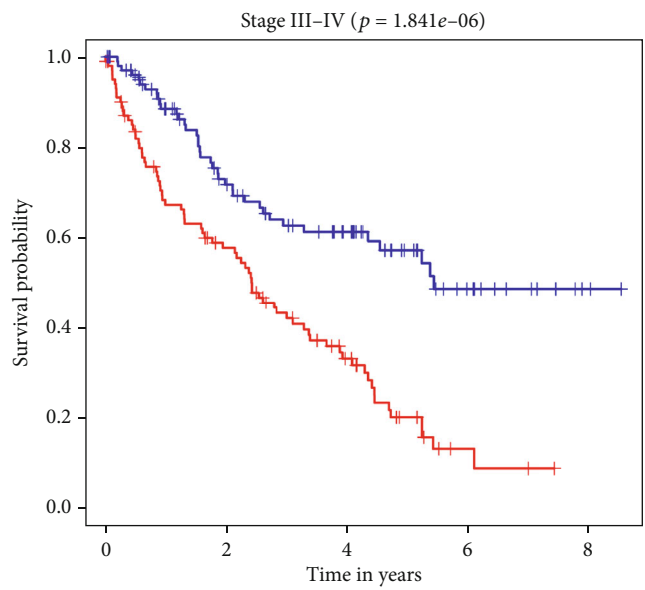
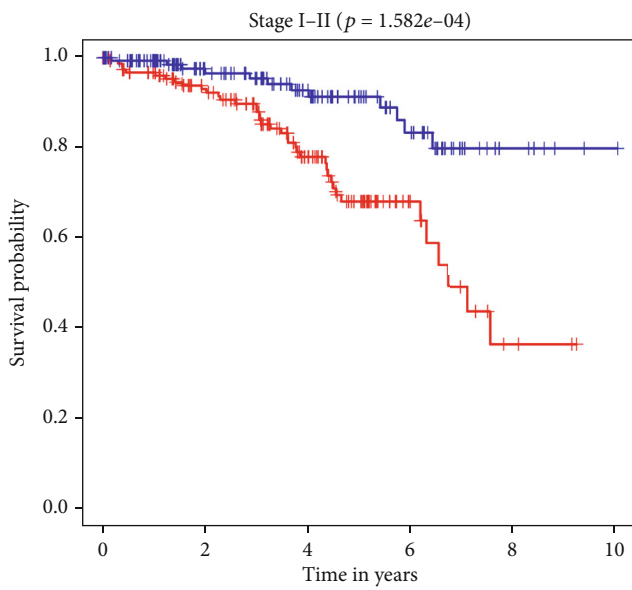


FIGURE 6: Continued.



(e)

(f)



(g)

(h)

FIGURE 6: Continued.

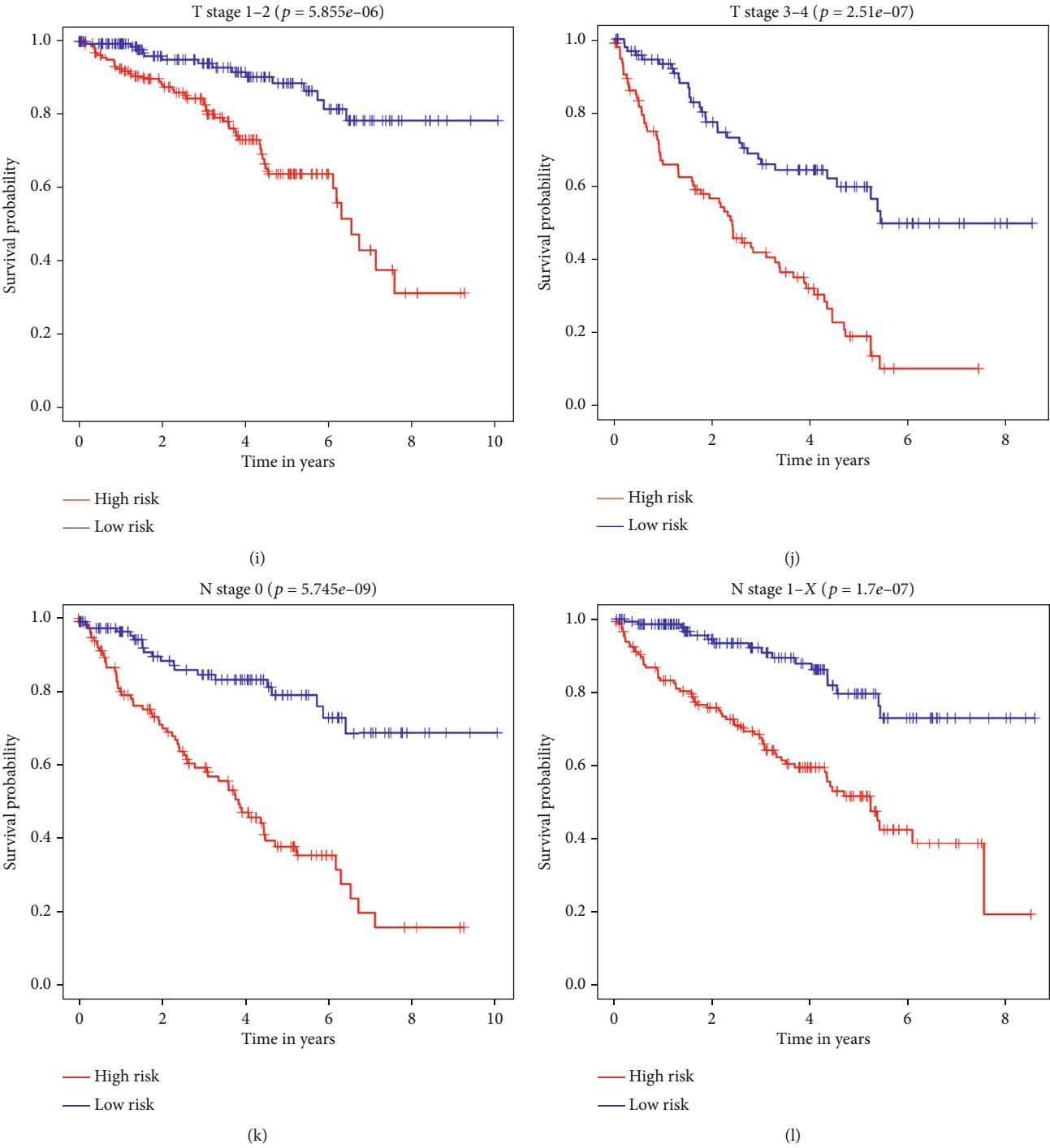


FIGURE 6: Continued.

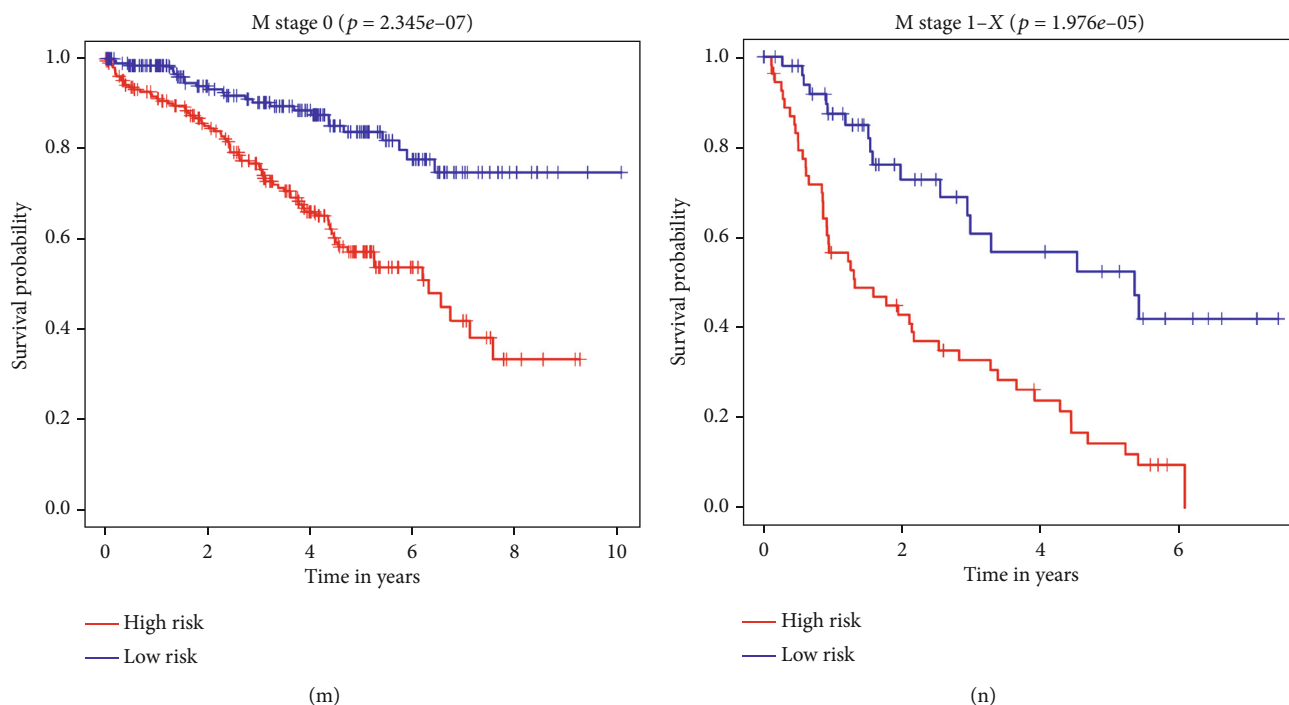


FIGURE 6: Kaplan-Meier survival analysis of ccRCC patients stratified by different clinical parameters. (a) Age ≤ 65 . (b) Age > 65 . (c) Male. (d) Female. (e) Grades 1-2. (f) Grades 3-4. (g) Stages I-II. (h) Stages III-IV. (i) T stages 1-2. (j) T stages 3-4. (k) N stage 0. (l) M stage 1-X. (m) M stage 0. (n) M stage 1-X.

$p = 1.549e - 06$, Figures 10(g) and 10(i)). Based on the nomogram, in the TCGA dataset, the predicted AUCs for 1-, 3-, and 5-year survival rates were 0.871, 0.804, and 0.787, respectively (Figure 10(h)), and in the E-MTAB-1980 dataset, the predicted AUCs for 1-, 3-, and 5-year survival rates were 0.897, 0.917, and 0.896, respectively (Figure 10(j)), indicating that the nomogram had good predictive power and accuracy.

3.11. Validation of Prognosis-Related RRG Expression. We used immunohistochemical results from the HPA online database to determine the protein expression of these 14 prognostic-related RRGs. The results showed that EIF4EBP1, FOXM1, PLG, and VWF were highly expressed in renal carcinoma compared with normal renal tissue, and ADAM8, CGN, G6PC, ITIH4, and MMP3 were low in expression in renal carcinoma compared with normal renal tissue. However, there was no significant difference in the expression of LTB4R and PRKCG between normal renal tissues and renal carcinoma tissues (Figure 11) (Supplemental Table S4).

4. Discussion

According to the latest global cancer statistics, RCC accounts for about 3% of all cancers and is increasing at 2% per year. Approximately 99,200 new cases of RCC and 39,100 RCC-related deaths were reported in Europe in 2018 [29]. As the most common histological subtype of RCC, ccRCC is a malignant parenchymal tumor derived from renal tubular cells, with a 5-year survival rate of only 11.7% in advanced patients [30–32]. However, approximately 25-30% of ccRCC

patients are diagnosed with advanced cancer, and 30% have distant metastases after surgery for early cancer [3, 4]. And the molecular mechanism is still unclear. Redox homeostasis depends on the balance between antioxidant and oxidant levels. During tumorigenesis and progression, when tumor growth exceeds the capacity of the existing vascular system to provide oxygen to tumor cells, tumor cells are often subjected to oxidative stress caused by ischemia, hypoxia, and independent anchored growth [33–35]. More and more evidence showed that redox homeostasis played a fundamental role in tumor genesis and metastasis progression [36–38]. Yet, current studies on cancer, including ccRCC, mainly focus on changes in oxidative stress. The expression pattern and role of RRGs in ccRCC is still unclear, and the redox omics characteristics of ccRCC have not been further studied.

In our current study, we identified a total of 344 differentially expressed RRGs between tumor and normal tissues based on the transcriptome data of ccRCC in the TCGA database. We systematically analyzed the biological functions and molecular mechanisms of these RRGs using bioinformatics techniques. In addition, by performing Cox regression analysis, we identified fourteen prognosis-related RRGs and constructed a RRG-based prognosis-related signature. We also explored the correlation between the prognostic signature and clinical parameters and the role of these prognostic RRGs in ccRCC. Moreover, we also explored the upstream regulatory networks of these RRGs and their relationship with immune cell infiltration.

After our thorough and in-depth analysis, we identified fourteen RRGs that were most associated with prognosis, including ADAM8, CGN, EIF4EBP1, FOXM1, G6PC, HAMP,

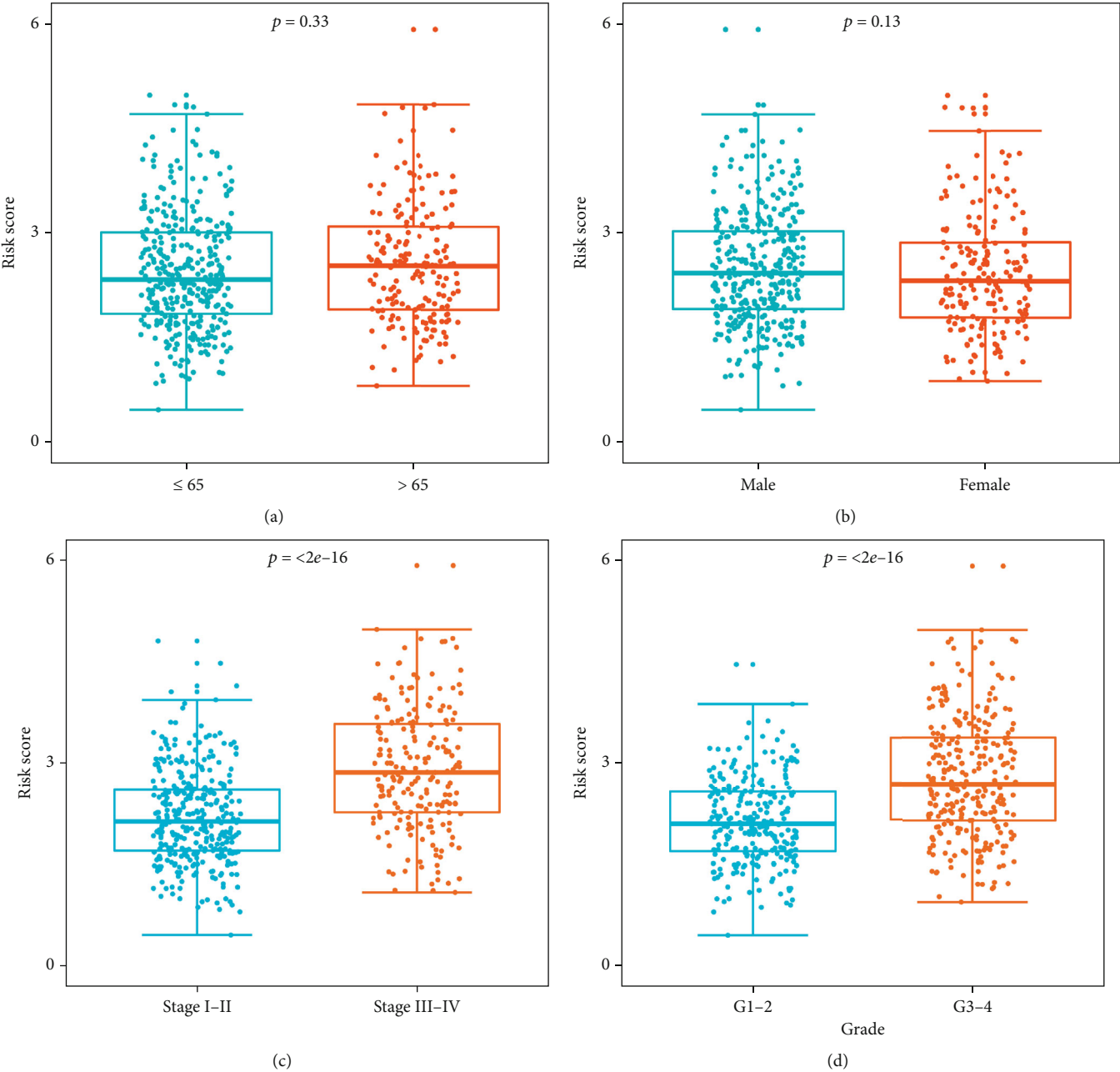


FIGURE 7: Continued.

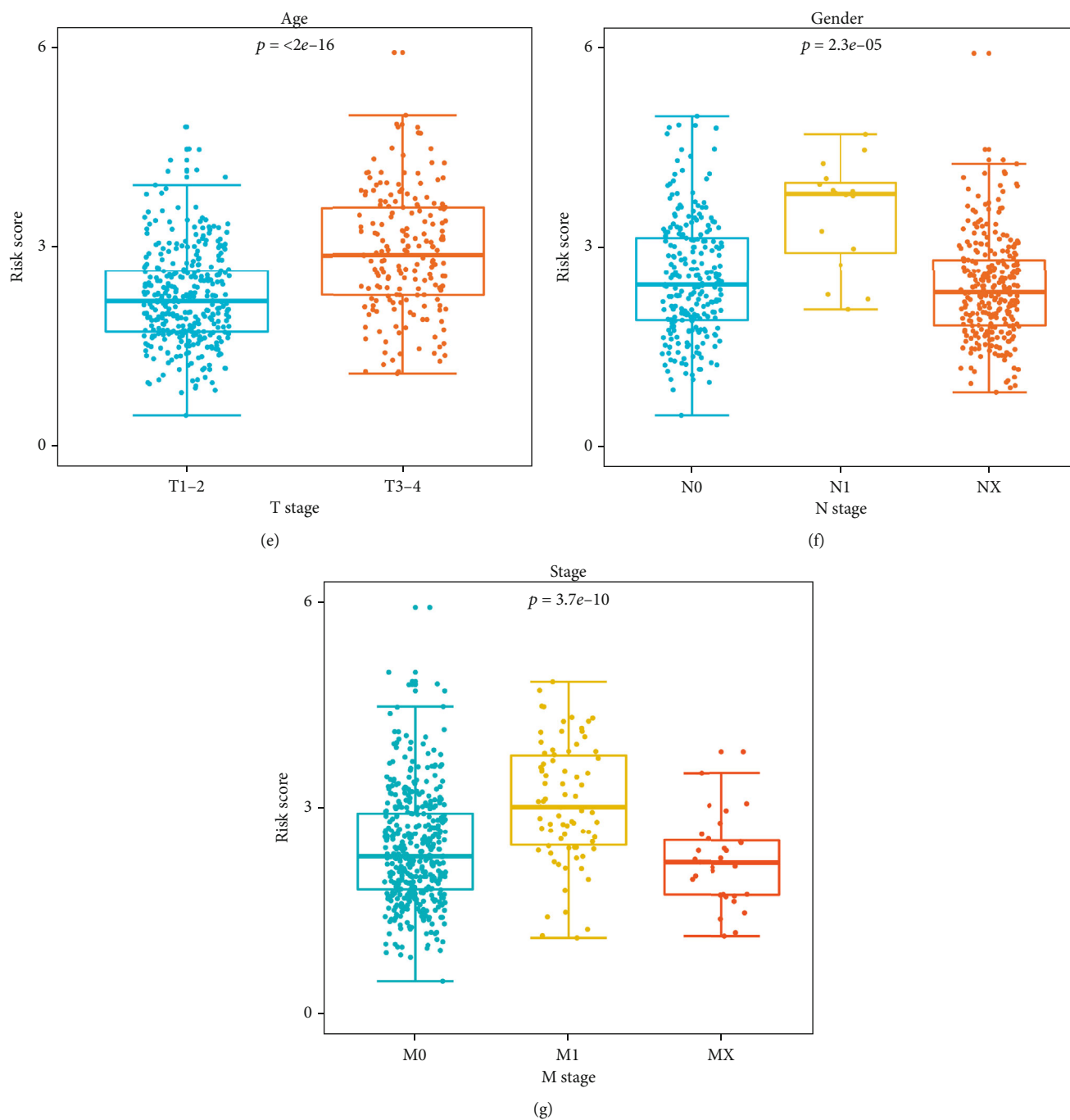


FIGURE 7: The expression differences of signature-based risk score stratified by different clinicopathological parameters. (a) Age. (b) Gender. (c) Stage. (d) Grade. (e) T stage. (f) N stage. (g) M stage.

HTR2C, *ITIH4*, *LTB4R*, *MMP3*, *PLG*, *PRKCG*, *SAA1*, and *VWF*. *ADAM8* is a member of the disintegrin and metalloproteases family with proteolytic activity, and plays an important role in cell adhesion, migration, proteolysis, and signal transduction. High expression of *ADAM8* in tumor cells has been shown to be associated with invasion and metastasis of cancer cells and is associated with poor prognosis in patients [39, 40]. *CGN* interactions with other proteins are involved in the regulation of tight junction assembly, cell growth, and gene expression [41]. Oliveto et al. [42] found

that highly expressed *CGN* was a predictor of survival in mesothelioma patients, and *miR-24-3p* promoted tumor progression and metastasis in mesothelioma patients by inhibiting the expression of *CGN*. The *EIF4EBP1* gene encodes a translation suppressor protein that competitively binds to eukaryotic translation initiation factor 4E, thereby inhibiting its protein expression [43]. Phosphorylated *EIF4EBP1* is thought to be an indicator of tumorigenic activity and is associated with poor survival in cancer patients, while nonphosphorylated *EIF4EBP1* acts as a tumor suppressor [44].

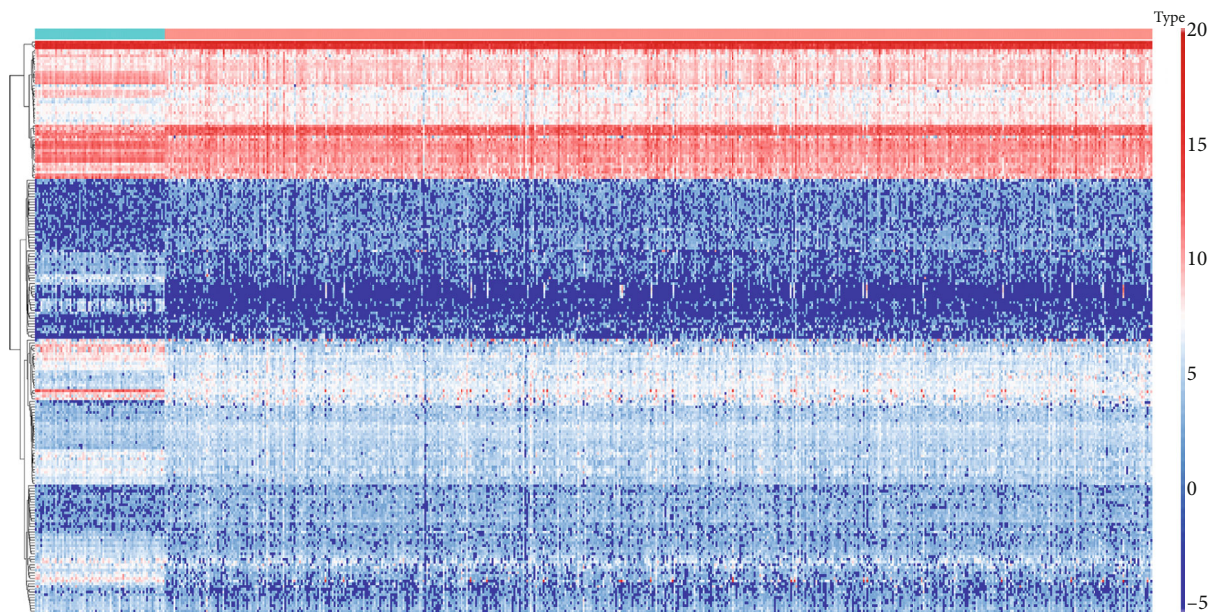
TABLE 2: The relationship between prognosis-related redox genes and clinicopathologic parameters.

Gene		Age ($\leq 65 / > 65$)	Gender (male/female)	Grade (G1-2/G3-4)	Stage (I-II/III-IV)	T stage (T1-2/T3-4)	N stage (N0/N1-X)	M stage (M0/M1-X)
<i>N</i>		353/186	353/186	249/282	331/205	349/190	241/298	428/109
ADAM8	<i>t</i>	0.733	NA*	6.708	6.059	5.807	0.995	4.203
	<i>p</i>	0.919	0.942	<0.001	<0.001	<0.001	0.640	<0.001
CGN	<i>t</i>	2.333	1.735	4.626	5.274	4.749	1.748	1.245
	<i>p</i>	0.140	0.387	<0.001	<0.001	<0.001	0.640	0.250
EIF4EBP1	<i>t</i>	2.360	NA*	NA*	NA*	NA*	0.779	NA*
	<i>p</i>	0.140	0.806	<0.001	<0.001	<0.001	0.655	<0.001
FOXM1	<i>t</i>	0.638	NA*	NA*	NA*	NA*	0.869	NA*
	<i>p</i>	0.919	0.530	<0.001	<0.001	<0.001	0.655	0.112
G6PC	<i>t</i>	1.027	3.144	4.643	5.276	4.730	1.144	3.983
	<i>p</i>	0.854	0.028	<0.001	<0.001	<0.001	0.640	<0.001
HAMP	<i>t</i>	NA*	1.529	6.518	5.939	4.891	0.999	2.855
	<i>p</i>	0.919	0.445	<0.001	<0.001	<0.001	0.640	0.012
HTR2C	<i>t</i>	NA*	0.903	NA*	NA*	NA*	0.481	0.100
	<i>p</i>	0.229	0.587	0.019	0.355	0.324	0.680	0.920
ITIH4	<i>t</i>	0.581	NA*	NA*	NA*	3.747	0.727	2.035
	<i>p</i>	0.919	0.636	<0.001	<0.001	<0.001	0.655	0.065
LTB4R	<i>t</i>	1.189	NA*	2.676	3.679	3.906	1.086	NA*
	<i>p</i>	0.823	0.587	0.009	<0.001	<0.001	0.640	0.018
MMP3	<i>t</i>	0.110	0.972	NA*	NA*	NA*	1.351	0.854
	<i>p</i>	0.954	0.587	<0.001	<0.001	<0.001	0.640	0.424
PLG	<i>t</i>	0.258	1.314	4.076	NA*	5.230	1.238	2.766
	<i>p</i>	0.945	0.529	<0.001	<0.001	<0.001	0.640	0.012
PRKCG	<i>t</i>	0.241	0.810	NA*	NA*	NA*	0.521	NA*
	<i>p</i>	0.945	0.587	<0.001	<0.001	<0.001	0.680	0.214
SAA1	<i>t</i>	0.289	2.725	NA*	7.910	7.124	0.126	4.796
	<i>p</i>	0.945	0.049	<0.001	<0.001	<0.001	0.900	<0.001
VWF	<i>t</i>	0.057	0.064	3.670	3.661	3.232	0.608	3.966
	<i>p</i>	0.954	0.949	<0.001	<0.001	0.001	0.680	<0.001

NA: not available. *Nonparametric Mann-Whitney rank sum test.

FOXM1 plays an important role in balancing genomic stability and maintaining cell proliferation and differentiation [45]. Studies have shown that FOXM1 is abnormally elevated in a variety of human malignancies and acts as a major activator of tumor cell invasion and metastasis [46]. G6PC plays an important role in the glycogen breakdown pathway. Studies have shown that glycogen plays a key role in promoting the survival of cancer cells, and inhibition of glycogen decomposition can induce apoptosis and early cell senescence [47]. HAMP plays an important role in the proliferation and metastasis of tumor cells [48]. Studies have

shown that dysregulated HAMP expression is associated with an increased risk of hepatocellular carcinoma [49]. HTR2C was found to be involved in the non-small-cell lung cancer pathway, directly affecting epidermal growth factor receptor tyrosine kinase inhibitor resistance [50]. ITIH4 is an acute-phase protein secreted by the liver into the blood circulation system, and it is believed to be closely related to the occurrence, progression, invasion, and metastasis of many solid tumors. Li et al. [51] found that ITIH4 is an effective serum marker for early warning and diagnosis of hepatocellular carcinoma. LTB4R is a potent lipid mediator that



Type
■ N
■ T

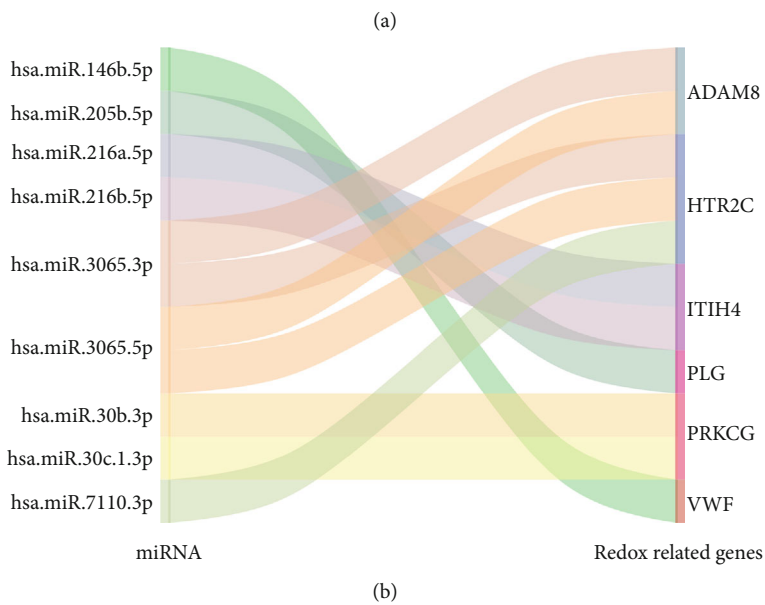


FIGURE 8: Continued.

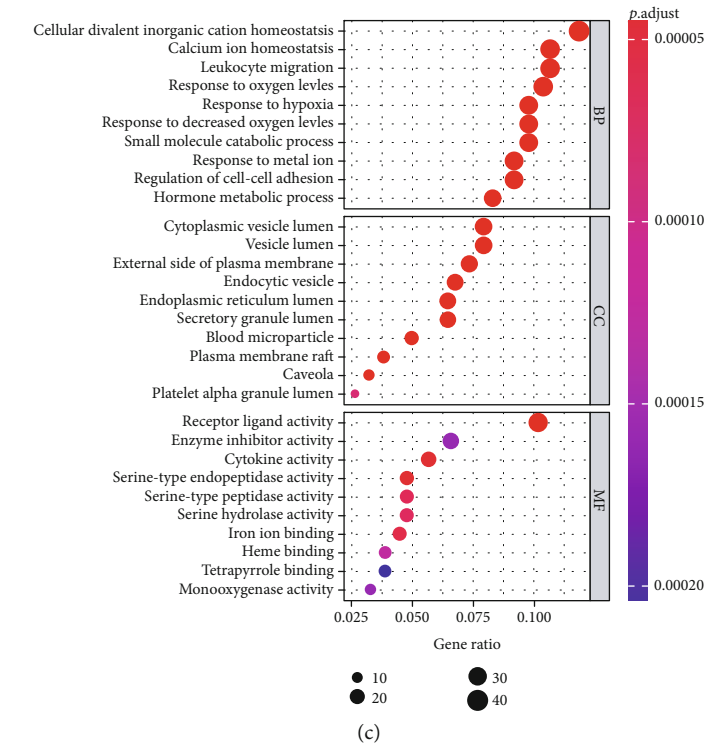


FIGURE 8: Multidimensional regulatory network of prognosis-related RRGs and differentially expressed miRNAs and the functional enrichment analysis of these RRGs. (a) Heat map of 211 differentially expressed miRNAs in the normal renal tissues and ccRCC tissues. (b) Sankey plot of the regulatory relationship between miRNAs and prognosis-related RRGs. (c) GO enrichment analysis of the differentially expressed RRGs. The top 10 enrichment analysis results, including biological processes, cell components, and molecular functions, are shown in the figure. (d) KEGG enrichment analysis of the differentially expressed RRGs. The first 30 results of functional enrichment analysis are shown in the figure.

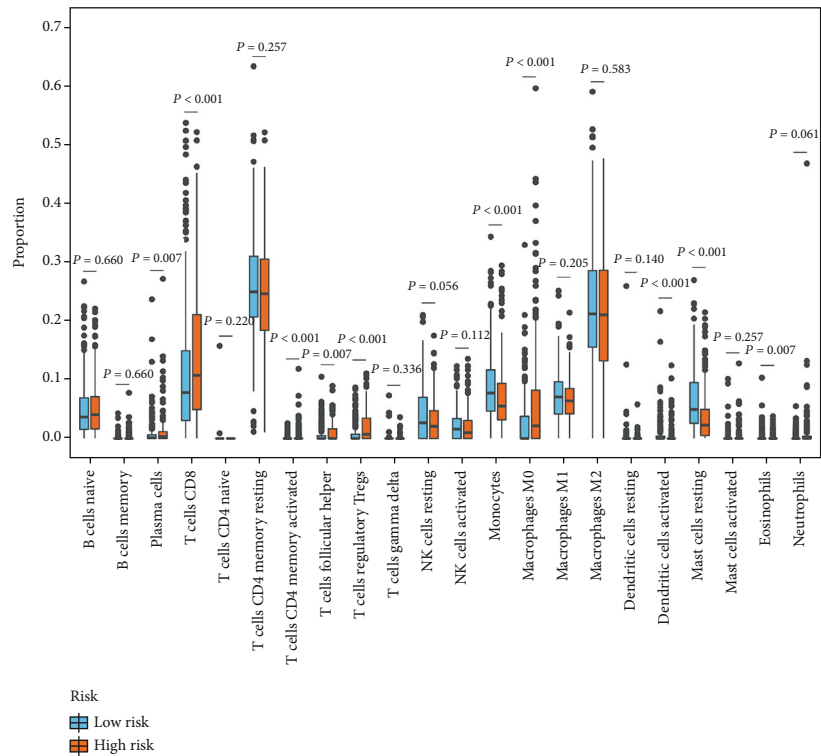
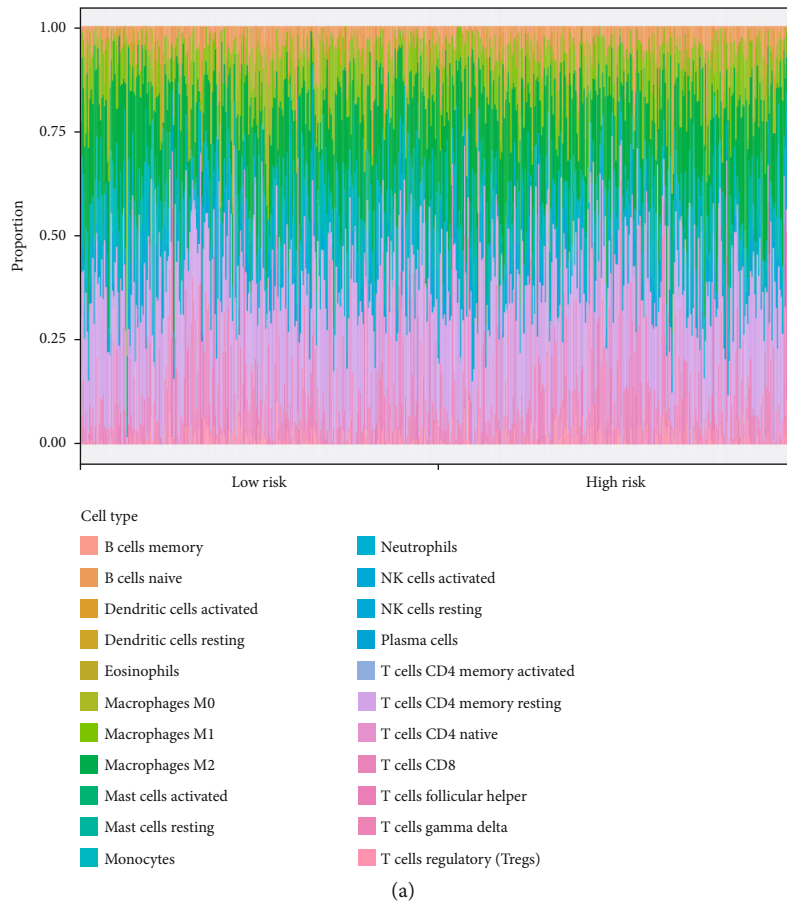


FIGURE 9: Continued.

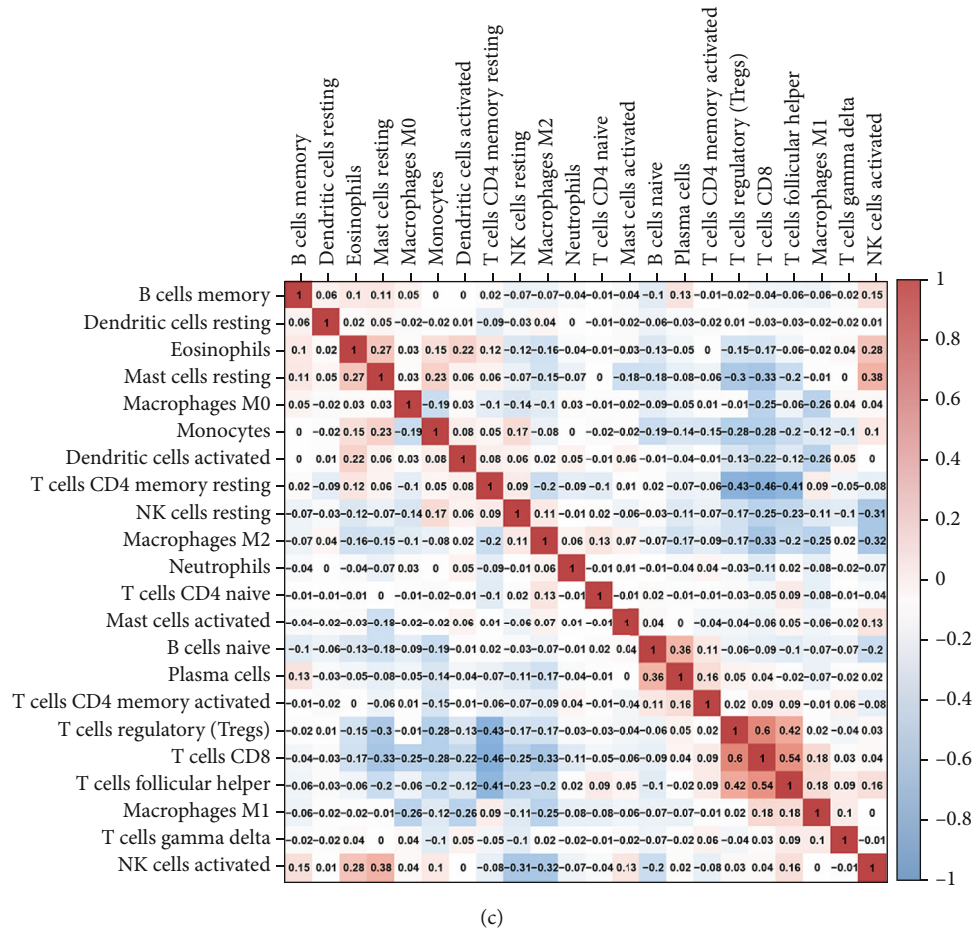


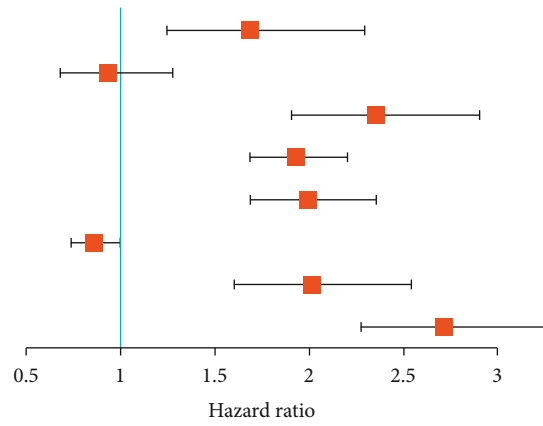
FIGURE 9: The infiltration difference of tumor-infiltrating immune cells between high-risk and low-risk groups in the TCGA cohort assessed by fourteen RRG-based prognostic signature. (a) The stacked bar chart shows the distribution of 22 immune cells in each sample of the TCGA cohort. ccRCC patients were grouped according to the median risk score. (b) Box plot shows the infiltration difference of tumor-infiltrating immune cells between the high-risk and low-risk groups in the TCGA cohort. (c) Correlation matrix of the proportion of immune cells. Red means positive correlation and blue means negative correlation.

regulates allergy, inflammation, and immune responses, and has been shown to be upregulated in a variety of tumors and to play a potential role in the early stages of tumor development [52, 53]. MMP3 is an extracellular matrix-degrading protease that plays an important role in a variety of tumors. Polette et al. [54] found that MMP3 expression was a prognostic marker for HNSCC invasion and lymph node metastasis. Radisky et al. [55] found that overexpression of MMP3 in breast epithelial cells was associated with epithelial-mesenchymal transformation in vitro and tumor promotion in vivo. PLG has broad substrate specificity, which not only supports the migration and invasion of tumor cells due to the enzymatic properties of fibrinolytic enzyme but also has antiangiogenesis and antitumor factors [56]. Zhao et al. [57] found that high expression of PLG in advanced high-grade serous ovarian cancer is a favorable prognostic biomarker. The PRKCG gene encodes γ PKC, which plays an important role in tumor genesis, proliferation, differentiation, and migration. Studies have found that mutations in the PRKCG gene increase breast cancer susceptibility [58]. Lu et al. [59] also found that PRKCG gene intron variation was significantly associated

with an increased risk of osteosarcoma. SAA1 is an acute-phase high-density lipoprotein-associated apolipoprotein that is significantly upregulated in injury, inflammation, and cancer [60]. Studies have shown that SAA1 is involved in a variety of functions, including inducing extracellular matrix-degrading enzymes for tissue repair, recruiting immune cells to inflammatory sites, and lipid transport and metabolism [61]. VWF is a multifunctional adhesive glycoprotein. Elevated plasma VWF antigen concentrations have been found in a variety of malignancies [62]. Aryal et al. [63] found that intraplatelet VWF could independently predict the recurrence of early hepatocellular carcinoma after resection. These results suggested that these fourteen RRGs may be involved in the occurrence and progression of ccRCC. However, the exact molecular mechanisms are unknown, and further exploration of possible mechanisms may be valuable.

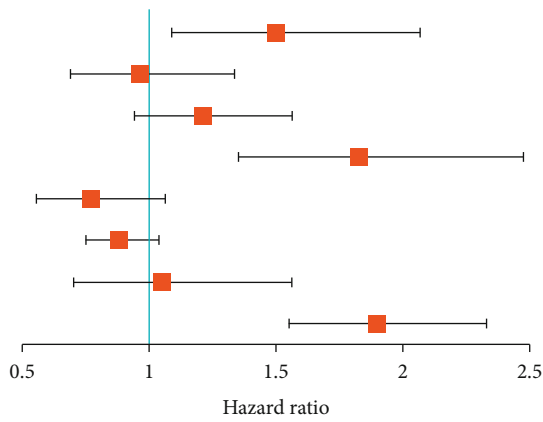
Next, we established a redox-associated prognostic signature based on these fourteen prognostic-related RRGs. Kaplan-Meier survival analysis found that patients in the high-risk group had worse OS than those in the low-risk group. ROC curve analysis showed that the prognostic

	<i>p</i> value	Hazard ratio
Age	<0.001	1.689 (1.244–2.294)
Gender	0.655	0.930 (0.678–1.276)
Grade	<0.001	2.354 (1.908–2.906)
Stage	<0.001	1.929 (1.687–2.205)
T	<0.001	1.993 (1.687–2.355)
N	0.049	0.856 (0.734–0.999)
M	<0.001	2.016 (1.603–2.536)
Risk score	<0.001	2.718 (2.275–3.247)

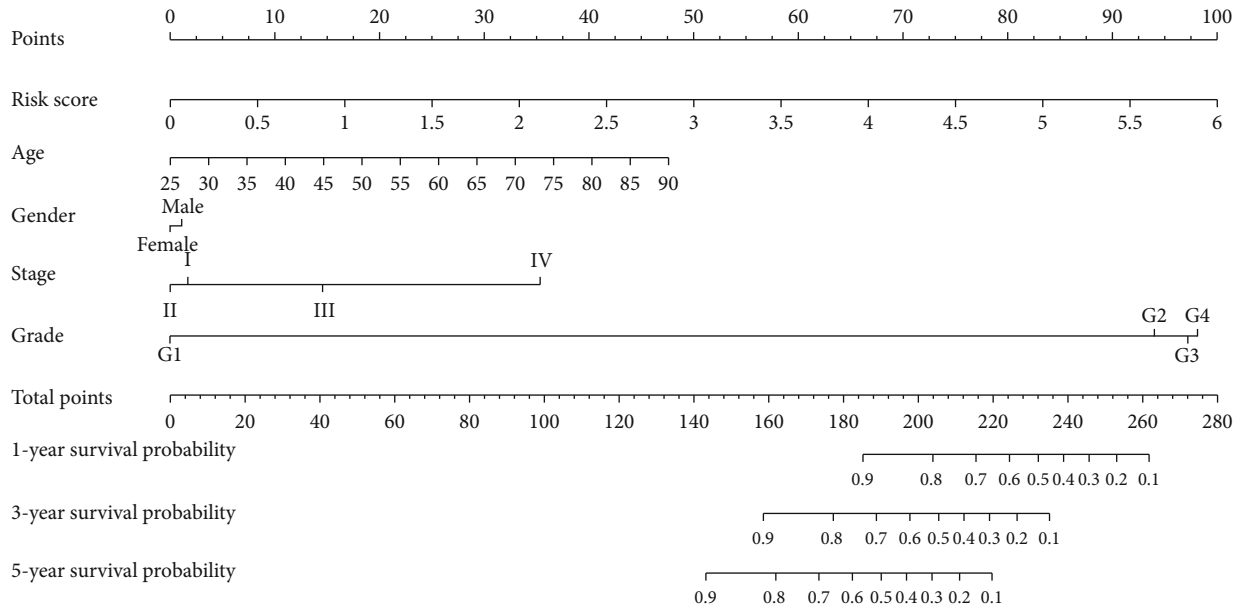


(a)

	<i>p</i> value	Hazard ratio
Age	<0.013	1.500 (1.089–2.065)
Gender	0.817	0.962 (0.692–1.338)
Grade	<0.135	1.213 (0.942–1.563)
Stage	<0.001	1.829 (1.352–2.475)
T	<0.111	0.769 (0.556–1.062)
N	0.125	0.881 (0.750–1.036)
M	<0.809	1.050 (0.706–1.563)
Risk score	<0.001	1.901 (1.551–2.328)

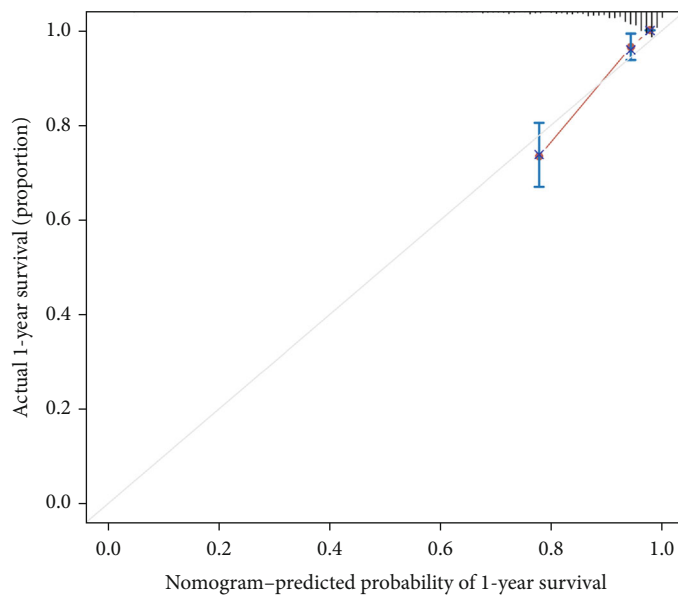


(b)

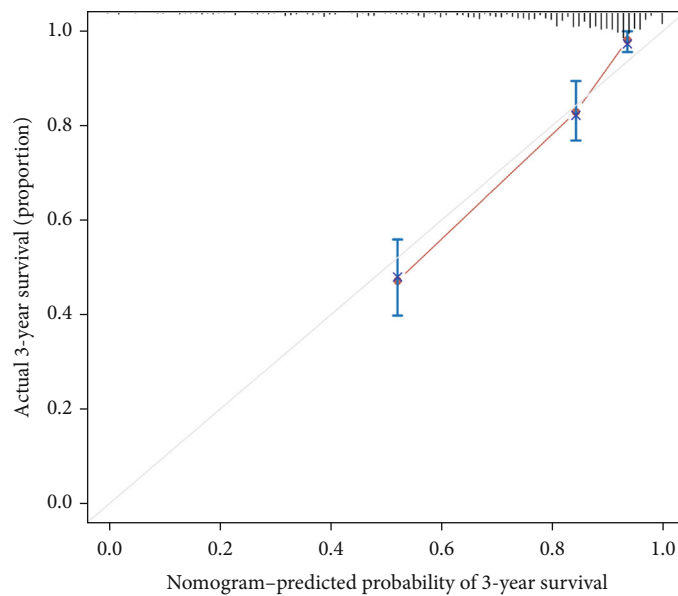


(c)

FIGURE 10: Continued.

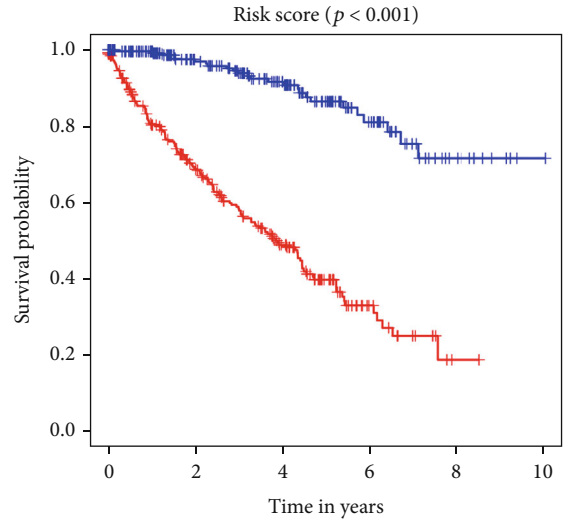
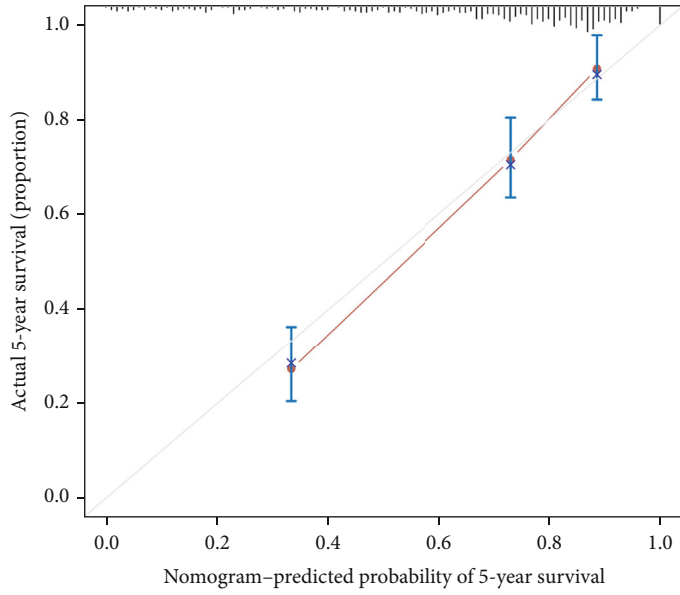


(d)



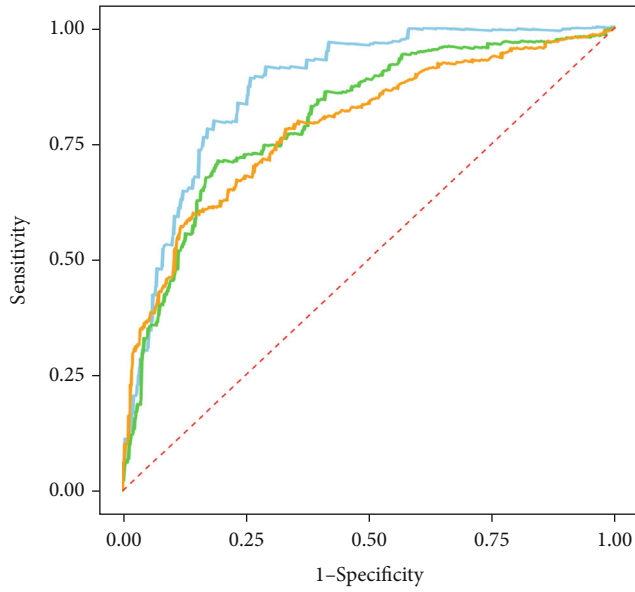
(e)

FIGURE 10: Continued.



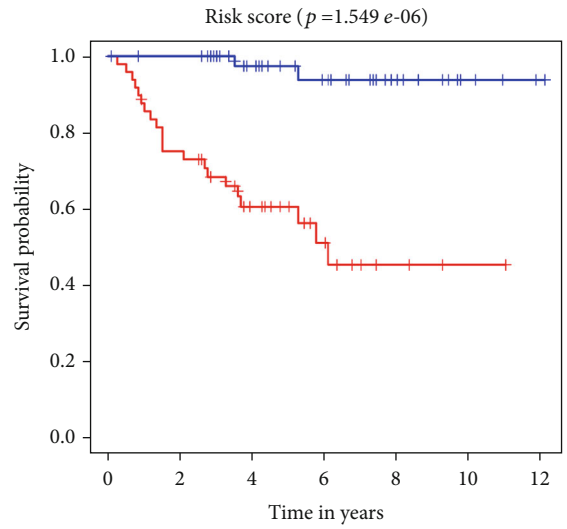
(f)

(g)



— AUC of 1 year survival = 0.871
— AUC of 3 year survival = 0.804
— AUC of 5 year survival = 0.787

(h)



— High risk
— Low risk

(i)

FIGURE 10: Continued.

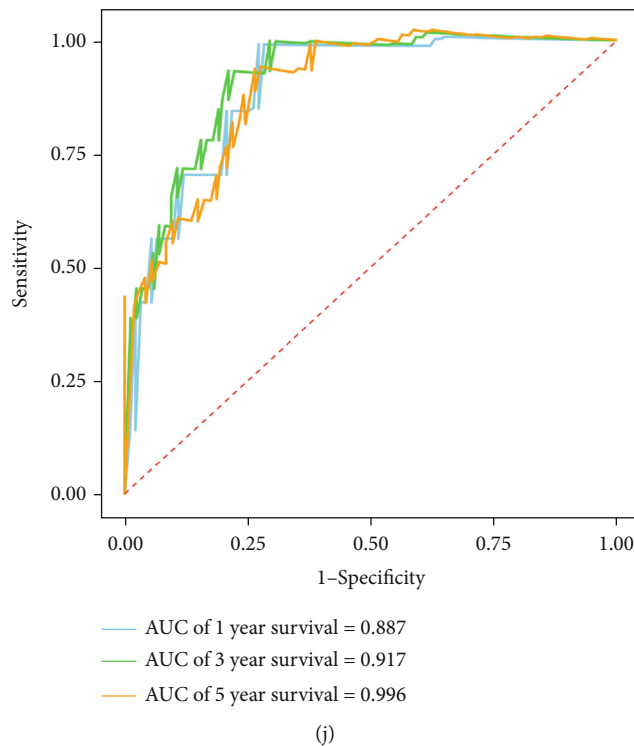


FIGURE 10: Cox regression analysis was performed on the common clinical characteristics and RRG-based signature in the TCGA cohort, and the establishment and verification of the nomogram. (a) Univariate Cox regression analysis of correlations between risk score for OS and clinical characteristics. (b) Multivariate Cox regression analysis of correlations between risk score for OS and clinical characteristics. (c) Nomogram for predicting the 1-year, 3-year, and 5-year OS of ccRCC patients in the TCGA cohort. (d, e, f) Calibration curves of the nomogram to predict OS at 1, 3, and 5 years. (g) Kaplan-Meier survival curve analysis of OS in the high- and low-risk subgroups of the TCGA cohort based on the nomogram. (h) Time-dependent ROC curves for predicting OS in the TCGA cohort based on the nomogram. The ROC curves and AUC were shown to predict ccRCC patients at 1, 3, and 5 years. (i) Kaplan-Meier survival curve analysis of OS in the high- and low-risk subgroups of the E-MTAB-1980 cohort based on the nomogram. (j) Time-dependent ROC curves for predicting OS in the E-MTAB-1980 cohort based on the nomogram. The ROC curves and AUC were shown to predict ccRCC patients at 1, 3, and 5 years.

signature could better screen out ccRCC patients with poor prognosis. Further analysis showed that after stratification by different clinical parameters, the prognosis of patients in each high-risk group was poor. And this prognosis-related signature was also associated with disease progression of ccRCC, and the higher the risk score, the more malignant the ccRCC tumor, suggesting that this signature has a good recognition in distinguishing the degree of malignancy of the tumor and prognosis of the patient.

In addition, we used the TCGA database to construct ccRCC network to explore the interaction between differentially expressed miRNAs and prognosis-related RRGs. A network of 9 differentially expressed miRNAs and 6 RRGs was established based on the results of coexpression analysis. These miRNAs may have the potential to activate oxidative stress or act as a great regulator of cancer triggering and deserve further investigation. To further understand the biological functions and molecular mechanisms of these differentially expressed RRGs, we performed GO and KEGG enrichment analysis. The results showed that these RRGs were significantly enriched in reactive oxygen species metabolic process, calcium ion homeostasis, antigen processing, treatment, peptide antigen presentation, HIF-1 signaling

pathway, transcriptional misregulation in cancer, and PI3K-Akt signaling pathway. The imbalance of the redox system plays an important role in the pathogenesis and progression of tumors. During tumor development, when tumor growth exceeds the capacity of the existing vascular system to provide oxygen to tumor cells, tumor cells are often subjected to oxidative stress caused by ischemia, hypoxia, and independent anchored growth [33–36]. These by-products of oxidative stress cause conformational changes in DNA, proteins, and lipids that further lead to glycosylation, phosphorylation, or oxidation, thereby affecting the function and stability of biomolecules [64]. When these proteins and lipids undergo apoptosis or oxidation, antigenic changes lead to tumor resistance to radiation therapy and the host immune system [65, 66]. Additionally, excessive ROS can react with residues of various amino acids of proteins (such as cysteine, histidine, lysine, arginine, proline, or threonine) to form carbonyl groups, changing the coding sequence and tertiary and quarter-level structures of proteins [67]. These mutated peptides may produce new epitopes. These results suggest that genes may influence the occurrence and development of tumors by regulating cell redox homeostasis and affecting immune cell function. Further studies found that, based on

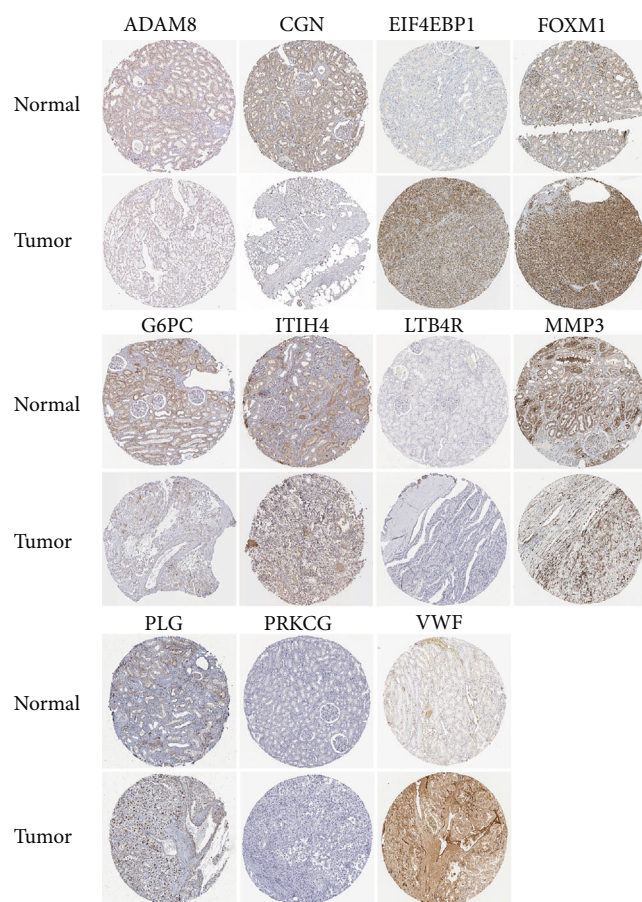


FIGURE 11: Validation of the expression of the prognostic RRGs in ccRCC and normal renal tissues in the HPA database.

the signature, there were differences in the degree of immune cell infiltration between high- and low-risk ccRCC groups.

Moreover, to expand the clinical application and availability of RRG-based prognostic signature and to establish a quantitative method for predicting patient prognosis, we constructed a nomogram combining clinical parameters. After drawing the calibration curve of each time cutoff point and verifying it with TCGA dataset and E-MTAB-1980 dataset for many times, it is suggested that the performance and accuracy of the nomogram are good.

Overall, our study provides new insights into the occurrence and progression of ccRCC from the perspective of redox. Our prognostic signature can better predict the survival probabilities of ccRCC patients, which may become a new prognostic biomarker for ccRCC. However, our study also has some limitations. First, our study is mainly based on a single bioinformatics information, and different characteristics of different platforms may lead to patient heterogeneity. Second, the model construction and validation of this study were designed by retrospective analysis, and the model still needs to be validated through a prospective clinical cohort. Finally, the specific biological function and molecular mechanism of prognostic RRGs in ccRCC are still unclear, and need to be further analyzed by *in vitro* and *in vivo* experiments.

5. Conclusions

In conclusion, we systematically explored the biological function and prognostic value of these differentially expressed RRGs in ccRCC by a variety of bioinformatics techniques. We also constructed redox-associated prognostic signature that could independently predict the prognosis of ccRCC patients. To our knowledge, this is the first report on the establishment of redox-associated prognostic signature of ccRCC. Our results may have important significance in revealing the mechanism of ccRCC and provide new therapeutic targets and prognostic biomarkers for ccRCC.

Abbreviations

RCC:	Renal cell carcinoma
ccRCC:	Clear cell renal cell carcinoma
RRGs:	Redox-related genes
TCGA:	The Cancer Genome Atlas
ROS:	Reactive oxygen species
ROC:	Receiver operating characteristic
HPA:	Human Protein Atlas
FC:	Fold change
FDR:	False discovery rate
WGCNA:	Weighted correlation network analysis
LASSO:	Least absolute shrinkage and selection operator
AUC:	Area under the receiver operating characteristic curve
OS:	Overall survival
GO:	Gene Ontology
KEGG:	Kyoto Encyclopedia of Genes and Genomes database
CIBERSORT:	Cell-type identification by estimating relative subsets of RNA transcripts
TFs:	Transcription factors.

Data Availability

The data and materials can be obtained by contacting the corresponding author.

Conflicts of Interest

The authors declare that there is no conflict of interest regarding the publication of this paper.

Authors' Contributions

This work was carried out in collaboration among all authors. Yue Wu designed the study and performed the data analysis. Xian Wei, Huan Feng, Bintao Hu, and Bo Liu performed the data analysis. Yang Luan, Yajun Ruan, Xiaming Liu, Zhuo Liu, and Jihong Liu performed the data analysis and revised the manuscript. Tao Wang designed the study and revised the manuscript. All authors read and approved the final manuscript.

Acknowledgments

This study was supported by the Medical Youth Top Talent Program of Hubei Province.

Supplementary Materials

Supplemental Table S1: a total of 4087 RRGs were obtained from the GeneCards, OMIM, NCBI, and GSEA-MSigDB databases. Supplemental Table S2: univariate Cox regression analysis of differentially expressed RRGs. Supplemental Table S3: transcription factors and redox genes regulatory networks. Supplemental Table S4: relevant links of immunohistochemical staining images of prognostic RRGs. Supplemental Figure S1: LASSO regression analysis for screening prognosis-related RRGs. Supplemental Figure S2: prognostic value of fifteen key RRGs in the TCGA cohort. Supplemental Figure S3: expression levels of these 14 RRGs in different cancer types in the TCGA cohort. (*Supplementary Materials*)

References

- [1] J. J. Hsieh, V. Le, D. Cao, E. H. Cheng, and C. J. Creighton, "Genomic classifications of renal cell carcinoma: a critical step towards the future application of personalized kidney cancer care with pan-omics precision," *The Journal of Pathology*, vol. 244, no. 5, pp. 525–537, 2018.
- [2] National Cancer Institute, "Cancer stat facts: kidney and renal pelvis cancer," February 2018, <https://seer.cancer.gov/statfacts/html/kidrp.html>.
- [3] P. I. Karakiewicz, A. Briganti, F. K.-H. Chun et al., "Multi-institutional validation of a new renal cancer-specific survival nomogram," *Journal of Clinical Oncology*, vol. 25, no. 11, pp. 1316–1322, 2007.
- [4] H. T. Cohen and F. J. McGovern, "Renal-cell carcinoma," *The New England Journal of Medicine*, vol. 353, no. 23, pp. 2477–2490, 2005.
- [5] V. Ficarra, A. Galfano, M. Mancini, G. Martignoni, and W. Artibani, "TNM staging system for renal-cell carcinoma: current status and future perspectives," *The Lancet Oncology*, vol. 8, no. 6, pp. 554–558, 2007.
- [6] X. Li, B. Turanli, K. Juszczak et al., "Classification of clear cell renal cell carcinoma based on PKM alternative splicing," *Helvicon*, vol. 6, no. 2, article e03440, 2020.
- [7] A. Caliskan, A. C. Andac, and K. Y. Arga, "Novel molecular signatures and potential therapeutics in renal cell carcinomas: insights from a comparative analysis of subtypes," *Genomics*, vol. 112, no. 5, pp. 3166–3178, 2020.
- [8] K. K. Griendling and M. Ushio-Fukai, "Reactive oxygen species as mediators of angiotensin II signaling," *Regulatory Peptides*, vol. 91, no. 1-3, pp. 21–27, 2000.
- [9] W. Dröge, "Free radicals in the physiological control of cell function," *Physiological Reviews*, vol. 82, no. 1, pp. 47–95, 2002.
- [10] A. Valencia and J. Morán, "Role of oxidative stress in the apoptotic cell death of cultured cerebellar granule neurons," *Journal of Neuroscience Research*, vol. 64, no. 3, pp. 284–297, 2001.
- [11] J. S. Ha, H. M. Lim, and S. S. Park, "Extracellular hydrogen peroxide contributes to oxidative glutamate toxicity," *Brain Research*, vol. 1359, pp. 291–297, 2010.
- [12] X. Lu, H. Xu, B. Sun, Z. Zhu, D. Zheng, and X. Li, "Enhanced neuroprotective effects of resveratrol delivered by nanoparticles on hydrogen peroxide-induced oxidative stress in rat cortical cell culture," *Molecular Pharmaceutics*, vol. 10, no. 5, pp. 2045–2053, 2013.
- [13] V. Helfinger and K. Schröder, "Redox control in cancer development and progression," *Molecular Aspects of Medicine*, vol. 63, pp. 88–98, 2018.
- [14] N. A. Simonian and J. T. Coyle, "Oxidative stress in neurodegenerative diseases," *Annual Review of Pharmacology and Toxicology*, vol. 36, no. 1, pp. 83–106, 1996.
- [15] N. S. Dhalla, R. M. Temsah, and T. Netticadan, "Role of oxidative stress in cardiovascular diseases," *Journal of Hypertension*, vol. 18, no. 6, pp. 655–673, 2000.
- [16] M. Valko, D. Leibfritz, J. Moncol, M. T. Cronin, M. Mazur, and J. Telser, "Free radicals and antioxidants in normal physiological functions and human disease," *The International Journal of Biochemistry & Cell Biology*, vol. 39, no. 1, pp. 44–84, 2007.
- [17] S. Reuter, S. C. Gupta, M. M. Chaturvedi, and B. B. Aggarwal, "Oxidative stress, inflammation, and cancer: how are they linked?," *Free Radical Biology & Medicine*, vol. 49, no. 11, pp. 1603–1616, 2010.
- [18] D. Zhou, L. Shao, and D. R. Spitz, "Reactive oxygen species in normal and tumor stem cells," *Advances in Cancer Research*, vol. 122, pp. 1–67, 2014.
- [19] J. G. Costa, N. Saraiva, I. Batinic-Haberle, M. Castro, N. G. Oliveira, and A. S. Fernandes, "The SOD mimic MnTnHex-2-PyP5+ reduces the viability and migration of 786-O human renal cancer cells," *Antioxidants*, vol. 8, no. 10, p. 490, 2019.
- [20] H. Miess, B. Dankworth, A. M. Gouw et al., "The glutathione redox system is essential to prevent ferroptosis caused by impaired lipid metabolism in clear cell renal cell carcinoma," *Oncogene*, vol. 37, no. 40, pp. 5435–5450, 2018.
- [21] R. Li, Y. Li, X. Liang, L. Yang, M. Su, and K. P. Lai, "Network pharmacology and bioinformatics analyses identify intersection genes of niacin and COVID-19 as potential therapeutic targets," *Briefings in Bioinformatics*, vol. 22, no. 2, pp. 1279–1290, 2021.
- [22] P. J. Thul, L. Åkesson, M. Wiking et al., "A subcellular map of the human proteome," *Science*, vol. 356, no. 6340, article eaal3321, 2017.
- [23] H. Sies, C. Berndt, and D. P. Jones, "Oxidative stress," *Annual Review of Biochemistry*, vol. 86, no. 1, pp. 715–748, 2017.
- [24] M. S. Leisegang, K. Schröder, and R. P. Brandes, "Redox regulation and noncoding RNAs," *Antioxidants & Redox Signaling*, vol. 29, no. 9, pp. 793–812, 2018.
- [25] N. Engedal, E. Žerovnik, A. Rudov et al., "From oxidative stress damage to pathways, networks, and autophagy via microRNAs," *Oxidative Medicine and Cellular Longevity*, vol. 2018, Article ID 4968321, 16 pages, 2018.
- [26] P. Karihtala, K. Porvari, Y. Soini, and K. M. Haapasari, "Redox regulating enzymes and connected microRNA regulators have prognostic value in classical Hodgkin lymphomas," *Oxidative Medicine and Cellular Longevity*, vol. 2017, Article ID 2696071, 8 pages, 2017.
- [27] Y. Zhang, S. Zheng, Y. Geng et al., "MicroRNA profiling of atrial fibrillation in canines: miR-206 modulates intrinsic cardiac autonomic nerve remodeling by regulating SOD1," *PLoS One*, vol. 10, no. 3, article e0122674, 2015.

- [28] M. Gómez de Cedrón, R. Acín Pérez, R. Sánchez-Martínez et al., “MicroRNA-661 modulates redox and metabolic homeostasis in colon cancer,” *Molecular Oncology*, vol. 11, no. 12, pp. 1768–1787, 2017.
- [29] J. Ferlay, M. Colombet, I. Soerjomataram et al., “Cancer incidence and mortality patterns in Europe: estimates for 40 countries and 25 major cancers in 2018,” *European Journal of Cancer*, vol. 103, pp. 356–387, 2018.
- [30] A. Lopez-Beltran, M. Scarpelli, R. Montironi, and Z. Kirkali, “2004 WHO classification of the renal tumors of the adults,” *European Urology*, vol. 49, no. 5, pp. 798–805, 2006.
- [31] H. Moch, A. L. Cubilla, P. A. Humphrey, V. E. Reuter, and T. M. Ulbright, “The 2016 WHO classification of tumours of the urinary system and male genital organs-part a: renal, penile, and testicular tumours,” *European Urology*, vol. 70, no. 1, pp. 93–105, 2016.
- [32] R. L. Siegel, K. D. Miller, and A. Jemal, “Cancer statistics, 2017,” *CA: A Cancer Journal for Clinicians*, vol. 67, no. 1, pp. 7–30, 2017.
- [33] T. Stylianopoulos, J. D. Martin, M. Snuderl, F. Mpekris, S. R. Jain, and R. K. Jain, “Coevolution of solid stress and interstitial fluid pressure in tumors during progression: implications for vascular collapse,” *Cancer Research*, vol. 73, no. 13, pp. 3833–3841, 2013.
- [34] S. S. Sabharwal and P. T. Schumacker, “Mitochondrial ROS in cancer: initiators, amplifiers or an Achilles’ heel?,” *Nature Reviews. Cancer*, vol. 14, no. 11, pp. 709–721, 2014.
- [35] Z. T. Schafer, A. R. Grassian, L. Song et al., “Antioxidant and oncogene rescue of metabolic defects caused by loss of matrix attachment,” *Nature*, vol. 461, no. 7260, pp. 109–113, 2009.
- [36] L. Yang, Z. He, J. Yao et al., “Regulation of AMPK-related glycolipid metabolism imbalances redox homeostasis and inhibits anchorage independent growth in human breast cancer cells,” *Redox Biology*, vol. 17, pp. 180–191, 2018.
- [37] M. A. Hawk and Z. T. Schafer, “Mechanisms of redox metabolism and cancer cell survival during extracellular matrix detachment,” *The Journal of Biological Chemistry*, vol. 293, no. 20, pp. 7531–7537, 2018.
- [38] D. C. Altieri, “Mitochondria on the move: emerging paradigms of organelle trafficking in tumour plasticity and metastasis,” *British Journal of Cancer*, vol. 117, no. 3, pp. 301–305, 2017.
- [39] U. Schlomann, G. Koller, C. Conrad et al., “ADAM8 as a drug target in pancreatic cancer,” *Nature Communications*, vol. 6, no. 1, article 6175, 2015.
- [40] C. Conrad, J. Benzel, K. Dorzweiler et al., “ADAM8 in invasive cancers: links to tumor progression, metastasis, and chemoresistance,” *Clinical Science*, vol. 133, no. 1, pp. 83–99, 2019.
- [41] M. S. Balda and K. Matter, “Tight junctions and the regulation of gene expression,” *Biochimica et Biophysica Acta (BBA) - Biomembranes*, vol. 1788, no. 4, pp. 761–767, 2009.
- [42] S. Oliveto, R. Alfieri, A. Miluzio et al., “A polysome-based microRNA screen identifies miR-24-3p as a novel promigratory miRNA in mesothelioma,” *Cancer Research*, vol. 78, no. 20, pp. 5741–5753, 2018.
- [43] T. E. Harris and J. C. Lawrence Jr., “TOR signaling,” *Science Signaling*, vol. 2003, no. 212, article re15, 2003.
- [44] G. Armengol, F. Rojo, J. Castellví et al., “4E-binding protein 1: a key molecular “funnel factor” in human cancer with clinical implications,” *Cancer Research*, vol. 67, no. 16, pp. 7551–7555, 2007.
- [45] C.-Y. Koo, K. W. Muir, and E. W. F. Lam, “FOXO1: from cancer initiation to progression and treatment,” *Biochimica et Biophysica Acta (BBA) - Gene Regulatory Mechanisms*, vol. 1819, no. 1, pp. 28–37, 2012.
- [46] D. Li, P. Wei, Z. Peng et al., “The critical role of dysregulated FOXO1-PLAUR signaling in human colon cancer progression and metastasis,” *Clinical Cancer Research*, vol. 19, no. 1, pp. 62–72, 2013.
- [47] E. Favaro, K. Bensaad, M. G. Chong et al., “Glucose utilization via glycogen phosphorylase sustains proliferation and prevents premature senescence in cancer cells,” *Cell Metabolism*, vol. 16, no. 6, pp. 751–764, 2012.
- [48] W. Guo, S. Zhang, Y. Chen et al., “An important role of the hepcidin-ferroportin signaling in affecting tumor growth and metastasis,” *Acta Biochimica et Biophysica Sinica*, vol. 47, no. 9, pp. 703–715, 2015.
- [49] W. D. Bao, Y. Fan, Y. Z. Deng et al., “Iron overload in hereditary tyrosinemia type 1 induces liver injury through the Sp1/Tfr2/hepcidin axis,” *Journal of Hepatology*, vol. 65, no. 1, pp. 137–145, 2016.
- [50] Z. Bing, Z. Cheng, D. Shi et al., “Investigate the mechanisms of Chinese medicine Fuzhengkangai towards EGFR mutation-positive lung adenocarcinomas by network pharmacology,” *BMC Complementary and Alternative Medicine*, vol. 18, no. 1, p. 293, 2018.
- [51] X. Li, B. Li, B. Li et al., “ITIH4: effective serum marker, early warning and diagnosis, hepatocellular carcinoma,” *Pathology & Oncology Research*, vol. 24, no. 3, pp. 663–670, 2018.
- [52] M. Venerito, D. Kuester, C. Harms, D. Schubert, T. Wex, and P. Malfertheiner, “Upregulation of leukotriene receptors in gastric cancer,” *Cancers*, vol. 3, no. 3, pp. 3156–3168, 2011.
- [53] M. Venerito, C. Helmke, D. Jechorek et al., “Leukotriene receptor expression in esophageal squamous cell cancer and non-transformed esophageal epithelium: a matched case control study,” *BMC Gastroenterology*, vol. 16, no. 1, p. 85, 2016.
- [54] M. Polette, C. Clavel, D. Muller, J. Abecassis, I. Binniger, and P. Birembaut, “Detection of mRNAs encoding collagenase I and stromelysin 2 in carcinomas of the head and neck by in situ hybridization,” *Invasion & Metastasis*, vol. 11, no. 2, pp. 76–83, 1991.
- [55] D. C. Radisky, D. D. Levy, L. E. Littlepage et al., “Rac1b and reactive oxygen species mediate MMP-3-induced EMT and genomic instability,” *Nature*, vol. 436, no. 7047, pp. 123–127, 2005.
- [56] A. A. van Tilborg, F. C. Sweep, A. J. Geurts-Moespot et al., “Plasminogen activators are involved in angiostatin generation in vivo in benign and malignant ovarian tumor cyst fluids,” *International Journal of Oncology*, vol. 44, no. 4, pp. 1394–1400, 2014.
- [57] S. Zhao, J. Dorn, R. Napieralski et al., “Plasmin(ogen) serves as a favorable biomarker for prediction of survival in advanced high-grade serous ovarian cancer,” *Biological Chemistry*, vol. 398, no. 7, pp. 765–773, 2017.
- [58] H. Mochizuki, T. Seki, N. Adachi, N. Saito, H. K. Mishima, and N. Sakai, “R659S mutation of gammaPKC is susceptible to cell death: implication of this mutation/polymorphism in the pathogenesis of retinitis pigmentosa,” *Neurochemistry International*, vol. 49, no. 7, pp. 669–675, 2006.
- [59] H. Lu, L. Zhu, L. Lian, M. Chen, D. Shi, and K. Wang, “Genetic variations in the PRKCG gene and osteosarcoma risk in a

- Chinese population: a case-control study," *Tumour Biology*, vol. 36, no. 7, pp. 5241–5247, 2015.
- [60] T. Yamada, "Serum amyloid A (SAA): a concise review of biology, assay methods and clinical usefulness," *Clinical Chemistry and Laboratory Medicine*, vol. 37, no. 4, pp. 381–388, 1999.
- [61] K. J. Strissel, M. T. Girard, J. A. West-Mays et al., "Role of serum amyloid A as an intermediate in the IL-1 and PMA-stimulated signaling pathways regulating expression of rabbit fibroblast collagenase," *Experimental Cell Research*, vol. 237, no. 2, pp. 275–287, 1997.
- [62] V. S. Schellerer, L. Mueller-Bergh, S. Merkel et al., "The clinical value of von Willebrand factor in colorectal carcinomas," *American Journal of Translational Research*, vol. 3, no. 5, pp. 445–453, 2011.
- [63] B. Aryal, M. Yamakuchi, T. Shimizu et al., "Bivalent property of intra-platelet VWF in liver regeneration and HCC recurrence: a prospective multicenter study," *Cancer Biomarkers*, vol. 26, no. 1, pp. 51–61, 2019.
- [64] J. Murray, C. E. Oquendo, J. H. Willis, M. F. Marusich, and R. A. Capaldi, "Monitoring oxidative and nitrative modification of cellular proteins; a paradigm for identifying key disease related markers of oxidative stress," *Advanced Drug Delivery Reviews*, vol. 60, no. 13-14, pp. 1497–1503, 2008.
- [65] R. Catera, G. J. Silverman, K. Hatzi et al., "Chronic lymphocytic leukemia cells recognize conserved epitopes associated with apoptosis and oxidation," *Molecular Medicine*, vol. 14, no. 11-12, pp. 665–674, 2008.
- [66] S. D. Brown, R. L. Warren, E. A. Gibb et al., "Neo-antigens predicted by tumor genome meta-analysis correlate with increased patient survival," *Genome Research*, vol. 24, no. 5, pp. 743–750, 2014.
- [67] M. Chevion, E. Berenshtein, and E. R. Stadtman, "Human studies related to protein oxidation: protein carbonyl content as a marker of damage," *Free Radical Research*, vol. 33, pp. S99–S108, 2000.

Research Article

Exploring the Role and Mechanism of pAMPK α -Mediated Dysregulation of Brf1 and RNA Pol III Genes

Teng Wu,¹ Dongkun Zhang,² Mingen Lin,^{3,4} Lihong Yu,¹ Ting Dai,¹ Shuai Li,¹ Fenghai Yu,¹ Lei Lu ^{1,4} Liling Zheng ⁵ and Shuping Zhong ⁴

¹GMU-GIBH Joint School of Life Sciences, Guangzhou Medical University, Guangzhou, China

²Department of Thoracic Surgery, Guangdong Provincial People's Hospital, Guangdong Academy of Medical Sciences, Guangzhou, China

³The First Affiliated Hospital of Shantou University Medical College, China

⁴Keck School of Medicine, University of Southern California, Los Angeles, CA, USA

⁵First Hospital of Quanzhou Affiliated to Fujian Medical University, China

Correspondence should be addressed to Lei Lu; llei1226@aliyun.com, Liling Zheng; zll111111@hotmail.com, and Shuping Zhong; szhong@usc.edu

Received 21 January 2021; Revised 30 March 2021; Accepted 5 April 2021; Published 21 April 2021

Academic Editor: Jayeeta Ghose

Copyright © 2021 Teng Wu et al. This is an open access article distributed under the Creative Commons Attribution License, which permits unrestricted use, distribution, and reproduction in any medium, provided the original work is properly cited.

TF IIB-related factor 1 (Brf1) is a key transcription factor of RNA polymerase III (Pol III) genes. Our early studies have demonstrated that Brf1 and Pol III genes are epigenetically modulated by histone H3 phosphorylation. Here, we have further investigated the relationship of the abnormal expression of Brf1 with a high level of phosphorylated AMPK α (pAMPK α) and explored the role and molecular mechanism of pAMPK α -mediated dysregulation of Brf1 and Pol III genes in lung cancer. Brf1 is significantly overexpressed in lung cancer cases. The cases with high Brf1 expression display short overall survival times. Elevation of Brf1 expression is accompanied by a high level of pAMPK α . Brf1 and pAMPK α colocalize in nuclei. Further analysis indicates that the carcinogen MNNG induces pAMPK α to upregulate Brf1 expression, resulting in the enhancement of Pol III transcription. In contrast, inhibiting pAMPK α decreases cellular levels of Brf1, resulting in the reduction of Pol III gene transcription to attenuate the rates of cell proliferation and colony formation of lung cancer cells. These outcomes demonstrate that high Brf1 expression reveals a worse prognosis in lung cancer patients. pAMPK α -mediated dysregulation of Brf1 and Pol III genes plays important roles in cell proliferation, colony formation, and tumor development of lung cancer. Brf1 may be a biomarker for establishing the prognosis of lung cancer. It is a new mechanism that pAMPK α mediates dysregulation of Brf1 and Pol III genes to promote lung cancer development.

1. Introduction

Lung cancer is a common malignant tumor. In recent years, the incidence of lung cancer in China has increased [1, 2]. It is a malignant tumor with the highest morbidity and mortality in the country. Based on cytological and histological characterization, lung cancer is divided into small-cell lung cancer (SCLC) and non-small-cell lung cancer (NSCLC). SCLC and NSCLC account for 15% and 80-85% of cases, respectively [3, 4]. SCLC is a heterogeneous neoplastic disease characterized by aggressiveness, rapid growth of cancer cells, and easy metastases [5], while NSCLC is a kind of

epithelial malignant disease apart from SCLC. NSCLC is not sensitive to chemotherapy, which is mainly performed by surgical resection with curative intent. The causes of lung cancer are complex, such as environmental pollution and genetic and epigenetic changes. The exact mechanism of lung cancer is not fully understood. Lung carcinogenesis involves multiple mechanisms: oncogene activation, such as K-Ras [6]; inactivation of tumor suppressor genes (LKB1) [7]; epidermal growth factor receptor (EGFR) mutation and amplification [8]; inhibition of immune system activity [9, 10]; and epigenetic alterations (DNA methylation, histone tail modifications, and small RNAs) [11]. To date, no studies

elucidate the roles of dysregulation of TF IIB-related factor 1 (Brf1) and its target genes, RNA polymerase III-dependent genes (Pol III genes) in lung cancer development, whereas dysregulation of Brf1 and Pol III genes is tightly related to tumor development.

Brf1 is a key transcription factor of tRNAs and 5S rRNA, which are Pol III genes. Brf1 specifically modulates the transcription of these genes [12–15]. Dysregulation of tRNAs and 5S rRNA genes is directly linked to cell transformation and tumorigenesis [16–18], and it also helps to enhance the cellular ability of protein synthesis for cell growth, proliferation and transformation, and tumor development. Increasing Brf1 expression elevates the activities of tRNA and 5S rRNA genes. In contrast, repressing Brf1 decreases the activity of these genes and inhibits cell proliferation and tumor development [17, 18]. Recent studies of ours and others indicate that Brf1 overexpression is founded in hepatocyte carcinoma (HCC), breast cancer, gastric carcinoma, and prostate cancer [19–22]. This shows that Brf1 plays an important role in human cancer development and tumor growth. However, it remains to be detected if Brf1 expression is increased in human cases of lung cancer and what is the significance of its expressional status in the diagnosis and prognosis of this disease.

5' AMP-activated protein kinase or 5' adenosine monophosphate-activated protein kinase (AMPK) is an enzyme. AMPK is composed of three subunits (α , β , and γ) to form a heterotrimeric protein complex, and these subunits play critical roles in its activity and stability [23]. AMPK increases glucose uptake and inhibits the synthesis of fatty acids, cholesterol, and triglycerides and promotes fatty acid uptake and β -oxidation [24]. It indicates that AMPK plays critical roles in the regulation of energy metabolism. AMPK is activated in low-energy cellular states by phosphorylating its subunits [25]. AMPK is a primary component of the LKB1 downstream pathway, while mutations of LKB1 are found in over 20% of patients with NSCLC and frequently associated with activating K-RAS mutations [26–28]. Tumor suppressor LKB1 mediates AMPK activity. As enhancements of Brf1 and Pol III gene activities are tightly related to human cancers, this suggests that AMPK activation may involve the modulation of Brf1 and Pol III gene transcription to increase cell proliferation and promote tumor development.

Our earlier studies have demonstrated that alcohol increases Brf1 expression in tissue culture and animal models, which facilitates cell proliferation and transformation, and tumor formation [15, 17, 19, 20, 29–32]. Chronic alcohol consumption results in the production of acetaldehyde and CYP2E1 induction (Cytochrome P450 2E1) [14]. Acetaldehyde is a by-product of alcohol metabolism catalyzed by ADH (alcohol dehydrogenase), which has direct mutagenic and carcinogenic effects *in vitro* and *in vivo* [14, 33]. CYP2E1 is associated with the release of ROS (reactive oxygen species) and conversion of procarcinogens to carcinogens [14]. Alcohol exposure increases cellular production of ROS, causing cellular stress to result in tissue injury and diseases [14]. ROS-induced oxidative stress activates the JNK1 pathway to increase Brf1 expression [31]. A recent study also indicates that levels of ROS of lung cancer cells are associated

with the alteration of pAMPK α [34], while AMPK activation is associated with protein synthesis [24, 25], which is controlled by Brf1 and Pol III genes. This implies that ROS and AMPK are potentially involved in Brf1 expression, which may be associated with lung cancer.

Here, we report, for the first time, that Brf1 expression is enhanced in human cases of lung cancer. High expression of Brf1 reveals short survival times ($p = 0.0013$). Activation of AMPK increases Brf1 promoter activity to upregulate Brf1 expression, resulting in elevation of tRNAs and 5S rRNA transcription. Repression of AMPK decreases cellular levels of Brf1, tRNAs, and 5S rRNA expression, leading to reducing the rates of cell proliferation and colony formation. Brf1 and pAMPK α are colocalized in lung cancer cell nuclei, which maybe synergistically regulate the transcription of Pol III genes. The study identifies a new pathway, pAMPK α , which modulates Brf1, tRNAs, and 5S rRNA transcription in lung cancer cells. This shows that both Brf1 and pAMPK α play an important role in lung cancer.

2. Materials and Methods

2.1. Human Tissue Samples. The 226 samples of paraffin-embedded, archived lung cancer tissue samples used in this study were histopathologically and clinically diagnosed at the Guangdong Provincial People's Hospital and Guangdong Academy of Medical Sciences and Shanghai Outdo Biotech Ltd after obtaining written informed consent and in accordance with the Institutional Review Board and the Declaration of Helsinki. No patient received any chemoradiotherapy prior to surgery [35]. The patients were followed up regularly after the operation at three-month intervals [35]. Eight freshly collected lung cancer tissues and matched adjacent nontumoral lung tissues were frozen and stored in liquid nitrogen until required for protein extraction [35]. Informed consent was obtained from each patient, and the study was approved by the Institute Research Ethics Committee of Guangdong General Hospital, Guangdong Academy of Medical Sciences (ID number: No. GDREC2016175H(R2)).

2.2. Cell Lines and Reagents. The lung cancer cell lines A549 and H1975, and normal human bronchial epithelial cell line 16HBE were purchased from the American Type Culture Collection (Manassas, VA) and cultured in RPMI 1640 containing 10% FBS, 100 IU/mL penicillin, and 100 μ g/mL streptomycin (HyClone, Utah, USA). All cells were tested for negative mycoplasma contamination and authenticated based on short tandem repeat fingerprinting before use. AMPK inhibitor, S7306 (Dorsomorphin (Compound C) 2HCl, Cat No. S7306), was purchased from Selleck and dissolved in sterile water. N-Methyl-N'-nitro-N-nitrosoguanidine (MNNG) was purchased from Accu. Standard, Inc (Cat No. R-081N) and dissolved in DMSO. Brf1 antibody was from Bethyl Laboratories Inc (Cat No. A301-228A). The MTT assay kit was from Boster Biotech (Cat No. AR1156).

2.3. Immunohistochemistry. We performed immunohistochemical staining with Brf1 antibody (1 : 200). Its details were described in our previous study [20, 30].

The levels of Brf1 immunostaining were evaluated independently by two pathologists who were blinded to the survival outcomes of the participants based on the proportion of positively stained tumor cells (stain area) and the intensity of staining [20]. The immunostaining results were performed by multiplying the staining intensity by the stained area (staining index (SI)) as previously described [30, 36, 37]. The Brf1 expression levels in lung cancer lesions were determined by the SI, which was 0, 1, 2, 3, 4, 6, 9, or 12. An optimal cutoff value was identified as follows: an SI score of ≥ 6 was used to define tumors as high Brf1 expression, and an SI score of ≤ 4 as low [30, 36, 37].

2.4. Immunoblot Analysis. Tissue samples of lung cancer were ground into powder with liquid nitrogen and lysed in lysis buffer with phosphatase and protease inhibitors [20]. Lung cancer cells were treated with $4\mu\text{M}$ MNNG or $10\mu\text{M}$ AMPK inhibitor, S7306, to extract total cell lysates, and the protein concentrations were measured using the BCA Protein Assay (Thermo Fisher Scientific, Cat No. 23225) [35]. Equal amounts of cell protein were subjected to electrophoresis in SDS-PAGE gels and then transferred to PVDF membranes (Millipore) for antibody blotting [35]. Bound primary antibody was visualized using horseradish peroxidase-conjugated secondary antibodies (Proteintech, Cat No. SA00001-1 or SA00001-2) and enhanced chemiluminescence reagents (Beyotime, Cat No. P0018S). Antibodies used in our study were as follows: Brf1 (1 : 2000), pAMPK α (CST, Cat No. 2535S, 1 : 1000), AMPK α (CST, Cat No. 2793S, 1 : 1000), and β -actin (Proteintech, Cat No. 20536-1-AP, 1 : 5000). All of the experiments were repeated at least three times [20].

2.5. Quantitative Real-Time PCR. Total RNAs were isolated with TRIzol (Invitrogen, Cat No. 15596026) following the manufacturer's protocol. Then, reverse transcription was performed (Takara, Cat No. RR036A). Target mRNA levels were determined by performing RT-qPCR with a TB Green[®] Premix Ex Taq[™] II (Tli RNaseH Plus) kit (Takara, Cat No. RR820A). GAPDH expression was used for normalization. The sequences of the primers were described previously [17, 18].

2.6. Immunofluorescence. For colocation detection, the lung cancer cells were fixed for 30 min in 4% formaldehyde/PBS, washed with 0.2% Triton-X 100/PBS [37]. The cell slices were blocked with 1% BSA/PBS for 1 h at room temperature and were incubated with Brf1 antibodies (1 : 200) overnight at 4°C and then incubated with anti-rabbit IgG (Proteintech, Cat No. SA00013-4, 1 : 200) for 1 h as secondary antibodies. The cell slices were immersed in 1x PBS and heated in a microwave oven at 42°C for 3 min to remove nonspecific bindings. Subsequently, pAMPK α antibodies (1 : 200) were incubated overnight at 4°C and then incubated with anti-rabbit IgG (Proteintech, Cat No. SA00013-2, 1 : 200) for 1 h as secondary antibodies [20].

Cell nuclei were counterstained with $2\mu\text{g}/\text{mL}$ DAPI (Biofroxx, Cat No. 1155MG010) for 5 min, and the slides were mounted in an antifade reagent (Life Technologies, Cat No. P36934). The cells were visualized under a fluorescence microscope (ZEISS, Germany) [30, 37].

2.7. siRNA Transfection and Brf1-Luc Reporter Assays. For siRNA knockdown, Brf1 siRNAs, AMPK α siRNA, and a control siRNA (mismatch RNA: mmRNA) were purchased from RiboBio. The sequences of primers and siRNAs used were as previously described [17, 18]. Transfections were performed using Lipofectamine 3000 and OPTI-MEM reagent (Life Technologies, Cat No. L3000015 and 11058021) when cells were approximately 40% confluent and transfected according to the manufacturer's instruction [37]. For Brf1-Luc promoter activity, cells were transfected with $0.5\mu\text{g}$ of the Brf1-Luc report constructs for 48 h. Cells were starved in FBS-free RPMI 1640 for 4 h and treated with different concentrations of MNNG for another 2 h. Cell pellets were dissolved in Promega reporter lysis buffer. The luciferase activities of these lysates were determined by a luminometer and the Promega Luciferase Kit (Promega, Cat No. E1910). The luciferase activities of the lysates were normalized to their protein amounts as described [31, 32]. The changes in luciferase activity were compared to the luciferase activity in the absence of MNNG. Means \pm SE is at least three independent experiments.

2.8. Colony Formation Assay. A549 cells were transfected with mismatch RNA (mmRNA), Brf1 siRNAs, and AMPK α siRNAs as described [31]. The transfected A549 cells (1×10^4 cells/well in 6-well plates) were mixed with equal volumes of 0.7% soft agar dissolved in RPMI 1640 (10% FBS) with or without $4\mu\text{M}$ MNNG and layered in triplicate onto 0.7% (RPMI 1640, 10% FBS) solidified agar. Cells were fed fresh complete media with MNNG twice weekly. Colonies were counted 2–3 weeks or longer after under a microscope and photographed as described previously [38].

2.9. Statistical Analyses. We carried out statistical analysis with Student's *t*-test, ANOVA and Tukey's multiple comparisons test, Kaplan-Meier and log-rank test, ROC curve, and Cox analysis. The details of the statistical analysis were described previously [37].

3. Results

3.1. Brf1 Expression in Lung Cancer Tissues and Its Significance. Brf1 plays an increasingly important role in human cancers. Emerging evidence indicates that Brf1 expression is elevated in the cases of human liver, breast, gastric, and prostate cancers [19–22]. To test Brf1 expression in the cases of lung cancer, we utilized the samples of this disease to determine the levels of Brf1 expression in tumor foci and paracarcinoma tissues by immunohistochemistry (IHC) staining. The result indicates that a strong signal of Brf1 was detected in tumor foci tissue (Figure 1(a), left panel), while a very weak reaction of Brf1 with its antibody was observed in paracarcinoma tissue (Figure 1(a), right panel). The overall reaction of Brf1

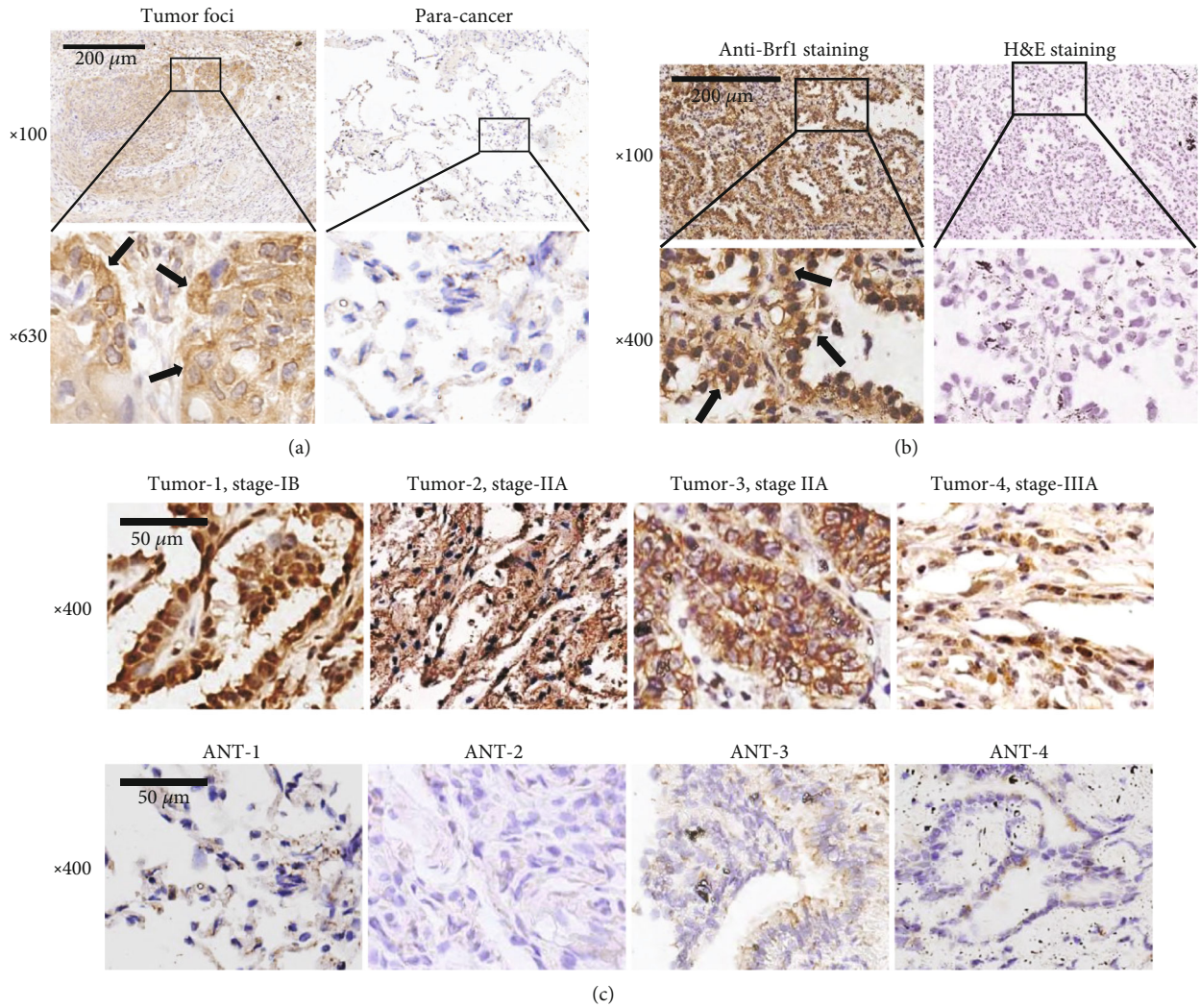


FIGURE 1: Immunohistochemical staining of Brf1 in lung cancer. (a) Comparison of Brf1 staining in tumor foci tissue with paracancer tissue (para-can) of lung cancer patients. Strong staining signals of Brf1 expression are seen in tumor foci of lung cancer (a, left panel). Weak signals of Brf1 staining are detected in para-can tissue of this disease (a, right panel). Top panel: 100x magnification (scale bar = 200 μm); bottom panel: 630x magnification. (b) Comparison of Brf1 IHC and H&E staining in the same cases of lung cancer. IHC staining about the signals of Brf1 expression in both cytoplasm and nuclei of tumor tissues of lung cancer; (b, left panel) H&E staining of tumor tissues of lung cancer; (b, right panel) 100x magnification (scale bar = 200 μm); 400x magnification. (c) Comparison of Brf1 expression in tumor foci with adjacent noncancerous tissue (ANT). The levels of Brf1 expression were detected in four lung cancer lesions (c, upper panel) and their paired ANT (c, lower panel). 400x magnification (scale bar = 50 μm). The results indicate that Brf1 expression was increased in the tumor tissues at different stages of lung cancer, compared to noncancerous tissues, ANT.

staining in tumor foci of lung cancer is markedly higher than that in paracarcinoma tissue (Figure 1(a)). Figure 1(b) reveals the results of Brf1 staining (Figure 1(b), left panel) and H&E staining (Figure 1(b), right panel). There are strong signals of Brf1 in the cytoplasm and nuclei of the tumor tissues of lung cancer (Figure 1(c), upper panel), whereas there are very weak or no signal of Brf1 expression in the corresponding adjacent noncancerous tissues (ANT) (Figure 1(c), lower panel). Results indicate that Brf1 expression in both early and advanced stages of lung cancer reveals strong signals in tumor tissues (Figure 1(c), upper panel). To further detect the relationship between Brf1 overexpression and clinical grades of lung cancer, we analyzed Brf1 expression in different stages of this disease. The paired analysis of Brf1 expres-

sion in tumor and normal tissues of lung cancer indicates that the levels of Brf1 expression in different clinical stage tumor tissues are significantly higher than that of normal tissues (Figure 2(a)). This implies that once tumorigenesis happens in the lung tissue, Brf1 expression will be significantly increased.

Furthermore, we determined the relationship between Brf1 expression and the overall survival period of lung cancer patients. The clinical information for the patients does not reveal any significant correlation of Brf1 expression with age, sex, and classification (Figure 2(c), Tables 1 and 2). We used four levels of intensity of Brf1 expression: negative staining, weak staining, moderate staining, and strong staining in these cases of lung cancer (Figures S1A and S1B). The

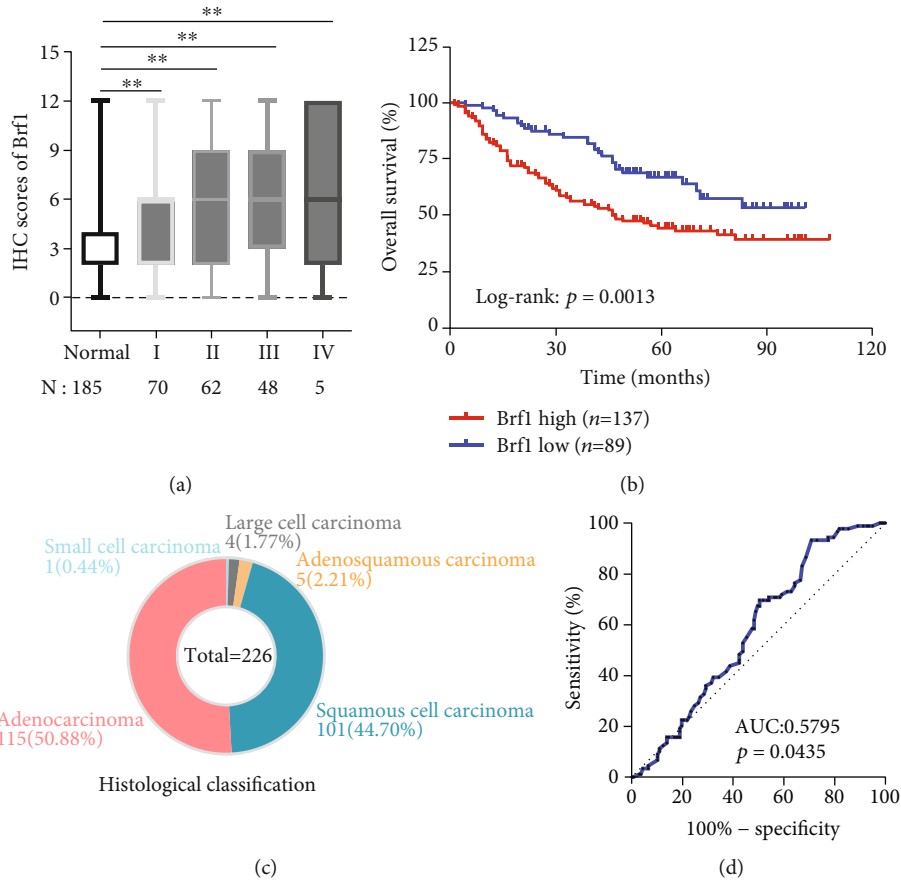


FIGURE 2: High Brf1 expression correlated with a poor prognosis of lung cancer. (a) The IHC staining scores of Brf1 expression. 185 cases in paired different clinical stages of lung cancer tumor tissues show high Brf1 expression, compared to low expression of Brf1 expression corresponding to normal tissues of these cases ($N = 185$). (b) 226 cases of human lung cancer patients were performed for Kaplan-Meier analysis of the overall survival period. Lung cancer patients ($N = 226$) with low versus high expression of Brf1 (Kaplan-Meier analysis with the log-rank test, $p < 0.01$). (c) Histological classification of the 226 cases of lung cancer. (d) ROC curve analysis. The result reveals that patients with high Brf1 expression display short survival times.

TABLE 1: Correlation between Brf1 expression and clinicopathological features in 226 primary lung cancers.

Parameters	Low Brf1 expression $N = 89$ (39.4%)	High Brf1 expression $N = 137$ (60.6%)	Chi-squared test p value	Fisher's exact test p value
Age				
<48	7 (7.9%)	6 (4.4%)		
≥ 48	82 (92.1%)	131 (95.6%)	0.272	0.381
Gender				
Male	53 (59.6%)	114 (83.2%)		
Female	36 (40.4%)	23 (16.8%)	0.000	0.000
Differentiation status				
Well/moderate	53 (59.6%)	77 (56.2%)		
Poor and others	36 (40.4%)	60 (43.8%)	0.619	0.680
Lymph node invasion (N stage)				
Absent	72 (80.9%)	91 (66.4%)		
Present	17 (19.1%)	46 (33.6%)	0.018	0.022
Clinical stage				
I, II	27 (30.3%)	75 (54.7%)		
III, IV	62 (69.7%)	62 (45.3%)	0.000	0.000

* p values determined by using SPSS 20.0. All statistical tests were two-sided.

TABLE 2: Effect of factors on overall survival in lung cancer patients in the univariate and multivariate Cox regression model.

Factors	Univariate*		Multivariate**†‡	
	HR (95% CI)	<i>p</i>	HR (95% CI)*	<i>p</i>
Age (<48/≥48)	2.69 (0.85-8.49)	0.091	—	—
Gender (male/female)	1.34 (0.85-2.12)	0.206	—	—
Differentiation (poor/well, moderate)	1.12 (0.76-1.65)	0.563	—	—
Lymph node invasion (present/absent)	0.49 (0.33-0.71)	0.000	—	—
Clinical stage (III-IV/I-II)	2.85 (1.92-4.22)	0.000	2.71 (1.82-4.02)	0.000
Brf1 (high/low)	0.55 (0.36-0.84)	0.006	0.60 (0.39-0.93)	0.021

*Hazard ratios and *p* values were obtained from Cox proportional hazards regression. All statistical tests were two-sided. †For the multivariate model, HR and *p* values were shown for the final set of stepwise selected variables only. ‡The parameters with *p* value less than 0.05 in the univariate were included in the multivariate Cox analysis using SPSS 20.0.

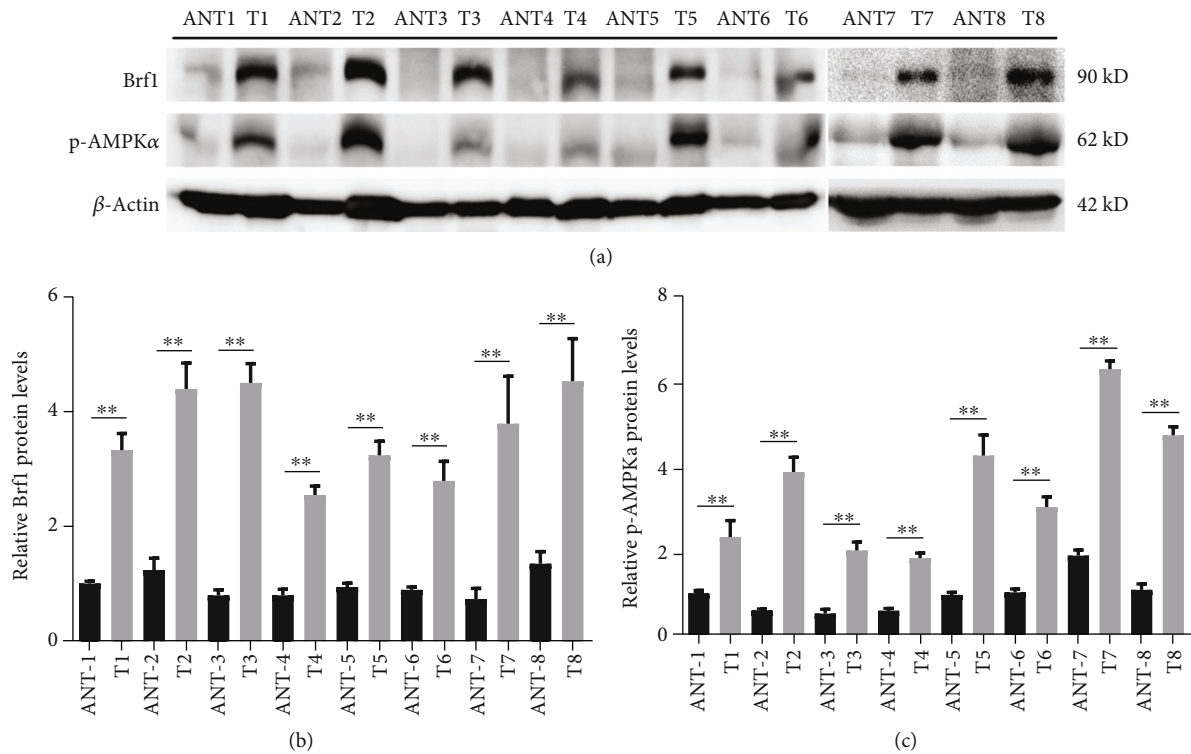


FIGURE 3: The relationship of AMPKα activation with Brf1 high expression in lung cancers. (a) Immunoblotting analysis of Brf1 and pAMPKα in 8 paired lung cancer tissues (T1: adenocarcinoma IIIB stage; T2: squamous cell carcinoma IIB stage; T3: adenocarcinoma IIA stage; T4: adenocarcinoma IA3 stage; T5: squamous cell carcinoma IIA stage; T6: adenocarcinoma IA1 stage; T7: adenocarcinoma IA3 stage; T8: adenocarcinoma IIIA stage). (b, c) The quantification of cellular levels of Brf1 (b) and pAMPKα (c) in the indicated lung cancer tissues was calculated and compared with the corresponding ANT. *p* values were determined by a two-tailed *t*-test. Data are presented as the mean ± SD of at least three independent experiments. **p* < 0.05, ***p* < 0.01.

strong staining of Brf1 in lesion tissues with staining index (SI) ≥ 6 was classified as high expression of Brf1. The result shows that about 60% of cases of lung cancer with high Brf1 expression display significant short overall survival times (Figure 2(b)). In addition, we also performed the ROC (receiver operator characteristic) curve analysis. The AUC result indicates that the accuracy of high Brf1 expression is a little low as a diagnostic biomarker for lung cancer (Figure 2(d)). Together, these studies indicate that Brf1 is overexpressed in lung cancer patients, and as a result, high expression of Brf1 reveals a worse prognosis. Brf1 may be a biomarker for the prognosis of the disease.

3.2. The Relationship between AMPK Activation and Brf1 Expression in Lung Cancer. The tumor suppressor gene, LKB1, is an upstream component and regulator of AMPK activation, but it is the most frequently mutated gene in lung cancer [26–28]. This suggests that mutant LKB1 loses its tumor suppressor function, leading to lung cancer development. Activated AMPK may be detected by its phosphorylation antibody in lung cancer samples, while the activated AMPK may mediate Brf1 expression and Pol III gene transcription. To test this hypothesis, we collected samples of human lung cancer to detect the levels of Brf1 proteins and phosphorylated AMPKα (pAMPKα) by immunoblot

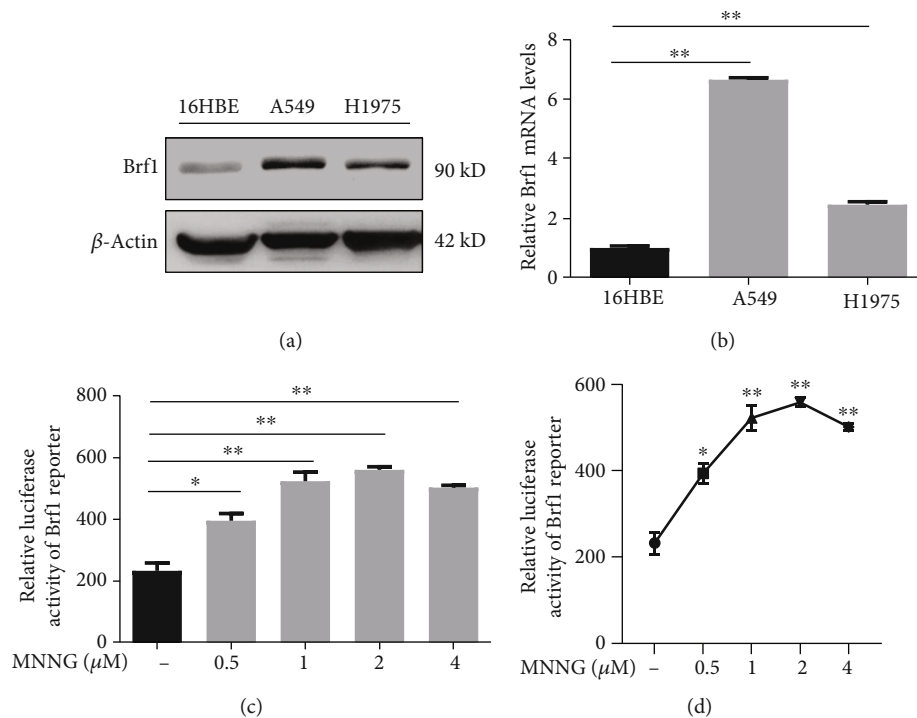


FIGURE 4: Brf1 expression in the cell lines of lung cancer and Brf1 promoter activity. (a) Immunoblotting analysis of Brf1 protein levels in the normal human bronchial epithelial cell line (16HBE) and lung cancer cell lines (A549 and H1975). (a) Is a representative result of immunoblotting. (b) RT-qPCR analysis of Brf1 mRNA levels in lung cancer cell lines (A549 and H1975) and nontumor line, 16HBE. (c, d) Brf1 promoter-luciferase activity. The A549 cells were transfected with 0.5 μ g Brf1-Luc plasmids. Luciferase assay indicates that the carcinogen MNNG increases the activity of the Brf1 promoter. All error bars represent the SD of at least three independent experiments. p values were determined by a two-tailed t -test. * $p < 0.05$, ** $p < 0.01$.

analysis and explore the correlation of the levels of pAMPK α with Brf1 expression. The results indicate that Brf1 expression is significantly increased in tumor tissues of lung cancer, compared to adjacent noncancerous tissue (ANT) samples in the same case (Figure 3(a)). Interestingly, pAMPK α levels in the tumor tissues are also much higher than those in corresponding ANT samples (Figure 3(a)). The quantitation of the immunoblot results of these samples indicates that the cellular levels of Brf1 (Figure 3(b)) and pAMPK α (Figure 3(c)) in tumor tissues are significantly higher than those in corresponding ANT samples. In addition, we also determined the cellular levels of Brf1 in the bronchial epithelial cells and lung cancer cell lines of humans. The immunoblot analysis reveals that the cellular levels of Brf1 in lung cancer cell lines, A549 and H1975, are higher than those in no lesion bronchial epithelial cell line, 16HBE (Figure 4(a)). We also determined the levels of Brf1 mRNA in the cell lines by RT-qPCR. The results indicate that the levels of Brf1 mRNA in A549 and H1975 cell lines are dramatically higher than those in bronchial epithelial cells (Figure 4(b)). High Brf1 expression is consistent with pAMPK α elevation in tumor tissues of lung cancer. We established the Brf1 promoter-luciferase reporter construct to test whether AMPK mediates Brf1 promoter activity. Figures 4(c) and 4(d) indicate that MNNG increases Brf1 transcription.

3.3. pAMPK α Mediates Brf1 Expression Resulting in the Enhancement of Pol III Gene Transcription. Given Brf1 expression with high levels of pAMPK α in the cases of human lung cancer (Figure 3), we further determine whether pAMPK α mediates Brf1 expression and Pol III gene transcription. A549 cells were cultured in 10% FBS/RMPI 1640 medium to 80–85% confluence and starved in FBS-free medium for 4 h. The cells were treated with different doses of carcinogen, MNNG. The resultant lysates and RNA were used to detect the protein and mRNA levels of Brf1 and pAMPK α . The results indicate that MNNG markedly induced pAMPK α (Figure 5(a), middle). More interestingly, MNNG also increases the accompanied cellular levels of Brf1 proteins and mRNAs in various MNNG doses in A549 cells (Figures 5(a), top and 5(b)). Since MNNG enhances Brf1 promoter activity in A549 cells (Figures 4(c) and 4(d)), similar results are also observed in the lung cancer cell line, H1975 (Figures S2 and S3C). Thus, we further determined whether MNNG-activated AMPK, pAMPK α , affects the target genes of Brf1. The results show that MNNG increases Pol III gene, tRNA^{Leu}, 5S rRNA, and tRNA^{Tyr} transcription in A549 (Figures 5(c)–5(e)) and H1975 cell lines (Figures S2B and S2C). This points out that pAMPK α really modulates the activities of Brf1 and Pol III genes.

To further confirm the roles of pAMPK α in Brf1 and Pol III gene expression, we pretreated A549 cells with pAMPK α

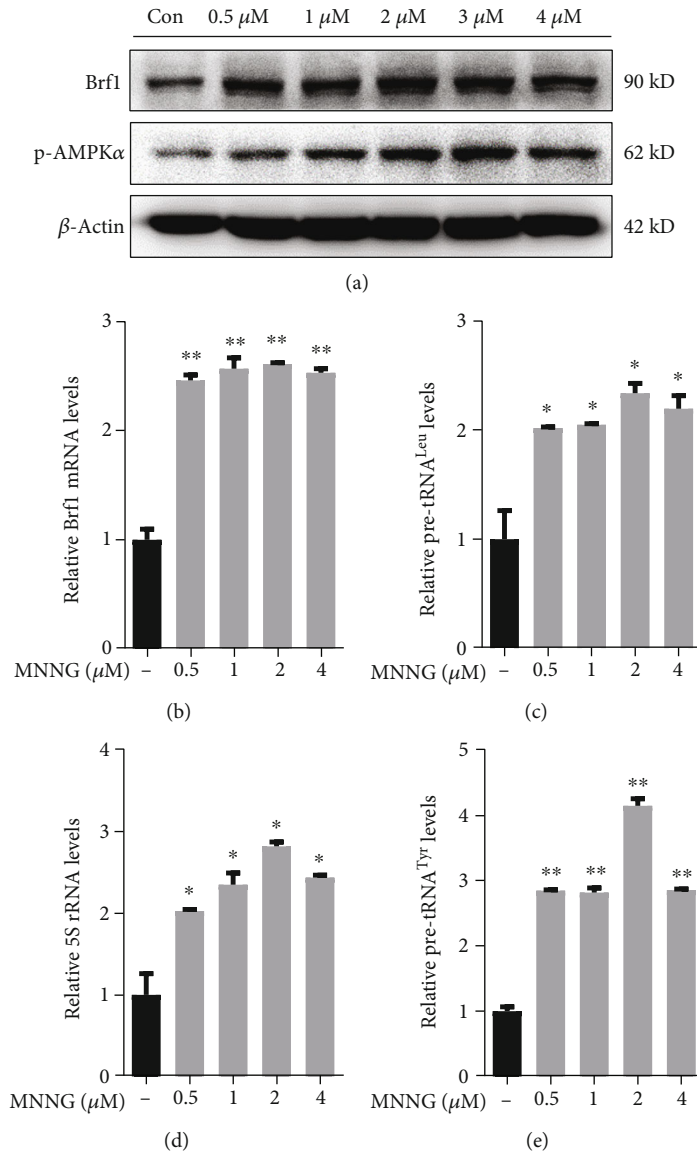


FIGURE 5: MNNG induces Brf1 expression and Pol III gene transcription. A549 cells were treated with different doses of the carcinogen MNNG. The resultant cell lysis and total RNA were extracted from the cells for immunoblotting analysis and RT-qPCR. (a) Immunoblotting analysis of cellular levels of Brf1 and pAMPK α . (b–e) RT-qPCR. Brf1 mRNA (b) and transcription levels of tRNA^{Leu} (c), 5S rRNA (d), and tRNA^{Tyr} (e). The results indicate that MNNG activated pAMPK α and enhanced Brf1 expression and Pol III gene transcription. All error bars represent the SD of at least three independent experiments. p values were determined by a two-tailed t -test. * $p < 0.05$, ** $p < 0.01$.

specific inhibitor, S7306, and then treated the cells with MNNG as indicated in Figures 6(a) and 6(b). The result displays that S7306 specifically decreases the level of MNNG-induced pAMPK α and also reduces the levels of Brf1 protein and mRNA, compared to control cells without the pretreatment by S7306 (Figures 6(a) and 6(b)). This shows that S7306 reduces the activation of AMPK α to result in a decrease in MNNG-induced Brf1 expression. Similar results were also observed in H1975 cells (Figures S3A and S3B). Besides, we transfected A549 cells with Brf1 siRNA to repress its expression. The results reveal that Brf1 siRNA can significantly reduce the cellular levels of Brf1, either protein or mRNA (Figures 6(c) and 6(d)), but not the levels

of pAMPK α and AMPK α (Figure 6(c)). Furthermore, our results reveal that repression of Brf1 expression dramatically inhibits the induction of pre-tRNA^{Leu} (Figure 6(e)) and 5S rRNA (Figure 6(f)) caused by MNNG in A549 cells. Our studies have demonstrated that repressing Brf1 expression decreases Pol III gene transcription (Figures 6(e) and 6(f)) [13, 17–19]. Thinking about the effect of nonspecific inhibition of the chemical inhibitor, S7306, we also utilized a specific inhibitor, AMPK α siRNA. Compared to control RNA (mismatch RNA, mmRNA), AMPK α siRNA markedly reduced the levels of Brf1 protein and mRNAs (Figures 7(a) and 7(b)) and also repressed the transcription of Pol III genes (Figures 7(c)–7(e)). These

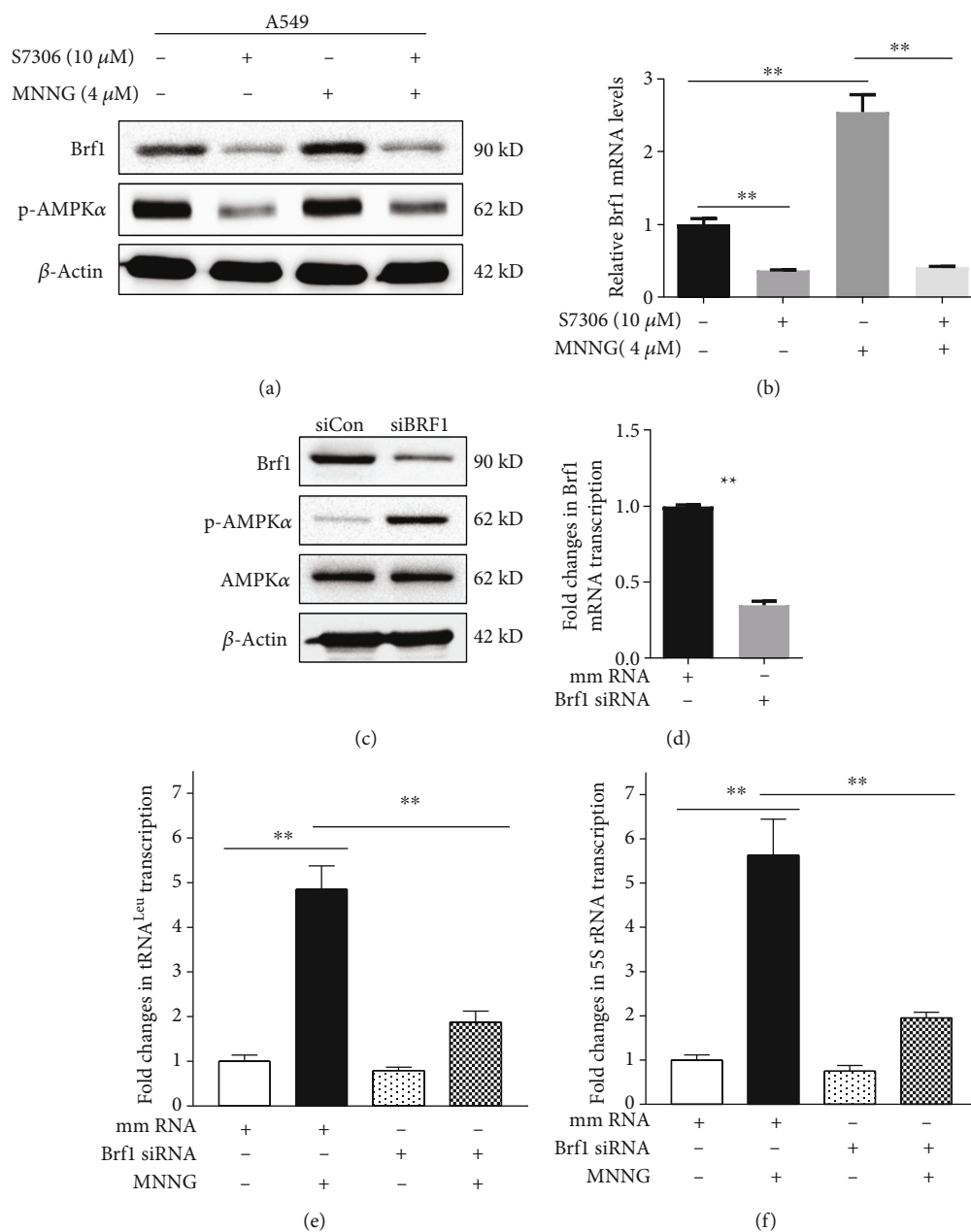


FIGURE 6: The role of Brf1 alteration in transcription of Pol III genes. (a) Immunoblotting analysis of Brf1 and pAMPK α protein levels. A549 cells were treated with AMPK inhibitor, S7306 (12 h with 10 μ M), and MNNG (1 h with 4 μ M). (b) RT-qPCR analysis of Brf1 mRNA levels in A549 cells treated with S7306 (12 h with 10 μ M) and MNNG (1 h with 4 μ M). (c) Immunoblotting analysis of Brf1, pAMPK α , and AMPK α protein levels in MNNG-treated A549 cells after siRNA-mediated knockdown of Brf1, compared to mm siRNA as control (siCon). (d) RT-qPCR analysis of Brf1 mRNA levels in A549 cells which were transfected with mmRNA or Brf1 siRNA to knock down Brf1. (e, f) RT-qPCR analysis. Pol III gene transcription in A549 cells was transfected with Brf1 siRNA or mmRNA for 48 h and then treated with MNNG (4 μ M) for 1 h. All error bars represent the SD of at least three independent experiments. p values were determined by a two-tailed t -test. * $p < 0.05$, ** $p < 0.01$.

results (Figures 6 and 7 and Figure S2–3) support the point that pAMPK α modulates the expression of Brf1 and Pol III gene transcription.

The above results indicate that AMPK α inhibitions (S7306 and AMPK α siRNA) reduce the cellular levels of Brf1, leading to decreases in Pol III gene activities (Figures 6 and 7). Therefore, we further determine the colocalization of Brf1 and pAMPK α in MNNG-treated lung can-

cer cells. Immunofluorescent staining indicates that Brf1 reaction with its specific antibody can be observed in the nuclei and plasma of A549 cells (Figure 8(a), red) and H1975 cells (Figure S4, red), while the pAMPK α signal is only in the nuclei of the cells (Figure 8(b), green; Figure S4, green). The colocalization signals of Brf1 and pAMPK α are seen in the nuclei of the cells (Figure 8, yellow-green and Figure S4). The colocalization of Brf1 and pAMPK α implies

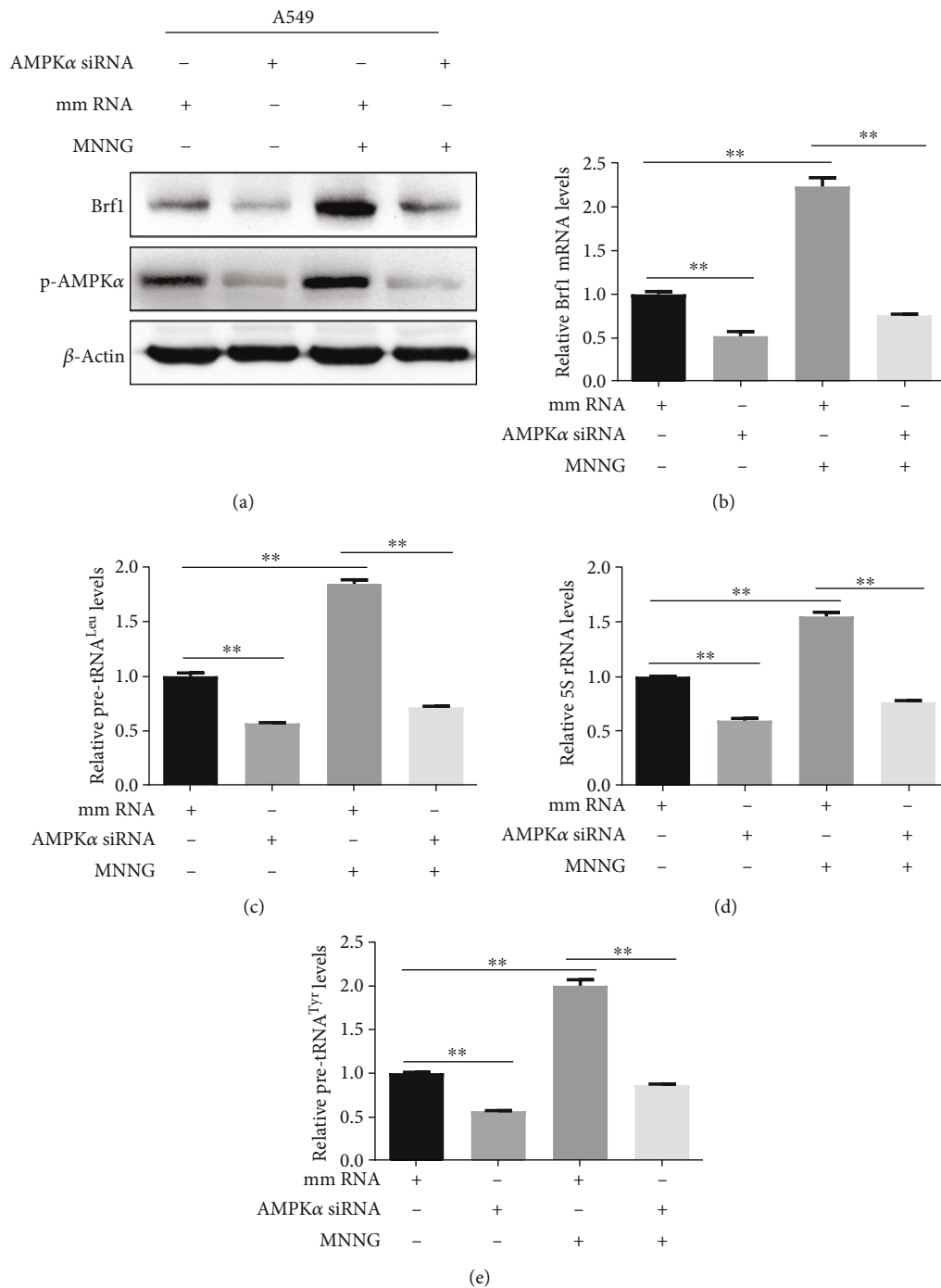


FIGURE 7: Repressing AMPK α expression decreases cellular levels of Brf1 and Pol III genes. (a) Immunoblotting analysis of Brf1 and pAMPK α protein levels in A549 cells were treated with MNNG (1 h with 4 μ M) after siRNA-mediated knockdown of AMPK α . (b) RT-qPCR analysis of Brf1 mRNA levels in A549 cells treated with MNNG (1 h with 4 μ M) after siRNA-mediated knockdown of AMPK α . (c–e) RT-qPCR analysis. A549 cells were transfected with mmRNA or AMPK α siRNA for 48 h and then treated with MNNG (1 h with 4 μ M). The cellular levels of pre-tRNA^{Leu} (c), 5S rRNA (d), and pre-tRNA^{Tyr} (e) transcription were determined by RT-qPCR. All error bars represent the SD of at least three replicates from two independent experiments. p values were determined by a two-tailed t -test. * p < 0.05, ** p < 0.01.

that pAMPK α and Brf1 may synergistically modulate Pol III gene activity [20, 30].

3.4. pAMPK α -Mediated the Alteration of Brf1 Results in Cellular Phenotypic Changes. The studies of ours and others have demonstrated that decreasing the expression of Brf1

and Pol III genes represses cell proliferation, cell transformation, and xenograft tumor growth [13, 17–19]. The above results have shown that activated AMPK α by the carcinogen MNNG increases the activities of Brf1 and Pol III genes (Figures 5–7, Figure S2). In contrast, inhibiting pAMPK α by its specific inhibitor decreases the activities of these

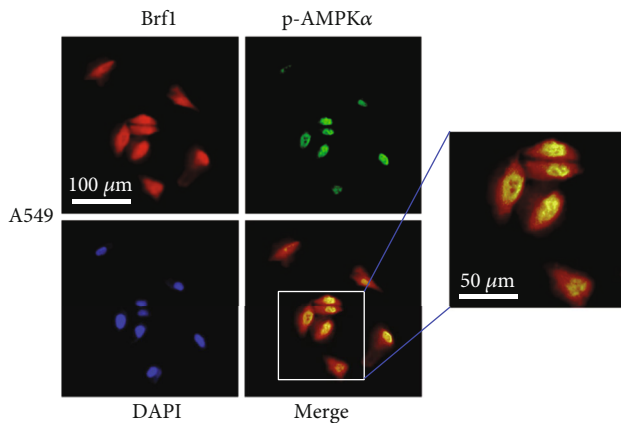


FIGURE 8: Colocalization of Brf1 and pAMPK α in lung cancer cells. Localizations of Brf1 and pAMPK α : Brf1 (red) and pAMPK α (green) and cell nuclei were stained with DAPI (blue) in A549 cells. The signals of Brf1 (red) and pAMPK α (green) were determined by immunofluorescence staining. The merging picture clearly shows that the colocalization signals of Brf1 and pAMPK α are seen in the nuclei of A549 cells (scale bar = 50 μ m).

genes (Figures 6 and 7 and Figure S3). Therefore, we further determine whether inhibiting AMPK α activity causes cellular phenotypic alteration. A549 cells were pretreated with the AMPK α inhibitor S7306 and then treated with MNNG to test the changes in cell phenotypes. The results indicate that inhibiting AMPK α by S7306 represses the proliferation of A549 cells, compared to control cells (Figures 9(a) and 9(b)). A higher dose of the inhibitor displays more inhibition of cell growth by S7306 (Figure 9(a)).

In addition, we also determined whether inhibiting AMPK α reduced the rate of colony formation of A549 cells. The results reveal that MNNG treatment significantly promotes colony formation of the cells, compared to the cells without MNNG treatment (Figure 9(c)), whereas inhibiting AMPK α dramatically decreases the rate of colony formation, which displays a significant difference between with and without S7306 treatment (Figure 9(d)). Moreover, we further transfected A549 cells with Brf1 siRNA and AMPK α siRNA. The results indicate that repression of either Brf1 or AMPK α by their siRNA, the rates of colony formation were significantly attenuated, compared to mm siRNA (Figures 9(e) and 9(f)). These results clearly prove that pAMPK α modulates Brf1 expression and Pol III gene transcription, causing cell phenotypic alteration of lung cancer cells.

4. Discussion

In the present study, we report that Brf1 expression is increased in the cases of human lung cancer. The cases with high Brf1 expression show a short survival period, which means that the prognosis of these cases is worse. Brf1 overexpression in lung cancer cases is accompanied by higher pAMPK α levels. Further analysis indicates that pAMPK α modulates the activities of Brf1 and Pol III genes. MNNG-increased pAMPK α enhances the cellular levels of Brf1 and Pol III gene expression. In contrast, inhibiting AMPK α acti-

vation reduces Brf1 expression, resulting in decreasing Pol III gene transcription. Brf1 and pAMPK α are colocalized in nuclei of lung cancer cells, which suggests that Brf1 and pAMPK α may synergistically modulate the activities of Pol III genes [20, 30]. Moreover, inhibiting AMPK α activity decreases the rates of proliferation and colony formation of lung cancer cells. These studies, for the first time, demonstrate that overexpression of Brf1 and higher levels of pAMPK α are in human lung cancer samples. The activated AMPK α , pAMPK α , upregulates Brf1 expression and Pol III gene transcription to accelerate cell proliferation and colony formation (Figure 10). These studies indicate that pAMPK α and Brf1 play an important role in lung cancer formation.

Brf1 is a key transcription factor. It specifically regulates its target genes, tRNAs and 5S rRNA transcription. Studies have demonstrated that dysregulation of Pol III genes is directly linked to cell transformation and tumorigenesis [16–18]. Upregulation of Pol III genes would serve to enhance the protein biosynthesis to promote cell proliferation and transformation and tumor development and growth, while Brf1 alteration in cells directly affects the products of tRNAs and 5S rRNA genes. Recent studies indicate that Brf1 expression is increased in human cancers of the liver, breast, stomach, and prostate [15, 19–22]. This implies that Brf1 overexpression is required for cancer cell growth in humans. Here, we report that Brf1 expression was enhanced in the cases of lung cancer (Figures 1–3, Figure S1). High Brf1 expression displays a worse prognosis (Figure 2). It suggests that Brf1 is a novel prognostic biomarker for human lung cancer.

LKB1 was originally defined as a tumor suppressor [39]. It is a component of AMPK upstream. Studies have demonstrated that LKB1 mutation in lung cancer is up to 20% or more [26–28]. The mutation of LKB1 often accompanies K-Ras activation in the disease, while activated oncogene, Ras, is able to increase the TFIIB activity to upregulate Pol III gene transcription [39–41]. Brf1 is an important subunit of the TFIIB complex. This points out that there may be an underlying relationship between Brf1 and lung cancer. Here, we report that Brf1 is overexpressed in cases of lung cancer. It proves the direct relationship between Brf1 and lung cancer. On the other hand, LKB1 activates AMPK activity, while activated AMPK α upregulates Brf1 and Pol III gene transcription (Figures 6 and 7) to promote lung cancer development in the status of K-Ras activation [41, 42]. A basic feature of cancer cells is the requirement of high nutrient intakes, macromolecular synthesis, and energy consumption to support tumor cell growth and survival [43]. The biological functions of Brf1 and Pol III genes are responsible for protein synthesis, whereas protein synthesis is essential for tumor cell growth. Eichner and his colleagues reported that AMPK is needed in glucose deprivation to induce Tfe3 activation, while Tfe3 activity increases the growth of rodent lung tumors [42]. Here, our study further demonstrates that the carcinogen MNNG activates AMPK α to increase the expression of Brf1 and Pol III genes (Figure 5). In contrast, inhibiting AMPK α decreases the expression of these genes (Figures 6 and 7). It shows that there is a new and much more important pathway, namely, pAMPK α , which upregulates

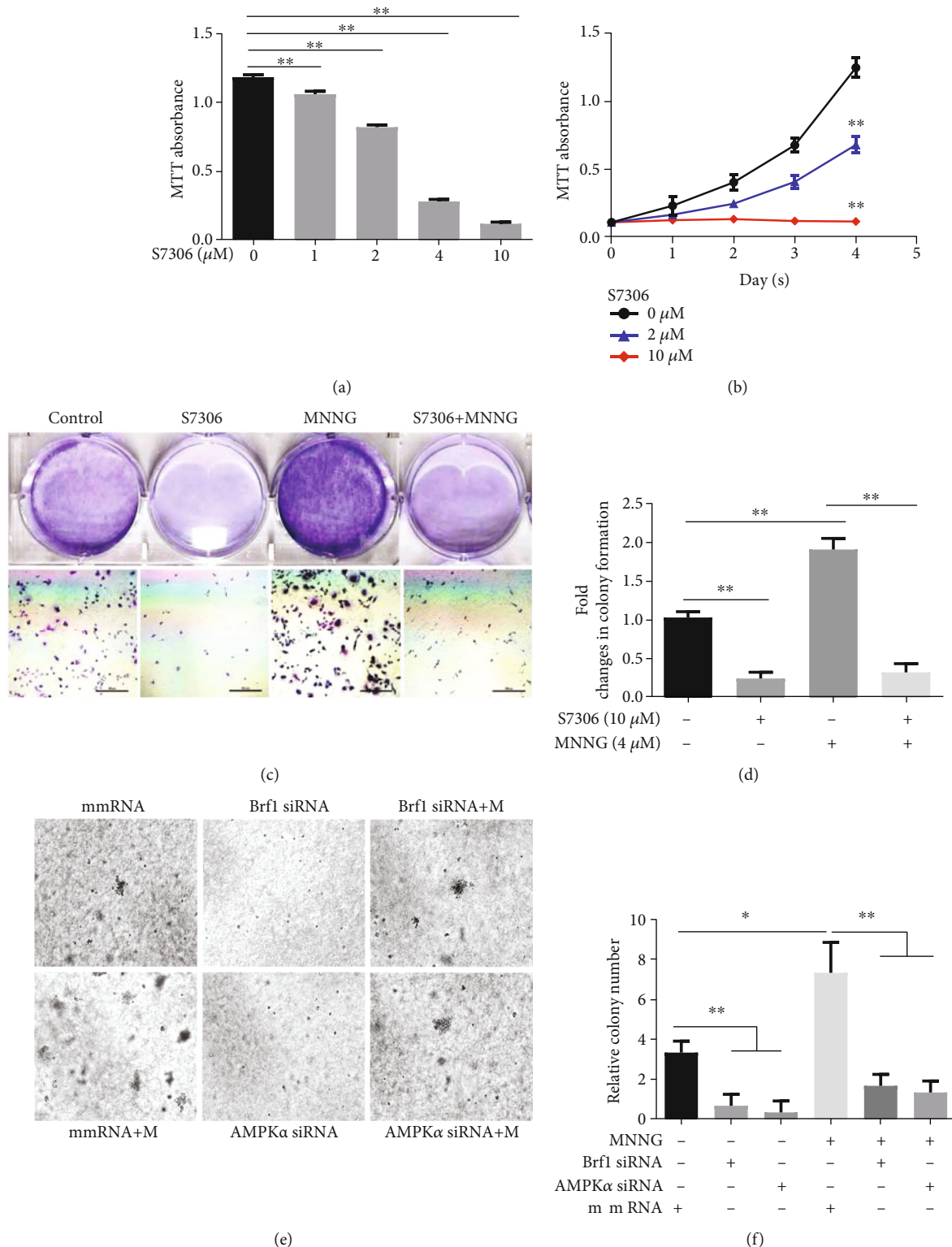


FIGURE 9: pAMPK α mediated the alteration of Brf1 resulting in cellular phenotypic changes. (a, b) MTT assay. A549 cells were pretreated with or without AMPK inhibitor S7306 for 4 days: (a) dose curve (4 days); (b) time course; (c) colony formation assays: A549 cells were cultured in RPMI 1640 alone or with S7306 or MNNG for 1 week or longer (scale bar = 500 μm). The colonies were stained with 0.1% crystal violet solution. (d) Quantification of the colony numbers of A549 cells calculated after being cultured alone or in S7306 or MNNG for 1 week. (e) A549 cells were transfected with mmRNA, Brf1 siRNA, or AMPK α siRNA, respectively. After knockdown of Brf1 or AMPK α for 48 h, the cells were seeded into soft agar and treated alone or with MNNG (4 μM) for 1-2 weeks to observe colony formation. (f) Quantification of the clonogenicity of A549 cells as described previously (e). All error bars represent the SD of at least three independent experiments. p values were determined by a two-tailed t -test. * $p < 0.05$, ** $p < 0.01$.

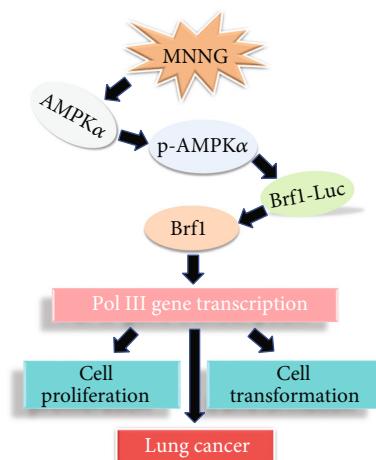


FIGURE 10: Schematic illustration of pAMPK α mediates dysregulation of Brf1 and Pol III gene transcription. In the study, high levels of Brf1 expression and pAMPK α are detected in human samples of lung cancer. Mechanism analysis indicates that the carcinogen MNNG induces pAMPK α to enhance Brf1 promoter activity, resulting in Brf1 expression and Pol III gene transcription, which increase the rates of cell proliferation and colony formation, eventually resulting in cancer development.

the activities of Brf1 and Pol III genes to promote human lung cancer development except AMPK-mediated Tfe3.

The studies of signaling events indicate that MAP kinases mediate Pol III gene transcription [39]. Hereafter, JNK1 and JNK2 were identified to differently mediate the activity of Brf1 and Pol III genes: JNK1 positively regulated the activities of Brf1 and Pol III genes to increase cell proliferation [44, 45]. In contrast, JNK2 negatively modulated Brf1 and Pol III genes to repress cell growth [44, 45]. Activated JNK1 upregulates Brf1 expression through the c-Jun and Elk1 pathways to promote liver tumor development [15, 31], whereas activation of JNK1 increases the Brf1 and Pol III gene activities to elevate the rates of breast cell growth and colony formation through ER α to facilitate cell transformation [17]. Here, we report that the carcinogen MNNG induces the activation of AMPK α to upregulate the expression of Brf1 and Pol III genes, resulting in increasing the rate of cell proliferation and colony formation (Figure 9) [20]. These studies indicate that dysregulation of Brf1 and Pol III genes is going through different signaling pathways in various organs. In other words, the modulations of Brf1 expression are of tissue specificity [14]. Furthermore, we have demonstrated that carcinogens (EGF and DEN) induce histone H3 phosphorylation at serine 10 and 28, while phosphorylated H3 epigenetically upregulates the transcription of Brf1 and Pol III genes [18, 38]. It implies that epigenetic regulation plays a key role in cancer development and tumor growth. These studies have been going in our laboratory.

5. Conclusion

In summary, our studies demonstrate that Brf1 is overexpressed in human lung cancer. High Brf1 expression displays

short survival times. The overexpression of Brf1 is accompanied by a high level of pAMPK α in the cases of lung cancer. Mechanism study reveals that activated AMPK α , pAMPK α , upregulates the activities of Brf1 and Pol III genes, while repressing AMPK α decreases Brf1 expression and Pol III gene transcription, resulting in the reduction of cell proliferation and colony formation (Figure 10) [29]. These studies demonstrate that pAMPK α -mediated Brf1 expression and Pol III gene transcription is a novel and direct pathway, which is tightly linked to protein synthesis, supporting cell growth and cell survival of lung cancer. Therefore, developing a specific inhibitor to repress the growth of cancer cells is a new strategy for the therapy of human lung cancer.

Abbreviations

AMPK:	5' AMP-activated protein kinase
pAMPK α :	Phosphorylated AMPK α
Brf1:	TF IIB-related factor 1
Pol III genes:	RNA polymerase III-dependent genes
TFIIIB:	Transcription factor III B complex
SCLC:	Small-cell lung cancer
NSCLC:	Non-small-cell lung cancer
LKB1:	Tumor suppressor liver kinase B1
IHC:	Immunohistochemistry
ANT:	Adjacent noncancerous tissue
SI:	Staining index
mm siRNA:	Mismatch siRNA
RT-qPCR:	Real-time quantitative PCR
Brf1-Luc:	Brf1 promoter-luciferase reporter
ER α :	Estrogen receptor α
MNNG:	N-Methyl-N'-nitro-N-nitrosoguanidine
ADH:	Alcohol dehydrogenase
CYP2E1:	Cytochrome P450 2E1
ROS:	Reactive oxygen species.

Data Availability

The datasets of the study are available on request to the corresponding authors.

Ethical Approval

The studies involving human samples were reviewed and approved by the Institute Research Ethics Committee of Guangdong General Hospital, Guangdong Academy of Medical Sciences (ID number: No. GDREC2016175H(R2)).

Conflicts of Interest

The authors declare no conflict of interest.

Authors' Contributions

Lu, Zheng, and Zhong participated in research design; Wu, Zhang, Lin, Yu, Dai, Li, and Yu conducted experiments; Zhong contributed new reagents or analytical tools; Wu and Yu performed data analysis; Lu, Zheng, and Zhong wrote or contributed to the writing of the manuscript. Teng Wu,

Dongkun Zhang, and Mingren Lin contributed equally to the present study.

Acknowledgments

The work was supported by a grant from the National Natural Science Foundation of China # 81300465 to L. Lu and supported by grants from the Science Foundation of Fujian Province (No. 2019J01601) and the Science and Technology Project of Quanzhou City (No. 2018C069R) to L. Zheng.

Supplementary Materials

Supplementary figures (Figure S1: immunohistochemical staining in the samples of lung cancer patients. Figure S2: carcinogen MNNG increases Brf1 expression and Pol III gene transcription. Figure S3: the roles of AMPK α in Brf1 expression in lung cancer cells. Figure S4: colocalization of Brf1 and pAMPK α in lung cancer cells.) are available at *Oxidative Medicine and Cellular Longevity* online. (Supplementary Materials)

References

- [1] Y. L. Wu, Y. Cheng, X. Zhou et al., "Dacomitinib versus gefitinib as first-line treatment for patients with _EGFR_ -mutation-positive non-small-cell lung cancer (ARCHER 1050): a randomised, open-label, phase 3 trial," *The Lancet Oncology*, vol. 18, no. 11, pp. 1454–1466, 2017.
- [2] W. Chen, R. Zheng, P. D. Baade et al., "Cancer statistics in China, 2015," *CA: a Cancer Journal for Clinicians*, vol. 66, no. 2, pp. 115–132, 2016.
- [3] N. Reguart, E. Marin, J. Remon, R. Reyes, and C. Teixido, "In search of the long-desired 'Copernican therapeutic revolution' in small-cell lung cancer," *Drugs*, vol. 80, no. 3, pp. 241–262, 2020.
- [4] M. R. Davidson, A. F. Gazdar, and B. E. Clarke, "The pivotal role of pathology in the management of lung cancer," *Journal of Thoracic Disease*, vol. 5, Suppl 5, pp. S463–S478, 2013.
- [5] C. Dayen, D. Debievre, O. Molinier et al., "New insights into stage and prognosis in small cell lung cancer: an analysis of 968 cases," *Journal of Thoracic Disease*, vol. 9, no. 12, pp. 5101–5111, 2017.
- [6] S. Aviell-Ronen, F. H. Blackhall, F. A. Shepherd, and M. S. Tsao, "K- _ras_ mutations in non-small-cell lung carcinoma: a review," *Clinical Lung Cancer*, vol. 8, no. 1, pp. 30–38, 2006.
- [7] W. A. Cooper, D. C. Lam, S. A. O'Toole, and J. D. Minna, "Molecular biology of lung cancer," *Journal of Thoracic Disease*, vol. 5, Suppl 5, pp. S479–S490, 2013.
- [8] R. S. Herbst, J. V. Heymach, and S. M. Lippman, "Lung cancer," *The New England Journal of Medicine*, vol. 359, no. 13, pp. 1367–1380, 2008.
- [9] N. Takahashi, H. Y. Chen, I. S. Harris et al., "Cancer cells co-opt the neuronal redox-sensing channel TRPA1 to promote oxidative-stress tolerance," *Cancer Cell*, vol. 33, no. 6, pp. 985–1003.e7, 2018.
- [10] S. Vlahopoulos, M. Adamaki, N. Khoury, V. Zoumpourlis, and I. Boldogh, "Roles of DNA repair enzyme OGG1 in innate immunity and its significance for lung cancer," *Pharmacology & Therapeutics*, vol. 194, pp. 59–72, 2019.
- [11] M. Jakopovic, A. Thomas, S. Balasubramaniam, D. Schrupp, G. Giaccone, and S. E. Bates, "Targeting the epigenome in lung cancer: expanding approaches to epigenetic therapy," *Frontiers in Oncology*, vol. 3, p. 261, 2013.
- [12] R. J. White, "RNA polymerase III transcription and cancer," *Oncogene*, vol. 23, no. 18, pp. 3208–3216, 2004.
- [13] D. L. Johnson and S. A. Johnson, "Cell biology. RNA metabolism and oncogenesis," *Science*, vol. 320, no. 5875, pp. 461–462, 2008.
- [14] C. Huang, Y. Zhang, and S. Zhong, "Alcohol intake and abnormal expression of Brf1 in breast cancer," *Oxidative Medicine and Cellular Longevity*, vol. 2019, Article ID 4818106, 9 pages, 2019.
- [15] G. Shi and S. Zhong, "Alcohol-associated cancer and deregulation of Pol III genes," *Gene*, vol. 612, pp. 25–28, 2017.
- [16] S. A. Johnson, L. Dubeau, and D. L. Johnson, "Enhanced RNA Polymerase III-dependent Transcription Is Required for Oncogenic Transformation*," *The Journal of Biological Chemistry*, vol. 283, no. 28, pp. 19184–19191, 2008.
- [17] Q. Zhang, J. Jin, Q. Zhong, X. Yu, D. Levy, and S. Zhong, "ER α mediates alcohol-induced deregulation of Pol III genes in breast cancer cells," *Carcinogenesis*, vol. 34, no. 1, pp. 28–37, 2013.
- [18] Q. Zhong, G. Shi, Q. Zhang, Y. Zhang, D. Levy, and S. Zhong, "Role of phosphorylated histone H3 serine 10 in DEN-induced deregulation of Pol III genes and cell proliferation and transformation," *Carcinogenesis*, vol. 34, no. 11, pp. 2460–2469, 2013.
- [19] Q. Zhong, S. Xi, J. Liang et al., "The significance of Brf1 overexpression in human hepatocellular carcinoma," *Oncotarget*, vol. 7, no. 5, pp. 6243–6254, 2016.
- [20] Z. Fang, Y. Yi, G. Shi et al., "Role of Brf1 interaction with ER α , and significance of its overexpression, in human breast cancer," *Molecular Oncology*, vol. 11, no. 12, pp. 1752–1767, 2017.
- [21] Y. Zhang, H. Wu, F. Yang et al., "Prognostic value of the expression of DNA repair-related biomarkers mediated by alcohol in gastric cancer patients," *The American Journal of Pathology*, vol. 188, no. 2, pp. 367–377, 2018.
- [22] C. J. Loveridge, S. Slater, K. J. Campbell et al., "BRF1 accelerates prostate tumorigenesis and perturbs immune infiltration," *Oncogene*, vol. 39, no. 8, pp. 1797–1806, 2020.
- [23] D. Stapleton, K. I. Mitchelhill, B. J. Mitchell et al., "Mammalian AMP-activated protein kinase subfamily (*)," *The Journal of Biological Chemistry*, vol. 271, no. 2, pp. 611–614, 1996.
- [24] S. M. Jeon, "Regulation and function of AMPK in physiology and diseases," *Experimental & Molecular Medicine*, vol. 48, no. 7, p. e245, 2016.
- [25] D. G. Hardie, F. A. Ross, and S. A. Hawley, "AMPK: a nutrient and energy sensor that maintains energy homeostasis," *Nature Reviews Molecular Cell Biology*, vol. 13, no. 4, pp. 251–262, 2012.
- [26] Z. Chen, K. Cheng, Z. Walton et al., "A murine lung cancer co-clinical trial identifies genetic modifiers of therapeutic response," *Nature*, vol. 483, no. 7391, pp. 613–617, 2012.
- [27] X. Han, F. Li, Z. Fang et al., "Transdifferentiation of lung adenocarcinoma in mice with _Lkb1_ deficiency to squamous cell carcinoma," *Nature Communications*, vol. 5, no. 1, p. 3261, 2014.
- [28] H. Ji, M. R. Ramsey, D. N. Hayes et al., "LKB1 modulates lung cancer differentiation and metastasis," *Nature*, vol. 448, no. 7155, pp. 807–810, 2007.

- [29] Z. Hong, M. Lin, Y. Zhang, Z. He, L. Zheng, and S. Zhong, "Role of betaine in inhibiting the induction of RNA Pol III gene transcription and cell growth caused by alcohol," *Chemico-Biological Interactions*, vol. 325, article 109129, 2020.
- [30] Z. Hong, Z. Fang, J. Lei et al., "The significance of Runx2 mediating alcohol-induced Brf1 expression and RNA Pol III gene transcription," *Chemico-Biological Interactions*, vol. 323, article 109057, 2020.
- [31] S. Zhong, K. Machida, H. Tsukamoto, and D. L. Johnson, "Alcohol induces RNA polymerase III-dependent transcription through c-Jun by co-regulating TATA-binding protein (TBP) and Brf1 expression*," *The Journal of Biological Chemistry*, vol. 286, no. 4, pp. 2393–2401, 2011.
- [32] M. Lin, C. Huang, W. Ren, J. Chen, N. Xia, and S. Zhong, "Mitogen- and stress-activated protein kinase 1 mediates Alcohol-upregulated transcription of Brf1 and tRNA genes to cause phenotypic alteration," *Oxidative Medicine and Cellular Longevity*, vol. 2020, Article ID 2067959, 13 pages, 2020.
- [33] V. Purohit, J. Khalsa, and J. Serrano, "Mechanisms of alcohol-associated cancers: introduction and summary of the symposium," *Alcohol*, vol. 35, no. 3, pp. 155–160, 2005.
- [34] C. Shan, Z. Lu, Z. Li et al., "4-Hydroxyphenylpyruvate dioxygenase promotes lung cancer growth via pentose phosphate pathway (PPP) flux mediated by LKB1-AMPK/H-DAC10/G6PD axis," *Cell Death & Disease*, vol. 10, no. 7, p. 525, 2019.
- [35] S. Li, Z. Zhuang, T. Wu et al., "Nicotinamide nucleotide transhydrogenase-mediated redox homeostasis promotes tumor growth and metastasis in gastric cancer," *Redox Biology*, vol. 18, pp. 246–255, 2018.
- [36] W. Li, C. P. Yu, J. T. Xia et al., "Sphingosine kinase 1 is associated with gastric cancer progression and poor survival of patients," *Clinical Cancer Research*, vol. 15, no. 4, pp. 1393–1399, 2009.
- [37] S. Li, T. Wu, Y. X. Lu et al., "Obesity promotes gastric cancer metastasis via diacylglycerol acyltransferase 2-dependent lipid droplets accumulation and redox homeostasis," *Redox Biology*, vol. 36, article 101596, 2020.
- [38] Q. Zhang, Q. Zhong, A. G. Evans, D. Levy, and S. Zhong, "Phosphorylation of histone H3 serine 28 modulates RNA polymerase III- dependent transcription," *Oncogene*, vol. 30, no. 37, pp. 3943–3952, 2011.
- [39] A. Hemminki, D. Markie, I. Tomlinson et al., "A serine/threonine kinase gene defective in Peutz-Jeghers syndrome," *Nature*, vol. 391, no. 6663, pp. 184–187, 1998.
- [40] S. Zhong, C. Zhang, and D. L. Johnson, "Epidermal growth factor enhances cellular TATA binding protein levels and induces RNA polymerase I- and III-dependent gene activity," *Molecular and Cellular Biology*, vol. 24, no. 12, pp. 5119–5129, 2004.
- [41] S. A. Johnson, L. Dubeau, M. Kawalek et al., "Increased expression of TATA-binding protein, the central transcription factor, can contribute to oncogenesis," *Molecular and Cellular Biology*, vol. 23, no. 9, pp. 3043–3051, 2003.
- [42] L. J. Eichner, S. N. Brun, S. Herzig et al., "Genetic analysis reveals AMPK is required to support tumor growth in murine Kras-dependent lung cancer models," *Cell Metabolism*, vol. 29, no. 2, pp. 285–302.e7, 2019.
- [43] R. A. Cairns, I. S. Harris, and T. W. Mak, "Regulation of cancer cell metabolism," *Nature Reviews Cancer*, vol. 11, no. 2, pp. 85–95, 2011.
- [44] S. Zhong and D. L. Johnson, "The JNKs differentially regulate RNA polymerase III transcription by coordinately modulating the expression of all TFIIB subunits," *Proceedings of the National Academy of Sciences of the United States of America*, vol. 106, no. 31, pp. 12682–12687, 2009.
- [45] S. Zhong, J. Fromm, and D. L. Johnson, "TBP is differentially regulated by c-Jun N-terminal kinase 1 (JNK1) and JNK2 through Elk-1, controlling c-Jun expression and cell proliferation," *Molecular and Cellular Biology*, vol. 27, no. 1, pp. 54–64, 2007.

Review Article

Advances in Understanding Mitochondrial MicroRNAs (mitomiRs) on the Pathogenesis of Triple-Negative Breast Cancer (TNBC)

Hung-Yu Lin ¹ and Pei-Yi Chu ^{2,3,4,5}

¹Research Assistant Center, Show Chwan Memorial Hospital, Changhua 500, Taiwan

²Department of Pathology, Show Chwan Memorial Hospital, Changhua 500, Taiwan

³School of Medicine, College of Medicine, Fu Jen Catholic University, New Taipei City 242, Taiwan

⁴Department of Health Food, Chung Chou University of Science and Technology, Changhua 510, Taiwan

⁵National Institute of Cancer Research, National Health Research Institutes, Tainan 704, Taiwan

Correspondence should be addressed to Pei-Yi Chu; chu.peiyi@msa.hinet.net

Received 14 January 2021; Revised 5 March 2021; Accepted 10 March 2021; Published 22 March 2021

Academic Editor: Kanhaiya Singh

Copyright © 2021 Hung-Yu Lin and Pei-Yi Chu. This is an open access article distributed under the Creative Commons Attribution License, which permits unrestricted use, distribution, and reproduction in any medium, provided the original work is properly cited.

Triple-negative breast cancer (TNBC) is characterized by poor outcome and the most challenging breast cancer type to treat worldwide. TNBC manifests distinct profile of mitochondrial functions, which dictates reprogrammed metabolism, fosters tumor progression, and notably serves as therapeutic targets. Mitochondrial microRNAs (mitomiRs) are a group of microRNAs that critically modulate mitochondrial homeostasis. By a pathway-centric manner, mitomiRs tightly orchestrate metabolic reprogramming, redox status, cell apoptosis, mitochondrial dynamics, mitophagy, mitochondrial DNA (mtDNA) maintenance, and calcium balance, leading to an emerging field of study in various cancer types, including TNBC. We herein review the recent insights into the roles and mechanism of mitomiRs in TNBC and highlight its clinical value in diagnosis and prognosis as well as vital advances on therapeutics of preclinical and clinical studies.

1. Introduction

Breast cancer (BC) is the most common cancer in women globally, accounting for about a quarter of female cancer [1, 2]. In spite of recent improvements in molecular and imaging diagnosis and treatments including hormone therapy, target therapy, chemotherapy, and radiotherapy, BC remains the leading cause of cancer death worldwide [1–3]. Based on the expression of estrogen receptor (ER), progesterone receptor (PR), human epidermal growth factor 2 (HER2), and proliferation marker protein Ki-67, BC can be categorized into four subtypes including luminal A, luminal B, HER2, and triple-negative breast cancer (TNBC) [4].

TNBC is tested negative for ER, PR, and HER2 by immunohistochemical staining, accounting for 15–20% of BC cases [5]. Advanced breast cancer comprises inoperable locally advanced breast cancer and metastatic (stage IV) breast can-

cer. As shown in Figure 1(a), the bone, the liver, and the lungs account, respectively, for about 67%, 40.8%, and 36.9% of the common metastatic sites, wherein basal-like BC (BLBC, accounting for 75% of the TNBC subtypes [6]) hits 40%, 35%, and 35%, respectively, of the metastatic BC [7]. More than 70% of the metastatic TNBC cases fails to survive after five years of diagnosis and exhibits worse prognosis than other BC subtypes [8]. Due to the lack of ER/PR/HER2 receptors, TNBC is unresponsive to endocrine and target therapy, such as tamoxifen, aromatase inhibitors, and/or anti-HER2-targeted therapies. As such, surgery, radiotherapy, and predominantly nonspecific chemotherapy (e.g., anthracycline and taxane regimens) remain the mainstay for management of these patients, yet with severe side effects worsening quality of life [9, 10]. Although the combination uses of chemotherapy regimens (e.g., capecitabine in conjunction with taxanes) have shown increased response rates,

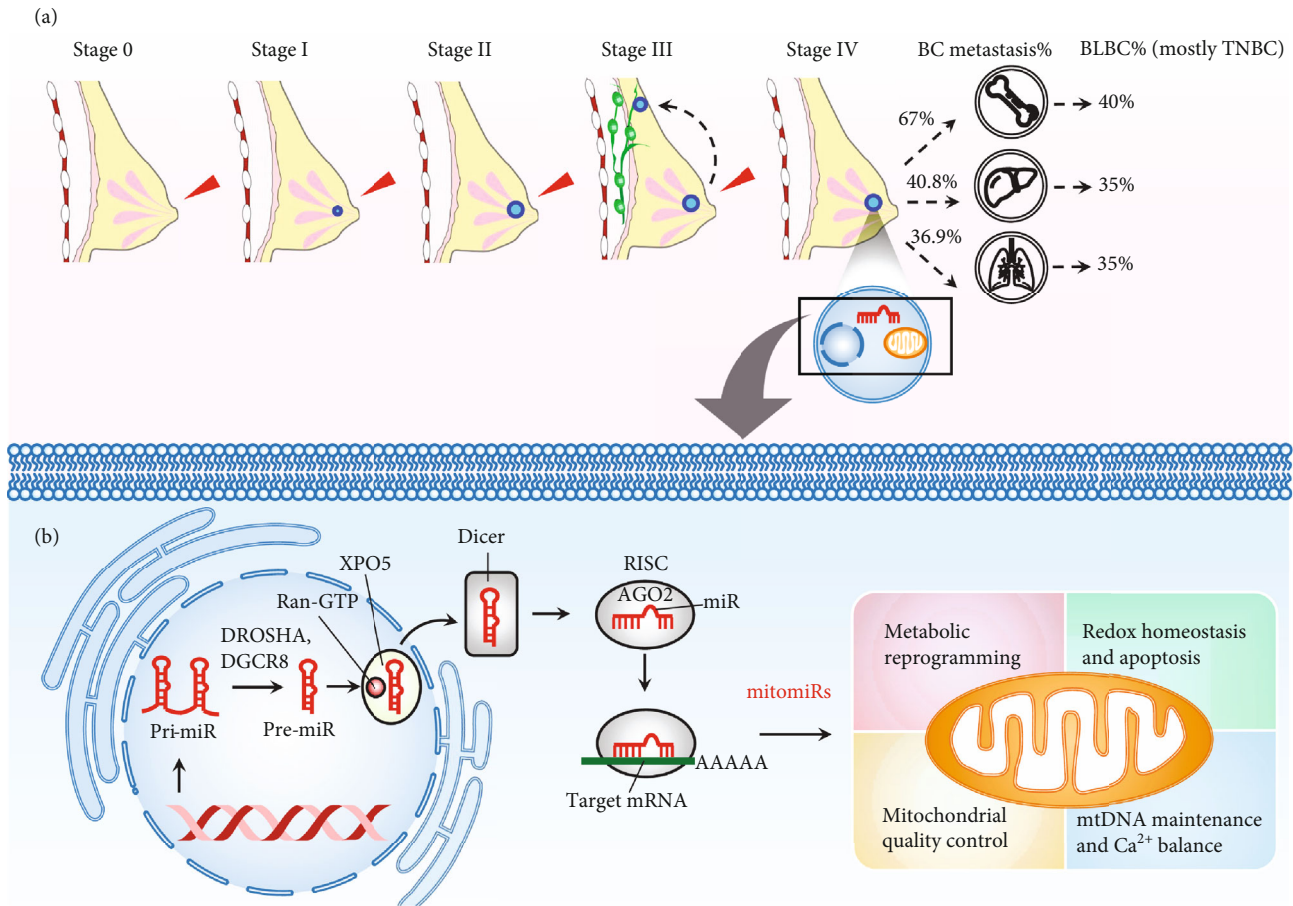


FIGURE 1: Graphic overview depicting the roles of mitomiRs in modulating mitochondrial homeostasis and its involvements in the scenario of TNBC progression. (a) TNBC stages classified by TNM system [7]. Advanced breast cancer comprises inoperable locally advanced breast cancer and metastatic (stage IV) breast cancer. The bone, the liver, and the lungs account, respectively, for about 67%, 40.8%, and 36.9% of the common metastatic sites, wherein basal-like BC (BLBC, accounting for 75% of the TNBC subtypes [6]) hits 40%, 35%, and 35%, respectively, of the metastatic BC [7]. (b) The mitomiR biogenesis and its impacts on mitochondrial dimensions. The precursor transcripts (pri-miR) are transcribed and posttranscriptionally cleaved by microprocessor (DROSHA and DGCR8) in the nucleus to liberate the pre-miR hairpin. The pre-miR is then exported to the cytoplasm by exportin 5 (XPO5) bound to guanosine 5'-triphosphate (Ran-GTP). In the cytoplasm, the DICER endoribonuclease cleaves the loop of the pre-miR to produce the mature miR. The resulting miR embeds in a groove of Argonaute (AGO) of the RNA-induced silencing complex (RISC) and ultimately targets a strand of mRNA by base pairing its 3' untranslated region (UTR). When bound to an mRNA, RISC inhibits translation, yet the main effect is to degrade the mRNA through deadenylation. mitomiRs are a particular cluster of miRs that predominantly occupy a sphere of influence on dimensions of mitochondrial homeostasis, including metabolic reprogramming, redox homeostasis, mitochondrial quality control, mtDNA maintenance, and Ca²⁺ balance.

the multiagent approach led to increased toxicities [11, 12]. Therefore, treatments for TNBC have since a major challenge for oncologists due to the absence of unambiguous molecular targets.

Mitochondria are dynamic organelles that produce energy through oxidative phosphorylation (OXPHOS) for the sophisticated biochemical reactions of a cell. Originated from eubacterial endosymbiosis, each of them has multiple copies of mitochondrial DNA (mtDNA), which is a circular, double-stranded DNA (16,569-base pairs in human) encoding 37 genes, including 13 proteins, 22 tRNAs, and 2 rRNAs [13]. Structurally, mitochondria have double-membrane system, composed of outer membrane and inner membrane, which compartmentalize intermembrane space, crista, and

matrix where OXPHOS takes place to generate ATP [13]. More than intracellular powerhouses, mitochondria play a central role in controlling physiological process and cellular fate by orchestrating metabolism, redox status, apoptosis, dynamics, mitophagy (a mechanism selectively degrading mitochondria by autophagy), mtDNA maintenance, and calcium balance [14, 15]. More recently, approaches aiming at disturbances of cellular metabolism and mitochondrial functions for the treatment of cancer, including BC, have been emerging [15, 16].

MicroRNAs (miRs) are small, approximately 22-nucleotide noncoding RNAs. miR genes are derived from within the introns and are subject to similar types of epigenetic regulation as are the protein-coding genes [17]. As

TABLE 1: Roles and mechanisms of mitomiRs in metabolic reprogramming.

mitomiR	Function	Target gene	Mechanism of action	Outcome	PMID	Reference
<i>Glucose metabolism</i>						
miR-29a	(-)TNBC	<i>ARG2</i>	↓AGR2→↓HIF-1 α	↑Apoptosis ↓Proliferation ↓Migration ↓Invasion ↓Tumor growth	33223849	Wang et al., 2020 [28]
miR-210	(+)TNBC	<i>GPD1L, CYGB</i>	↓GPD1L→↑HIF-1 α →↑glycolysis ↓CYGB→↓p53→↑glycolysis	↓Apoptosis ↑Tumor growth	32908121	Du et al., 2020 [29]
miR-140	(-)TNBC	<i>GLUT1</i>	↓GLUT1→↓glycolysis	↑OCR/↓ECAR ↓Proliferation ↓Tumor growth	31184216	He et al., 2019 [30]
let-7a	(-)TNBC	<i>STAT3</i>	↓STAT3→↓hnRNPA1→↓PKM2 →↓Glycolysis	↓Proliferation	30368881	Yao et al., 2019 [31]
miR-155	(+)TNBC	<i>PIK3R1, FOXO3a</i>	↓PI3K/↓FOXO3a→↑cMYC →↑HK2/↑PKM2/↑LDHA →↑Glycolysis	↑Tumor growth	29527004	Kim et al., 2018 [32]
miR-128	(-)TNBC	<i>INSR, IRS1</i>	↓INSR/↓INS1→↓p-AKT/↓HK2/↓PFK →↓Glycolysis	↓Mitochondrial bioenergetics ↓Proliferation ↓Tumor growth	29116653	Xiao et al., 2018 [33]
miR-342	(-)TNBC	<i>MCT1</i>	↓MCT1→↓lactate uptake	↓Proliferation ↓Migration ↑OCR/↓ECAR ↓Proliferation ↓Migration ↓Invasion ↓Tumor growth ↓Tumor metastasis	30115973	Romero-Cordoba et al., 2018 [34]
miR-30a	(-)TNBC	<i>LDHA</i>	↓LDHA→↓glycolysis	↓ATP production ↓Lactate production ↓Migration ↓Tumor metastasis	28461244	Li et al., 2017 [35]
miR-21	(+)TNBC	<i>CAB39L, SESN1</i>	↓CAB39L, ↓SESN1→↓p-AMPK→↑mTOR	↑Proliferation ↑Migration ↑Invasion ↑Tumor growth	28698800	Pulito et al., 2017 [36]
miR-340	(-)TNBC	<i>MCU</i>	↓MCU→↓[Ca ²⁺] _m →↓LDH →↓Glycolysis	↓ATP production ↓Lactate production ↓Migration ↓Tumor metastasis	29137386	Yu et al., 2017 [37]
miR-101	(-)TNBC	<i>AMPK</i>	↓AMPK→↓glycolysis	↓Proliferation	27145268	Liu et al., 2016 [38]
miR-18a	(-)TNBC	<i>HIF1A</i>	↓HIF-1 α →↓hypoxic gene expression	↓Tumor growth ↓Tumor metastasis	25069832	Krutilina et al., 2014 [39]
miR-143	(-)TNBC	<i>HK2</i>	↓HK2→↓glycolysis	↑Apoptosis ↓Proliferation ↓Tumor growth	22354042	Jiang et al., 2012 [40]
miR-155	(+)TNBC	<i>mir-143</i>	↑miR-155→↓C/EBP β → ↓miR-143→↑HK2→↑glycolysis	↑Tumor growth	22354042	Jiang et al., 2012 [40]
<i>Fatty acid metabolism</i>						
miR-1291	(-)TNBC	<i>ESRRA</i>	↓ERR α →↓CPT1C	↓Proliferation ↓Tumor growth ↑TNBC sensitivity to 2-DG	32641987	Chen et al., 2020 [41]
let-7a	(-)TNBC	<i>SCD</i>	↓SCD, ↓G6PD, ↓FASN, ↓ASSDHPPT →↑OCR/↑ECR/↑ $\Delta\Psi_m$	↓Proliferation ↑TNBC sensitivity to doxorubicin	25669981	Serguienko et al., 2015 [42]
miR-195	(-)TNBC	<i>ACACA, FASN, HMGCR</i>	↓Cellular triglyceride ↓Cellular cholesterol ↓ $\Delta\Psi_m$	↓EMT ↓Proliferation ↓Migration ↓Invasion	26632252	Singh et al., 2015 [43]

TABLE 1: Continued.

mitomiR	Function	Target gene	Mechanism of action	Outcome	PMID	Reference
<i>Glutamine/cystine metabolism</i>						
miR-27a	(-)TNBC	<i>SLC7A11, CTH</i>	↓xCT→↓cystine uptake ↓CTH→↓cystine production	↓Mammosphere formation ↓CSC markers ↑TNBC sensitivity to doxorubicin and paclitaxel	32066826	Ueda et al., 2020 [36]
<i>OXPHOS</i>						
miR-4485	(-)TNBC	<i>16S rRNA</i>	↓16S rRNA→↓ETC enzymes	↑Cell death ↓Proliferation ↓Tumor growth	28220193	Sripada et al., 2017 [44]
miR-663	(-)TNBC	<i>UQC2</i>	↓UQC2→↓complex III activity	↑OXPHOS subunits ↓Invasion ↓Tumor growth	29066618	Carden et al., 2017 [45]

(+): oncogenic; (-): tumor suppressor; “↑”: enhanced; “↓”: reduced; $\Delta\Psi_m$: mitochondrial membrane potential; AASDHPPT: 4-phosphopantetheinyl transferase; ACACA: acetyl-CoA carboxylase; AGR2: anterior gradient 2; $[Ca^{2+}]_m$: mitochondrial calcium; AMPK: AMP-activated protein kinase; CAB39L: calcium-binding protein 39-like; C/EBP β : CCAAT-enhancer-binding protein β ; CPT1C: carnitine palmitoyltransferase 1C; CTH: cystathionine gamma-lyase; CYGB: cytoglobin; ECAR: extracellular acidification rate; EMT: epithelial-mesenchymal transition; ERR α (encoded by *ESRRA*): estrogen-related receptor alpha; FASN: fatty acid synthase; FOXO3a: forkhead box O3; G6PD: glucose-6-phosphate dehydrogenase; GLUT1: glucose transporter 1; GPD1L: glycerol-3-phosphate dehydrogenase 1; *HIF1A/HIF-1 α* : hypoxia-inducible factor 1-alpha; HK2: hexokinase 2; HMGCR: 3-hydroxy-3-methylglutaryl CoA reductase; INSR: insulin receptor; IRS1: insulin receptor substrate 1; LDHA: lactate dehydrogenase A; MCT1: monocarboxylate transporter 1; MCU: mitochondrial calcium uniporter; mtDNA: mitochondrial DNA; mt-ROS: mitochondrial reactive oxygen species; OCR: oxygen consumption rate; OXPHOS: oxidative phosphorylation; PFK: phosphofructokinase; PI3K: phosphoinositide 3-kinases; PKM2: pyruvate kinase M1/2; SCD: stearoyl-CoA desaturase; SESN1: sestrin-1; STAT3: signal transducers and activators of transcription 3; UQC2: ubiquinol-cytochrome c reductase complex assembly factor 2; xCT (encoded by *SLC7A11*): cystine/glutamate transporter.

shown in Figure 1(b), a miR gene is initially transcribed by RNA polymerase II into a primary miRNA (pri-miRNA) and then processed in the nucleus by microprocessor complex comprising an endoribonuclease Drosha and a double-stranded RNA-binding protein DiGeorge syndrome critical region 8 (DGCR8) into a ~70 nt precursor miR (pre-miR) [18], which are then exported to the cytoplasm by an exportin 5/guanosine 5'-triphosphate (XPO5/RanGTP) complex. In the cytoplasm, the loop of a pre-miRNA is cleaved by the endonuclease Dicer to generate a mature miR [19]. The regulatory functions of a mature miR are accomplished by associating with the Argonaute (AGO) of the RNA-induced silencing complex (RISC) [20]. As such, a miR ultimately targets a strand of mRNA by base pairing its 3' untranslated region (UTR) and negatively regulates mRNA expression in most cases. When bound to an mRNA, RISC inhibits translation, yet the main effect is to degrade the mRNA through deadenylation [17].

mitomiRs are a group of miRs that intimately regulate mitochondrial functions. mitomiRs can exert the repressive effect on gene expression to modulate mitochondrial functions by two ways: one major type of mitomiRs targets mRNAs in the cytoplasm; the other type of mitomiRs is imported into mitochondria to target mtDNA-encoded mRNAs. With regard to the gene origin of the mitomiRs, the vast majority of them are nuclear-encoded, while few of the mitomiRs are encoded by mtDNA (e.g., miR-1974, miR-1977, and miR-1978) [21].

Mounting evidence in recent years has noted the translational implication of mitomiRs in metabolic disorder, degenerative diseases, and cancer [22–24]. Their functions in modulating multiple aspects of mitochondrial homeostasis permit alterations in cancer metabolism, growth, metastasis,

and sensitivity to clinical drugs. More importantly, mitomiRs' potential as a predictive panel and therapeutic targets is notably emerging. As such, we herein focus on the novel biological roles and mechanisms of mitomiRs on the mitochondria-centric metabolic network in the context of TNBC (Figure 1). Moreover, we highlight recent insights into the advanced understating of predictive value and therapeutic implication of mitomiRs.

2. Roles of mitomiRs in Regulating Metabolic Reprogramming of TNBC

Cancer cells are characterized by significant metabolic reprogramming which facilitate survival and rapid proliferation in a nutrient-deprived tumor microenvironment [25, 26]. Otto Warburg firstly identified that cancer cells maintain high levels of glycolysis for ATP production, regardless of oxygen availability, a phenomenon thereafter termed as the Warburg effect [27]. Since then, an increasing volume of study focused on cancer-associated metabolic reprogramming within crucial metabolic pathways, including altered metabolism of glucose, fatty acid, and amino acids as well as perturbed OXPHOS, in an attempt to find out metabolic susceptibilities during cancer progression. The potential preclinical/clinical reagents targeting metabolic reprogramming of TNBC have been reviewed (32296646). In this regard, we summarized a number of mitomiRs that have been reported to significantly regulate TNBC progression by acting to metabolic reprogramming (Table 1).

Several lines of study noted that mitomiRs perturb glycolysis-associated targets to inhibit TNBC. Jiang et al. have demonstrated that miR-155/miR-143 axis modulates tumor development by dictating glycolysis [40]. They showed that

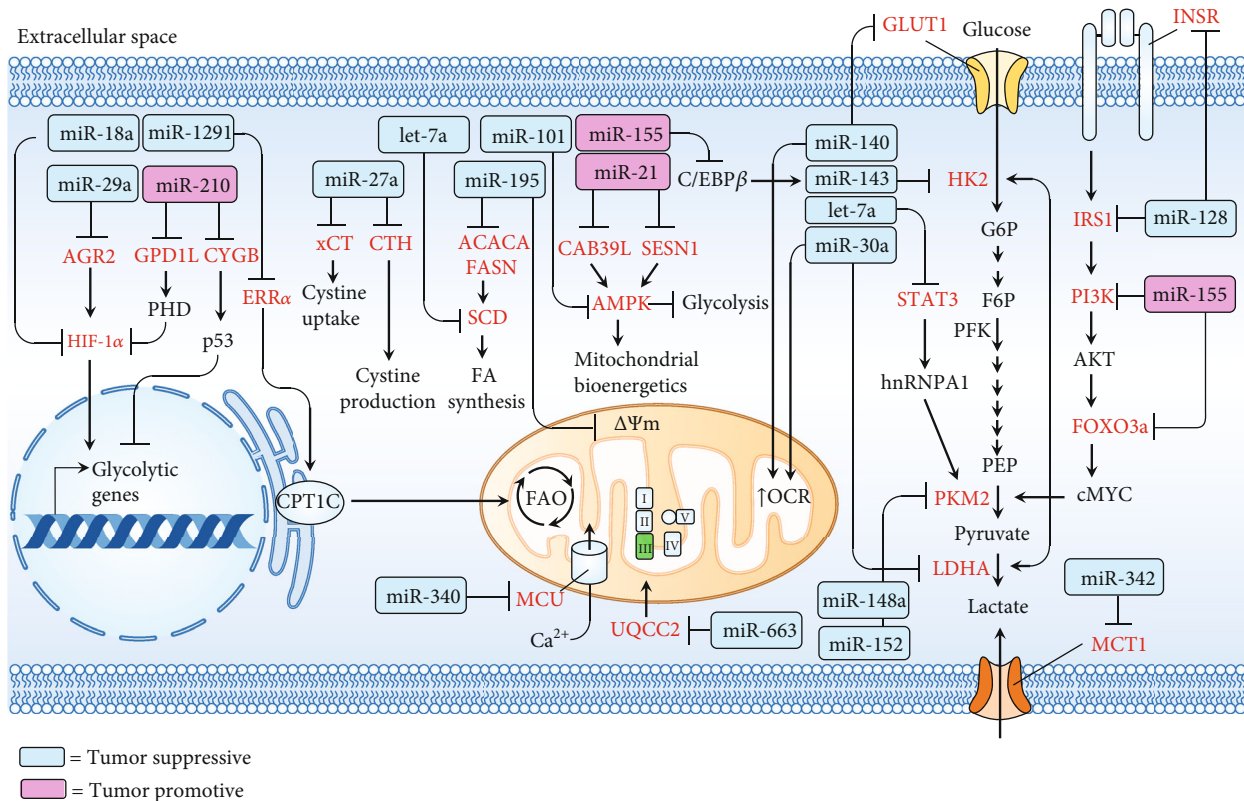


FIGURE 2: Integrative network depicting that tumor-suppressive (blue rectangle) or tumor-promotive (pink rectangle) mitomiRs act on specific target genes (red) that are involved in metabolic reprogramming. $\Delta\Psi_m$: mitochondrial membrane potential; ACACA: acetyl-CoA carboxylase; AGR2: anterior gradient 2; AMPK: AMP-activated protein kinase; CAB39L: calcium-binding protein 39-like; C/EBP β : CCAAT-enhancer-binding protein β ; CPT1C: carnitine palmitoyltransferase 1C; CTH: cystathionine gamma-lyase; CYGB: cytoglobin; ERR α : estrogen-related receptor alpha; F6P: fructose 6-phosphate; FASN: fatty acid synthase; G6P: glucose 6-phosphate; GLUT1: glucose transporter 1; GPD1L: glycerol-3-phosphate dehydrogenase 1; HIF-1 α : hypoxia-inducible factor 1-alpha; HK2: hexokinase 2; INSR: insulin receptor; IRS1: insulin receptor substrate 1; LDHA: lactate dehydrogenase A; MCT1: monocarboxylate transporter 1; MCU: mitochondrial calcium uniporter; mtDNA: mitochondrial DNA; mt-ROS: mitochondrial reactive oxygen species; OCR: oxygen consumption rate; PEP: phosphoenolpyruvate; PFK: phosphofruktokinase; PI3K: phosphoinositide 3-kinases; PKM2: pyruvate kinase M1/2; SCD: stearoyl-CoA desaturase; SESN1: sestrin-1; STAT3: signal transducers and activators of transcription 3; UQCC2: ubiquinol-cytochrome c reductase complex assembly factor 2; xCT: cystine/glutamate transporter.

miR-155 and miR-143 have TNBC-promoting and TNBC-inhibiting effect, respectively. Mechanistically, tumorigenic inflammatory signals augment glycolysis through miR-155, which suppresses miR-143 by targeting CCAAT-enhancer-binding protein β (C/EBP β). The resulting decrease in miR-143 leads to an unleashed targeting inhibition on hexokinase 2 (HK2), leading to an increase in HK2 and consequently an induced glycolysis [40]. miR-18a was demonstrated to inhibit TNBC growth and metastasis in both *in vivo* and *in vitro* models and expression of hypoxic genes [39]. The molecular basis of miR-18a lies in the direct binding to the *HIF1A* UTR [39]. Inhibition of TNBC proliferation *in vitro* can be achieved by the overexpression of miR-101, which exerts repressive effect on gene expression of AMPK [38]. Yu et al. have shown that miR-340 inhibits glycolysis through modulating mitochondrial calcium homeostasis in TNBC [37]. Specifically, miR-340 targets the UTR of mitochondrial calcium uniporter (MCU) gene and represses the expression to reduce tumor growth and metastasis [37]. Li et al. demonstrated that miR-30a inhibits glycolysis and enhances mitochondrial respi-

ratory activity by targeting lactate dehydrogenase A (LDHA), whereby the growth and metastasis of TNBC is reduced [35]. miR-342 was reported to disturb glucose metabolism and lactate uptake of TNBC by targeting monocarboxylate transporter 1 (MCT1) [34]. miR-128 was shown to specifically inhibit insulin receptor (INSR) and insulin receptor substrate 1 (IRS1) to abate glycolytic signaling pathway and mitochondrial respiration, resulting in decreased tumor growth [33]. Both miR-148a and miR-152 were shown to directly target pyruvate kinase M1/2 (PKM2) to counteract glycolytic metabolism of TNBC cells, leading to decreased cancer cell proliferation and angiogenesis [46]. Yao et al. have identified that let-7a represses signal transducers and activators of transcription 3 (STAT3) expression level to subsequently mediate hnRNPA1/PKM2 signaling, leading to a decrease in glucose metabolism and TNBC proliferation [31]. miR-140 showed antiglycolytic and antiproliferative effect on TNBC through direct binding to glucose transporter 1 (GLUT1) [30]. Li et al. showed that miR34a inhibitor promotes cell proliferation and glucose uptake, indicating the anti-TNBC effect of

TABLE 2: Roles and mechanisms of mitomiRs in the perturbation of redox homeostasis.

mitomiR	Function	Target gene	Mechanism of action	Outcome	PMID	Reference
miR-34a	(-)TNBC	<i>BCL-2</i>	↓ <i>BCL-2</i> /↑ <i>BAX</i> →↑ <i>ROS</i> /↓ $\Delta\Psi_m$	↓Mammosphere formation ↓Tumor growth	32319481	Ahir et al., 2020 [54]
miR-27a	(-)TNBC	<i>SLC7A11</i> <i>CTH</i> <i>NFE2L2</i>	↓ <i>xCT</i> , ↓ <i>CTH</i> , ↓ <i>NRF2</i> →↑ <i>ROS</i> , ↓autophagic flux	↓Mammosphere formation ↓ <i>CSC</i> markers ↑TNBC sensitivity to doxorubicin and paclitaxel	32066826	Ueda et al., 2020 [36]
miR-324	(-)TNBC	<i>ACK1</i>	↓ <i>ACK1</i> →↑ <i>ROS</i> → ↑DNA oxidative damage	↓Proliferation ↓Tumor growth	31751910	Zhang et al., 2019 [52]
miR-4485	(-)TNBC	<i>16S rRNA</i>	↓ <i>16S rRNA</i> →↓ <i>ETC</i> enzyme activity→↑ <i>ROS</i> /↓ $\Delta\Psi_m$	↑Cell death ↓Proliferation ↓Tumor growth	28220193	Sripada et al., 2017 [44]
let-7a	(-)TNBC	<i>SCD</i>	↓ <i>SCD</i> →↑ <i>OCR</i> →↑ <i>ROS</i>	↑ <i>SOD2</i> , <i>TXNRD1</i> , <i>HO-1</i> ↓Proliferation ↑Cell cycle arrest ↑TNBC sensitivity to doxorubicin	25669981	Serguienko et al., 2015 [42]
miR-373	(+)TNBC	<i>TXNIP</i>	↓ <i>TXNIP</i> →↑ <i>TRX</i> →↓ <i>ROS</i> →↑ <i>HIF-1α</i> →↑ <i>TWIST1</i> 1→↑miR-373	↑EMT ↑Migration and invasion ↑Tumor growth ↑Tumor metastasis	26196741	Chen et al., 2015 [53]
miR-200a	(-)TNBC	<i>KEAP1</i>	↓ <i>KEAP1</i> →nuclear translocation of <i>NRF2</i> →↑ <i>NQO1</i>	↑Antioxidant pathway ↓Anchorage-independent cell growth	21926171	Eades et al., 2011 [51]

(+): oncogenic; (-): tumor suppressor; “↑”: enhanced; “↓”: reduced; $\Delta\Psi_m$: mitochondrial membrane potential; *ACK1*: activated CDC42 kinase 1; *BAX*: Bcl-2-associated X protein; *BCL-2*: B cell lymphoma 2; *CTH*: cystathionine gamma-lyase; *CSCs*: cancer stem cells; *ETC*: electron transport chain; *HAX-1*: HCLS1-associated protein X-1; *HO-1*: heme oxygenase 1; *NQO1*: NAD(P)H quinone dehydrogenase 1; *NRF2* (encoded by *NFE2L2*): nuclear factor erythroid 2-related factor 2; *ROS*: reactive oxygen species; *SCD*: stearyl-CoA desaturase; *SOD2*: superoxide dismutase mitochondrial; *TRAIL*: tumor necrosis factor-related apoptosis-inducing ligand; *TNBCSC*: triple-negative breast cancer stem cell; *TRX*: thioredoxin; *TWIST1*: twist family BHLH transcription factor 1; *TXNIP*: thioredoxin-interacting protein; *TXNRD1*: thioredoxin reductase 1; *xCT* (encoded by *SLC7A11*): cystine/glutamate transporter.

miR34a [47]. More recently, Wang et al. demonstrated that miR-29a overexpression exerts inhibitory effect on proliferation, migration, and invasion of TNBC cells through targeting the anterior gradient 2 (*ARG2*)/*HIF-1 α* axis [28]. Furthermore, circular RNA circPVT1 was identified as a miR sponge, leading to suppressing the expression of miR-29a and promoting *in vivo* tumor growth [28].

In addition to glucose metabolism, some mitomiRs act toward fatty acid metabolism to exert inhibitory effect on TNBC. For example, miR-195 was shown to target acetyl-CoA carboxylase (*ACACA*), fatty acid synthase (*FASN*), and 3-hydroxy-3-methylglutaryl CoA reductase (*HMGCR*) to suppress epithelial-mesenchymal transition (EMT), proliferation, migration, and invasion [43]. Serguienko et al. have demonstrated that let-7a targets *SCD* (stearyl-CoA desaturase) to reduce cell proliferation and sensitivity to doxorubicin [42]. More recently, Chen et al. reported that miR-1291 targets estrogen-related receptor alpha (*ERR α*) to inhibit the expression level of carnitine palmitoyltransferase 1C (*CPT1C*), causing a decrease in cell proliferation *in vitro* and tumor growth *in vivo* [41].

With regard to amino acid metabolism, Ueda et al. demonstrated that miR-27a play a suppressive role over TNBC by disturbing glutamine/cystine dynamics. Specifically, miR-27a directly bind to UTR of cystine/glutamate transporter (*xCT*) and cystathionine gamma-lyase (*CTH*), whereby cystine uptake and production, respectively, are compromised, lead-

ing to a decrease in mammosphere formation and cancer stem cell markers as well as an increase in sensitivity to doxorubicin and paclitaxel [36]. On the other hand, some mitomiRs were shown to curb TNBC by impeding OXPHOS. miR-4485 and miR-663 have been identified to hinder mitochondrial function by direct binding to the UTR of mtDNA-encoded 16S rRNA and ubiquinol-cytochrome c reductase complex assembly factor 2 (*UQCC2*), respectively [44, 45].

In contrast, some reports have explored that a group of mitomiRs responsible for metabolic reprogramming can act to promote the development of TNBC. In this regard, miR-21 was shown to exert its function by targeting calcium-binding protein 39-like (*CAB39L*) and sestrin-1 (*SESN1*) to promote proliferation and invasion of TNBC [48]. Kim et al. have reported that miR-155 promotes glycolysis and growth of TNBC by targeting an axis comprising phosphoinositide 3-kinase regulatory subunit 1, forkhead box O, and c-MYC (*PI3R1-FOXO3a-cMYC* axis) [32]. A recent report conducted by Du et al. identified that miR-210 exerts a positive effect in glucose metabolism, lactate production, extracellular acidification rate (ECAR), proliferation, and starvation-induced apoptosis. The molecular underpinnings were found to lie in direct binding of miR-210 to *GPD1L* and *CYGB*, whereby *HIF-1 α* stabilization and p53 suppression can, respectively, be maintained [29]. An integrative network summarizing the roles and pathways of mitomiRs is illustrated in Figure 2.

TABLE 3: Roles and mechanisms of mitomiRs in cell apoptosis.

mitomiR	Function	Target gene	Mechanism of action	Effect on TNBC	PMID	Reference
miR-34a	(-)TNBC	BCL2	↓BCL-2→↑BAX	↑Apoptosis ↓Migration ↓Mammosphere formation ↓Tumor growth	32319481	Ahir et al., 2020 [54]
miR-224	(+)TNBC	CASP9	↓Caspase-9	↓Apoptosis ↑Proliferation ↑Migration ↑Invasion	30886656	Zhang et al., 2019 [60]
miR-125a/miR-181a	(-)TNBC	BCL2	↓BCL-2→↑BAX	↑Phospho-p53 ↑PARP cleavage ↑Apoptosis	31541355	Majzoub et al., 2019
miR-20b	(-)TNBC	VEGF	↓BCL-2→↑BAX →Caspase-9/3	↑Apoptosis ↓Proliferation ↓Migration ↓Invasion	28550685	Lu et al., 2018 [59]
miR-15/16	(-)TNBC	BMI1	↓BCL-2/↑BAX/↑BID →↓ΔΨm→↑caspase-9/3	↑Cell death ↓Proliferation ↓Migration	27596816	Patel et al., 2016 [58]
miR-223	(-)TNBC	HAX1	↓HAX-1	↑TRAIL-induced apoptosis of TNBCSC	27618431	Sun et al., 2016 [57]
miR-145	(-)TNBC	cIAP	↓cIAP→↑FADD→ ↑Caspase-8/3→↑tBID	↑TNF-α-induced apoptosis	26733177	Zheng et al., 2016 [56]
miR-101	(-)TNBC	MCL1	↓MCL-1→↓ΔΨm	↑Apoptosis ↓Proliferation ↓Tumor growth ↑TNBC sensitivity to paclitaxel	26036638	Liu et al., 2015 [55]

2-DG: 2-deoxy-D-glucose; ΔΨm: mitochondrial membrane potential; BAX: Bcl-2-associated X protein; BCL-2: B cell lymphoma 2; BID: BH3 interacting-domain death agonist; CASP9: caspase-9; cIAP: cellular inhibitor of apoptosis; FADD: Fas-associated protein with death domain; HAX-1: HCLS1-associated protein X-1; MCL-1: induced myeloid leukemia cell differentiation protein Mcl-1; PARP: poly ADP-ribose polymerase; tBID: truncated BH3 interacting-domain death agonist; TRAIL: tumor necrosis factor-related apoptosis-inducing ligand; TNBCSC: triple-negative breast cancer stem cell; VEGF: vascular endothelial growth factor.

3. Roles of mitomiRs in Redox Homeostasis and Cell Apoptosis

The increased demand for cellular ATP and accelerated oxidation of nutrient molecules trigger the generation of reactive oxygen species (ROS) derived from electron transport chain of mitochondria [49]. A moderate elevated ROS benefits cellular proliferation, whereas excessive ROS production can lead to oxidative damage to proteins, lipids, and DNA [50]. As such, intracellular ROS status plays a critical role in cell growth and survival. Indeed, a cluster of miRs functions to dictate the imbalance between the production of ROS and the activity of antioxidant defence system, resulting in the disruption of redox homeostasis and ultimately cancer cell apoptosis [22]. A study conducted by Eades et al. has demonstrated that miR-200a serves as repressor on TNBC cells by perturbing antioxidant defence mechanism [51]. Specifically, miR-200a directly targets Kelch-like ECH-associated protein 1 (KEAP1), leading to the NF-E2-related factor 2 (NRF2) stabilization and nuclear translocation to act forward the activation of Nrf2-dependent NAD(P)H-quinone oxidoreductase 1 (NQO1) gene transcription [51]. By targeting SCD, let-7a is able to alter fatty acid metabolism, leading to boosted mitochondrial activity and oxidative stress, as evidenced by an

increase in oxygen consumption rate (OCR), ROS expression level, and the expression level of superoxide dismutase 2 (SOD2), thioredoxin reductase 1 (TXRND1), and heme oxygenase 1 (HO-1) [42]. Likewise, miR-27a was shown to disrupt glutathione- (GSH-) associated antioxidant mechanism by targeting xCT, which mediates the uptake of cystine, a precursor for GSH biosynthesis [36]. miR-324 has been reported to induce ROS level through inhibiting a driver of tumor progression, activated CDC42 kinase 1 (ACK1) [52]. In contrast, miR-373 plays an anti-ROS role in TNBC by targeting thioredoxin-interacting protein (TXNIP), which functions to inhibit antioxidant protein thioredoxin (Trx) by interacting with its redox-specific active cysteine residues [53]. The ROS-suppressing hallmark of miR-373/TXNIP acted to promote HIF-1α/twist family BHLH transcription factor 1 (TWIST1) pathway, leading to increased invasive behaviour of TNBC cells [53].

Furthermore, some mitomiRs induce ROS production by targeting genes involved in the integrity of mitochondria. In this regard, miR-4485 was demonstrated to translocate to mitochondria to exert direct binding activity to mtDNA-encoded 16S rRNA, resulting in a decrease in electron transport chain (ETC) enzyme activity and mitochondrial ATP production, as well as an increase in expression level of

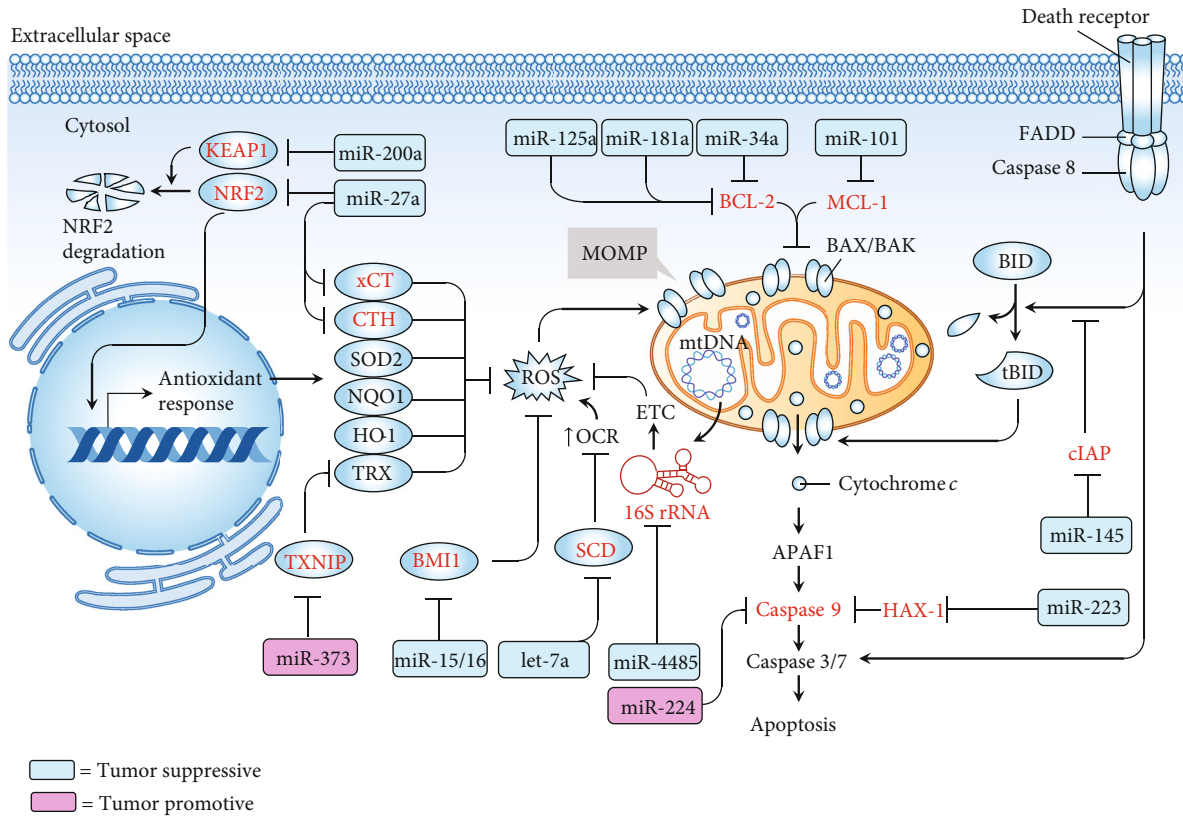


FIGURE 3: mitomiRs implicated in the regulatory network of redox homeostasis and the fate of apoptosis in the scenario of TNBC. Tumor-suppressive (blue rectangle) or tumor-promotive (pink rectangle) mitomiRs and their target genes (red) act on specific target genes (red). APAF1: apoptotic protease activating factor 1; BAX: Bcl-2-associated X protein; BCL-2: B cell lymphoma 2; BID: BH3 interacting-domain death agonist; BMI1: B cell-specific Moloney murine leukemia virus integration site 1; CTH: cystathionine gamma-lyase; cIAP: cellular inhibitor of apoptosis; ETC: electron transport chain; FADD: Fas-associated protein with death domain; HAX-1: HCLS1-associated protein X-1; HO-1: heme oxygenase 1; MCL-1: induced myeloid leukemia cell differentiation protein Mcl-1; MOMP: mitochondrial outer membrane permeabilization; mtDNA: mitochondrial DNA; NQO1: NAD(P)H quinone dehydrogenase 1; NRF2: nuclear factor erythroid 2-related factor 2; OCR: oxygen consumption rate; SCD: stearoyl-CoA desaturase; ROS: reactive oxygen species; SOD2: superoxide dismutase mitochondrial; tBid: truncated BH3 interacting-domain death agonist; TRAIL: tumor necrosis factor-related apoptosis-inducing ligand; TRX: thioredoxin; TWIST1: twist family BHLH transcription factor 1; TXNIP: thioredoxin-interacting protein; TXNRD1: thioredoxin reductase 1; xCT (encoded by SLC7A11): cystine/glutamate transporter.

ROS [44]. The tumor-suppressive effect *in vivo* was verified by overexpression of miR-4485 in TNBC cells [44]. In addition, Ahir et al. recently identified that miR-34a is implicated in effectively suppressing growth and mammosphere formation of TNBC [54]. The inhibitory role of miR-34a on B cell lymphoma 2 (BCL-2) permits the formation of permeabilization pore on the outer membrane of the mitochondria (OMM), promoting the intracellular ROS production [54]. Table 2 summarizes the mitomiRs acting toward the regulation of redox homeostasis and the biological roles and mechanisms in TNBC.

Several lines of study have revealed a group of mitomiRs modulate the carcinogenesis and sensitivity to drugs of TNBC by targeting genes implicated in apoptotic signaling. Liu et al. have demonstrated that miR-101 play a positive role in the induction of TNBC apoptosis by targeting induced myeloid leukemia cell differentiation protein Mcl-1 (MCL-1), a prosurvival member of the Bcl-2 family [55]. Overexpression of miR-101 was shown to inhibit tumor growth and sensitize cells to paclitaxel-induced apoptosis [55]. Sim-

ilarly, Zheng et al. demonstrated that miR-145 has a promotive role in receptor-interacting protein Fas-associated protein with death domain caspase-8 (RIP1-FADD-casp8) apoptosis signaling induced by TNF- α [56]. By targeting cellular inhibitor of apoptosis (cIAP1), miR-145 can exert TNBC-suppressive function, leading to the activation of the extrinsic pathway, whereby activated casp8 act to cleave BH3 interacting-domain death agonist (BID) to initiate the mitochondrial apoptotic pathway [56]. miR-223 has been shown to specifically suppress the expression of HCLS1-associated protein X-1 (HAX-1), an antiapoptotic protein that inhibits the activation of caspase-9 [57]. miR-223 overexpression potentiated proapoptotic effect induced by TNF-related apoptosis-inducing ligand (TRAIL) over triple-negative breast cancer stem cells (TNBCSCs) [57]. Patel et al. revealed that miR-15a/miR-16 overexpression in TNBC cells results in increased intrinsic pathway of apoptosis through direct of B cell-specific Moloney murine leukemia virus integration site 1 (BMI1), an oncogene involving mitochondrial homeostasis [58]. miR-20b was shown to target

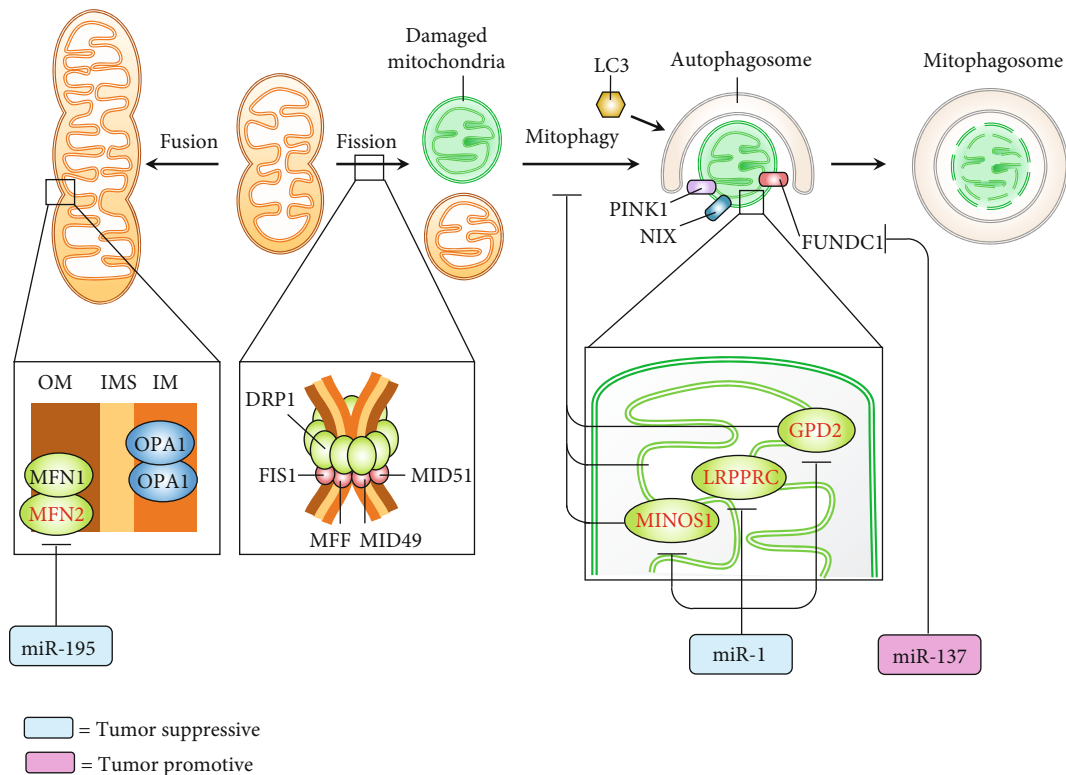


FIGURE 4: mitomiRs (miR-195, miR-1, and miR-137) regulate mitochondrial quality control machinery, e.g., mitochondrial dynamics and mitophagy. Tumor-suppressive (blue rectangle) or tumor-promotive (pink rectangle) mitomiRs and their target genes (red). DRP1: dynamin-related protein 1; FIS1: mitochondrial fission 1 protein; FUNDC1: FUN14 domain containing 1; GPD2: glycerol-3-phosphate dehydrogenase 2; LC3: microtubule-associated proteins 1A/1B light chain 3B; LDH: lactate dehydrogenase; LRPPRC: leucine-rich pentatricopeptide-repeat containing; MCU: mitochondrial calcium uniporter; MFF: mitochondrial fission factor; MFN: mitofusins; MID49/51: mitochondrial dynamics protein MID49/51; MINOS1: mitochondrial inner membrane organizing system 1; NIX: NIP-3-like protein X; OPA1: optic atrophy 1; PINK1: PTEN-induced kinase 1.

VEGF and cause decreased BCL-2 and increased BAX and activation of cell apoptosis, resulting in an inhibitory effect on proliferation, migration, and invasion of TNBC cells [59]. Both groups, Ahir et al. and Majzoub et al., have recently shown that BCL-2 is a specific target of miR-34a [54] and miR-125a/miR-181a [55]. These mitomiRs can exert suppressive effect on TNBC cells by inducing apoptosis as well as reducing cell migration [55] and tumor growth [54]. Conversely, miR-224 has been reported to be tumor-promotive in TNBC. Zhang et al. showed that miR-224 provides apoptotic resistance and enhances proliferation, migration, and invasion by targeting caspase-9 [60]. Collectively, the recent understandings of mitomiRs in targeting apoptosis pathway in the context of TNBC are listed in Table 3. The schematic sophisticated network encompassing tumor-suppressive/tumor-promotive mitomiRs targeting molecules central to redox homeostasis and apoptosis is illustrated in Figure 3.

4. Roles of mitomiRs in Regulating Mitochondrial Dynamics and Mitophagy

Mitochondria are highly dynamic organelles. The dynamic properties comprising fusion, fission, and degradation not only play critical role for their optimal function in energy gen-

eration but also have profound impact on human diseases, including cancer [61]. The multiple events of mitochondrial fusion require hydrolysis of GTP and mitochondrial membrane potential [62]. Mitofusins 1 and 2 (MFN1/2) are both GTP-hydrolyzing enzymes of the dynamin superfamily. They are located on the outer membrane of mitochondria (OMM) and required for OMM fusion [63]. The fusion of inner membrane of mitochondria (IMM) is mediated by another member of the dynamin superfamily, optic atrophy 1 (OPA1), located in IMM [64]. On the other hand, the mitochondrial fission largely relied on the activity of dynamin-related protein 1 (DRP1), a GTP-hydrolyzing enzyme [65, 66]. DRP1 is recruited from the cytosol to associate with corresponding receptors residing on OMM, including mitochondrial fission 1 protein (FIS1), mitochondrial fission factor (MFF), mitochondrial dynamics protein MID49 (MID49), and mitochondrial dynamics protein MID51 (MID51) [67–69]. Mitochondrial fission acts to promote segregation of damaged mitochondria, which subsequently facilitates mitochondrial fragments of the appropriate size for engulfment by autophagosomes. The degradation of dysfunctional mitochondria by autophagy, or mitophagy, is a major mechanism for mitochondrial quality control [61].

More recently, the emerging role of mitomiRs in TNBC progression via regulating the mitochondrial quality control

TABLE 4: Roles and mechanisms of mitomiRs in mitochondrial homeostasis on dynamics, mitophagy, calcium transport, and mtDNA maintenance.

mitomiR	Function	Target gene	Mechanism of action	Outcome	PMID	Reference
<i>Mitochondrial dynamics</i>						
miR-195	(-)TNBC	MFN2	↓MFN2 ↓OPA1 ↑DRP1	↑Mitochondrial fission ↓OCR ↓Mitochondrial ATP ↑ROS ↑Apoptosis	30932749	Purohit et al., 2019 [70]
<i>Mitophagy</i>						
miR-137	(+)BCSC	FUNDC1	↓FUNDC1/↓NIX/↓LC3-II →↓Mitophagy	↑Mitochondrial biogenesis ↓ROS ↑ATP production ↓Apoptosis	32945512	Hu et al., 2020 [72]
miR-1	(-)BCSC	MINOS1 GPD2 LRPPRC	↓MINOS1/↓GPD2/↓LRPPRC →↑Disorganized cristae →↑PINK1→↑LC3-II →↑Mitophagy	Cell cycle arrest at G0/G1 ↓Tumor growth	31765945	Zhang et al., 2019 [71]
<i>Mitochondrial calcium transport</i>						
miR-4488	(-)TNBC	CX3CL1	↓MCU (TNBC)→ ↑miR-4488 EVs (TNBC)→ ↓CX3CL1 (ECs)	↓Angiogenesis ↓Tumor metastasis ↑Survival time of mice	33067576	Zheng et al., 2020 [74]
miR-340	(-)TNBC	MCU	↓MCU→↓[Ca ²⁺] _m →↓LDH	↓Glucose uptake ↓ATP production ↓Lactate production ↓Migration ↓Tumor metastasis	29137386	Yu et al., 2017 [37]
miR-195	(-)TNBC	CYP27b1	↑[Ca ²⁺] _m ↑[Ca ²⁺] _C ↓ΔΨ _m	↓EMT ↓Proliferation ↓Migration ↓Invasion	26632252	Singh et al., 2015 [43]
<i>mtDNA maintenance</i>						
miR-499a	(+)TNBCSC	POLB	↑POLB→↑mtDNA stability	↑Tumorigenic genes ↑CSC genes ↑Proliferation	33278391	Manda et al., 2020 [76]
miR-128	(-)TNBC	INSR, IRS1	↓INSR/↓INS1→↓mtDNA content	↓Mitochondrial bioenergetics ↓Proliferation ↓Tumor growth	29116653	Xiao et al., 2018 [33]
miR-199a	(-)TNBC	TFAM	↓TFAM→↓mtDNA content	↑Cisplatin-induced apoptosis ↓Proliferation	28126676	Fan et al., 2017 [75]
miR-4485	(-)TNBC	16S rRNA	↓16S rRNA→↓ETC enzyme activity→↓mitochondrial ATP	↑Cell death ↓Proliferation ↓Tumor growth	28220193	Sripada et al., 2017 [44]

(+): oncogenic; (-): tumor suppressor; “↑”: enhanced; “↓”: reduced; ΔΨ_m: mitochondrial membrane potential; BCSC: breast cancer stem cell; ↑[Ca²⁺]_C: cytosolic calcium; [Ca²⁺]_m: mitochondrial calcium; CX3CL1: C-X3-C motif chemokine ligand 1; CYP27B1: cytochrome P450 family 27, subfamily B, polypeptide 1; DRP1: dynamin-related protein 1; ECs: endothelial cells; EVs: extracellular vesicles; FUNDC1: FUN14 domain containing 1; GPD2: glycerol-3-phosphate dehydrogenase 2; INSR: insulin receptor; IRS1: insulin receptor substrate 1; LC3: microtubule-associated proteins 1A/1B light chain 3B; LDH: lactate dehydrogenase; LRPPRC: leucine-rich pentatricopeptide-repeat containing; MCU: mitochondrial calcium uniporter; MFN: mitofusin; MINOS1: mitochondrial inner membrane organizing system 1; NIX: NIP-3-like protein X; OPA1: optic atrophy 1; PINK1: PTEN-induced kinase 1; POLB: DNA polymerase beta; ROS: reactive oxygen species; TFAM: mitochondrial transcription factor A; UQCRC2: ubiquinol-cytochrome C reductase core protein 2.

machinery has been revealed (Figure 4). In this regard, Purohit et al. reported that miR-195 exerts anti-TNBC effect by targeting MFN2. The dysregulated mitochondrial dynamics was evidenced by decreased MFN2 and OPA1, increased

DRP1, and enhanced mitochondrial fission. miR-195 also led to declined mitochondrial OXPHOS and bioenergetics and increased ROS level and cell apoptosis [70]. Zhang et al. demonstrated that overexpression of miR-1 exerts a

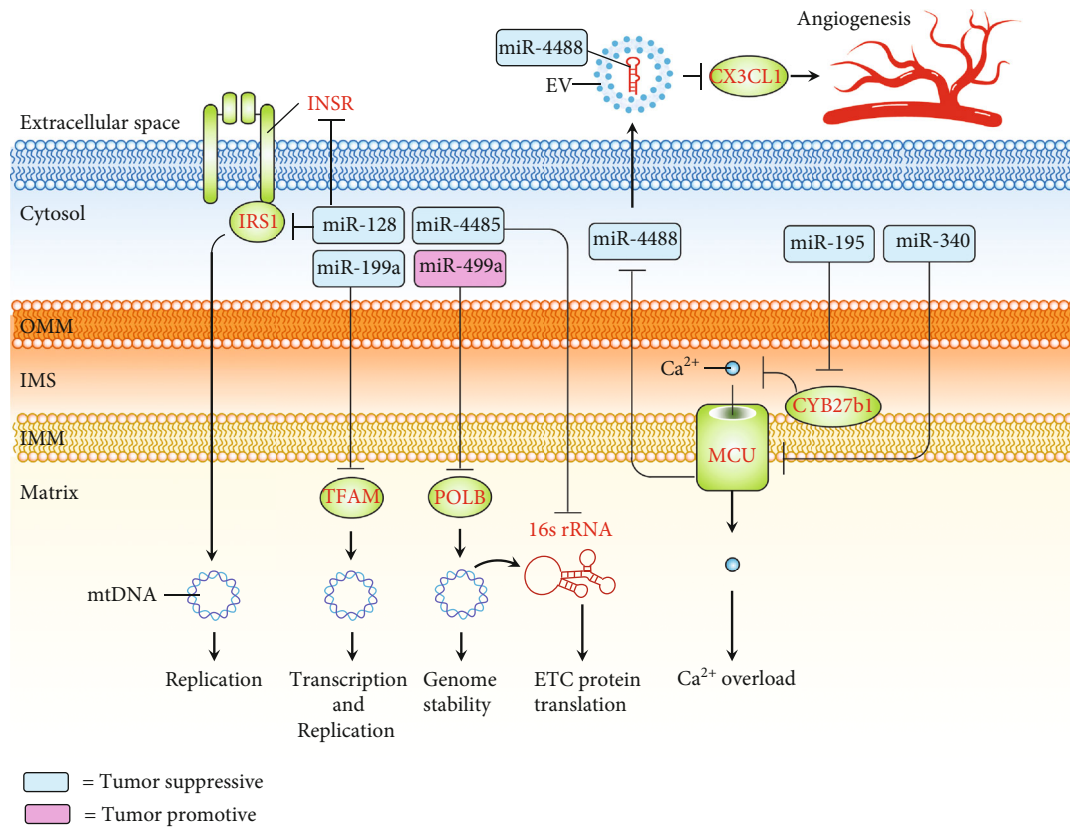


FIGURE 5: Schematic pipeline depicting mitomiRs that exert tumor-suppressive or tumor-promotive role on TNBC through acting on mechanisms involved in mtDNA maintenance or mitochondrial calcium uptake. Tumor-suppressive (blue rectangle) or tumor-promotive (pink rectangle) mitomiRs and their target genes (red). CX3CL1: C-X3-C motif chemokine ligand 1; CYP27B1: cytochrome P450 family 27, subfamily B, polypeptide 1; INSR: insulin receptor; IRS1: insulin receptor substrate 1; MCU: mitochondrial calcium uniporter; mtDNA: mitochondrial DNA; POLB: DNA polymerase beta; ROS: reactive oxygen species; TFAM: mitochondrial transcription factor A.

tumor-suppressive effect by simultaneously targeting mitophagy-associated genes including MINOS1 (mitochondrial inner membrane organizing system 1), GPD2 (glycerol-3-phosphate dehydrogenase 2), and LRPPRC (leucine-rich pentatricopeptide-repeat containing), leading to an induction of mitophagy in breast cancer stem cells [71]. On the other hand, Hu et al. showed that miR-137 play a tumor-promotive role in breast cancer stem cells [72]. By direct targeting FUN14 domain containing 1 (FUNDC1), miR-137 repressed the mitophagy by reducing the expression of FUNDC1, NIP-3-like protein X (NIX), and LC3-II, resulting in an increase in mitochondrial biogenesis and bioenergetics and a decrease in ROS level and cell apoptosis [72]. Table 4 highlights the mitomiRs involved in mitochondrial dynamic and mitophagy.

5. mitomiRs and Calcium Transport

A growing body of literature has revealed the implications of mitochondrial calcium uptake in tumorigenesis [73]. Indeed, some of the studies unravelled the roles of a cluster of mitomiRs in inhibiting TNBC progression by disturbing mitochondrial calcium uptake. Table 4 outlines the recent findings regarding this issue. Specifically, Singh et al. demon-

strated that miR-195 acts toward increased mitochondrial calcium by targeting cytochrome P450 family 27, subfamily B, polypeptide 1 (CYP27B1), leading to dysfunctional mitochondria as evidenced by loss of mitochondrial membrane potential. They confirmed its antitumor role by showing that overexpression of miR-195 impedes EMT, proliferation, migration, and invasion of TNBC cells [43]. Yu et al. showed that miR-340 negatively regulates mitochondrial calcium uniporter (MCU) by direct interacting with MCU 3'UTR. Downregulated MCU was shown to inhibit tumor Warburg effect, leading to a significant decrease in cell migration and invasion *in vitro* and lung metastasis *in vivo* [37]. Interestingly, Zheng et al. revealed that knockdown of MCU induces generation and secretion of miR-4488-containing extracellular vesicles (EVs) from TNBC cells. The miR-4488-containing EVs uptaken by endothelial cells acted to target an angiogenic activator C-X3-C motif chemokine ligand 1 (CX3CL1), resulting in suppressed angiogenic activity. Furthermore, the administration of miR-4488-containing EVs inhibited tumor metastasis and increased survival time of tumor-bearing mice [74]. The schematic pipeline regarding the roles and mechanisms of mitomiRs directing at mitochondrial calcium balance is illustrated in Figure 5.

TABLE 5: Clinicopathological relevance of mitomiRs.

mitomiRs	Specimen	Expression	Clinical relevance	PMID	Reference
miR-4488	Serum EVs	↓	Low expression in TNBC patients	33067576	Zheng et al., 2020 [74]
miR-21	Serum	↓	Decreased level in BC patients after metformin treatment	28698800	Pulito et al., 2017 [48]
miR-34a	Serum Tissue	↓	Low expression predicts poor OS of TNBC patients	31616515 31897330	Li et al., 2019 [47] Kim et al., 2019 [77]
miR-29a	Tissue	↓	Low expression predicts poor OS of BC patients	33223849	Wang et al., 2020 [28]
miR-1	Tissue	↓	Low expression in BC patients	31765945	Zhang et al., 2019 [71]
miR-324	Tissue	↓	Low expression correlated with large tumor size and advanced TNM stage (III-IV) of BC patients	31751910	Zhang et al., 2019 [52]
miR-342	Tissue	↓	Low expression predicts poor OS of TNBC patients	30115973	Romero-Cordoba et al., 2018 [34]
miR-128	Tissue	↓	Low expression predicts poor OS and DFS of TNBC patients	29116653	Xiao et al., 2018 [33]
miR-125b	Tissue	↓	Low expression in BC tissue and TNBC cell line	29434858	Hu et al., 2018
miR-4485	Tissue	↓	Low expression in BC patients	28220193	Sripada et al., 2017 [44]
miR-663	Tissue	↓	Low expression predicts poor OS of BC patients	29066618	Carden et al., 2017 [45]
miR-195	Tissue	↓	Low expression in TNBC patients	29183284	Qattan et al., 2017 [79]
miR-148a, miR-152	Tissue	↓	Low expression in TNBC tissue compared to adjacent normal tissue	25703326	Xu et al., 2015 [46]
miR-101	Tissue	↓	Low expression associated with advanced TNM stage (III-IV) and lymph node infiltration of TNBC patients	26036638	Liu et al., 2015 [55]
miR-195	Plasma	↑	High expression in TNBC patients	29183284	Qattan et al., 2017 [79]
miR-210	Plasma	↑	High expression in TNBC patients	29183284	Qattan et al., 2017 [79]
miR-16	Plasma	↑	High expression in TNBC patients	29183284	Qattan et al., 2017 [79]
miR-221	Serum Tissue	↑	High expression in serum and tumor tissue of BC patients	26503209	Ye et al., 2016 [80]
miR-27a	Serum	↑	High expression in BC patients and in TNBC cell line	26662313	Zhou et al., 2016 [81]
miR-155	Tissue	↑	High expression in tumor tissue indicates elevated glucose uptake of TNBC patients	29527004	Kim et al., 2018 [32]
miR-210	Tissue	↑	High expression in TNBC patients	29183284	Qattan et al., 2017 [79]
miR-16	Tissue	↑	High expression in TNBC patients	29183284	Qattan et al., 2017 [79]
miR-373	Tissue	↑	High expression predicts lymph node metastasis of BC patients	26196741	Chen et al., 2015 [53]

“↑”: enhanced; “↓”: reduced; BC: breast cancer; DFS: disease-free survival; EVs: extracellular vesicles; OS: overall survival; TNBC: triple-negative breast cancer; TNM: tumor, node, metastasis.

6. mitomiRs and mtDNA Maintenance

A line of research identified a group of mitomiRs functioning to modulate the maintenance of mtDNA in the context of TNBC (Table 4). Sripada et al. showed that miR-4485 suppresses tumor growth and cell proliferation of TNBC by targeting 16S rRNA encoded by mtDNA [44]. Fan et al. demonstrated that miR-199a directly targets mitochondrial transcription factor A (TFAM) and causes a significant decrease in mtDNA content, leading to reduced proliferation and potentiate proapoptotic effect induced by cisplatin [75]. In addition, Xiao et al. reported that miR-128 exerts a mtDNA-reducing effect through targeting INSR/IRS1, resulting in a decrease in mitochondrial bioenergetics, proliferation, and tumor growth of TNBC [33]. More recently, miR-499a was identified as a driver of TNBCSC development. In this regard, Manda et al. showed that miR-499a acts to mediate the suppression of DNA polymerase beta (POLB), which plays a master role in the repair and genome stability

of mtDNA [76]. We summarized the mechanisms of mitomiRs acting on mtDNA maintenance of TNBC in Figure 5.

7. Prognostic Value, Therapeutic Implications, and Future Perspective

The expression of several mitomiRs can potentially be regarded as predictive, diagnostic, and prognostic biomarkers for TNBC (Table 5). A cluster of low-expressed mitomiRs is identified in tumor tissue [28, 33, 34, 44–47, 52, 55, 71, 77–79], while some of them are high-expressed [32, 53, 79, 80]. Of note, some mitomiRs showed clinical significance in predicting disease outcome. There are a group of mitomiRs enabling predicting survival time [33, 34, 45, 47, 77], while another set of them indicates advanced stage or metastasis [52, 53, 55]. Importantly, circulating mitomiRs identified as relevant biomarkers provide an opportunity to establish a rapid clinical panel which can be less invasive and more accessible [47, 48, 74, 79–81].

TABLE 6: mitomiR-based therapeutics and targeting mechanisms in preclinical study of TNBC.

Approach/reagent	Effecting mitomiR	Experimental model	PMID	Reference
<i>Metabolic reprogramming</i>				
siRNA-circPVT1	↑miR-29a	<i>In vivo, in vitro</i>	33223849	Wang et al., 2020 [28]
Lentivirus-miR-128	↑miR-128	<i>In vivo, in vitro</i>	29116653	Xiao et al., 2018 [33]
Small molecule (metformin)	↓miR-21	<i>In vitro, in vivo</i>	28698800	Pulito et al., 2017 [48]
<i>Apoptosis</i>				
Nanoparticle-loaded miR-34a	↑miR-34a	<i>In vivo, ex ovo, in vitro</i>	32319481	Ahir et al., 2020 [54]
Nanoparticle-loaded anti-miR-10b	↓miR-10b	<i>In vivo, ex ovo, in vitro</i>	32319481	Ahir et al., 2020 [54]
Cisplatin+thiosemicarbazone compound 4	↑miR-125a, ↑miR-181a	<i>In vitro</i>	31541355	Majzoub et al., 2019
shRNA-lncCAMTA1	↑miR-20b	<i>In vitro</i>	28550685	Lu et al., 2018 [59]
Anti-miR-221	↓miR-221	<i>In vitro</i>	26503209	Ye et al., 2016 [80]
<i>Redox signaling</i>				
Natural product (ursolic acid)	↓miR-499a	<i>Ex ovo, in vitro</i>	33278391	Manda et al., 2020 [76]
Physical agent (ultrasound)	↑miR-200c	<i>In vitro</i>	32313093	Shi et al., 2020 [85]
Natural product (parthenolide)	↑miR-29b	<i>In vitro</i>	31313842	De Blasio, 2019 [84]
shRNA-LINC00963	↑miR-324	<i>In vitro, in vivo</i>	31751910	Zhang et al., 2019 [52]
Adenovirus-MDA-7	↓miR-221	<i>In vitro, in vivo</i>	30842276	Pradhan et al., 2019 [82]
CuO-Nw-FA	↑miR-425	<i>In vivo, ex ovo, in vitro</i>	26520043	Ahir et al., 2016 [83]
Histone deacetylase inhibitor (SAHA)	↑miR-200a	<i>In vitro</i>	21926171	Eades et al., 2011 [51]
<i>Mitochondrial calcium transport</i>				
Exosome	↑miR-4488	<i>In vivo, in vitro</i>	33067576	Zheng et al., 2020 [74]

“↑”: enhanced; “↓”: reduced; circPVT1: circular RNA PVT1; CuO-Nw-FA: copper oxide nanowire conjugated with folic acid; lncRNA: long noncoding RNA; MITF: melanogenesis-associated transcription factor; SAHA: suberoylanilide hydroxamic acid.

TABLE 7: Interventional clinical trials for mitomiRs.

Intervention	Effecting mitomiR	Cancer type	Trial number	Phase (status)
<i>Metabolic reprogramming</i>				
Cobomarsen (MRG-106)	↓miR-155	T-cell lymphoma/mycosis fungoides	NCT03713320; NCT03837457	Phase 2 (terminated)
TargomiRs	↑miR-16	Mesothelioma NSCLC	NCT02369198	Phase 1 (completed)
<i>Apoptosis</i>				
MRX-34	↑miR-34a	Liver cancer Lymphoma SCLC NSCLC Melanoma Multiple myeloma Renal cell carcinoma	NCT01829971	Phase 1 (terminated)

“↑”: enhanced; “↓”: reduced; NSCLC: non-small-cell lung cancer; SCLC: small cell lung cancer.

Recent insights into therapeutic approaches in preclinical model pave new paths to potential treatments for TNBC (Table 6). These strategies exert treatment effect by targeting various aspects implicated in mitochondrial homeostasis, including metabolic reprogramming, apoptosis, redox signaling, and mitochondrial calcium transport. Most common approaches employed genetic manipulation, including siRNA, shRNA, and antisense for mitomiR inhibition [28, 52, 59, 80]. Although some approaches conducted by virus-based gene delivery demonstrated treatment efficiency [33, 82], the potential adverse effects to humans must be taken into consideration

in the future should they be registered for clinical trials. The use of chemotherapeutics combo could be promising but still need more advanced study, such as *in vivo* model (31541355). Nanoparticle-loaded mitomiRs provide a potential way to achieve highly efficient delivery into tumor (32319481). Interestingly, Ahir et al. demonstrated a mitomiR-promoting nanotechnology using copper oxide nanowire fabricated with folic acid (CuO-Nw-FA) that enables enhanced cellular uptake in TNBC cells without imparting significant toxicity in normal cellular system [83]. Oral hypoglycemic drug [48], natural products [76, 84],

epigenetic modifier [51], and physical agent [85] have been shown to effectively inhibit TNBC cell proliferation. More notably, the notion of using mitomiR-containing EVs may offer a treatment strategy with advantage of high purity, specificity, and biodistribution as less safety concern [74]. Of note, some clinical trials utilizing mitomiR-based treatment for several types of cancer have been registered (Table 7). Unfortunately, due to the occurrence of immune-related serious adverse events, the trial using miR-34a was terminated (NCT01829971). The termination of anti-miR-155-based drug is due to business reasons, but not concerns regarding safety or lack of efficacy (NCT03713320). The miR-26-based approach, TargomiRs, may be a next glimmer of hope for cancer treatment. The first-in-human, phase 1 trial of TargomiR patients with malignant pleural mesothelioma has completed. The results showed acceptable safety profile and early signs of activity of TargomiRs in patients [86], supporting the feasibility of further study.

8. Conclusions

Due to the absence of unambiguous molecular targets for TNBC, its clinical treatment is still a challenging issue. The hallmarks of altered metabolism and mitochondrial fitness in TNBC provide an opportunity for advancing new diagnostic/prognostic tools and therapeutic approaches. mitomiRs are a subgroup of microRNAs that closely regulate mitochondrial functionality by targeting genes present in the cytosol or mitochondria. Growing evidence has elucidated its effectiveness and mechanism of action in the context of TNBC, making mitomiRs an emerging field of study. Indeed, the predictive, prognostic, and diagnostic value of a number of mitomiRs has been revealed. There is increasing novel mitomiR-based therapeutics aiming for efficient inhibition on tumor growth. It is important to note that some mitomiRs were qualified for the early stage of clinical trial. In spite of these inspiring advances, there is still a need to gain deeper insight into mitomiR-dictated mechanisms with respect to mitochondrial homeostasis, to develop accessible prediction panel with satisfactory sensitivity/specificity and to explore interventions suitable for clinical use. To summarize, mitomiRs represent attractive therapeutic targets for the treatment of TNBC.

Data Availability

No data were used to support this study.

Conflicts of Interest

The authors declare that there is no conflict of interest regarding the publication of this paper.

Acknowledgments

The authors would like to thank James Waddell for his assistance with the proofreading and revision of this article. This research was funded by the Ministry of Science and Technology, Taiwan (MOST 106-2314-B-442-001-MY3, MOST 109-

2314-B-442-001, and MOST 109-2314-B-075B-002), National Health Research Institutes (NHRI-109BCCO-MF-202015-01), and Show Chwan Memorial Hospital, Taiwan (SRD-109023, SRD-109024, SRD-109025, and RD107063).

References

- [1] C. Fitzmaurice, D. Abate, N. Abbasi et al., "Global, regional, and national cancer incidence, mortality, years of life lost, years lived with disability, and disability-adjusted life-years for 29 cancer groups, 1990 to 2017," *JAMA Oncology*, vol. 5, no. 12, pp. 1749–1768, 2019.
- [2] F. Bray, J. Ferlay, I. Soerjomataram, R. L. Siegel, L. A. Torre, and A. Jemal, "Global cancer statistics 2018: GLOBOCAN estimates of incidence and mortality worldwide for 36 cancers in 185 countries," *CA: a Cancer Journal for Clinicians*, vol. 68, no. 6, pp. 394–424, 2018.
- [3] L. A. Torre, R. L. Siegel, E. M. Ward, and A. Jemal, "Global cancer incidence and mortality rates and trends—an update," *Cancer Epidemiology, Biomarkers & Prevention*, vol. 25, no. 1, pp. 16–27, 2016.
- [4] A. Goldhirsch, W. C. Wood, A. S. Coates, R. D. Gelber, B. Thurlimann, and H. J. Senn, "Strategies for subtypes—dealing with the diversity of breast cancer: highlights of the St Gallen International Expert Consensus on the Primary Therapy of Early Breast Cancer 2011," *Annals of Oncology*, vol. 22, no. 8, pp. 1736–1747, 2011.
- [5] F. Fabbri, S. Salvi, and S. Bravaccini, "Know your enemy: genetics, aging, exposomic and inflammation in the war against triple negative breast cancer," *Seminars in Cancer Biology*, vol. 60, pp. 285–293, 2020.
- [6] A. Angius, P. Cossu-Rocca, C. Arru et al., "Modulatory role of microRNAs in triple negative breast cancer with basal-like phenotype," *Cancers*, vol. 12, no. 11, p. 3298, 2020.
- [7] N. Harbeck, F. Penault-Llorca, J. Cortes et al., "Breast cancer," *Nature Reviews. Disease Primers*, vol. 5, no. 1, p. 66, 2019.
- [8] M. Bonotto, L. Gerratana, E. Poletto et al., "Measures of outcome in metastatic breast cancer: insights from a real-world scenario," *The Oncologist*, vol. 19, no. 6, pp. 608–615, 2014.
- [9] J. D. Brenton, L. A. Carey, A. A. Ahmed, and C. Caldas, "Molecular classification and molecular forecasting of breast cancer: ready for clinical application?," *Journal of Clinical Oncology*, vol. 23, no. 29, pp. 7350–7360, 2005.
- [10] A. A. Jitariu, A. M. Cimpean, D. Ribatti, and M. Raica, "Triple negative breast cancer: the kiss of death," *Oncotarget*, vol. 8, no. 28, pp. 46652–46662, 2017.
- [11] G. Bianchini, J. M. Balko, I. A. Mayer, M. E. Sanders, and L. Gianni, "Triple-negative breast cancer: challenges and opportunities of a heterogeneous disease," *Nature Reviews. Clinical Oncology*, vol. 13, no. 11, pp. 674–690, 2016.
- [12] A. K. Conlin and A. D. Seidman, "Taxanes in breast cancer: an update," *Current Oncology Reports*, vol. 9, no. 1, pp. 22–30, 2007.
- [13] R. M. Andrews, I. Kubacka, P. F. Chinnery, R. N. Lightowlers, D. M. Turnbull, and N. Howell, "Reanalysis and revision of the Cambridge reference sequence for human mitochondrial DNA," *Nature Genetics*, vol. 23, no. 2, p. 147, 1999.
- [14] S. W. Tait and D. R. Green, "Mitochondrial regulation of cell death," *Cold Spring Harbor Perspectives in Biology*, vol. 5, no. 9, 2013.

- [15] T. Rodrigues and L. S. Ferraz, "Therapeutic potential of targeting mitochondrial dynamics in cancer," *Biochemical Pharmacology*, vol. 182, p. 114282, 2020.
- [16] A. Reda, A. Refaat, A. A. Abd-Rabou et al., "Role of mitochondria in rescuing glycolytically inhibited subpopulation of triple negative but not hormone-responsive breast cancer cells," *Scientific Reports*, vol. 9, no. 1, p. 13748, 2019.
- [17] G. J. Goodall and V. O. Wickramasinghe, "RNA in cancer," *Nature Reviews. Cancer*, vol. 21, no. 1, pp. 22–36, 2021.
- [18] R. W. Carthew and E. J. Sontheimer, "Origins and mechanisms of miRNAs and siRNAs," *Cell*, vol. 136, no. 4, pp. 642–655, 2009.
- [19] K. Saito, A. Ishizuka, H. Siomi, and M. C. Siomi, "Processing of pre-microRNAs by the Dicer-1-Loquacious complex in *Drosophila* cells," *PLoS Biology*, vol. 3, no. 7, article e235, 2005.
- [20] S. Li, S. L. Lian, J. J. Moser et al., "Identification of GW182 and its novel isoform TNGW1 as translational repressors in Ago2-mediated silencing," *Journal of Cell Science*, vol. 121, no. 24, pp. 4134–4144, 2008.
- [21] S. Bandiera, S. Ruberg, M. Girard et al., "Nuclear outsourcing of RNA interference components to human mitochondria," *PLoS One*, vol. 6, no. 6, article e20746, 2011.
- [22] C. Lu, D. Zhou, Q. Wang et al., "Crosstalk of microRNAs and oxidative stress in the pathogenesis of cancer," *Oxidative Medicine and Cellular Longevity*, vol. 2020, Article ID 2415324, 13 pages, 2020.
- [23] M. A. Ortega, O. Fraile-Martinez, L. G. Guijarro et al., "The regulatory role of mitochondrial microRNAs (MitomiRs) in breast cancer: translational implications present and future," *Cancers*, vol. 12, no. 9, p. 2443, 2020.
- [24] P. K. Purohit and N. Saini, "Mitochondrial microRNA (MitomiRs) in cancer and complex mitochondrial diseases: current status and future perspectives," *Cellular and Molecular Life Sciences*, vol. 78, no. 4, pp. 1405–1421, 2021.
- [25] R. J. DeBerardinis and N. S. Chandel, "Fundamentals of cancer metabolism," *Science Advances*, vol. 2, no. 5, article e1600200, 2016.
- [26] N. N. Pavlova and C. B. Thompson, "The emerging hallmarks of cancer metabolism," *Cell Metabolism*, vol. 23, no. 1, pp. 27–47, 2016.
- [27] W. H. Koppenol, P. L. Bounds, and C. V. Dang, "Otto Warburg's contributions to current concepts of cancer metabolism," *Nature Reviews. Cancer*, vol. 11, no. 5, pp. 325–337, 2011.
- [28] J. Wang, K. Huang, L. Shi, Q. Zhang, and S. Zhang, "<p>CircPVT1 promoted the progression of breast cancer by regulating MiR-29a-3p-mediated AGR2-HIF-1 α pathway</p>," *Cancer Management and Research*, vol. - Volume 12, pp. 11477–11490, 2020.
- [29] Y. Du, N. Wei, R. Ma, S. Jiang, and D. Song, "A miR-210-3p regulon that controls the Warburg effect by modulating HIF-1 α and p53 activity in triple-negative breast cancer," *Cell Death & Disease*, vol. 11, no. 9, p. 731, 2020.
- [30] Y. He, F. Deng, S. Zhao et al., "Analysis of miRNA-mRNA network reveals miR-140-5p as a suppressor of breast cancer glycolysis via targeting GLUT1," *Epigenomics*, vol. 11, no. 9, pp. 1021–1036, 2019.
- [31] A. Yao, Y. Xiang, Y. R. Si et al., "PKM2 promotes glucose metabolism through a let-7a-5p/Stat3/hnRNP-A1 regulatory feedback loop in breast cancer cells," *Journal of Cellular Biochemistry*, vol. 120, no. 4, pp. 6542–6554, 2019.
- [32] S. Kim, E. Lee, J. Jung et al., "MicroRNA-155 positively regulates glucose metabolism via PIK3R1-FOXO3a-cMYC axis in breast cancer," *Oncogene*, vol. 37, no. 22, pp. 2982–2991, 2018.
- [33] M. Xiao, C. Lou, H. Xiao et al., "MiR-128 regulation of glucose metabolism and cell proliferation in triple-negative breast cancer," *The British Journal of Surgery*, vol. 105, no. 1, pp. 75–85, 2018.
- [34] S. L. Romero-Cordoba, S. Rodriguez-Cuevas, V. Bautista-Pina et al., "Loss of function of miR-342-3p results in MCT1 overexpression and contributes to oncogenic metabolic reprogramming in triple negative breast cancer," *Scientific Reports*, vol. 8, no. 1, p. 12252, 2018.
- [35] L. Li, L. Kang, W. Zhao et al., "miR-30a-5p suppresses breast tumor growth and metastasis through inhibition of LDHA-mediated Warburg effect," *Cancer Letters*, vol. 400, pp. 89–98, 2017.
- [36] S. Ueda, M. Takanashi, K. Sudo, K. Kanekura, and M. Kuroda, "miR-27a ameliorates chemoresistance of breast cancer cells by disruption of reactive oxygen species homeostasis and impairment of autophagy," *Laboratory Investigation*, vol. 100, no. 6, pp. 863–873, 2020.
- [37] C. Yu, Y. Wang, J. Peng et al., "Mitochondrial calcium uniporter as a target of microRNA-340 and promoter of metastasis via enhancing the Warburg effect," *Oncotarget*, vol. 8, no. 48, pp. 83831–83844, 2017.
- [38] P. Liu, F. Ye, X. Xie et al., "mir-101-3p is a key regulator of tumor metabolism in triple negative breast cancer targeting AMPK," *Oncotarget*, vol. 7, no. 23, pp. 35188–35198, 2016.
- [39] R. Krutilina, W. Sun, A. Sethuraman et al., "MicroRNA-18a inhibits hypoxia-inducible factor 1 α activity and lung metastasis in basal breast cancers," *Breast Cancer Research*, vol. 16, no. 4, p. R78, 2014.
- [40] S. Jiang, L. F. Zhang, H. W. Zhang et al., "A novel miR-155/miR-143 cascade controls glycolysis by regulating hexokinase 2 in breast cancer cells," *The EMBO Journal*, vol. 31, no. 8, pp. 1985–1998, 2012.
- [41] Y. Chen, Y. Zhou, F. Han et al., "A novel miR-1291-ERR α -CPT1C axis modulates tumor cell proliferation, metabolism and tumorigenesis," *Theranostics*, vol. 10, no. 16, pp. 7193–7210, 2020.
- [42] A. Serguenco, I. Grad, A. B. Wennerstrom et al., "Metabolic reprogramming of metastatic breast cancer and melanoma by let-7a microRNA," *Oncotarget*, vol. 6, pp. 2451–2465, 2015.
- [43] R. Singh, V. Yadav, S. Kumar, and N. Saini, "MicroRNA-195 inhibits proliferation, invasion and metastasis in breast cancer cells by targeting FASN, HMGCR, ACACA and CYP27B1," *Scientific Reports*, vol. 5, no. 1, p. 17454, 2015.
- [44] L. Sripada, K. Singh, A. V. Lipatova et al., "hsa-miR-4485 regulates mitochondrial functions and inhibits the tumorigenicity of breast cancer cells," *Journal of Molecular Medicine (Berlin, Germany)*, vol. 95, no. 6, pp. 641–651, 2017.
- [45] T. Carden, B. Singh, V. Mooga, P. Bajpai, and K. K. Singh, "Epigenetic modification of miR-663 controls mitochondria-to-nucleus retrograde signaling and tumor progression," *The Journal of Biological Chemistry*, vol. 292, no. 50, pp. 20694–20706, 2017.
- [46] Q. Xu, L. Z. Liu, Y. Yin et al., "Regulatory circuit of PKM2/NF- κ B/miR-148a/152-modulated tumor angiogenesis and cancer progression," *Oncogene*, vol. 34, no. 43, pp. 5482–5493, 2015.
- [47] Z. Li, X. Gong, W. Zhang et al., "Inhibition of miRNA-34a promotes triple negative cancer cell proliferation by promoting

- glucose uptake," *Experimental and Therapeutic Medicine*, vol. 18, pp. 3936–3942, 2019.
- [48] C. Pulito, F. Mori, A. Sacconi et al., "Metformin-induced ablation of microRNA 21-5p releases Sestrin-1 and CAB39L antitumoral activities," *Cell discovery*, vol. 3, no. 1, p. 17022, 2017.
- [49] G. Barja, "Mitochondrial oxygen radical generation and leak: sites of production in states 4 and 3, organ specificity, and relation to aging and longevity," *Journal of Bioenergetics and Biomembranes*, vol. 31, no. 4, pp. 347–366, 1999.
- [50] D. Trachootham, J. Alexandre, and P. Huang, "Targeting cancer cells by ROS-mediated mechanisms: a radical therapeutic approach?," *Nature Reviews. Drug Discovery*, vol. 8, no. 7, pp. 579–591, 2009.
- [51] G. Eades, M. Yang, Y. Yao, Y. Zhang, and Q. Zhou, "miR-200a regulates Nrf2 activation by targeting *Keap1* mRNA in breast cancer cells," *The Journal of Biological Chemistry*, vol. 286, no. 47, pp. 40725–40733, 2011.
- [52] N. Zhang, X. Zeng, C. Sun et al., "LncRNA LINC00963 promotes tumorigenesis and radioresistance in breast cancer by sponging miR-324-3p and inducing ACK1 expression," *Molecular Therapy-Nucleic Acids*, vol. 18, pp. 871–881, 2019.
- [53] D. Chen, B. L. Dang, J. Z. Huang et al., "MiR-373 drives the epithelial-to-mesenchymal transition and metastasis via the miR-373-TXNIP-HIF1 α -TWIST signaling axis in breast cancer," *Oncotarget*, vol. 6, pp. 32701–32712, 2015.
- [54] M. Ahir, P. Upadhyay, A. Ghosh et al., "Delivery of dual miRNA through CD44-targeted mesoporous silica nanoparticles for enhanced and effective triple-negative breast cancer therapy," *Biomaterials Science*, vol. 8, no. 10, pp. 2939–2954, 2020.
- [55] X. Liu, H. Tang, J. Chen et al., "MicroRNA-101 inhibits cell progression and increases paclitaxel sensitivity by suppressing MCL-1 expression in human triple-negative breast cancer," *Oncotarget*, vol. 6, no. 24, pp. 20070–20083, 2015.
- [56] M. Zheng, Z. Wu, A. Wu, Z. Huang, N. He, and X. Xie, "MiR-145 promotes TNF- α -induced apoptosis by facilitating the formation of RIP1-FADDcaspase-8 complex in triple-negative breast cancer," *Tumour Biology*, vol. 37, no. 7, pp. 8599–8607, 2016.
- [57] X. Sun, Y. Li, M. Zheng, W. Zuo, and W. Zheng, "MicroRNA-223 increases the sensitivity of triple-negative breast cancer stem cells to TRAIL-induced apoptosis by targeting HAX-1," *PLoS One*, vol. 11, no. 9, article e0162754, 2016.
- [58] N. Patel, K. R. Garikapati, M. J. Ramaiah, K. K. Polavarapu, U. Bhadra, and M. P. Bhadra, "miR-15a/miR-16 induces mitochondrial dependent apoptosis in breast cancer cells by suppressing oncogene BMI1," *Life Sciences*, vol. 164, pp. 60–70, 2016.
- [59] P. Lu, Y. Gu, L. Li, F. Wang, X. Yang, and Y. Yang, "Long non-coding RNA CAMTA1 promotes proliferation and mobility of the human breast cancer cell line MDA-MB-231 via targeting miR-20b," *Oncology Research*, vol. 26, no. 4, pp. 625–635, 2018.
- [60] L. Zhang, X. Zhang, X. Wang, M. He, and S. Qiao, "MicroRNA-224 promotes tumorigenesis through downregulation of caspase-9 in triple-negative breast cancer," *Disease Markers*, vol. 2019, Article ID 7378967, 9 pages, 2019.
- [61] D. C. Chan, "Mitochondrial dynamics and its involvement in disease," *Annual Review of Pathology*, vol. 15, no. 1, pp. 235–259, 2020.
- [62] F. Legros, A. Lombes, P. Frachon, and M. Rojo, "Mitochondrial fusion in human cells is efficient, requires the inner membrane potential, and is mediated by mitofusins," *Molecular Biology of the Cell*, vol. 13, no. 12, pp. 4343–4354, 2002.
- [63] T. Koshiba, S. A. Detmer, J. T. Kaiser, H. Chen, J. M. McCaffery, and D. C. Chan, "Structural basis of mitochondrial tethering by mitofusin complexes," *Science*, vol. 305, no. 5685, pp. 858–862, 2004.
- [64] P. Mishra, V. Carelli, G. Manfredi, and D. C. Chan, "Proteolytic cleavage of Opa1 stimulates mitochondrial inner membrane fusion and couples fusion to oxidative phosphorylation," *Cell Metabolism*, vol. 19, no. 4, pp. 630–641, 2014.
- [65] A. Pagliuso, P. Cossart, and F. Stavru, "The ever-growing complexity of the mitochondrial fission machinery," *Cellular and Molecular Life Sciences*, vol. 75, no. 3, pp. 355–374, 2018.
- [66] J. R. Jimah and J. E. Hinshaw, "Structural insights into the mechanism of dynamin superfamily proteins," *Trends in Cell Biology*, vol. 29, no. 3, pp. 257–273, 2019.
- [67] O. C. Loson, Z. Song, H. Chen, and D. C. Chan, "Fis1, Mff, MiD49, and MiD51 mediate Drp1 recruitment in mitochondrial fission," *Molecular Biology of the Cell*, vol. 24, no. 5, pp. 659–667, 2013.
- [68] L. D. Osellame, A. P. Singh, D. A. Stroud et al., "Cooperative and independent roles of the Drp1 adaptors Mff, MiD49 and MiD51 in mitochondrial fission," *Journal of Cell Science*, vol. 129, no. 11, pp. 2170–2181, 2016.
- [69] H. Otera, N. Miyata, O. Kuge, and K. Mihara, "Drp1-dependent mitochondrial fission via MiD49/51 is essential for apoptotic cristae remodeling," *The Journal of Cell Biology*, vol. 212, no. 5, pp. 531–544, 2016.
- [70] P. K. Purohit, R. Edwards, K. Tokatlidis, and N. Saini, "MiR-195 regulates mitochondrial function by targeting mitofusin-2 in breast cancer cells," *RNA Biology*, vol. 16, no. 7, pp. 918–929, 2019.
- [71] S. Zhang, C. Liu, and X. Zhang, "Mitochondrial damage mediated by miR-1 overexpression in cancer stem cells," *Molecular Therapy-Nucleic Acids*, vol. 18, pp. 938–953, 2019.
- [72] Q. Hu, Y. Yuan, Y. Wu, Y. Huang, Z. Zhao, and C. Xiao, "MicroRNA-137 exerts protective effects on hypoxia-induced cell injury by inhibiting autophagy/mitophagy and maintaining mitochondrial function in breast cancer stem-like cells," *Oncology Reports*, vol. 2020, p. 1, 2020.
- [73] R. Peruzzo, R. Costa, M. Bachmann, L. Leanza, and I. Szabo, "Mitochondrial metabolism, contact sites and cellular calcium signaling: implications for tumorigenesis," *Cancers*, vol. 12, no. 9, p. 2574, 2020.
- [74] X. Zheng, S. Lu, Z. He et al., "MCU-dependent negative sorting of miR-4488 to extracellular vesicles enhances angiogenesis and promotes breast cancer metastatic colonization," *Oncogene*, vol. 39, no. 46, pp. 6975–6989, 2020.
- [75] X. Fan, S. Zhou, M. Zheng, X. Deng, Y. Yi, and T. Huang, "MiR-199a-3p enhances breast cancer cell sensitivity to cisplatin by downregulating TFAM (TFAM)," *Biomedicine & Pharmacotherapy*, vol. 88, pp. 507–514, 2017.
- [76] S. Mandal, N. Gamit, L. Varier, A. Dharmarajan, and S. Warrior, "Inhibition of breast cancer stem-like cells by a triterpenoid, ursolic acid, via activation of Wnt antagonist, sFRP4 and suppression of miRNA-499a-5p," *Life Sciences*, vol. 265, p. 118854, 2021.
- [77] D. Kim, J. Lee, J. Kang et al., "Notch1 in tumor microvascular endothelial cells and tumoral miR-34a as prognostic markers in locally advanced triple-negative breast cancer," *Journal of Breast Cancer*, vol. 22, no. 4, pp. 562–578, 2019.

- [78] G. Hu, X. Zhao, J. Wang et al., “miR-125b regulates the drug-resistance of breast cancer cells to doxorubicin by targeting HAX-1,” *Oncology Letters*, vol. 15, pp. 1621–1629, 2017.
- [79] A. Qattan, H. Intabli, W. Alkhayal, C. Eltabache, T. Tweigieri, and S. B. Amer, “Robust expression of tumor suppressor miRNA’s let-7 and miR-195 detected in plasma of Saudi female breast cancer patients,” *BMC Cancer*, vol. 17, no. 1, p. 799, 2017.
- [80] Z. Ye, R. Hao, Y. Cai, X. Wang, and G. Huang, “Knockdown of miR-221 promotes the cisplatin-inducing apoptosis by targeting the BIM-Bax/Bak axis in breast cancer,” *Tumour Biology*, vol. 37, no. 4, pp. 4509–4515, 2016.
- [81] S. Zhou, Q. Huang, S. Zheng, K. Lin, J. You, and X. Zhang, “miR-27a regulates the sensitivity of breast cancer cells to cisplatin treatment via BAK-SMAC/DIABLO-XIAP axis,” *Tumour Biology*, vol. 37, no. 5, pp. 6837–6845, 2016.
- [82] A. K. Pradhan, P. Bhoopathi, S. Talukdar et al., “MDA-7/IL-24 regulates the miRNA processing enzyme DICER through downregulation of MITF,” *Proceedings of the National Academy of Sciences of the United States of America*, vol. 116, no. 12, pp. 5687–5692, 2019.
- [83] M. Ahir, S. Bhattacharya, S. Karmakar et al., “Tailored-CuO-nanowire decorated with folic acid mediated coupling of the mitochondrial-ROS generation and miR425-PTEN axis in furnishing potent anti-cancer activity in human triple negative breast carcinoma cells,” *Biomaterials*, vol. 76, pp. 115–132, 2016.
- [84] A. De Blasio, R. Di Fiore, G. Pratelli et al., “A loop involving NRF2, miR-29b-1-5p and AKT, regulates cell fate of MDA-MB-231 triple-negative breast cancer cells,” *Journal of Cellular Physiology*, vol. 235, no. 2, pp. 629–637, 2019.
- [85] D. Shi, L. Guo, X. Sun et al., “UTMD inhibit EMT of breast cancer through the ROS/miR-200c/ZEB1 axis,” *Scientific Reports*, vol. 10, no. 1, p. 6657, 2020.
- [86] N. van Zandwijk, N. Pavlakis, S. C. Kao et al., “Safety and activity of microRNA-loaded minicells in patients with recurrent malignant pleural mesothelioma: a first-in-man, phase 1, open-label, dose-escalation study,” *The Lancet Oncology*, vol. 18, no. 10, pp. 1386–1396, 2017.

Research Article

HIF-1 Inhibitor YC-1 Reverses the Acquired Resistance of EGFR-Mutant HCC827 Cell Line with MET Amplification to Gefitinib

Qian Jin , Jisheng Zheng, Ming Chen, Na Jiang, Xianrong Xu, and Feihua Huang 

Department of Respiratory Medicine, Tongde Hospital of Zhejiang Province, Hangzhou, Zhejiang 310012, China

Correspondence should be addressed to Qian Jin; jinqian0504@hotmail.com and Feihua Huang; 042111364@fudan.edu.cn

Received 17 October 2020; Revised 30 January 2021; Accepted 14 February 2021; Published 3 March 2021

Academic Editor: Kanhaiya Singh

Copyright © 2021 Qian Jin et al. This is an open access article distributed under the Creative Commons Attribution License, which permits unrestricted use, distribution, and reproduction in any medium, provided the original work is properly cited.

Background. Acquired resistance occurred in the majority of nonsmall cell lung cancer (NSCLC) patients receiving epidermal growth factor receptor-tyrosine kinase inhibitors (EGFR-TKIs) therapy, and this may be related to the activation of the HIF-1 pathway. Therefore, we examined the influence of the hypoxia-inducible factor-1 (HIF-1) pathway inhibition on the sensitivity of HCC827 gefitinib-resistant (HCC827 GR) cells with MET amplification to gefitinib. **Methods.** We established HCC827 GR cell line with MET amplification and set four groups with different treatment. An MTT assay, a colony formation analysis, and a wound healing assay were performed to determine the sensitivity change of HCC827 GR cells after different treatments. HIF-1 α , p-EGFR, and p-Met levels were detected with western blot. Correlations among HIF-1 α , p-EGFR, and p-Met levels of HCC827 GR cells with different treatments were analyzed with Pearson's correlation analysis. **Results.** HIF-1 inhibitor YC-1 enhanced the sensitivity of HCC827 GR cells to gefitinib. p-Met level was correlated with HIF-1 α level, while there was no correlation between p-Met level and p-EGFR level. **Conclusion.** HIF-1 inhibitor YC-1 is able to reverse the acquired resistance of HCC827 GR to gefitinib, and the regulation of the HIF-1 pathway on MET may be one of the mechanisms.

1. Introduction

The acquired resistance of anticancer drugs is a major cause for therapeutic failure in nonsmall cell lung cancer (NSCLC) leading to tumor recurrence, progression, and poor prognosis [1]. For NSCLC patients with EGFR sensitive mutation, epidermal growth factor receptor-tyrosine kinase inhibitors (EGFR-TKIs) have been used clinically as the first-line treatment [2–4]. However, tumor progression inevitably occurred in the majority of NSCLC patients receiving EGFR-TKIs therapy despite the initial obvious and rapid effects of EGFR-TKIs [5]. Many mechanisms such as T790M mutation, human EGFR-2 amplification, and MET amplification may lead to acquired resistance of EGFR-TKIs [6, 7], but there must be many other mechanisms that need further researches.

Hypoxia is a remarkable characteristic of lung cancer [8]. Tumors in hypoxia condition are easier to have gene mutation, more resistant to antitumor therapy, more invasive, and more antiapoptotic [9]. Under hypoxia condition, the hypoxia-inducible factor 1 (HIF-1) signaling pathway is acti-

vated and plays an important role on the biological effects of hypoxia [8]. HIF-1 consists of a functional α subunit and a β subunit [10]. In a previous study, the quantity of NSCLC stem cells which were resistant to EGFR-TKIs in EGFR mutant NSCLC was increased under hypoxia condition, and the HIF-1 α level was elevated in acquired EGFR-TKI-resistant NSCLC cells [11, 12]. Therefore, we aim at the HIF-1 pathway as a potential target to affect the sensitivity of NSCLC cells to EGFR-TKIs.

In our previous published research, we used HIF-1 inhibitor and activator to regulate the activity of the HIF-1 pathway and found that HIF-1 inhibitor can enhance the sensitivity of HCC827 cells (EGFR-TKIs sensitive EGFR exon 19 mutant NSCLC cell line) to EGFR-TKIs [13]. In order to learn the effect of the HIF-1 pathway on EGFR-TKI acquired resistant NSCLC, we design the present research.

3-(5'-hydroxymethyl-2'-furyl)-1-benzylindazole (YC-1) is a kind of benzyl indazole by chemically synthesizing [14]. It had been found as a HIF-1 inhibitor without cytotoxicity [15]. For the present study, YC-1 and gefitinib were selected

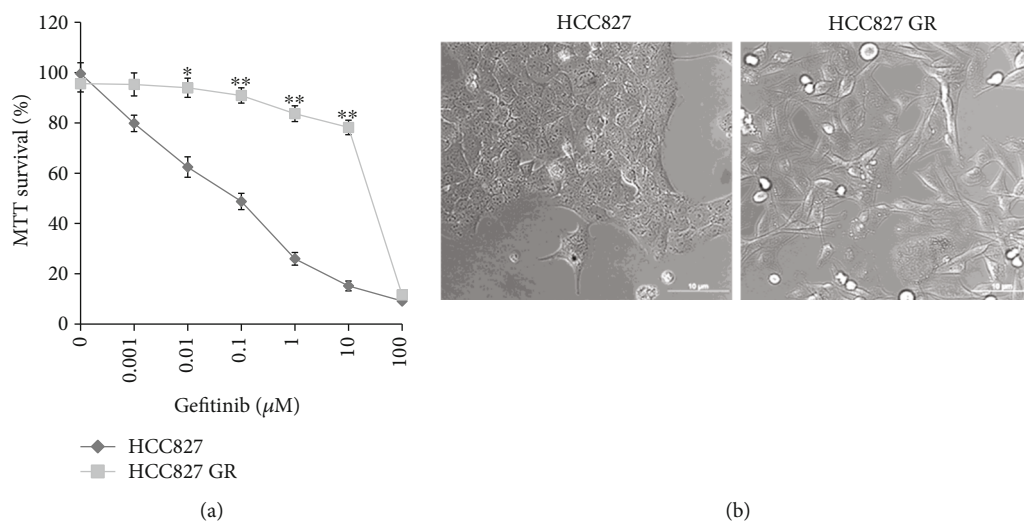


FIGURE 1: HCC827 GR cell line was established. (a) Gefitinib sensitivity between parental HCC827 cells and HCC827 GR cells was compared. Cell viability was measured by MTT assay. Data are presented as mean \pm standard deviation from three independent experiments. * $P < 0.05$ and ** $P < 0.01$ for HCC827 GR cells versus parental cells. (b) Morphological changes from parental HCC827 cells to HCC827 GR cells. Original magnification, $\times 200$.

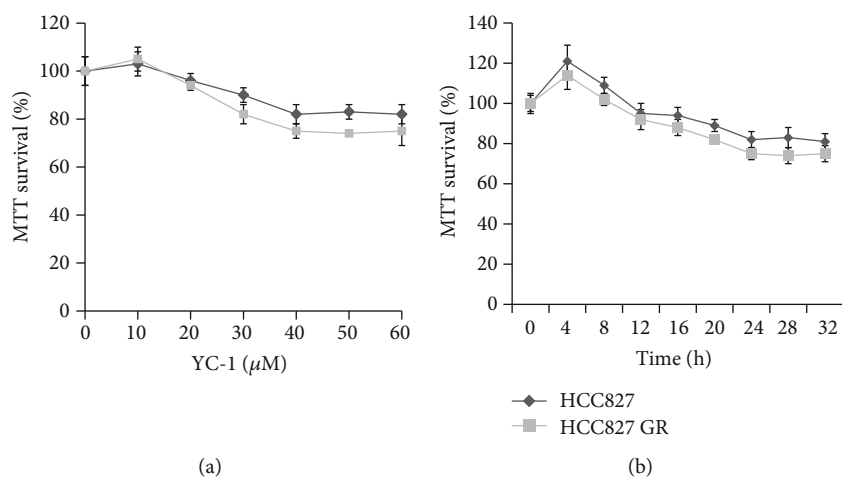


FIGURE 2: Effect of YC-1 on cell viability of parental HCC827 cells and HCC827 GR cells. (a) Cells were exposed to 10, 20, 30, 40, 50, and 60 μM YC-1 and 0.066% DMSO for 24 h. YC-1 concentrations higher than 40 μM were not able to further inhibit the viability of HCC827 and HCC827GR cells. (b) Cells were treated with 40 μM YC-1 for different incubation times, and an increase of the YC-1 exposure time resulted in a decrease of the cell viability. Cell viability was measured by MTT assay. Data are presented as mean \pm standard deviation from three independent experiments.

as HIF-1 inhibitor and EGFR-TKI, respectively. HCC827 gefitinib-resistant (HCC827 GR) cell line was selected as the acquired EGFR-TKI resistant NSCLC cell line. HCC827 GR is generated by exposing HCC827 cells to increasing concentrations of gefitinib, and MET amplification is the mechanism of its acquired resistance [7, 16, 17]. In EGFR-TKI-sensitive NSCLC cells, EGFR was able to regulate MET level through the HIF-1 pathway [18]. In acquired EGFR-TKI-resistance NSCLC cells with MET amplification, EGFR lost its regulation on MET, and whether the HIF-1 pathway remained the regulation on MET kept unclear [7]. In order to make clear the correlation between HIF-1 and MET, acquired gefitinib-resistant HCC827 GR cells with MET

amplification was considered to be the ideal cell line for the present study.

Here, we researched whether HIF-1 inhibiting can reverse the acquired gefitinib resistance of HCC827 GR and detected the levels of p-EGFR, HIF-1 α , and p-Met to explore whether the relative mechanism was associated with the regulation of HIF-1 on MET.

2. Materials and Methods

2.1. Reagents. Reagents and suppliers were as follows: Droplet Digital PCR QX200 system (Bio-Rad Laboratories Inc., Hercules, CA, USA); antibodies against phosphorylated

hepatocyte growth factor receptor (p-Met), c-Met, phosphorylated EGFR (p-EGFR), and EGFR protein (Abcam, Cambridge, MA, USA); and QIAamp DNA Mini Kit (Qiagen, Hilden, Germany). Other reagents and suppliers had been described in our previous research of Jin et al. 2019 [13].

2.2. Establishment of HCC827 GR Cell Line. Human commercially available HCC827 cell line was bought from China Academy of Cell Resource Center, Shanghai Institutes for Biological Sciences as the parental cell. Cell viability of HCC827 in different gefitinib concentrations was measured by MTT assay. HCC827 was continuously exposed to gefitinib beginning at $0.001 \mu\text{M}$ (equivalent to IC20 in parental HCC827) and increased in a stepwise manner to $1 \mu\text{M}$ to generate a resistant cell line. The gefitinib concentrations were increased stepwise to $0.006 \mu\text{M}$, $0.05 \mu\text{M}$, $0.1 \mu\text{M}$, $0.5 \mu\text{M}$, and $1 \mu\text{M}$, equivalent to IC30, IC40, IC50, IC60, and IC70 in parental cells, respectively, until these cells recovered near-normal growth kinetics. The total procedure took 6 months. In order to confirm the successful establishment of HCC827 GR cell line, cell viability of HCC827 GR in different gefitinib concentrations was measured by MTT assay after culturing HCC827 GR in gefitinib-free condition for at least 4 days. At the same time, HCC827 cells were cultured in gefitinib-free condition concomitantly, and their sensitivity to gefitinib was not changed through the gefitinib sensitivity examination every 5 passages [19].

2.3. MET Amplification Detection. In the process of HCC827 GR cell line established, MET levels from parental HCC827 cell to HCC827 GR cell (the gefitinib concentration was increased gradually from $0 \mu\text{M}$ to $1 \mu\text{M}$) were detected. MET levels of HCC827 GR cell with different treatment were detected too. Cells were collected and washed with PBS for 2 times. DNA was abstracted and purified with QIAamp DNA Mini Kit. MET amplifications were analyzed with ddPCR copy number variation (CNV) assay. QX200 ddPCR system was used to perform ddPCR. All procedures were performed according to instructions.

We followed the methods of Jin et al. 2019 [13] for the method of cell culture, medication treatment of YC-1, western blot assay, MTT assay, colony formation assay, cell migration assay, and statistical analyses. Concrete contents were described in supplementary material (available here)

3. Result

3.1. HCC827 GR Cell Line Was Established. The parental cell HCC827 was continuously exposed to gefitinib beginning at $0.001 \mu\text{M}$ and increased in a stepwise manner to $1 \mu\text{M}$. Finally, the HCC827 GR cell line was established as shown in Figure 1(a). Gefitinib had less effect on HCC827 GR cells than that on HCC827 cells. The IC50 of gefitinib on HCC827 GR cells and HCC827 cells was $26.53 \pm 0.96 \mu\text{M}$ and $0.08 \pm 0.02 \mu\text{M}$. Moreover, the morphology of HCC827 GR cells were more elongated than their parental HCC827 cells (Figure 1(b)).

3.2. YC-1 Enhances the Sensitivity of HCC827 GR Cells to Gefitinib. The concentration of YC-1 on HCC827 GR cells

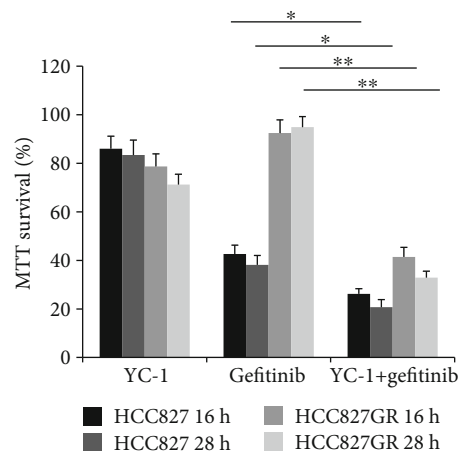


FIGURE 3: MTT assay in parental HCC827 cells and HCC827 GR cells with different treatments. Cell viability of cells with different treatments (blank control, YC-1, gefitinib, YC-1, and gefitinib combined, for 16 h and 28 h) was evaluated by MTT assay. The concentration of YC-1 was $40 \mu\text{M}$, and the final concentration of gefitinib was 20 nM . Error bars represented the mean \pm standard deviation (SD). Data were obtained from three independent experiments. * $P < 0.05$ and ** $P < 0.01$.

was determined through an MTT assay. The concentration of $40 \mu\text{M}$ was finally chosen for this experiment, for a higher concentration of YC-1 was not able to further inhibit the viability of HCC827 GR cells (Figure 2(a)). Increase of the YC-1 exposure time resulted in a decrease of the cell viability, and the effect of $40 \mu\text{M}$ YC-1 on HCC827 GR cells started at the time of 12 h and reached its optimum at the time of 24–28 h (Figure 2(b)). In order to avoid a false negative result caused by large groups of cell death while YC-1 and gefitinib combined, two time points of 16 h and 28 h were set for this study. Colony formation analysis, MTT assay, and wound healing assay were utilized to evaluate the sensitivity of HCC827 GR cells to gefitinib. In MTT assay, compared with gefitinib alone treated HCC827 GR cells, a reduction in cell viability was shown when HCC827 GR cells were treated with YC-1 and gefitinib combined for both 16 h and 28 h ($P < 0.01$; Figure 3), though this phenomenon was also presented in HCC827 cells ($P < 0.05$; Figure 3). In the colony formation analysis, YC-1 alone for both 16 h and 28 h can inhibit the colony formation ability of HCC827 GR cells ($P < 0.05$; Figure 4). Gefitinib and YC-1 together can also inhibit the colony formation ability of HCC827 GR cells ($P < 0.01$; Figure 4). In the wound healing assay, compared with gefitinib treatment alone, gefitinib and YC-1 combined treatment was able to inhibit cell migration ($P < 0.01$; Figure 5). YC-1 treatment alone for both 16 h and 28 h can also inhibit cell migration ability ($P < 0.05$; Figure 5).

3.3. Sensitivity of HCC827 Cells and HCC827 GR Cells to Gefitinib before and after Treatment with YC-1. HCC827 cells and HCC827 GR cells were treated with gefitinib at different concentrations (0.001 , 0.01 , 0.1 , 1 , 10 , and $100 \mu\text{M}$) and $40 \mu\text{M}$ YC-1 combined with gefitinib at different

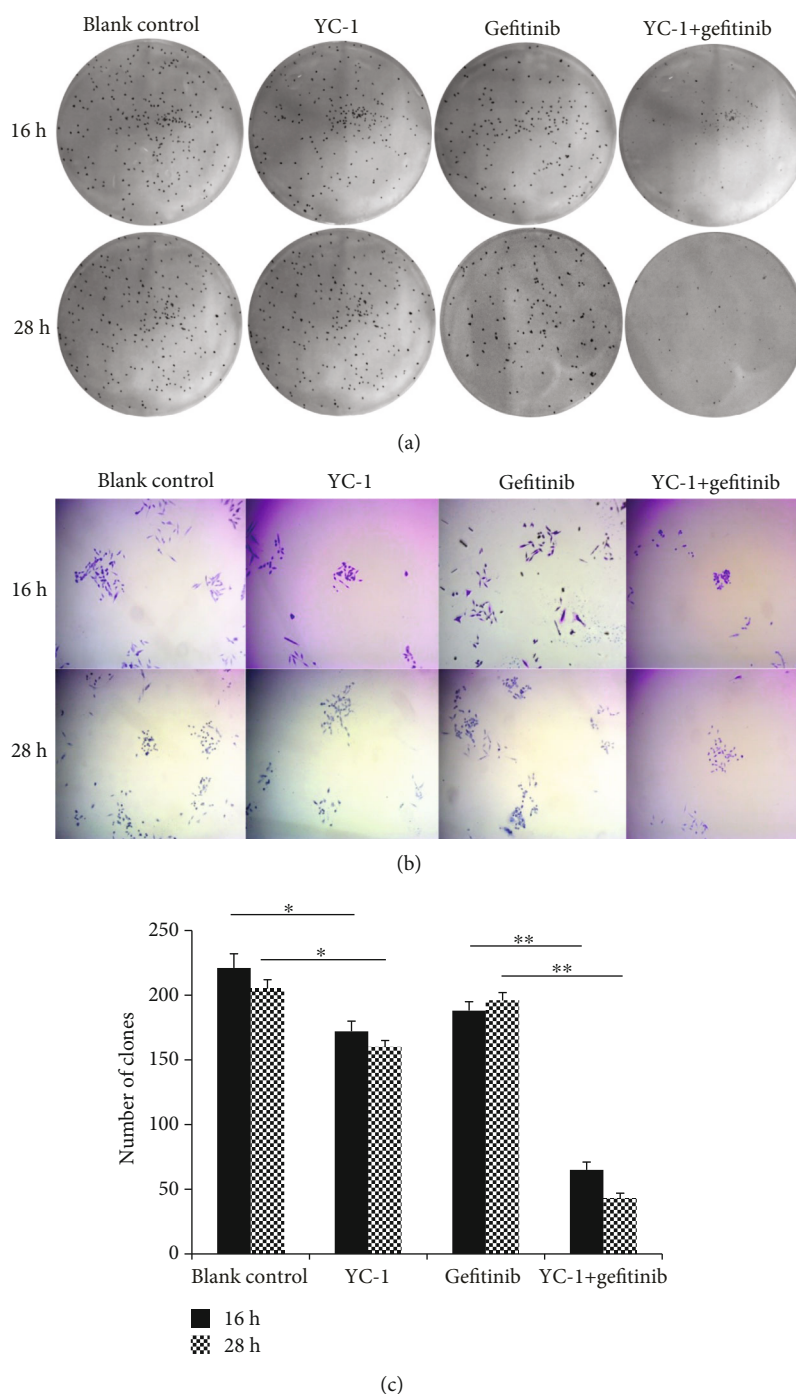


FIGURE 4: Colony formation analysis in HCC827 GR cells with different treatments. HCC827 GR cells were seeded and cultured on dishes with different treatments (blank control, YC-1, gefitinib, YC-1, and gefitinib combined, for 16 h and 28 h), then, cells were culture for 2 weeks in media without drugs. (a) Colony formation of HCC827 GR cells observed by naked eyes. (b) Colony formation of HCC827 GR cells observed under microscope (magnification, $\times 40$). (c) Quantified results of colony formation analysis. The concentration of YC-1 was $40 \mu\text{M}$, and the final concentration of gefitinib was 20 nM . Error bars represented the mean \pm SD. Data were obtained from three independent experiments. * $P < 0.05$ and ** $P < 0.01$.

concentrations. Cell viability was measured by MTT. Compared with gefitinib alone-treated HCC827 cells, a reduction in cell viability was observed when HCC827 cells were treated with $40 \mu\text{M}$ YC-1 and gefitinib at concentrations of 0.01 , 0.1 , and $1 \mu\text{M}$ ($P = 0.0348$, $P = 0.0085$, and $P = 0.01726$, respec-

tively). Compared with gefitinib alone-treated HCC827 GR cells, cell viability was reduced when HCC827 GR cells were treated with $40 \mu\text{M}$ YC-1 and gefitinib at concentrations of 0 , 0.001 , 0.01 , 0.1 , 1 , and $10 \mu\text{M}$ ($P = 0.0089$, $P = 0.0075$, $P = 0.00116$, $P < 0.001$, $P < 0.001$, and $P < 0.001$, respectively).

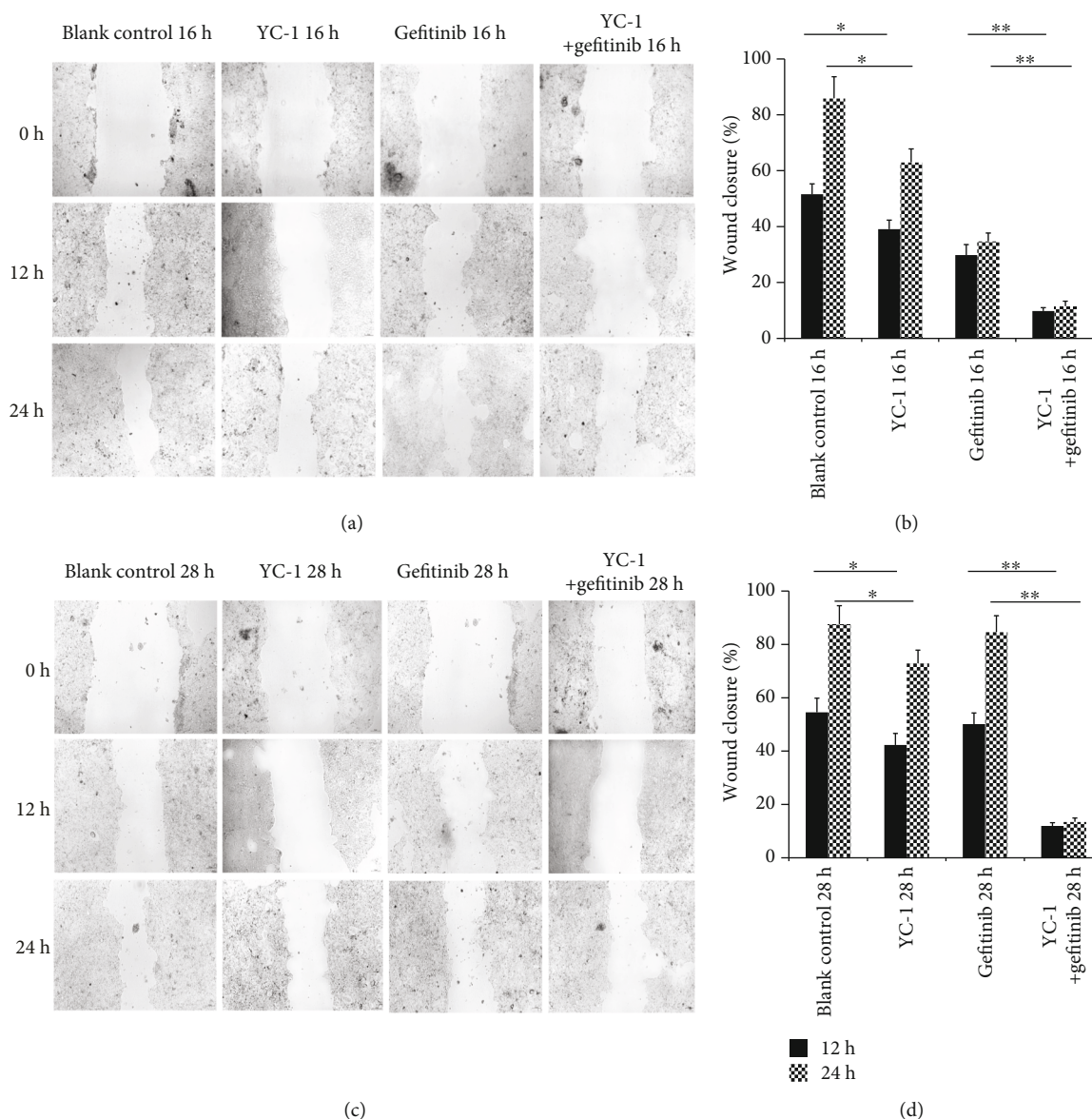


FIGURE 5: Wound healing assay in HCC827 GR cells with different treatments. HCC827 GR cells were pretreated with different treatments (blank control, YC-1, gefitinib, YC-1, and gefitinib combined, for 16 h and 28 h) before receiving the wound healing assay. (a) Wound healing status of HCC827 GR cells with different treatments for 16 h was presented after wounding for 12 and 24 h (magnification, $\times 100$). (b) Wound-healing percentages after wounding for 12 and 24 h were calculated to evaluate cell migration ability of HCC827 GR cells with different treatments for 16 h. (c) Wound healing status of HCC827 GR cells with different treatments for 28 h was presented after wounding for 12 and 24 h (magnification, $\times 100$). (d) Wound-healing percentages after wounding for 12 and 24 h were calculated to evaluate cell migration ability of HCC827 GR cells with different treatments for 28 h. The concentration of YC-1 was $40 \mu\text{M}$, and the final concentration of gefitinib was 20 nM . Error bars represented the mean \pm SD. Data were obtained from three independent experiments. $*P < 0.05$ and $**P < 0.01$.

At the gefitinib concentration of $0.1 \mu\text{M}$, the sensitivity to gefitinib of HCC827 GR cells treated with $40 \mu\text{M}$ YC-1 was enhanced compared with that of HCC827 cells treated with $40 \mu\text{M}$ YC-1 ($P = 0.0062$). At other gefitinib concentrations, there was no significant difference at the sensitivity to gefitinib between HCC827 cells and HCC827 GR cells treated with $40 \mu\text{M}$ YC-1 (Figure 6). These indicated that $40 \mu\text{M}$ YC-1 was able to reverse the resistance of HCC827 GR cells to gefitinib and even presented enhanced sensitivity of

HCC827 GR cells to gefitinib at treatment concentration compared with the parental cells.

3.4. The Detection of MET Amplification in HCC827 GR Cells and the Influence of HIF-1 Pathway Downregulation to MET Amplification. After the HCC827 GR cell line was established, MET amplification was detected. The MET level of HCC827 GR cells reached to more than 5 times of its parental cell. In the process of the HCC827 GR cell line established in

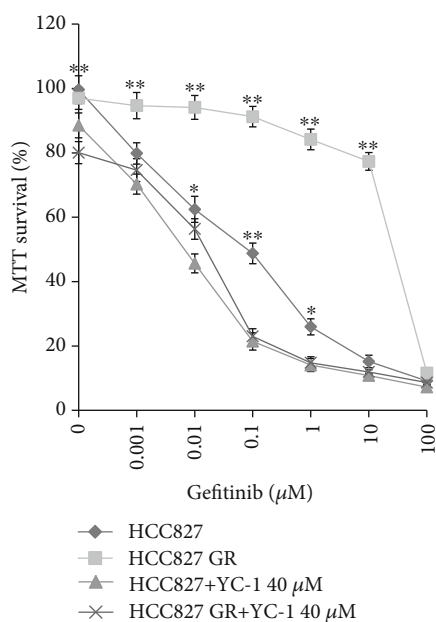


FIGURE 6: Comparison of gefitinib sensitivity among HCC827 cells, HCC827 GR cells, HCC827 cells treated with YC-1, and HCC827 GR cells treated with YC-1. Cell viability was measured by MTT assay. The concentration of YC-1 was 40 μM . Data were obtained from three independent experiments and presented as mean \pm SD. * $P < 0.05$ and ** $P < 0.01$ for HCC827 cells and HCC827 GR cells versus those treated with YC-1.

a stepwise manner, the level of MET increased gradually. When the concentration of gefitinib reached to 1 μM , a high level of MET amplification emerged.

In different treatment groups of HCC827 GR, MET amplification was inhibited in the YC-1-treated group and YC-1 and gefitinib combined group for both 16 h and 28 h ($P < 0.001$ of both groups for 16 h and 28 h). It indicated that downregulation of the HIF-1 pathway was able to inhibit MET amplification (Figure 7).

3.5. Correlation between p-Met and HIF-1 α Levels in HCC827 GR Cells with Different Treatments. Protein levels of p-EGFR, EGFR, HIF-1 α , c-Met, and p-Met in different HCC827 GR groups were tested with western blot analysis. In the blank control group, the HIF-1 α level and p-Met level were much higher than those in their parental HCC827 cells ($P = 0.0029$ and $P < 0.001$, respectively). In groups containing YC-1 treatment, levels of HIF-1 α and p-Met were decreased compared with groups without YC-1 treatment (for HIF-1 α levels comparison, $P = 0.0359$, $P = 0.0125$, $P = 0.0297$, and $P = 0.0101$, respectively; $P < 0.001$ for all p-Met levels comparison; Figure 8). In the above groups, the p-Met level was correlated with HIF-1 α level ($P < 0.001$; $R^2 = 0.959$; Figure 9(a)), but there was no correlation between the p-Met level and p-EGFR level ($P = 0.697$; $R^2 = 0.027$; Figure 9(b)).

4. Discussion

In the present study, the inhibition of the HIF-1 pathway by YC-1 can make the HCC827 GR cell more sensitive to gefi-

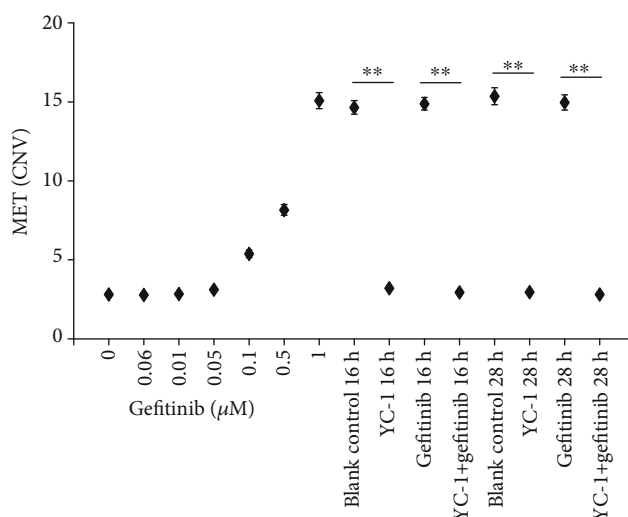


FIGURE 7: MET amplification detected by ddPCR CNV assay. In the process of the HCC827 GR cell line established, MET levels from parental HCC827 cell to HCC827 GR cell (the gefitinib concentration was increased gradually from 0 μM to 1 μM) were shown. MET levels of HCC827 GR cell with different treatment (blank control, YC-1, gefitinib, and YC-1 and gefitinib combined for 16 h and 28 h) were shown too. The concentration of YC-1 was 40 μM , and the final concentration of gefitinib was 20 nM. Data were obtained from three independent experiments and presented as mean \pm SD. ** $P < 0.01$.

tinib. Through the comparison of gefitinib sensitivity among HCC827 cells, HCC827 GR cells, HCC827 cells treated with YC-1, and HCC827 GR cells treated with YC-1, it finally revealed that HIF-1 inhibitor YC-1 reversed the acquired resistance of HCC827 GR cells to gefitinib. In our previous research, we also found that the HIF-1 inhibitor was able to enhance the sensitivity of HCC827 cells to gefitinib [13].

Hypoxic tumor cells activate a series of signal pathways to adapt to the hypoxic condition. In these signal pathways, the HIF-1 signal pathway is the most well-defined and important pathway. HIF-1 pathway has more than 100 target genes which allow the tumor cells to survive and proliferate in hypoxic condition [20, 21]. HIF-1 keeps a stable construction in hypoxia. Then, it transfers to the nucleus and activates the expression of its target genes [8]. These activated genes prevent apoptosis and promote therapy resistance by regulating cell metabolism, survival, drug efflux, signaling, and DNA repair [22–26]. Thus, inhibiting the HIF-1 pathway is able to enhance the sensitivity of anticancer therapy theoretically.

For the HIF-1 pathway in EGFR-TKI therapy resistance, previous research showed the upregulation of HIF-1 α [12]. Furthermore, the quantity of NSCLC stem cells which were resistant to EGFR-TKIs in EGFR mutant NSCLC was increased under hypoxic condition [11]. In acquired EGFR-TKI-resistant NSCLC cells with MET amplification, EGFR lost its regulation on MET, and whether the HIF-1 pathway remained the regulation on MET kept unclear [7]. Meanwhile, HCC827 GR is generated by exposing HCC827 cells to increasing concentrations of gefitinib, and MET amplification is the mechanism of its acquired resistance [16, 17]. In

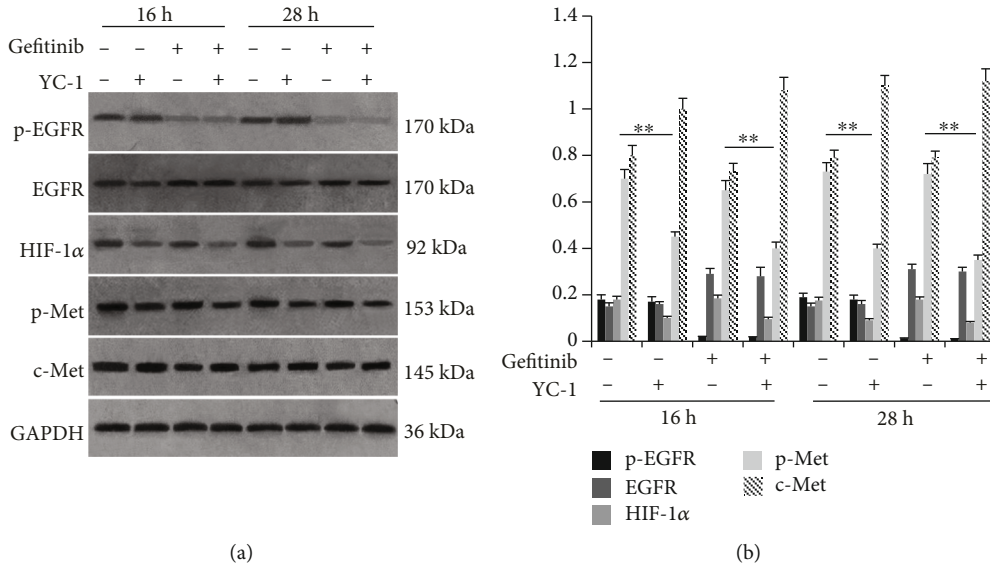


FIGURE 8: Expression of p-EGFR, EGFR, HIF-1 α , p-Met, and c-Met in HCC827 GR cells with different treatments. (a) Western blot analysis was performed to detect p-EGFR, EGFR, HIF-1 α , p-Met, and c-Met protein expression levels in HCC827 GR cells with different treatments (blank control, YC-1, gefitinib, YC-1, and gefitinib combined, for 16 h and 28 h). (b) Quantified densitometric scanning of the blots. The concentration of YC-1 was 40 μ M, and the final concentration of gefitinib was 20 nM. Error bars represented the mean \pm SD. Data were obtained from three independent experiments. ** $P < 0.01$.

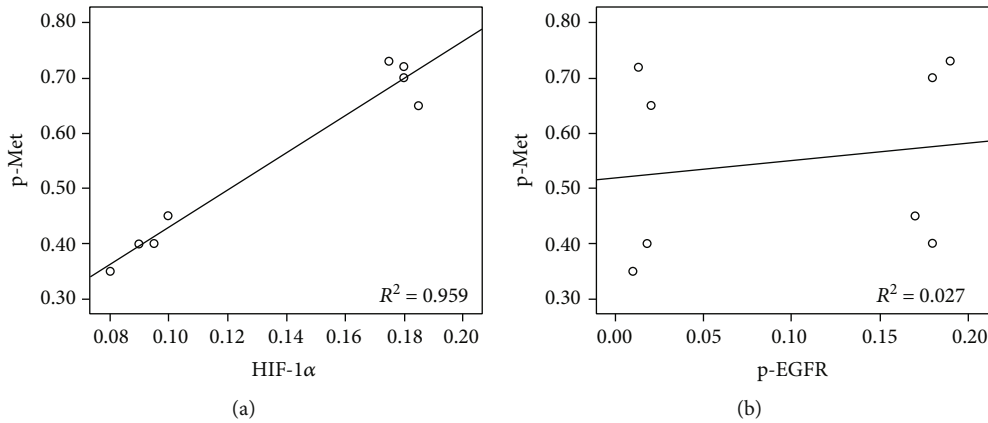


FIGURE 9: Pearson's correlation analysis between p-Met, HIF-1 α , and p-EGFR levels. (a) There was a positive correlation between HIF-1 α and p-Met levels in HCC827 GR cells with different treatments ($P < 0.001$; $R^2 = 0.959$). (b) There was no correlation between p-Met and p-EGFR levels in HCC827 GR cells with different treatments ($P = 0.697$; $R^2 = 0.027$).

our study, MET amplification of HCC827 GR was presented by ddPCR CNV assay, and the correlations between HIF-1 α , p-EGFR, and p-Met levels were analyzed by Pearson's correlation analysis. Our study showed that the p-Met level was correlated with the HIF-1 α level, but there was no correlation between p-Met level and p-EGFR level. So, we speculated that the HIF-1 pathway keeps its regulation on MET while EGFR loses its regulation on MET in HCC827 GR cells with MET amplification. Accordingly, the regulation of the HIF-1 pathway on MET may be one of the mechanisms of YC-1 reversing the acquired resistance of HCC827 GR to gefitinib.

Despite the necessity of further researches to find out other possible mechanisms of YC-1 reversing the acquired

resistance of HCC827 GR to gefitinib, the present study discovers that HIF-1 inhibitor YC-1 is able to reverse the acquired resistance of HCC827 GR with MET amplification to gefitinib. Therefore, the HIF-1 pathway may be a significant target for reversing the acquired resistance of NSCLC with MET amplification to EGFR-TKIs.

5. Conclusions

HIF-1 inhibitor YC-1 is able to reverse the acquired resistance of HCC827 GR to gefitinib, and the regulation of HIF-1 pathway on MET may be one of the mechanisms.

Data Availability

The data used to support the findings of this study are available from the corresponding author upon request.

Conflicts of Interest

The authors declare that they have no competing interests.

Acknowledgments

The authors would like to thank Miss Guizhi Zhao, Professor Jianying Zhou, and the respiratory research laboratory staff of First Affiliated Hospital of Zhejiang University School of Medicine for providing technical assistance. This study was funded by Medicine and Health Projects of Zhejiang Province [2016KYB053] and Chinese Medicine Scientific Projects of Zhejiang Province [2018ZA020].

Supplementary Materials

The supplementary material described methods of cell culture, medication treatment, western blot assay, MTT assay, colony formation assay, cell migration assay and statistical analyses. (*Supplementary Materials*)

References

- [1] V. Sosa Iglesias, L. Giuranno, L. J. Dubois, J. Theys, and M. Vooijs, "Drug resistance in non-small cell lung cancer: a potential for NOTCH targeting?," *Frontiers in oncology*, vol. 8, p. 267, 2018.
- [2] A. C. Z. Gelatti, A. Drilon, and F. C. Santini, "Optimizing the sequencing of tyrosine kinase inhibitors (TKIs) in epidermal growth factor receptor (EGFR) mutation-positive non-small cell lung cancer (NSCLC)," *Lung Cancer*, vol. 137, pp. 113–122, 2019.
- [3] J. Franek, J. C. Cappelleri, K. A. Larkin-Kaiser, K. D. Wilner, and R. Sandin, "Systematic review and network meta-analysis of first-line therapy for advanced EGFR-positive non-small-cell lung cancer," *Future Oncology*, vol. 15, no. 24, pp. 2857–2871, 2019.
- [4] W. H. Hsu, J. C. Yang, T. S. Mok, and H. H. Loong, "Overview of current systemic management of EGFR-mutant NSCLC," *Annals of Oncology*, vol. 29, supplement_1, pp. i3–i9, 2018.
- [5] S. M. Lim, N. L. Syn, B. C. Cho, and R. A. Soo, "Acquired resistance to EGFR targeted therapy in non-small cell lung cancer: mechanisms and therapeutic strategies," *Cancer Treatment Reviews*, vol. 65, pp. 1–10, 2018.
- [6] D. Westover, J. Zugazagoitia, B. C. Cho, C. M. Lovly, and L. Paz-Ares, "Mechanisms of acquired resistance to first- and second-generation EGFR tyrosine kinase inhibitors," *Annals of Oncology*, vol. 29, supplement_1, pp. i10–i19, 2018.
- [7] J. A. Engelman, K. Zejnullahu, T. Mitsudomi et al., "MET amplification leads to gefitinib resistance in lung cancer by activating ERBB3 signaling," *Science*, vol. 316, no. 5827, pp. 1039–1043, 2007.
- [8] S. K. Burroughs, S. Kaluz, D. Wang, K. Wang, E. G. Van Meir, and B. Wang, "Hypoxia inducible factor pathway inhibitors as anticancer therapeutics," *Future Medicinal Chemistry*, vol. 5, no. 5, pp. 553–572, 2013.
- [9] W. Wilson and M. Hay, "Targeting hypoxia in cancer therapy," *Nature Reviews. Cancer*, vol. 11, no. 6, pp. 393–410, 2011.
- [10] G. L. Wang, B. H. Jiang, E. A. Rue, and G. L. Semenza, "Hypoxia-inducible factor 1 is a basic-helix-loop-helix-PAS heterodimer regulated by cellular O₂ tension," *Proc Natl Acad Sci USA*, vol. 92, no. 12, pp. 5510–5514, 1995.
- [11] A. Murakami, F. Takahashi, F. Nurwidya et al., "Hypoxia increases gefitinib-resistant lung cancer stem cells through the activation of insulin-like growth factor 1 receptor," *PLoS One*, vol. 9, article 86459, 2014.
- [12] F. Morgillo, "Antitumour efficacy of MEK inhibitors in human lung cancer cells and their derivatives with acquired resistance to different tyrosine kinase inhibitors," *British Journal of Cancer*, vol. 105, no. 3, pp. 382–392, 2011.
- [13] Q. Jin, J. Zhou, X. Xu, F. Huang, and W. Xu, "Hypoxia-inducible factor-1 signaling pathway influences the sensitivity of HCC827 cells to gefitinib," *Oncology Letters*, vol. 17, no. 4, pp. 4034–4043, 2019.
- [14] F. N. Ko, C. C. Wu, S. C. Kuo, F. Y. Lee, and C. M. Teng, "YC-1, a novel activator of platelet guanylate cyclase," *Blood*, vol. 84, no. 12, pp. 4226–4233, 1994.
- [15] Y. S. Chun, E. J. Yeo, E. Choi et al., "Inhibitory effect of YC-1 on the hypoxic induction of erythropoietin and vascular endothelial growth factor in Hep3B cells¹," *Biochemical Pharmacology*, vol. 61, no. 8, pp. 947–954, 2001.
- [16] W. J. Jang, S. K. Jung, J. S. Kang et al., "Anti-tumor activity of WK88-1, a novel geldanamycin derivative, in gefitinib-resistant non-small cell lung cancers with Met amplification," *Cancer Science*, vol. 105, no. 10, pp. 1245–1253, 2014.
- [17] J. K. Rho, Y. J. Choi, S. Y. Kim et al., "MET and AXL inhibitor NPS-1034 exerts efficacy against lung cancer cells resistant to EGFR kinase inhibitors because of MET or AXL activation," *Cancer Research*, vol. 74, no. 1, pp. 253–262, 2014.
- [18] L. Xu, M. B. Nilsson, P. Saintigny et al., "Epidermal growth factor receptor regulates MET levels and invasiveness through hypoxia-inducible factor-1 α in non-small cell lung cancer cells," *Oncogene*, vol. 29, no. 18, pp. 2616–2627, 2010.
- [19] J. A. Engelman, T. Mukohara, K. Zejnullahu et al., "Allelic dilution obscures detection of a biologically significant resistance mutation in EGFR-amplified lung cancer," *The Journal of Clinical Investigation*, vol. 116, no. 10, pp. 2695–2706, 2006, Epub 2006 Aug 10.
- [20] C. Wigerup, S. Pahlman, and D. Bexell, "Therapeutic targeting of hypoxia and hypoxia-inducible factors in cancer," *Pharmacology & Therapeutics*, vol. 164, pp. 152–169, 2016.
- [21] N. A. Warfel and W. S. El-Deiry, "HIF-1 signaling in drug resistance to chemotherapy," *Current Medicinal Chemistry*, vol. 21, no. 26, pp. 3021–3028, 2014.
- [22] K. M. Comerford, T. J. Wallace, J. Karhausen, N. A. Louis, M. C. Montalto, and S. P. Colgan, "Hypoxia-inducible factor-1-dependent regulation of the multidrug resistance (MDR1) gene," *Cancer Research*, vol. 62, no. 12, pp. 3387–3394, 2002.
- [23] M. C. Brahimi-Horn, G. Bellot, and J. Pouyssegur, "Hypoxia and energetic tumour metabolism," *Current Opinion in Genetics & Development*, vol. 21, no. 1, pp. 67–72, 2011.
- [24] L. Liu, X. Ning, L. Sun et al., "Hypoxia-inducible factor-1 alpha contributes to hypoxia-induced chemoresistance in gastric cancer," *Cancer Science*, vol. 99, no. 1, pp. 121–128, 2008.

- [25] D. Wu, B. Chen, F. Cui, X. He, W. Wang, and M. Wang, "Hypoxia-induced microRNA-301b regulates apoptosis by targeting Bim in lung cancer," *Cell Proliferation*, vol. 49, no. 4, pp. 476–483, 2016.
- [26] F. Liu, L. Hu, Y. Ma et al., "Increased expression of monoamine oxidase A is associated with epithelial to mesenchymal transition and clinicopathological features in non-small cell lung cancer," *Oncology Letters*, vol. 15, no. 3, pp. 3245–3251, 2018.